MECHANICAL, THERMAL AND SORPTION STUDIES OF INDUSTRIAL WASTE REINFORCED NATURAL RUBBER

Thesis submitted to
the University of Calicut in partial fulfilment of
the requirements for the award of the degree of

DOCTOR OF PHILOSOPHY IN CHEMISTRY

by

BASHPA P

Under the supervision of

Dr. Tania Francis

DEPARTMENT OF CHEMISTRY
ST. JOSEPH'S COLLEGE (AUTONOMOUS) DEVAGIRI,
CALICUT, KERALA – 673008
(Affiliated to University of Calicut)

JANUARY 2024

DECLARATION

I hereby declare that the work presented in the thesis entitled **"MECHANICAL, THERMAL AND SORPTION STUDIES OF INDUSTRIAL WASTE REINFORCED NATURAL RUBBER"** is based on the original work done by me under the guidance of **Dr. Tania Francis**, Assistant Professor & Head, Department of Chemistry, St. Joseph's College (Autonomous) Devagiri, Kozhikode and has not been included in any other thesis submitted previously for the award of any degree. The contents of the thesis are undergone plagiarism check using 'iThenticate' software at C.H.M.K. Library, University of Calicut, and the similarity index found within the permissible limit. I also declare that the thesis is free from AI generated contents.

Kozhikode **Bashpa P**

Date:

Signature of the Supervising teacher:

Name: Dr. Tania Francis

DEPARTMENT OF CHEMISTRY
ST. JOSEPH'S COLLEGE (AUTONOMOUS) DEVAGIRI
CALICUT - 673 008, KERALA, INDIA.
'College with potential for excellence',
Accredited by **NAAC** with Grade **A**$^{++}$
Affiliated to University of Calicut

Dr. Tania Francis
Assistant Professor & Head

Tel: +91 9496928889; 9895726068
Email: francistania76@gmail.com

Date:

CERTIFICATE

This is to certify that the research work embodied in the thesis entitled **"MECHANICAL, THERMAL AND SORPTION STUDIES OF INDUSTRIAL WASTE REINFORCED NATURAL RUBBER"** submitted by **Bashpa P** to the University of Calicut for the award of degree of **Doctor of Philosophy in Chemistry** under the Faculty of Science is an authentic record of precise research work carried out at the Department of Chemistry, St. Joseph's College (Autonomous) Devagiri, Calicut, Kerala under my supervision and guidance. The contents of the thesis have been checked for plagiarism using the 'iThenticate' software at C.H.M.K. Library, University of Calicut, and the similarity index falls under the permissible limit. I certify that the contents of this thesis have not been submitted elsewhere for any degree or diploma. I also certify that the corrections/suggestions recommended by adjudicators have been incorporated into the thesis

Kozhikode **Dr. Tania Francis**

ACKNOWLEDGEMENT

The work mentioned in this thesis would never have been achieved without the generous help of many people who have always encouraged me. I use this occasion to acknowledge and sincerely thank them for helping me make this thesis possible.

First and foremost, I am deeply grateful to Dr. Tania Francis, Assistant Professor and Head, Department of Chemistry, St. Joseph's College (Autonomous) Devagiri, Calicut, for being my Ph.D. supervisor. Her inspiration, unwavering assistance, intellectual stimulation, astute direction, incredibly priceless thoughts, and recommendations from the beginning to the end helped me to grasp the subject. Her erudite recommendations, wise counsel, boundless curiosity, and tender demeanour inspired me. I appreciate the countless ideas and contributions that will always be my lifelong source of scientific knowledge.

I wish to thank Rev. Fr. Biju K. Isaac (CMI), Manager, Prof. Boby Jose, Principal and Dr. Satheesh George, Principal-in-charge of St. Joseph's College (Autonomous) Devagiri, Calicut, for permitting me to do part-time research and providing financial support for the publication of research articles. I also record my gratitude and respect to the former Principals, Dr. Sabu K Thomas, Dr. Sibichen M Thomas, Dr. Jose John Mallikasseri and former Head of the Department of Chemistry, Dr. Joy Joseph, for their support and help throughout my research period.

I am grateful to all the faculty members of the Department of Chemistry, laboratory and library staff of St. Joseph's College (Autonomous) Devagiri, Calicut, for their help and support.

I sincerely thank the members of the Research Advisory Committee (RAC), Prof. Abraham Joseph, Prof. Renuka N.K., and Prof. M.T. Ramesan (Department of Chemistry, University of Calicut), for their valuable suggestions and encouragement during my research.

My acknowledgement could never be completed without acknowledging my laboratory seniors, who have helped me understand the hard truths of research by teaching me about laboratory culture and providing an excellent example for me to follow. I appreciate Ms. Annie Stephy and Dr. Meril Shelly for their supportive advice and assistance during my research period.

I am fortunate enough to express my gratitude for the help of a few exceptional individuals. I have no idea how to convey my appreciation and heartfelt thanks to the following individuals: Dr. Dileep P., Assistant Director, JJ Murphy Research Centre, Rubber Park India (P) Ltd., Valayanchirangara, Ernakulam, Dr. Silviya Elanthikkal, Deanship of Scientific Research, Imam Abdulrahman Bin Faisal University, Dammam, Saudi Arabia, Prof. P. Venugopalan, Retired Professor, Department of Chemistry, Panjab University, Chandigarh, Mr. Mehar Singh, Research Scholar, Physical Chemistry Division, Panjab University, Chandigarh, and Dr. P. Lalitha, Director R&D, Bharat Ratna Prof. CNR Rao Research Centre, Avinashilingam Institute for Home Science and Higher Education for Women, Coimbatore stand out among them and sincerely thank for their invaluable assistance and support for conducting various analyses.

I am grateful to the unknown reviewers who repeatedly rejected my manuscripts from various journals. Their feedback enabled me to improve the quality of my research publications. I also thank the reviewers who recommended my articles for publication in prestigious peer-reviewed journals.

I thank the Management and Principals of N.S.S. College, Manjeri and Ottapalam, for allowing me to do part-time research.

I wish to thank my husband and my dear children for their adorable affection and motivation, without which I could not complete this task. I embrace the opportunity to express my deep gratitude to my Parents, Parents-in-law, and all my family and friends for their encouragement.

My sincere gratitude goes out to Shri. Balu and Shri. Rajesh K, Bina Photostat, Calicut University, for their excellent proof corrections and computer processing of the thesis.

Above all, I thank God Almighty for the grace shown to me, whose kindness has supported me during all my meek attempts to bumble through the challenging field of research.

As I near the conclusion of my six-year PhD journey, I am truly pleased with my achievements. My personal and professional development has been profoundly impacted by this life-changing experience, which taught me the priceless lesson that persistence eventually pays off. The unwavering commitment and determination shown by those around me have profoundly influenced my character.

Bashpa P.

Dedicated to

My Beloved Husband

&

My Dear Children

ABSTRACT

The rapid growth of industrialisation is having a negative effect on the environment due to the enormous quantity of different types of industrial waste being released into the atmosphere. The traditional methods of landfilling and other methods of disposing of industrial waste are no longer enough to deal with the surplus of these wastes. As a result, the reutilisation of these wastes is becoming increasingly popular. It is inevitable to concentrate on the efficient and effective utilisation of various types of industrial wastes to reduce production costs and prevent pollution. In addition to recycling industrial wastes, there is a great need for high-performance rubber composites for a wide range of applications.

Polyurethane waste (PUW) from the footwear, magnesium carbonate waste (MCW) from the condom, and sodium sulphate waste (SSW) from the pigment industries were collected, removed other impurities, and incorporated into natural rubber (NR) as reinforcing fillers. The influence of clay on property enhancement is also studied by adding it as an additional filler to the NR-PUW composites. NR-waste composites were prepared through a two-roll mill mixing process. The rheological, mechanical, thermal and sorption properties of NR-PUW, NR-MCW, NR-SSW composites and NR-PUW-clay compounds were investigated. All the fabricated composites showed significant improvement in mechanical, thermal, and sorption properties compared to NR. NR composites with 5 parts per hundred (phr) PUW, 3 phr MCW and 7.5 phr SSW showed the best mechanical

properties among other composites prepared. Various established mechanical modelling techniques were used to confirm the better filler adhesion on the NR matrix. NR compound with 5 phr PUW and 10 phr clay showed better mechanical properties, while compound with 5 phr PUW and 20 phr clay had good sorption resistance. The model-free approaches successfully tracked the path during the thermal degradation and predicted the produced composite's activation energy changes and multistep degradation kinetics. The fabricated composites and compounds find huge potential as a replacement for NR, benefitting the production of common industrial rubber products with high tensile strength, heat resistance, and solvent absorption resistance. Another important finding of this study is that it is essential to reuse industrial waste from a circular economy perspective to reduce production costs and prevent environmental pollution. Additionally, this technology can be used in other rubber systems such as SBR, NBR, and ENR to produce high-performance rubber composites for various industrial applications.

Keywords: Natural rubber composites, Industrial waste reutilisation, Mechanical, Thermal, Sorption.

സംഗ്രഹം

വ്യാവസായികവൽക്കരണത്തിന്റെ ദ്രുതഗതിയിലുള്ള വളർച്ച പരിസ്ഥിതിയെ പ്രതികൂലമായി ബാധിക്കുന്നു. ഇതിന് കാരണം വിവിധ തരം വ്യാവസായിക മാലിന്യങ്ങൾ അന്തരീക്ഷത്തിലേക്ക് പുറന്തള്ളുന്നതാണ്. ഈ മാലിന്യങ്ങൾ കൈകാര്യം ചെയ്യാൻ പരമ്പരാഗത രീതിയിലുള്ള ലാൻഡ് ഫില്ലിംഗും, മറ്റ് രീതികളും ഇനി പര്യാപ്തമല്ല. ചെലവ് കുറയ്ക്കുന്നതിനും മലിനീകരണം തടയുന്നതിനും വിവിധ തരം വ്യാവസായിക മാലിന്യങ്ങളുടെ കാര്യക്ഷമവും ഫലപ്രദവുമായ പുനരുപയോഗത്തിൽ ശ്രദ്ധ കേന്ദ്രീകരിക്കേണ്ടത് അനിവാര്യമാണ്. ഇതിനു പുറമെ വിപുലമായ വ്യാവസായിക റബ്ബർ ഉല്പന്നങ്ങളുടെ നിർമ്മിതിക്കായ് ഉയർന്ന പ്രവർത്തനക്ഷമതയുള്ള റബ്ബർ സംയുക്തങ്ങളുടെ ആവശ്യകതയും ഇന്ന് വളരെ പ്രസക്തമാണ്.

പാദരക്ഷ നിർമാണ കമ്പനിയിൽ നിന്നുള്ള പൊളിയൂറിത്തീൻ മാലിന്യം (PUW), കോണ്ടം വ്യവസായത്തിൽ നിന്നുള്ള മഗ്നീഷ്യം കാർബണേറ്റ് മാലിന്യം (MCW), പിഗ്മെന്റ് വ്യവസായങ്ങളിൽ നിന്നുള്ള സോഡിയം സൾഫേറ്റ് മാലിന്യം (SSW) എന്നിവ ശേഖരിച്ച്, മറ്റു മാലിന്യങ്ങൾ മാറ്റിയ ശേഷം, പ്രകൃതിദത്ത റബ്ബറിൽ (NR) ശക്തിപ്പെടുത്തുന്ന ഫില്ലറുകളായി സംയോജിപ്പിച്ചു. ഗുണങ്ങൾ മെച്ചപ്പെടുത്തലിൽ കളിമണ്ണിന്റെ സ്വാധീനം പഠിക്കാൻ, ഇത് NR-PUW കോമ്പോസിറ്റുകളിലേക്ക് ഒരു അധിക ഫില്ലറായി ചേർത്തു. NR-മാലിന്യ സംയോജനങ്ങൾ രണ്ട്-റോൾ മിൽ മിക്സിംഗ് പ്രക്രിയയിലൂടെ തയ്യാറാക്കി.

NR-PUW, NR-MCW, NR-SSW കോമ്പോസിറ്റുകളുടെയും NR-PUW-കളിമൺ സംയുക്തങ്ങളുടെയും റിയോളജിക്കൽ, മെക്കാനിക്കൽ, തെർമൽ, സോർപ്ഷൻ പ്രോപ്പർട്ടികൾ പഠിച്ചു. എല്ലാ ഫാബ്രിക്കേറ്റഡ് കോമ്പോസിറ്റുകളും NR നെ അപേക്ഷിച്ച് മെക്കാനിക്കൽ, തെർമൽ, സോർപ്ഷൻ ഗുണങ്ങളിൽ കാര്യമായ പുരോഗതി കാണിച്ചു. 5 phr PUW, 3 phr MCW, 7.5 phr SSW എന്നിവയുള്ള NR കോമ്പോസിറ്റുകൾ മറ്റ് കോമ്പോസിറ്റുകളേക്കാൾ മികച്ച ഗുണങ്ങൾ കാണിച്ചു. NR മാട്രിക്സിൽ മികച്ച ഫില്ലർ അഡീഷൻ സ്ഥിരീകരിക്കാൻ വിവിധ സ്ഥാപിത മെക്കാനിക്കൽ മോഡലിംഗ് ടെക്നിക്കുകൾ ഉപയോഗിച്ചു. 5 phr PUW ഉം 10 phr കളിമണ്ണും ഉള്ള NR സംയുക്തം മികച്ച മെക്കാനിക്കൽ ഗുണങ്ങൾ കാണിച്ചു, അതേസമയം 5 phr PUW ഉം 20 phr കളിമണ്ണും ഉള്ള സംയുക്തത്തിന് നല്ല സോർപ്ഷൻ പ്രതിരോധമുണ്ട്. മോഡൽ-ഫ്രീ അപ്രോച്ചുകൾ തെർമൽ ഡിഗ്രേഡേഷൻ സമയത്ത് പാത്ത് വിജയകരമായി ട്രാക്ക് ചെയ്യുകയും ഉൽപ്പാദിപ്പിച്ച സംയുക്തത്തിന്റെ ഊർജ്ജ മാറ്റങ്ങളും മൾട്ടിസ്റ്റെപ്പ് ഡിഗ്രേഡേഷൻ ഗതിവിഗതികളും പ്രവചിക്കുകയും ചെയ്തു. ഫാബ്രിക്കേറ്റഡ് റബ്ബർ-വേസ്റ്റ് കോമ്പോസിറ്റുകളും റബ്ബർ-വേസ്റ്റ്-ക്ലേ സംയുക്തങ്ങളും NR-ന് പകരമായി വലിയ വ്യാവസായിക സാധ്യതകൾ കണ്ടെത്തുന്നു, ഇത് ഉയർന്ന സ്വഭാവമുള്ള സാധാരണ വ്യാവസായിക റബ്ബർ ഉൽപ്പന്നങ്ങളുടെ ഉത്പാദനത്തിന് ഗുണം ചെയ്യും

സൂചക പദങ്ങൾ: പ്രകൃതിദത്ത റബ്ബർ കോമ്പോസിറ്റുകൾ, വ്യാവസായിക പാഴ്വസ്തുക്കളുടെ പുനരുപയോഗം, മെക്കാനിക്കൽ, തെർമൽ, സോർപ്ഷൻ

CONTENTS

LIST OF FIGURES

LIST OF TABLES

LIST OF ABBREVIATIONS

ASTM	:	American Society for Testing and Materials
BET	:	Brunauer-Emmett-Teller
BJH	:	Barrett-Joyner-Halenda
CAGR	:	Compound annual growth rate
CB	:	Carbon black
CBS	:	N-Cyclohexyl-2-benzothiazolesulphenamide
CEA	:	Central Electricity Authority
CMC	:	Carboxymethyl cellulose
CNT	:	Carbon nanotube
CPCB	:	Central Pollution Control Board
CRI	:	Cure rate index
CSA	:	Calcium sulphoaluminate
DLS	:	Dynamic light scattering
DTG	:	Derivative thermogravimetry
EDX	:	Energy dispersive X-ray spectroscopy
ENR	:	Epoxidized natural rubber
EPDM	:	Ethylene propylene diene monomer
EPS	:	Expanded polystyrene
EVA	:	Ethylene vinyl acetate
FESEM	:	Field emission scanning electron microscopy
FTIR	:	Fourier Transform infrared
FWO	:	Flynn-Wall-Ozawa
HRTEM	:	High-resolution transmission electron microscopy
ISNR	:	Indian standard natural rubber
IUPAC	:	International Union of Pure and Applied Chemistry
KAS	:	Kissinger-Akahira-Sunose
LMC	:	Light magnesium carbonate

MA	:	Maleic anhydride
MCW	:	Magnesium carbonate waste
MoEF	:	Ministry of Environment and Forests
MPa	:	Megapascal
MSW	:	Municipal solid waste
Mt/year	:	Million tonnes per year
NBR	:	Nitrile butadiene rubber
N-N	:	Nicolais-Narkis
NR	:	Natural rubber
PCS	:	Photon correlation spectroscopy
PE	:	Polyethylene
PET	:	Polyethene terephthalate
phr	:	Parts per hundred
PMMA	:	Polymethyl methacrylate
PP	:	Polypropylene
PRI	:	Plasticity retention index
PU	:	Polyurethane
PUW	:	Polyurethane waste
PVC	:	Polyvinyl chloride
R & D	:	Research and Development
SBR	:	Styrene butadiene rubber
SSW	:	Sodium sulphate waste
SWM	:	Solid waste management
TGA	:	Thermogravimetric analysis
TMQ	:	2,2,4-Trimethyl-1,2-dihydroquinoline
TMTD	:	Tetramethylthiuram disulphide
TPD	:	Tons per day
T-P-T	:	Turcsányi-Pukànszky-Tüdõs
XRD	:	X-ray diffraction

LIST OF SYMBOLS

t_{90}	:	Ideal cure time
t_{s2}	:	Scorch time
M_H	:	Maximum torque
M_L	:	Minimum torque
E_a	:	Activation energy
A	:	Arrhenius frequency factor
E_D	:	Activation energy of diffusion
E_P	:	Activation energy of permeation
ΔH	:	Heat of sorption
α	:	Degree of conversion
δ	:	Hildebrand solubility parameter
Q_∞	:	Equilibrium mol %
D	:	Diffusion coefficient
S	:	Sorption coefficient
P	:	Permeation coefficient
Q_t %	:	Percentage uptake of solvents
n	:	Interaction parameter of the penetrant with the polymer
k	:	Mode of transport
B	:	Interaction parameter
R	:	Universal gas constant
β	:	Heating rate
T_i	:	Onset degradation temperature
T_{max}	:	Maximum degradation temperature

PREFACE

The use of waste materials from the footwear, condom, and pigment industries as a reinforcing filler in natural rubber (NR) to fabricate high-performance rubber composites is the subject of the thesis entitled "Mechanical, Thermal and Sorption Studies of Industrial Waste Reinforced Natural Rubber." The effect of clay on NR composites reinforced with the footwear industry waste has also been studied.

The introductory chapter emphasises the hazardous effects of industrial wastes on the environment and how crucial it is to recycle them. Nowadays, landfills handle most industrial waste disposal, which harms the environment. Various forms of solid industrial wastes and their generation, management, and treatment are covered in great detail. An exploration of the potential applications of industrial wastes and an in-depth analysis of their viability as an NR filler is studied. Details on fillers that could improve various properties of NR are provided, along with an overview of the material. A comprehensive discussion of current research on organic, inorganic, and biological wastes utilised as rubber fillers is provided. The present investigation's goals and scope are also included.

The specifications for the materials and the basic principles of the experimental techniques utilised for this investigation are provided in the Materials and Methods chapter. The features of industrial waste materials and their composite compositions with NR have been investigated. The gathered industrial wastes, clay, and fabricated NR-

waste composites were characterised using various analytical methods. The techniques for analysing the mechanical, thermal and sorption properties of NR-waste composites have been described. The tensile strength and Young's modulus of the produced composites have been verified using well-established theoretical models. TG analysis was employed to study the NR composite's non-isothermal degradation kinetics using isoconversional model-free approaches.

Chapter 3 explains the properties of various industrial wastes collected and used as fillers for reinforcement in NR. These wastes include rigid polyurethane waste (PUW) from the footwear industry, light magnesium carbonate waste (MCW) from the condom industry and recovered sodium sulphate waste (SSW) from the pigment industry. A brief explanation of the properties of clay, which is used as an additional filler along with PUW, is also included. Various analytical techniques were used to characterise the collected wastes after separating unwanted materials and powdering.

Natural rubber-polyurethane waste (NR-PUW) composites are fabricated and thoroughly characterised in Chapter 4. The assessment of the rheological, mechanical, thermal, and sorption characteristics of the NR-PUW composites was explained. The established theoretical models validated the fabricated composite's tensile strength and Young's modulus. The kinetics of the fabricated composite's non-isothermal thermal degradation were studied using different model-free isoconversional methods. Along with multiple sorption characteristics, the sorption properties of NR-PUW composites have also been investigated in different aliphatic, aromatic, and industrial solvents.

Natural rubber-magnesium carbonate waste (NR-MCW) composites were fabricated and characterised in Chapter 5. Research and descriptions have been carried out on the curing, mechanical, thermal, and sorption properties of NR-MCW composites. The thermal degradation kinetics of NR-MCW composites have been investigated using various model-free techniques. Investigations on various sorption characteristics and the sorption capabilities of NR-MCW composites in different aliphatic and aromatic solvents have been presented.

The sixth chapter describes how the natural rubber-sodium sulphate waste (NR-SSW) composite was made and characterised. The rheological, mechanical, and thermal characteristics of the generated NR-SSW composites have been examined. Model-free isocorvesional approaches were utilised to investigate the thermal breakdown kinetics of NR-SSW composites. The sorption properties of the NR-SSW composites in different solvents and various sorption parameters were studied.

Chapter 7 covers synthesising and characterising natural rubber-polyurethane waste-clay (NR-PUW-clay) compounds, and their mechanical, thermal and curing characteristics were discussed. The sorption properties of NR-PUW-clay compounds in different solvents were investigated along with different sorption parameters.

The conclusions of the reported work, recommendations for further research, and pertinent references are given at the end of the thesis.

CONTENTS

ABSTRACT

The selection of a material for a specific application is carried out by analysing the performance under different mechanical, thermal and electrical conditions for any material. In this aspect polymer composites become a unique group whose properties can be tuned in accordance with the applications. The present research work carries out an extensive study on composites of ethylene-co-vinyl acetate (EVA) with modified chitosan as fillers keeping in mind the necessity of waste to energy goal.

As an initial step towards the development of composites, modification of chitosan via graft polymerization is carried out. These modified chitosans namely, chitosan-g-PANi, chitosan-g-MMA, chitosan-g-HEMA and chitosan/phytic acid polyelectrolyte complex, were used as fillers in the polymer composites that were processed via melt-mixing. The processed polymer composites were characterized using infrared spectroscopy, mechanical and thermogravimetric analysis. The ones that comprised of chitosan-g-PANi were further explored for their dielectric properties. The thermal degradation kinetics and thermodynamic parameters were calculated for the developed materials. Non-isothermal model free methods viz, Flynn-Wall-Ozawa (FWO), Kissinger-Akahira-Sunose (KAS), Starink, Tang, Friedman (FR) and Vyazovkin were employed for the calculation. The activation energy values obtained by the differential FR method shows an increase compared to the integral methods like FWO, KAS, Starink and Tang. This is due to the lack of assumptions and approximations employed during the calculations via FR method.

The mechanical testing showed that the composites other than EVA/chitosan-g-PANi showed decrease in tensile strength with increase filler content. Samples with grafted PANi showed increased tensile strength with increase in filler concentration. The model-free kinetic methods pointed towards the endothermic nature of the degradation process progressed by the formation of activated complexes for all four systems. The study signifies the need for better understanding towards the degradation properties which will aid in developing methods in industrial scale recycling of similar materials. Further the developed materials can be investigated towards flame retardant and food packaging applications.

Keywords: EVA based composites, grafting, degradation kinetics, mechanical, dielectrics

സംഗ്രഹം

ഏതെങ്കിലും മെറ്റീരിയലിന്റെ വ്യത്യസ്ത മെക്കാനിക്കൽ, തെർമൽ, ഇലക്ട്രിക്കൽ സാഹചര്യങ്ങളിൽ പ്രകടനം വിശകലനം ചെയ്തുകൊണ്ടാണ് ഒരു നിർദ്ദിഷ്ട ആപ്ലിക്കേഷനായി ഒരു മെറ്റീരിയൽ തിരഞ്ഞെടുക്കുന്നത്. ഈ വശത്ത്, പോളിമർ കോമ്പോസിറ്റുകൾ ഒരു അദ്വിതീയ ഗ്രൂപ്പായി മാറുന്നു, അവയുടെ ഗുണവിശേഷതകൾ ആപ്ലിക്കേഷനുകൾക്ക് അനുസൃതമായി ട്യൂൺ ചെയ്യാൻ കഴിയും. ഊർജ്ജ ലക്ഷ്യത്തിലേക്കുള്ള മാലിന്യത്തിന്റെ ആവശ്യകത കണക്കിലെടുത്ത് ഫില്ലറുകളായി പരിഷ്കരിച്ച ചിറ്റോസൻ ഉപയോഗിച്ച് എഥിലീൻ-കോ-വിനൈൽ അസറ്റേറ്റ് (ഇവിഎ) സംയുക്തങ്ങളെക്കുറിച്ചുള്ള വിപുലമായ പഠനം നിലവിലെ ഗവേഷണ പ്രവർത്തനങ്ങൾ നടത്തുന്നു.

കമ്പോസിറ്റുകളുടെ വികസനത്തിലേക്കുള്ള പ്രാരംഭ ഘട്ടമെന്ന നിലയിൽ, ഗ്രാഫ്റ്റ് പോളിമറൈസേഷൻ വഴി ചിറ്റോസന്റെ പരിഷ്കരണം നടത്തുന്നു. ചിറ്റോസാൻ-ജി-പാനി, ചിറ്റോസാൻ-ജി-എംഎംഎ, ചിറ്റോസാൻ-ജി-ഹീമ, ചിറ്റോസാൻ/ഫൈറ്റിക് ആസിഡ് പോളി ഇലക്ട്രോലൈറ്റ് കോംപ്ലക്സ് എന്നിങ്ങനെയുള്ള പരിഷ്കരിച്ച ഈ ചിറ്റോസാനുകൾ, മെൽറ്റ്-മിക്സിംഗ് വഴി സംസ്കരിച്ച പോളിമർ കോമ്പോസിറ്റുകളിൽ ഫില്ലറുകളായി ഉപയോഗിച്ചു. ഇൻഫ്രാറെഡ് സ്പെക്ട്രോസ്കോപ്പി, മെക്കാനിക്കൽ, തെർമോഗ്രാവിമെട്രിക് വിശകലനം എന്നിവ ഉപയോഗിച്ചാണ് പ്രോസസ്സ് ചെയ്ത പോളിമർ കോമ്പോസിറ്റുകളുടെ സവിശേഷത. ചിറ്റോസാൻ-ജി-പാനി അടങ്ങിയവ അവയുടെ വൈദ്യുത ഗുണങ്ങൾക്കായി കൂടുതൽ പര്യവേക്ഷണം ചെയ്തു. വികസിപ്പിച്ച മെറ്റീരിയലുകൾക്കായി താപ ഡീഗ്രേഡേഷൻ ചലനാത്മകതയും തെർമോഡൈനാമിക് പാരാമീറ്ററുകളും കണക്കാക്കി. ഫ്ലിൻ-വാൾ-ഒസാവ (എഫ്ഡബ്ല്യുഒ), കിസിംഗർ-അകാഹിറ-സുനോസ് (കെഎഎസ്), സ്റ്റാറിങ്ക്, ടാങ്, ഫ്രീഡ്മാൻ (എഫ്ആർ), വ്യാസോവ്കിൻ എന്നീ നോൺ-ഐസോതെർമൽ മോഡൽ ഫ്രീ രീതികളാണ് കണക്കുകൂട്ടലിനായി ഉപയോഗിച്ചത്. എഫ്ഡബ്ല്യുഒ, കെഎഎസ്, സ്റ്റാറിങ്ക്, ടാങ് തുടങ്ങിയ അവിഭാജ്യ രീതികളുമായി താരതമ്യപ്പെടുത്തുമ്പോൾ ഡിഫറൻഷ്യൽ എഫ്ആർ രീതിയിലൂടെ ലഭിക്കുന്ന ആക്റ്റിവേഷൻ എനർജി മൂല്യങ്ങൾ വർദ്ധനവ് കാണിക്കുന്നു. എഫ്ആർ രീതിയിലൂടെയുള്ള കണക്കുകൂട്ടലുകളുടെ സമയത്ത് ഉപയോഗിച്ച അനുമാനങ്ങളുടെയും ഏകദേശങ്ങളുടെയും അഭാവമാണ് ഇതിന് കാരണം.

മെക്കാനിക്കൽ പരിശോധനയിൽ EVA/chitosan-g-PANi ഒഴികെയുള്ള സംയുക്തങ്ങൾ ഫില്ലർ ഉള്ളടക്കം വർദ്ധിപ്പിക്കുന്നതിനനുസരിച്ച് ടെൻസൈൽ ശക്തി കുറയുന്നതായി കാണിച്ചു. ഗ്രാഫ്റ്റ് ചെയ്ത പാനി ഉപയോഗിച്ചുള്ള സാമ്പിളുകൾ ഫില്ലർ കോൺസൺട്രേഷൻ വർദ്ധിപ്പിച്ചുകൊണ്ട് വർദ്ധിച്ച ടെൻസൈൽ ശക്തി കാണിച്ചു. നാല് സിസ്റ്റങ്ങൾക്കുമായി സജീവമാക്കിയ കോംപ്ലക്സുകളുടെ രൂപീകരണത്തിലൂടെ പുരോഗമിച്ച ഡീഗ്രഡേഷൻ പ്രക്രിയയുടെ എൻഡോതെർമിക് സ്വഭാവത്തിലേക്ക് ചൂണ്ടിക്കാണിച്ച മോഡൽ രഹിത ചലനാത്മക രീതികൾ. സമാന വസ്തുക്കളുടെ വ്യാവസായിക തലത്തിൽ പുനരുപയോഗം ചെയ്യുന്നതിനുള്ള രീതികൾ വികസിപ്പിക്കുന്നതിന് സഹായിക്കുന്ന ഡീഗ്രേഡേഷൻ പ്രോപ്പർട്ടികളെ കുറിച്ച് നന്നായി മനസ്സിലാക്കേണ്ടതിന്റെ ആവശ്യകതയെ പഠനം സൂചിപ്പിക്കുന്നു. കൂടുതൽ വികസിപ്പിച്ച വസ്തുക്കൾ ഫ്ലെം റിട്ടാർഡന്റ്, ഫുഡ് പാക്കേജിംഗ് ആപ്ലിക്കേഷനുകൾ എന്നിവയിലേക്ക് അന്വേഷിക്കാവുന്നതാണ്.

സൂചകപദങ്ങൾ: EVA അടിസ്ഥാനമാക്കിയുള്ള സംയുക്തങ്ങൾ, ഗ്രാഫ്റ്റിംഗ്, ഡീഗ്രേഡേഷൻ കൈനറ്റിക്സ്, മെക്കാനിക്കൽ, ഡൈഇലക്ട്രിക്സ്

Chapter 1
Introduction

This chapter discusses the need to recycle industrial wastes as they seriously harm the environment. The majority of industrial waste is currently dumped in landfills, which harms the ecosystem. The generation, handling, and treatment of various industrial solid wastes are covered in detail. A complete discussion on the possibility of using industrial solid waste as a filler in different rubbers is included, and an inquiry into their potential for reuse is explained. A description of natural rubber and information on fillers that could improve various properties of natural rubber is provided. Recent research on the use of biological, inorganic, and organic wastes as fillers in rubber is detailed. Additionally, the current study's scope and objectives are mentioned.

The presence of fundamental elements for survival, like air, water, and soil, on the earth makes it unique from all other planets in the solar system. But environmental pollution is a serious issue and one of the most critical problems currently affecting humanity and all other life forms on our planet today. Nine million individuals (one in every six fatalities) died in 2019 due to the effects of pollution, which has been constant since 2015 (1). The term "environmental pollution" refers to the physical and biological components of the earth and atmosphere becoming contaminated to the point where it interferes with regular environmental processes. While developing nations grapple with serious, unique, and swiftly escalating pollution problems, developed countries are becoming more and more concerned about environmental issues worldwide. Foreign and domestic companies acting with little concern for the impact on the local environment exacerbate the influential combination of industrialisation, urban development, and high consumption trends (2,3). Environmental pollution is more of a social issue than a health one because it can damage homes and communities (4). The way that developing nations develop has a direct impact on pollution issues. Despite this, many developing nations lack the infrastructure for effective policy implementation or the capacity to design environmental pollution control measures. The economic progress of a country goes hand in hand with industrial development. It can supply the items that citizens need and improve their financial well-being. The distribution of the industry's growth will significantly impact how society develops in the future. Additionally, the industry is a

substantial user of natural resources and an essential pollution producer.

The adoption of liberalisation policies in India in 1991 made it easier than ever for private and foreign capital and technology to enter the industrial sector. India was able to establish a robust and diverse industrial structure as a result, placing our nation among emerging economies. Managing various industrial wastes substantially threatens the living system, which is a significant problem in India (5). The risks that various industrial pollutants offer to living systems regarding their negative impacts and possible hazards are growing daily. In India, unregulated imports, illegal dumping sites, and insufficient information on the production and disposal of hazardous waste are the main issues related to industrial waste. For effective management and handling of dangerous wastes in the nation, the Ministry of Environment and Forests (MoEF) issued the Hazardous Waste (Management & Handling) Rules, 1989, which were subsequently revised in 2000, 2003, and 2016 (6).

1.1. Solid waste

Solid wastes are undesirable or pointless byproducts of human activity, ranging from industrial waste to municipal garbage, and some may contain complicated and dangerous compounds. Figure 1.1 shows the main categories of solid waste.

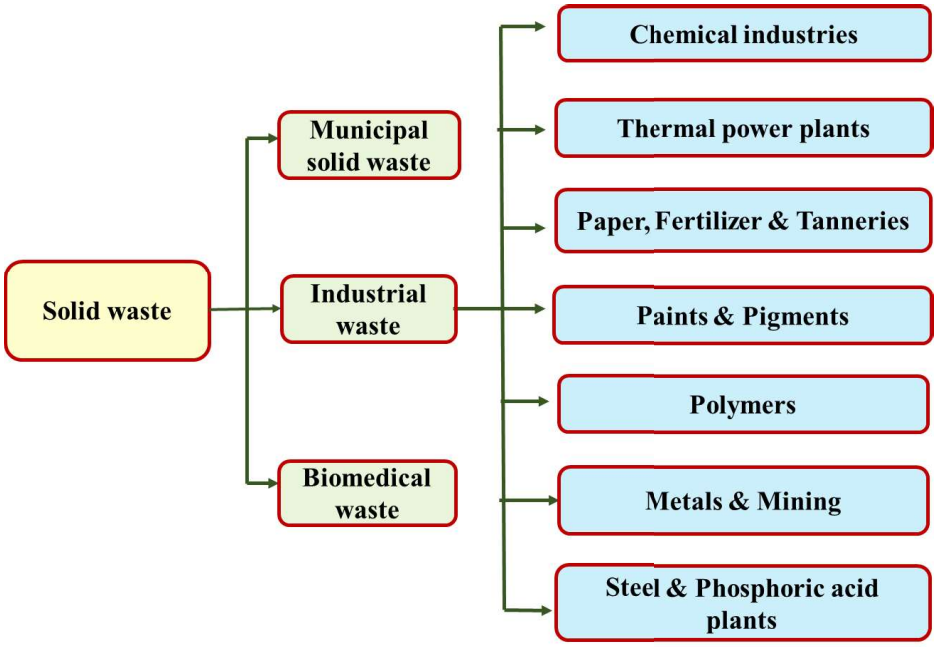

Figure 1.1. Major classification of solid waste

The total amount of solid waste produced in India is 160038.9 metric tonnes per day (TPD), of which 152749.5 TPD is collected with a 95.4 % collection efficiency. 79956.3 TPD of solid waste is processed at 50 %, 29427.2 TPD is landfilled at 18.4 % and 31.7 % of the waste produced, or 50655.4 TPD, remains unaccounted for (7). Maharashtra, Uttar Pradesh, West Bengal, Gujarat, and Delhi's National capital territory produce approximately half of the nation's solid waste out of India's twenty-eight states and eight union territories. Figure 1.2 shows India's solid waste generation trend by the states in TPD (8).

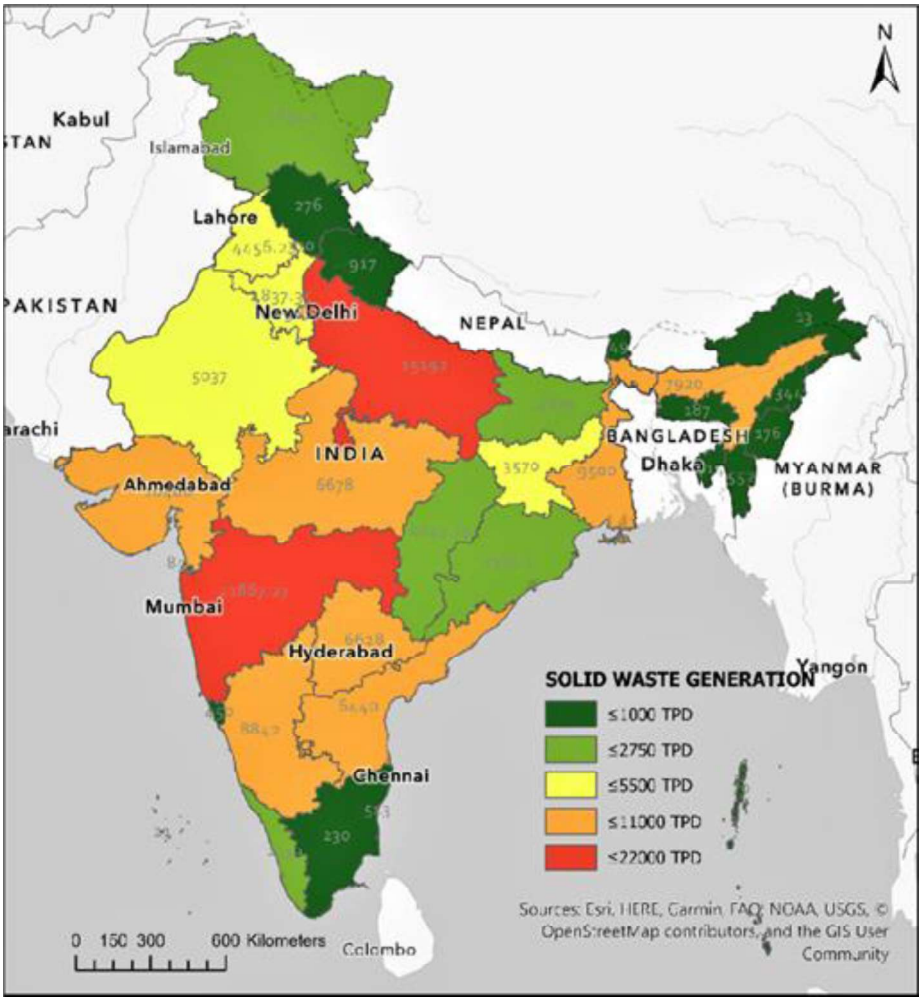

Figure 1.2. State-wise solid waste generation in India

1.1.1. Municipal solid waste

Municipal solid waste (MSW), commonly known as garbage or trash, comprises the everyday materials we use and discard, including clothing, furniture, newspapers, bottles, product packaging, paint, grass clippings, food scraps, appliances, and batteries. Our workplaces, schools, hospitals, and residences generate MSW and its production is projected to rise from an estimated 2.01 billion tonnes in 2016 to 3.40

billion by 2050 (9). East Asia and the Pacific are projected to have produced 468 million tonnes of MSW. In contrast, the Middle East and North Africa made the least amount in 2016 at 129 million tonnes. MSW is produced globally at a rate of 1.2 kg per person per day, or 1300 million tonnes per year (Mt/year). By 2025, this enormous amount of MSW is expected to increase to 2200 Mt/year, and managing this massive volume of MSW poses a severe threat to the sustainability of the environment (10). The production of MSW causes significant ecological pollution, primarily due to the emission of gases that contribute to the greenhouse effect, such as methane and carbon dioxide, as well as the high proportion of organic materials that make up solid waste and their frequently improper disposal. Municipal administrations are under pressure to create more effective techno-economic and political solutions to manage the expanding amounts of MSW due to this environmental danger (11). An overview of the global MSW generation is given in Figure 1.3 (12).

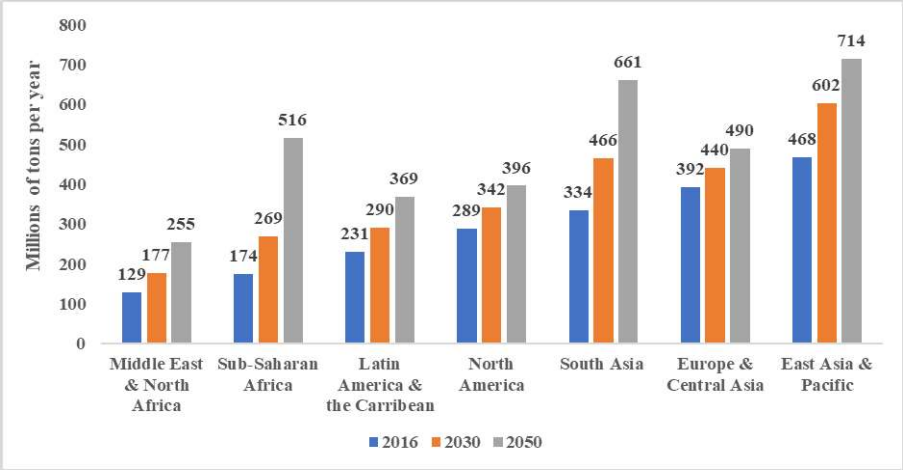

Figure 1.3. Forecast of global MSW generation

There are 377 million people living in metropolitan areas in India, and they produce an estimated 55 million tonnes of MSW each year. India's urban population is expected to increase to 600 million by 2030 and 814 million by 2050. So, by 2030, India is expected to produce 165 million tonnes of MSW, and by 2050, 436 million tonnes. By 2030, MSW is anticipated to emit 41.09 million tonnes of greenhouse gases annually (13). India's massive population generates 0.15 million tonnes of MSW daily, of which 0.14 million tonnes (or 90 %) are collected (14).

1.1.2. Biomedical waste

Any waste produced during people's or animal's diagnosis, treatment, or immunisation might be considered biomedical waste (15). This waste could include potentially dangerous elements, including infectious agents, sharps, chemical or radioactive compounds, or other medical wastes that, if managed improperly, could endanger the environment and public health. Sharps, pathological, infectious, and chemical wastes are a few categories that need to be separated for effective biomedical waste management. After that, waste is gathered, transported, and stored as per the rules and regulations. Before the waste is disposed of in a way that minimises hazards to human health and the environment, it is treated using techniques like burning, autoclaving, or chemical disinfection.

1.1.3. Major industrial solid wastes in India

The industrial sector's rapid expansion in India is to blame for much of the waste produced today. The following industrial solid

wastes are considered a massive threat to the environment in India. The primary industrial solid wastes produced in India are lime from the pulp and paper industries, gypsum from the fertiliser and related industries, red mud from the aluminium, zinc, and copper industries, blast furnace slag and steel melting slag from integrated iron and steel mills, and coal ash from thermal power plants. These are briefly explained below.

1.1.3.1. Coal ash

The tiny powder particles left behind from burning coal and heavier elements settling to the furnace's bottom are considered as coal ash. India's thermal power plants that burn coal produce an average of 200 million metric tonnes of ash annually, which has been gradually rising. By 2032, this number will reach 600 million (16). The Central Electricity Authority's (CEA) most recent estimates indicate that Indian power plants produced 217.04 million metric tonnes of ash in 2018-19 based on information from 195 thermal power units (17). Such enormous amounts of ash provide management difficulties for plant managers and several public health issues for the local people surrounding the ash disposal sites. The usual disposal of ash as slurry currently uses roughly 40,000 hectares of land, just in terms of land use.

1.1.3.2. Integrated iron and steel plant slag

During various phases of metallurgical processes, steel factories produce enormous amounts of waste materials. These include tar sludge, blast furnace slag, Linz-Donawitz (LD) slag, coke bridge,

and blast furnace flue dust. The source of production, raw material quality, and metallurgical processes all significantly impact the composition of these materials (18). Waste from steel plants is often disposed of in landfills, which harms the environment.

1.1.3.3. Red mud

One of the top ten mineral producing nations in the world is India. Commercial production of aluminium metal from bauxite ore consists mainly of two processes. The Bayer process first produces alumina, and then in the second stage, aluminium metal is produced by electrolysing the alumina in the Hall-Heroult cell. However, the extraction of alumina from bauxite is linked to significant environmental issues (19). The primary waste product is red mud or bauxite residue, and depending on the bauxite's quality, between 55 and 65 % of the bauxite processed is turned into red mud. Around the world, red mud is disposed of on land or in the neighbouring sea or ocean. The nearby water, land, and air are all harmed by its high alkalinity. The Central Pollution Control Board (CPCB) of India provided the report, which states that the yearly production of red mud worldwide is 140 million tonnes, with 75-80 % of that amount being produced in Australia and China, and that India generates about 9 million tonnes of it annually (20).

1.1.3.4. Lime mud

Lime mud is produced as waste in pulp and paper mills since calcium oxide cannot be recovered due to the high silica concentration (21). When lime mud is disposed of, it is frequently dumped into low-

lying areas, into water supplies directly, or as run-off during the monsoon, endangering the ecosystem severely.

1.1.3.5. Phosphogypsum

Phosphogypsum is a byproduct of the fertiliser industry during the production of phosphoric acid. About 12 million tonnes of phosphogypsum are produced annually in India. Only around 40-50 % of it is reused in the production of cement, fertiliser for farming, gypsum board, etc. The remaining phosphogypsum is disposed of as landfill and deposited in water streams in slurry form, which pollutes the environment (22).

1.1.3.6. Polymer waste

One of the industries with the quickest growth rate, polymer production contributes to the Indian economy at an annual growth rate of 18 %. More than 4 million people work in the polymer manufacturing industry. India's plastic consumption is expected to reach 20.89 million tonnes in 2021-22 and 22 million tonnes by 2023; therefore, the sector needs to implement circular economy concepts to reduce waste and pollution and provide new chances for growth and innovation. With packaging materials accounting for a sizable portion of the plastic trash produced, India is the second-largest user of plastic in the world. Approximately 9.46 million metric tonnes of plastic garbage are produced in the nation each year, but only 60 % of that amount is recycled, according to a report by the CPCB (23). The residual wastes frequently wind up in rivers, seas, and landfills, harming the ecosystem and marine life. There are serious repercussions

from this widespread plastic pollution, including harm to human health and the ecosystem.

In addition to these significant industrial wastes, footwear manufacturing generates substantial amounts of rigid polyurethane (PU) waste during sole production. The condom manufacturing industry uses massive quantities of light magnesium carbonate as a finishing powder and is discarded after use. The pigment industries produce enormous amounts of sodium sulphate during production processes. Waste like chrome shavings, buffing dust, and keratin waste from the leather sector are also to be considered (24). All the abovementioned industrial wastes are disposed of in landfills, which causes soil, water, and air pollution to affect the living system significantly. It is high time to introduce technologies to effectively and safely remove and reutilise these industrial wastes, emphasising the circular economy approach.

1.2. Current solid waste management methods in India

The management of solid waste is a significant issue in India due to the country's rapid urbanisation, industrialisation, and economic development (25). Waste management involves separating waste at the source and using specialised facilities for waste processing to separate recyclable elements. The best waste management systems offer a tailored and organised processing of materials that maximises resource recovery from waste (26,27). An adequate system should minimise the initial production of materials through source reduction, followed by reusing and recovering to reduce the number of materials compared to

the traditional disposal method, symbolised by the four Rs as stated below in Figure 1.4.

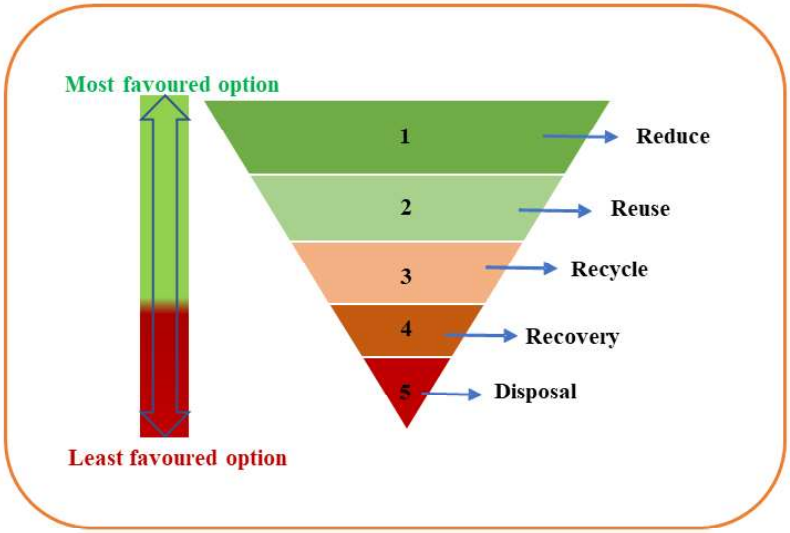

Figure 1.4. Hierarchy of waste management

- The most popular option, reduce, calls for reducing the waste we produce by consuming less plastic.
- The second choice is reuse, which entails utilising items more than once to conserve resources, energy, and money.
- The next item on the list is recycling, which involves transforming garbage into fresh goods.
- After the reduce, reuse, and recycle procedures have been optimised, recovery takes place. The final option is disposal; however, this is the least favoured option and the last resort.

The significant steps involved in solid waste management (SWM) are as follows:

1.2.1. Collection and transport of waste

Regular collections of industrial solid waste should be made, and current techniques should be used to load it onto packer or container trucks before transporting it manually or mechanically. The garbage is compressed to a high density at the collection centres before being transferred to the disposal locations.

1.2.2. Incineration

In essence, burning industrial waste involves oxidising any combustible components that may be present. Waste is a heterogeneous mass comprising water, minerals, metals, and organic substances. Industrial waste incineration releases air pollutants, particularly fine particles and hazardous gases, which are harmful to the environment and must be controlled. Other issues with incineration include the challenge of ash disposal in landfills due to heavy metal residues and the removal of liquid waste from floor drainage, quench water, scrubber effluents, and other liquid wastes.

1.2.3. Landfill

The most economical and popular way for many nations to dispose of their solid waste is through landfilling. Town dumps were once typically used in low-lying locations close to water sources. The consequences of this dirty dumping included water contamination, unpleasant smell, fire, insects, rats, etc. Nowadays, sanitary landfilling is used, which calls for the selection of dumping sites using science, controlled deposition, improved compaction techniques, leachate collection to stop water contamination, and site monitoring to prevent environmental pollution.

1.2.4. Composting

Composting is a controlled environmental process that involves the microbial bio-oxidation of biodegradable organic materials. After a brief thermophilic stage brought on by oxidation, there is a cooling phase during which deteriorated organic matter forms. After being allowed to mature at room temperature, this material becomes a stable, humus-like substance called compost that has preserved the mineral ingredients good for soil and plants. However, this method is limited to the management of biodegradable industrial wastes.

1.2.5. Recycling

Recycling is reprocessing the disposed waste material into a valuable product. Recyclability is the capacity of a substance to regain the characteristics that it possessed when it was first created. It promotes environmental sustainability by keeping raw material inputs out of the economy and rerouting waste produced from it.

1.3. Reutilisation of industrial waste

Intensive Research and Development (R&D) efforts have been focused on finding compatible and cost-effective remedies for waste minimisation and its utilisation today (28). Recent SWM strategies include newer or re-engineered processes that decrease toxic emissions, maximise current levels of waste utilisation, and develop high-value products. Recently, synergistic usage of solid waste from various industries with different compounds to produce value-added products has also been gaining momentum. Table 1.1 briefly explains various researcher's attempts on utilising different industrial wastes.

Table 1.1. List of recent literature on the reutilisation of industrial waste

Sl. No.	Source of waste	Area of application	Findings & benefits of reutilisation	Reference
1.	Ethylene vinyl acetate (EVA) from the footwear industry and construction/demolition waste (CDW)	Preparation of lightweight concrete	➢ The concrete with 50 % EVA showed an increase in material toughness. ➢ It is suggested that lightweight concrete can be produced using EVA waste and CDW.	Lima *et al.* (29)
2.	Ilmenite red mud waste (RMUD) from the production of TiO_2	Additive to concrete	➢ The density and slump loss of RMUD concrete and fly ash (FA) concrete are comparable. ➢ Water absorbability and permeability of both concretes are nearly the same. ➢ Shrinkage during 360 days was almost the same for both.	Chylinski *et al.* (30)
3.	Soda sludge, calcium sulphate, fly ash with lime, and fly ash	Fillers in asphalt mixtures	➢ Improved adhesion between the bitumen and fillers was noticed. ➢ Asphalt with higher water resistance and durability was obtained.	Dimulescu *et al.* (31)

4.	Waste plastic bags	Replacing cement in the production of building bricks and concrete blocks.	➢ The flexural test demonstrated that as the plastic component in the bricks and concrete blocks grew, so did the bending moment and, consequently, the bending stress.	Hassanien *et al.* (32)
5.	Waste from steel, paper, pulp and galvanising industries	Reutilisation in steel production and their repolymerisation potential	➢ Can act as a replacement for fly ash in geopolymers ➢ Geopolymers-rich waste showed more compressive strength and similar workability	Kumar *et al.* (33)
6.	Waste glass powder (GP) from bottles and window panes	Converted to glass hydrated lime (GL) and used as fillers in asphalt pavements	➢ At lower optimal asphalt content, GL-GP mixes demonstrated superior resilience against fatigue, rutting, and low-temperature cracking. ➢ The usage of 74 tonnes of GP, GL and GP fillers decreased the material cost and potential for global warming by up to 35 %.	Choudhary *et al.* (34)
7.	Phosphogypsum waste from chemical industries	Replacement of cement in concrete	➢ Partial replacement of cement with 10 %, 20 % and 30 % phosphogypsum waste in concrete is proposed. ➢ The prepared concrete is suitable for lying rigid pavement.	Prathap *et al.* (35)

8.	Silica fume, sugarcane ash, and fly ash	Partial replacement of conventional cement.	➢ There was a drop in strength attributes such as split tensile strength, modulus of rupture, and compressive strength. ➢ Reduction in construction cost and CO_2 emission	Debbarma *et al.* (36)
9.	Carbon dust waste from aluminium factories	Production of cement mortar	➢ The compressive strength of the mortar was improved by partially substituting carbon dust (5 and 10 %) for cement. ➢ Carbon dust integration resulted in the creation of a more dense and compact structure.	Irshidat *et al*. (37)
10.	Marble dust waste, desulphurisation gypsum, flue gas ceramics dust waste, and Napier grass ash.	Production of calcium sulphoaluminate (CSA) cement	➢ Shorter initial and final setting times were noticed. ➢ When conventional Portland cement is mixed with 20–40 wt. % CSA cement, rapid setting and great early strength are attained.	Julphunthong *et al.* (38)

1.4. Composites

Composites are hybrid materials that consist of two components: a matrix, which is a continuous phase, and a reinforcement or filler, which is a discontinuous phase with variable properties. These two components create a material with distinct qualities (39). Figure 1.5 provides the classification of composites based on matrix and dispersed phase characteristics.

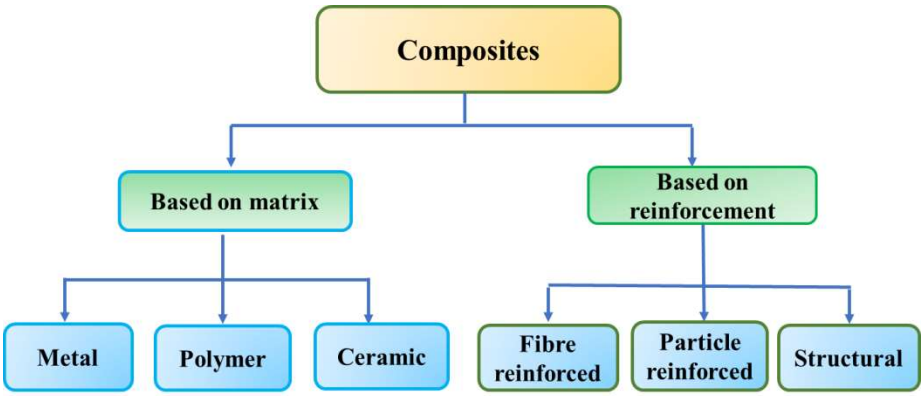

Figure 1.5. Classification of composites

The increased mechanical, thermal, optical, and solvent absorption resistance of polymer matrix composites make them increasingly popular despite the availability of numerous metal and ceramic-based composites. The fillers used in the polymer matrix, which are reinforcing materials, provide high strength and stiffness.

1.5. Natural rubber as matrix

When fabricating composite materials, elastomers with distinctive properties, including stiffness, low density, strength, and simplicity of processing, are frequently used as a matrix. Elastomers

often have an amorphous structure, considerable molecular weight, and weak intermolecular forces. High toughness, good tensile strength, and exceptional elongation at break can all be found in an elastomeric matrix. These matrices are frequently used in the wire, cable, space, automotive, and sports industries.

Natural rubber (NR), one of the most important elastomers for human society, is an essential raw resource that goes into the production of over 40,000 distinct products. NR is extensively used in various fields like automobile, consumer goods, healthcare, construction, electrical, marine, agriculture, fashion and apparel, adhesives and coatings, etc. (40). NR is made from latex, a milky fluid generated by many plants that contains proteins, carbohydrates, alkaloids, etc. Hevea brasiliensis, the rubber tree, is the principal source of NR latex. NR comprises viscoelastic cis-1-4 polyisoprene units with a high molecular weight. NR's chemical composition in polymer matrix composites is more common despite the availability of many metal and ceramic-based composites due to their enhanced mechanical, thermal, optical, and solvent absorption resistance. A polymer matrix loaded with reinforcing components gives the matrix high strength and stiffness. Figure 1.6 illustrates NR's chemical structure.

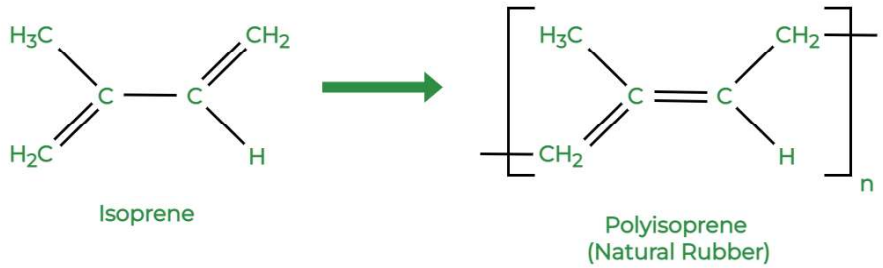

Figure 1.6. NR's chemical structure

1.6. Fillers

In addition to curatives, the rubber may contain certain compounds known as fillers to satisfy particular industrial specifications. The primary goals of adding fillers to rubber are to increase processability, improve reinforcement, and make it more affordable. Particulate fillers, hybrid fillers, fibrous fillers, and laminates are the four main categories for fillers. In general, filler materials are stiffer than the matrix, and the extent to which they can improve a material's properties relies on the nature of the material, its shape, and whether it is reinforcing or not. The classification of fillers is displayed in Figure 1.7.

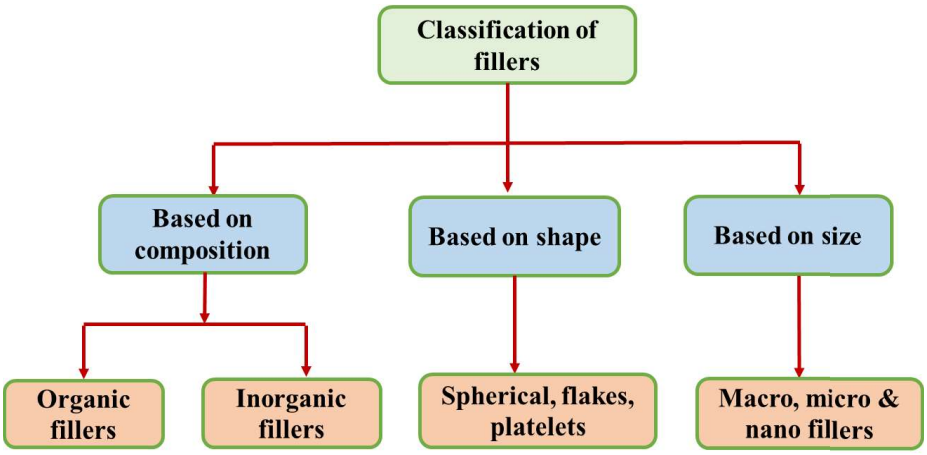

Figure 1.7. Classification of fillers

1.7. Natural rubber composites

NR-based composites have a wide range of industrial uses in many different industries, including the manufacture of shoes, tyres, sporting goods, hoses, glues, belts, gaskets, etc. In order to improve

mechanical qualities significantly, vulcanisation is the most important step in the rubber industry (41). NR is mixed with curing ingredients during vulcanisation, including accelerator, crosslinking agent, activator, etc. To fulfil the demands of the industry today, NR composites with curing chemicals alone are insufficient. The neat rubber is given a boost in several qualities by adding fillers, which are insoluble foreign substances (42). Particle size, shape, aspect ratio, and specific surface area of the filler all influence the rubber-filler composite's improved properties (43). In the past, silica and carbon black were frequently utilised as fillers to reinforce NR (44,45). However, the downside of these fillers is that they cause the formation of aggregates in the rubber matrix (46). This defect is rectified by adding nano and hybrid fillers with a highly specific surface area, and the mechanical characteristics of rubber composites are improved by strengthening the bond between the rubber and the filler (47,48). Rubber-filler compatibility is a crucial factor for homogenous filler dispersion on the matrix, which results in superior performance. However, most fillers do not have this advantage, primarily because filler and rubber have different polarities (47). The rubber industry now encounters the abovementioned problems while making high-performance NR-filler composites.

1.8. Reutilisation of industrial waste as fillers in rubber

Urbanisation and industrial growth produce vast quantities of waste, and it is now in the national interest to recycle these materials effectively. In developed nations today, the adoption of green chemistry guidelines and the notion of global economic sustainability

is growing in popularity (49). Therefore, sustainable development aims to manage these industrial wastes in an eco-friendly manner so that new materials can be designed for additional applications (50). Numerous attempts have been made to create unique, sustainable composites to recycle and repurpose waste materials as fillers in rubber. A thorough examination of the possibilities for repurposing industrial waste from different categories may be found below.

1.8.1. Organic/ Carbon based fillers

The mechanical properties of polymer materials are enhanced by introducing powdered organic fillers. Carbon-based rubber composites are made from a proper combination of the rubber matrix and organic fillers produced by appropriate processing techniques (34). The hydrodynamic interactions between the rubber and nanofiller surfaces are the primary factor enhancing the carbon nanofiller's reinforcing effect (51). The reports on reusing organic or carbon-based, inorganic, and bio-material waste from various sectors are given in Tables 1.2. to 1.4.

Table 1.2. Literature on recycling industrial waste with carbon content

Sl. No.	Source of waste	Area of application	Findings & benefits of reutilisation	Reference
1.	Expanded polystyrene (EPS) waste from S-tech Thermocool industry	NR with grafted maleic anhydride (MA).	➢ NR/EPS blends have low torque, higher scorch & cure time with silica-filled NR. ➢ Tensile strength with 1 % MA is enhanced by 14 %, modulus at 300 % by 26 %, and tear strength by 28 %.	Sekharan *et al.* (52)
2.	Recycled carbon black (RCB) from waste tyre	NR	➢ RCB modified with H_2O_2 was used to replace CB in NR. ➢ RCB increases the torque and crosslink density of the composites. ➢ Tensile strength, elongation at break, abrasion resistance, ageing resistance, and heat build-up were increased.	Dwivedi *et al.* (53)
3.	Ground tyre rubber (GTR) from water jet milling	Blends of waste high-density polyethene (w-HDPE) and GTR	➢ Improvement in impact strength is noticed for GTR content by up to 30 %. ➢ Impact strength is improved from 17 % to 28 % using maleic anhydride as a compatibilizer. ➢ The use of additives achieves improved properties.	Simon *et al.* (54)
4.	Polymeric waste from the cable industry	Polyethylene (PE) by rotational moulding	➢ Cable waste contains several polymeric fractions, PE, polyvinyl chloride (PVC), etc. ➢ About 35 % of waste can be incorporated without a reduction in mechanical properties.	Diaz *et al.* (55)

5.	Waste Polyamide (w-PA) from scrap tyres and waste polyethene terephthalate (w-PET)	Preparation of polyamide-glass fibre composites and w-PA/w-PET blends	➢ 5 % glass fibre doubled the impact resistance of composites. ➢ Incorporating 15 % glass fibre enhanced the tensile, elongation, and Young's modulus. ➢ w-PA/ w-PET blends with 75 % PET and 25 % PA showed higher impact resistance.	Ferreira *et al.* (56)
6.	Recycled PET (r-PET) flakes from PET bottle waste	Production of r-PET textile fibres	➢ r-PET fibre has lower tensile strength than virgin PET fibres (v-PET). ➢ Compared to v-PET, r-PET raw materials resulted in more uneven yarn. ➢ r-PET samples had slightly higher hairiness values for ring-spun yarns than v-PET samples.	Sarioglu *et al.* (57)
7.	Pyrolysis of epoxy-based polymer composite waste	Recovery of carbon fibres for reuse.	➢ Free carbon fibres from the polymer matrix are obtained by pyrolysis at 550 °C for 1 hour. ➢ The fibres had no pores, material fracture and carbonisation.	Abdou *et al.* (58)
8.	Polypropylene (PP) waste from the textile industry	Styrene-butadiene rubber (SBR)	➢ Waste PP fibre and powder replace carbon black partially. ➢ 1 phr PP fibre containing SBR showed the highest maximum torque and increased hardness, whereas elongation at break decreased.	Pajtasova *et al.* (59)
9.	Waste PU from the refrigeration industry	SBR/NR	➢ Composites have a high plastic strength but a poor elastic strength. ➢ Using the Lorenz- Park Equation, the filled composites showed values over 0.7, suggesting a significant filler–rubber interaction.	Hiranobe *et al.* (60)

10.	PU waste after glycolysis	NR/CB	➢ High M_L and t_{90} values for the rubber mix plasticised using polyurethane glycolysate. ➢ After accelerated thermal ageing (70 °C, air, 7 and 14 days), the NR/CB composites made with glycolysate had higher hardness and tensile strength than comparable vulcanizates made using naphthenic oil.	Wloch *et al.* (61)
11.	Waste polyvinyl chloride (PVC)	Preparation of novel substrate with super absorbent resin (SAR)	➢ The interfacial adhesion between PVC and SAR is improved by modification. ➢ The substrate showed increases in tensile strength, elongation at break, and compression strength of 84 %, 52 %, and 6.4 %, respectively. ➢ The prepared substrate exhibited good reusability and plant cultivation capacity.	Zhang *et al.* (62)
12.	Recycled PET waste (R-PET)	NR/ Epoxidized NR (ENR)	➢ Cure time and torque values were increased with PET loading for NR compared to ENR. ➢ The crosslink density of both NR and ENR increased with PET content. ➢ Thermogravimetric analysis (TGA) proved the enhancement in thermal stability by incorporating PET in both compounds.	Nabil *et al.* (63)
13.	Chloroprene rubber waste (CRW) from rejected gloves	NR blends	➢ CRW, CB, silica, and $CaCO_3$ were added to NR as fillers.	Hayeemasae *et al.* (64)

			➢ NR-CRW blends showed a faster curing rate on adding CB and $CaCO_3$. ➢ Silica-filled NR-CRW blends showed higher tensile strength.	
14.	Waste rubber to replace original rubber in NR mix	NR	➢ Replacing 10-30 % gum rubber with waste filler does not alter the desired properties. ➢ An increase in the abrasion resistance of the composite was noticed.	Yehia *et al.*(65)
15.	Modified ground tyre rubber (GTR) by microwave irradiation	NR	➢ Enhanced tensile strength and crosslink density of the GTR-NR composite were reported. ➢ The addition of GTR increased the thermal stability.	Colom *et al.* (66)

1.8.2. Inorganic fillers

Inorganic fillers improve rubber blend's interfacial interactions, thereby thermal and mechanical properties by stabilising their interfaces. Multi-functional inorganic fillers include silica, $CaCO_3$, clay, zeolite, and organoclay as inorganic compatibilizers (67,68). Due to the strong interactions between the rubber and filler phases, silica is among the most widely used fillers (69). Prospective replacements for these materials, including organo-montmorillonite, mica, bio-based fibres, and biochar, have been researched for better performance (70,71). For instance, mica-based fillers are now employed in elastomers and various general applications such as plastic components, adhesives, etc. (72).

1.8.3. Bio-fillers

As a result of environmental concerns, bio-fillers, also known as natural fillers, are being employed more frequently to create different polymer composites. Compared to synthetic fillers like CB, silica, graphene, carbon nanotube (CNT), and carbon nanofiber, bio-fillers have the advantages of being renewable, abundant, and inexpensive (73,74). Additionally, bio-fillers have various benefits, including low density, sustainability, and reduced manufacturing energy usage (75). Bio-fillers made from plant fibres are less compatible with rubber matrices since they are hydrophilic (76).

Table 1.3. Scholarly works on the reuse of inorganic industrial waste as fillers

Sl. No.	Filler	Matrix	Findings	Reference
1.	Silica fume waste from the zirconia industry	NR	➢ Composite with 20 phr silica waste increased the tensile strength (12 %), modulus (107 %), and tear strength (28 %) with NR gum. ➢ Hybrid filler with silane coupling agent increased the thermal stability by 6 °C.	Dileep *et al.* (77)
2.	Marble and granite dust from cutting industry	PP	➢ The addition of dust to the PP reduces the crystallinity of the composites. ➢ The thermal resistance of the composites is considerably improved. ➢ The density and water absorption of the composites increased with filler loading.	Awad *et al*. (78)
3.	Grit waste from the cellulose industry	NR	➢ Hardness is increased with an increase in the filler, while abrasion loss decreases up to 10 phr loading. ➢ Stress reinforcement is more	Dognani *et al.* (79)

			significant for treated waste (20 phr loading).	
4.	Foundry waste (FW) modified with the silane coupling agent	NR	➢ Composition of FW is 72 % SiO_2, 12 % Al_2O_3, and 3.7 % CaO ➢ Modified FW increases torque and decreases T_{90}. ➢ The tear strength of modified FW is increased by 21 %. ➢ Hardness and modulus are higher than the neat matrix.	Xie *et al.* (80)
5.	Gypsum waste (GW) from the ceramic industry	ENR	➢ Cure studies revealed that torque increases with filler content. ➢ The tensile strength of the GW-ENR composite showed an increase of up to 10 phr GW. ➢ Hardness and modulus showed a progressive increase. ➢ TGA showed a slight enhancement in thermal stability by adding GW to ENR.	Roy *et al.* (81)
6.	Ferrous waste byproducts from the metallurgical industry	Products applied in water and wastewater decontamination	➢ It has a high potential for valorisation in the circular economy context. ➢ It can be transformed into high-	Matei *et al.* (82)

			quality goods for environmental restoration.	
7.	Marble powder from the marble industry	NR	➢ The filler is waste marble powder treated with ammonium carbonate (TMP). ➢ TMP-filled compounds have a higher elongation at break, similar tensile strength, and hardness with the neat NR. ➢ TMP-filled compounds showed lower air permeability than unfilled compounds.	Dasgupta *et al.* (83)
8.	Marble sludge waste (MSW) from the marble-cutting industry	NR	➢ The chemical composition of MSW is 68 % $CaCO_3$ with traces of silica, FeO, etc. ➢ Tensile strength and modulus increased up to 70 phr MSW composite. ➢ An increase in hardness and compression with filler loading was reported.	Ahmed *et al.* (84)
9.	Silica fume (SF) waste from the ferrosilicon factory	NBR & Ethylene propylene diene monomer (EPDM)	➢ The composition of SF is 95 % SiO_2 and is modified using polymethyl methacrylate (PMMA) (mSF).	El-Sabbagh *et al.* (85)

			➢ A decrease in cure time with the addition of mSF was noticed. ➢ The tensile strength of both NBR and EPDM composites increased at smaller loading of SF and then decreased at high content.	
10.	Fly ash (FA) from lignite combustion	SBR	➢ The particle size used is 10 µm, and composition analysis showed 45 % SiO_2. ➢ Fly ash waste can replace 40 % CB without decreasing the mechanical properties compared to SBR/50 phr CB. ➢ Elongation at break and abrasion resistance were increased.	Orczykowski *et al*. (86)
11.	Red brick waste (RBW) from the red brick manufacturing industry	NBR	➢ RBW consisted mainly of SiO_2, Al_2O_3, and FeO. ➢ Tensile strength and hardness were maximum for 40 phr composite, ➢ Solvent uptake decreased with an increase in filler loading. ➢ Dielectric studies showed that composites with 30 phr RBW	Shafik *et al.* (87)

			exhibited high dielectric constant and less loss.	
12.	Ceramic waste from the ceramic industry modified with the silane coupling agent.	NR	➢ Ceramic waste particles were ball milled to reduce size to125 µm. X-ray fluorescence (XFR) spectrum proved Si & Al are the significant components. ➢ Tensile strength, modulus, and elongation at break were higher for filler-NR compounds. ➢ A decrease in tear strength and abrasion loss with increased filler loadings was reported.	Kondarage *et al.* (88)
13.	Sludge waste from the production of concentrated NR latex	NR	➢ Scorch time and optimum cure time were decreased. ➢ Hardness and modulus were increased on increasing filler loading. ➢ The addition of filler resulted in greater tensile strength, tear strength and abrasion resistance.	Intiya *et al.* (89)
14.	FA collected from the electric power plants	NR	➢ NR composites filled with high CaO and low CaO were prepared. ➢ The qualities of NR composites are	Krainoi *et al.* (90)

			impacted by the variation in components, which can be viewed as a substitute filler for CB-based composites. ➢ The use of both fillers shortened the NR composite's production time.	
15.	Inorganic filler-based eggshell (ES) waste	NR	➢ The mechanical and swelling properties were significantly enhanced when the coated filler was utilised in the NR matrix, particularly at 20 wt. % ES. ➢ The glass transition temperature (T_g) shifts to a lower temperature when resin concentration increases, as shown by differential scanning calorimetry (DSC) thermograms. ➢ Bio enveloping ES can be an alternative for green tyre and vehicle applications.	Moustafa *et al.* (91)

Table 1.4. Literature on reutilisation of biodegradable waste

Sl. No.	Filler	Matrix	Findings	Reference
1.	Chitin nano whiskers from Shrimp shell waste	NBR	➢ Tensile and tear strength were increased by 116 % and 54 %, respectively. ➢ Thermal stability was increased for 6 phr loaded nanocomposites. ➢ Dynamic mechanical analysis (DMA) results showed increased storage and loss modulus.	Dominic *et al.* (92)
2.	Nanocellulose from rice husk.	NR	➢ 30 wt. % of CB is replaced with 25 wt. % CB and 5 wt. % nanofiller. ➢ Thermal studies showed a decrease in onset degradation temperature on adding nanofiller. ➢ DMA studies proved no appreciable change in T_g for the composites.	Dominic *et al.* (93)
3.	Leather waste (WL) from the tannery industry	NR	➢ The strength at rupture rose from 1.38 to 2.18 MPa (NR/WL60) with the amount of leather waste. Additionally, Young's modulus increased to 0.1206 MPa from 0.0026 MPa. ➢ The solid density decreased due to the increase in the amount of leather. ➢ TGA showed an enhancement in the thermal resistance for composites.	Garcia *et al.* (94)

4.	Waste leather fibre (WLF) from the leather industry	NBR	➢ From 0 to 50 wt. %, the tensile and tear strength improved with the WLF concentration. ➢ The hardness and resistance of the developed materials were increased with WLF content. ➢ The increasing storage modulus compared to raw NBR showed good WLF and NBR matrix compatibility.	Hang *et al.* (95)
5.	Mixed office paper waste (MOW)	Synthesis of carboxymethyl cellulose (CMC)	➢ The rheological properties of 3 % aq. solution of CMC product showed non-Newtonian pseudoplastic behaviour.	Joshi *et al.* (96)
6.	Sugarcane bagasse ash (SBA)	NR	➢ Cure characteristics revealed that torque increases as SBA increases, and there is a decrease in cure time. ➢ DSC studies showed no change in the T_g by the incorporation of SBA. ➢ Increase in the tensile strength and modulus with SBA content.	Santos *et al.* (97)
7.	Hydro char (HC), obtained by hydrothermal carbonisation of hardwood waste (sawdust)	NR	➢ Partial replacement of CB with HC increases the torque and reduces the cure time. ➢ At higher loading of HC, the crosslink density is reduced. ➢ It accelerates the vulcanisation reaction, as evidenced by decreased scorch time.	Lubura *et al.* (98)

8.	Peanut shell powder (PSP) and coconut shell powder (CSP)	NR	➢ Biodegradation studies showed that filler accelerates biodegradation, and chemically treated filler resists degradation. ➢ The tensile strength of the composites has decreased by 2-5 % due to chemical treatment. ➢ Research on hardness indicated that chemically treated filler-rubber composites retained more hardness.	Sareena *et al.* (99)
9.	Crop residues as an alternative to vulcanizates	NR	➢ Higher torque indicates a high degree of crosslinking and hardness. ➢ Vulcanizates with straw added had higher barrier qualities and thermo-oxidative ageing resistance of all the examined samples.	Masłowski *et al.* (100)
10.	Waste walnut shell	EPDM	➢ 30 % silane-modified walnut shell content in EPDM showed the highest elastic modulus and tensile strength. ➢ The swelling ratio of the EPDM compound has lowered due to the walnut shell's high density.	Gungor *et al.* (101)
11.	Coconut shell bio-waste	SBR	➢ An Increase in tensile strength by ~36 % and tear strength by ~30 %. ➢ Thermal stability is improved as the onset temperature increases from 250 ºC to 370 ºC.	Sahoo *et al.* (102)

12.	Sunflower husks, rice husks and buckwheat hulls	PU foam	➢ Higher apparent density, lower water absorption, and higher compressive strength on adding filler. ➢ The foam composed of PU and 5 wt. % rice hulls had the highest fire resistance.	Czerwonka *et al.* (103)
13.	Bio fillers based on cellulose, chitin, starch, and their composites	NR	➢ Better crystallinity and higher biodegradability are noticed. ➢ Applications in fields like medical, food packaging, footwear, sensors and water purification were reported.	Thomas *et al.* (74)
14.	Waste fodder potato proteins (WFPP) from the starch industry	carboxylated acrylonitrile-butadiene rubber	➢ Improved crosslink density. ➢ An enhancement in mechanical properties was reported. ➢ Susceptibility for bio decomposition was increased	Prochoń *et al.* (104)
15.	Hydrothermally treated lignin	SBR and SBR blend.	➢ Bis(triethoxysilylpropyl)tetrasulphide silane was utilised as a coupling agent for in situ surface compatibilization. ➢ Modified lignin showed semi-reinforcing behaviour.	Sekar *et al.* (105)

1.9. Research gap

The ecology is adversely affected by the notable surge in industrialization due to the excessive discharge of diverse industrial wastes. The overproduction of industrial wastes can no longer be solved by conventional means like landfills. Therefore, the reutilisation of these wastes is becoming more popular. It is imperative to concentrate on the effective and efficient use of various industrial wastes for repurposing to reduce production costs and prevent pollution. In addition to recycling industrial waste, high-performance rubber composites are desperately needed for a wide range of applications.

There are many reports on the use of biomaterials as rubber fillers for specific applications. However, the literature lacks information about repurposing industrial solid wastes from the footwear, condom, and pigment industries. The ecosystem is severely contaminated by the production of large volumes of the aforementioned wastes, which are usually disposed of in landfills. Consequently, there is ample opportunity to utilise these industrial wastes as fillers with reinforcement in NR to create NR-waste composites, which would enhance NR's mechanical, thermal, and sorption properties.

1.10. Scope and objectives of the present work

The primary aim of the current work is to propose innovative technologies for the reutilisation of waste materials from the footwear, condom, and pigment industries and fabricating NR-waste composites

with enhanced properties for possible applications in the rubber industry. The circular economy approach to cost reduction and pollution control is the paramount relevance of this work. The main goals and objectives of the current work are listed below.

1. To collect, remove other impurities, and powder the following industrial wastes.

a) Polyurethane waste (PUW) from the footwear industry.

b) Magnesium carbonate waste (MCW) from the condom manufacturing industry.

c) Sodium sulphate waste (SSW) from the pigment industry.

2. To characterise the powdered industrial wastes by using various analytical techniques such as Fourier-transform infrared spectroscopy (FTIR), X-ray diffraction (XRD) analysis, dynamic light scattering (DLS) method, field emission scanning electron microscopy (FESEM), high-resolution tunnelling electron microscopy-energy dispersive X-ray (HRTEM-EDX) analysis, Brunauer–Emmett–Teller (BET) analysis, and thermogravimetric analysis (TGA).

3. To employ the powdered waste materials as fillers in NR for fabricating NR-waste composites by two-roll mill mixing method.

4. To characterise the prepared NR-waste composites using attenuated total reflectance-Fourier Transform infrared spectroscopy (ATR-FTIR), Field emission scanning electron

microscopy (FESEM), and thermogravimetric analysis (TGA) techniques.

5. To study the prepared NR-waste composite's rheological, mechanical, thermal and sorption properties.

6. To compare the experimental results with various established mechanical models and to study the non-isothermal degradation kinetics by isoconversional model-free approaches.

7. To employ clay as an additional filler in industrial wastes-filled NR composites and to study its rheological, mechanical, thermal, and sorption properties.

The primary outcome of this work is to reutilise industrial solid wastes as potential fillers in NR and other synthetic rubbers to fabricate new rubber composites with improved mechanical, thermal, and sorption properties. The fabricated rubber composites may find their potential for manufacturing common industrial components like pad assemblies, mud flaps, automobile parts, gaskets, seals, drive couplings, etc. The proposed approach will help to lower production costs, prevent environmental pollution, and promote a circular economy approach.

Chapter 2
Materials and Methods

The material specifications and the experimental methodology employed for the current investigation are given in this chapter. The features of industrial waste materials and their composite compositions with NR have been covered. Various analytical techniques have been explained to characterise the collected industrial wastes, clay and fabricated natural rubber-waste composites. The methods for examining the cure, mechanical, thermal and sorption properties of NR-waste composites have been explained. Established modelling techniques, namely the Nicolais-Narkis (N-N), Lu, and Turcsányi-Pukànszky-Tüdõs (T-P-T) models were employed to validate the tensile strength and Einstein and Guth models for Young's modulus of the fabricated composites. The reported study involves the application of Flynn-Wall-Ozawa (FWO), Kissinger-Akahira-Sunose (KAS), Tang, and Starink model-free methods to investigate the kinetics of non-isothermal degradation reaction utilising thermogravimetric analysis.

2.1. Materials

Various materials used for the fabrication of composites in the present investigation, their specifications and properties are described.

2.1.1. Natural rubber

Natural rubber (NR), an elastomeric hydrocarbon polymer, is found in the sap of the rubber tree, Hevea brasiliensis, as a milky colloidal suspension or latex. The rubber particles are dispersed steadily in an essentially watery media to form latex. It has a rubber content of 35-40 %, a water content of 55-60 %, and a solids content of 5 % (proteins, sugars, resins and salts). Rubber is made by adding acetic acid or formic acid, which acts as a coagulant, to the latex and coagulating it. The coagulated substance is dried and sheeted out. In the current work, Indian standard natural rubber (ISNR 5) grade NR was procured from the Rubber Research Institute of India at Kottayam. The following Table 2.1 lists the Indian Standard Specification for ISNR 5.

Table 2.1. Specifications of ISNR 5

Property	Value
Dirt content (% by mass)	Max. 0.05
Volatile matter (% by mass)	Max. 0.80
Ash content (% by mass)	Max. 0.60
Nitrogen content (% by mass)	Max. 0.60
Initial plasticity	Min. 30
Plasticity retention index (PRl)	Min. 60
Solubility parameter ($MPa^{1/2}$)	16.6

2.1.2. Polyurethane waste from the footwear industry

PU offers an intriguing polymer family by reacting various polyols with polyisocyanates because their mechanical, thermal, and chemical properties may be customised to fit desired applications. Manufacturing the soles for shoes and chappals uses a sizeable amount of PU in the form of crosslinked microcellular foams (106,107). The PU market alone is projected to be valued at USD 5.9 billion in 2024, rising at a compound annual growth rate (CAGR) of 7.6 % (108). The significant growth is linked to the expansion of the footwear industry, which is marked by changes in lifestyle and fashion as well as superior qualities, including high mechanical strength, which makes PU shoes sturdy and long-lasting (109,110). The PU sole is ideal for foot comfort since it has a soft texture, excellent elasticity, and a lower density than other soles. It also has excellent resistance against wear, tear, bending, high hardness, and superior shock absorption. Today, PU soles are used in various shoe styles, including athletic, casual, boots, formal, slippers, and sandals.

Global footwear exports climbed by 30.8 % in volume and 80.8 % in value over the past nine years due to a 20.5 % growth in global footwear manufacturing. China and India account for roughly 65 % of worldwide manufacturing, making Asia the region that produces and uses the most footwear items (108). India is just behind China in the world's shoe production, with a yearly production of close to 16 billion pairs. Figure 2.1 shows the global production and consumption of footwear in 2020.

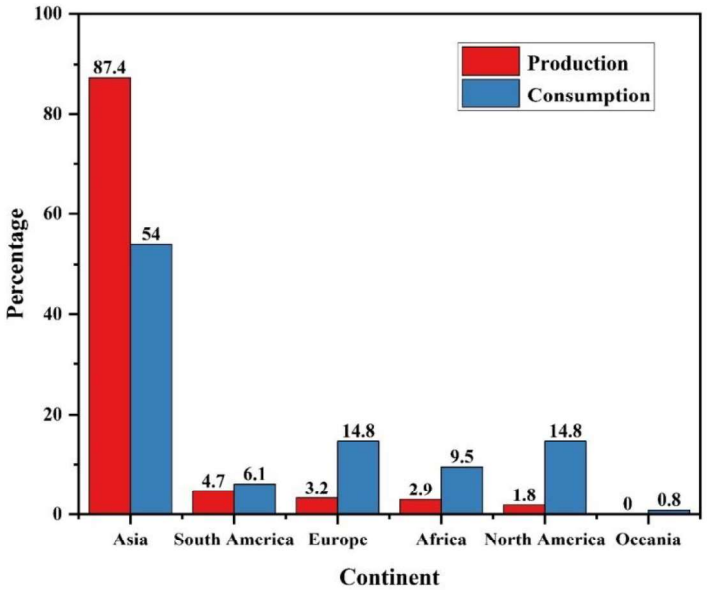

Figure 2.1. Global footwear production and consumption

Due to the widespread use of PU in the footwear industry and the significant amount of it that is dumped in landfills worldwide, PU poses a substantial threat to the environment today. The considerable impact of polyurethane waste (PUW) from the footwear industry and post-consumer footwear waste recycling on environmental degradation calls for careful consideration (111). Due to continual changes in regulatory requirements and environmental concerns, PU recycling is currently receiving attention on a global scale.

PUW was collected from M/s Veekesy Elastomers Pvt. Ltd. Kozhikode, Kerala. PU is made in the footwear industries by copolymerising butane-1,4-diol (Huntsman International (I) Pvt. Ltd., India) and diphenylmethane 4,4'-diisocyante (Huntsman International (I) Pvt. Ltd., India) and combining it with a chosen dye to give desired

colour. The diol, diisocyante and dye were allowed to travel through the pouring machine into the mould after all three components had been thoroughly combined to undergo polymerisation. The mould is heated first to ensure uniform mixing and then chilled to harden in the appropriate shape. After 5-6 usages, the mixer machine needs to be cleaned using dichloromethane. After cleaning, dye, diol, and diisocyanate are again permitted to enter the mixer. The PU produced after cleaning the mixer is discarded as it can't be utilised for manufacturing the sole. In a mixer machine, 5 kg of PUW is typically generated each day when only one dye is used, and this amount can increase up to 25 kg when different dyes are used. The digital images of the PU-based shoe sole waste collected, the cut pieces and powdered PUW, respectively, are displayed in Figure 2.2 (a-c).

Figure 2.2. Digital images of (a) PUW, (b) cut pieces of PUW and (c) powdered PUW

2.1.3. Magnesium carbonate waste from the condom industry

One of the most prevalent and well-liked birth control methods today is using male condoms (112). Latex, which is vulcanised to

boost the rubber's strength and durability, makes up the majority of condoms. During its manufacturing, fatty acids and surfactants are used as a binding agent and stabiliser to the latex. Zinc oxide is also incorporated to protect the rubber from UV radiation and fungal deterioration. Accelerators and antioxidants are also added to prevent harmful nitrosamine formation and oxidative degradation. Compared to water-based lubricants, silicone-based lubricants maintain slippery properties for a much more extended period. Magnesium carbonate and calcium carbonate are frequently used to make condoms less sticky (113). Many manufacturers now employ pharmaceutical-grade light magnesium carbonate (LMC) to lessen the stickiness of condoms. By 2022, it is anticipated that the Indian condom industry will reach $180 million due to increased consumer knowledge of sexually transmitted infections (STIs) and human immunodeficiency virus (HIV) attacks, thanks to the Government of India's initiatives. HLL Lifecare Ltd., Reckitt Benckiser (India) Ltd., Mankind Pharma, TTK Protective Devices Ltd., Cupid Ltd., and Raymond Ltd. are significant companies that dominate the Indian condom market.

Light magnesium carbonate waste (MCW) was procured from the Government of India-owned company, HLL Lifecare Ltd., Thiruvananthapuram, Kerala. HLL Lifecare Ltd. has eight condom manufacturing units nationwide. Its manufacturing facility in Thiruvananthapuram, Kerala, was established in 1969 and has undergone continuous modernisation with an annual production capacity of 1947 million condoms. The finishing powder used in the last phases of condom production was either silica or LMC. About

75-85 tonnes of MCW are produced annually in a condom manufacturing unit, and no attempts to repurpose it have been reported. This MCW is usually dumped in landfills, which makes drinking water harder. The careless disposal of MCW and the resultant water pollution prompted to focus on the possibility of its reutilisation. Figure 2.3 includes a digitised image of MCW.

Figure 2.3. Digital image of MCW.

2.1.4. Sodium sulphate waste from the pigment industry

The leading producer of inorganic pigments and surfactants, Ultramarine and Pigments Ltd., Chennai, India, provided sodium sulphate waste (SSW). The digital representation of SSW is displayed in Figure 2.4.

Figure 2.4. Digital image of SSW

Ultramarine blue (sodium-alumino-silicate) is a pigment containing mineral-rich zeolite with trace levels of polysulphide. The most intricate of the mineral colours, ultramarine ($Na_{8-10}Al_6Si_6O_{24}S_{2-4}$), includes the blue cubic mineral lazurite and is a complicated sodium silicate that has sulphur (the major component in lapis lazuli) (114). The unpaired electron in the S^{3-} radical anion gives the pigment its blue colour. Ultramarine blue is non-toxic, does not contaminate clothing, and is exceptionally stable in heat and light. It can also withstand high temperatures. It is regarded as an excellent tinting agent and an optical brightener and gives resilience to plastic structures. Figure 2.5 depicts the entire production process of ultramarine blue.

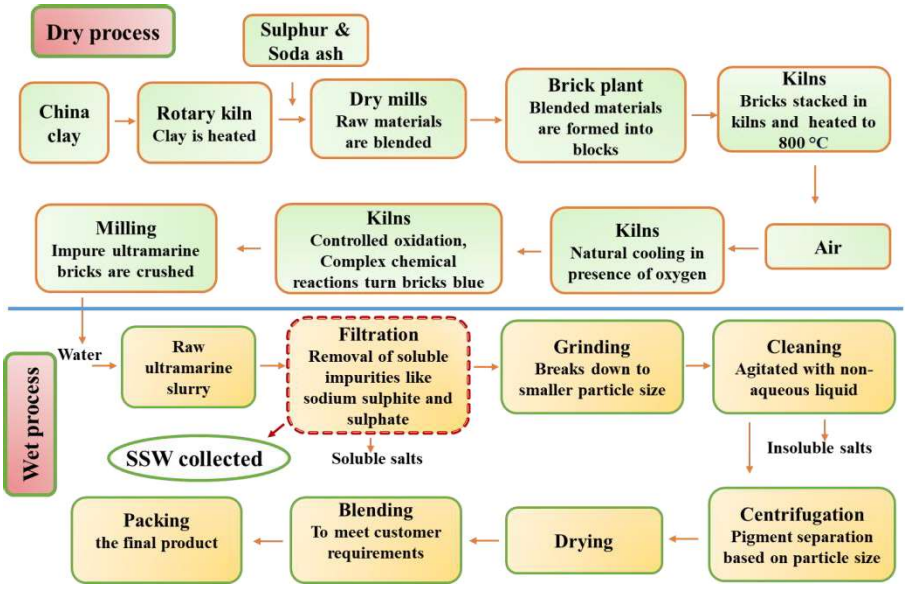

Figure 2.5. Manufacture of ultramarine blue

A sizable amount of water is required to purify the ultramarine blue slurry during production, and the generated wastewater has extraordinarily high levels of soluble inorganic salts, especially sodium salts, which severely pollute the water (115,116). The wastewater from the pigment industry includes a significant amount of dissolved sodium sulphate. Sulphate can be converted to sulphide, released into the atmosphere as H_2S, or precipitated as an insoluble salt of lead or barium (117). Sodium sulphate concentrations range from 100 mg/L to 3000 mg/L in industrial wastewater. Although the health effects of sulphate are acute (diarrhoea) and relatively short-lived, a significant reduction in sulphate concentration in drinking water is advised (118). High sulphate concentrations can produce scaling in pipes and sprinkler blockage when combined with iron and calcium. They can cause corrosion cracking, dealloying, pitting, corrosion of crevices and

metals, and corrosion of public works (119). Skin and eye irritation are two health effects caused by sodium sulphate, which can have long-term repercussions on aquatic life. Biological treatment techniques have little to no impact on removing sodium sulphate (120). The most favoured method for recovering sodium sulphate from aqueous streams involves evaporation followed by crystallisation, but this method is unprofitable when the salt concentration is relatively low. When salt concentration is low, membrane-based separation technologies have become more desirable.

2.1.5. Clay

Clay is a prominent type of hydrous aluminium silicate having a sheet-like (layer-like) structure and small particle sizes. Significant quantities of potassium, sodium, and calcium are also commonly found, while iron partially replaces magnesium and aluminium. Clay is widely used to enhance the stiffness, electrical insulation, thermal stability, barrier qualities, and other properties of polymers (121,122). In this work, clay was utilised as a supplementary filler with PUW to examine its effect on enhancing the mechanical, thermal, and sorption properties of NR-PUW composites. Hydrated clay was collected from English Indian Clays Ltd. (EICL), Thiruvananthapuram, Kerala, and is displayed in Figure 2.6.

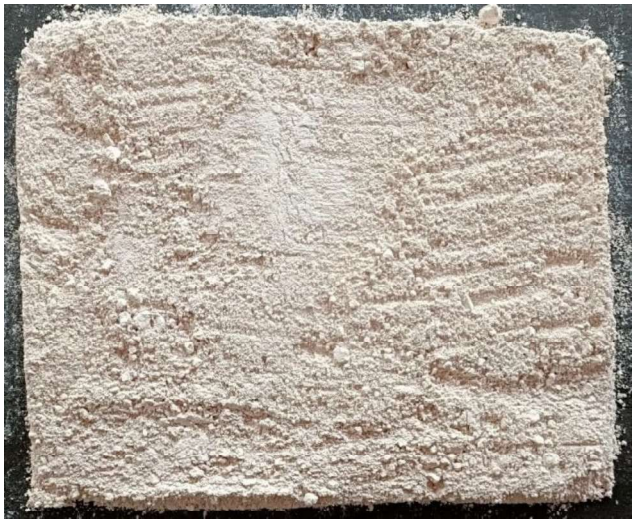

Figure 2.6. Digital image of hydrated clay dried at 50 °C for 6 hours

2.2. Chemicals

Specifications and attributes of various substances employed in this study, except the matrix and fillers, are described.

2.2.1. Zinc oxide

Zinc oxide is a common activator in the rubber formulation, and the following specifications (Table 2.2) apply to the zinc oxide (white seal grade) provided by Pondy Oxides and Chemicals Ltd., Chennai.

Table 2.2. Specifications of zinc oxide

Property	Value
Specific gravity	5.50
ZnO content (%)	98.00
Acidity (%)	0.40
Heat loss (%), max (2 hours at 100 °C)	0.50

2.2.2. Stearic acid

Stearic acid was also used as an activator and bought from Godrej Industries Ltd., Gujarat. It had the following specifications as specified in Table 2.3.

Table 2.3. Specifications of stearic acid

Property	Value
Appearance	Light cream to brown
Specific gravity	0.90
Melting point (°C)	50-69
Acid value	195-205
Iodine value (max)	20
% ash by mass (max)	0.1

2.2.3. N-Cyclohexyl-2-benzothiazolesulphenamide

N-cyclohexyl-2-benzothiazolesulphenamide (CBS), acquired from Nocil Ltd., Mumbai, was employed as an accelerator and had the following specifications (Table 2.4).

Table 2.4. Specifications of CBS

Property	Value
Specific gravity at 25 °C	1.27
Melting point (°C)	97-99
% ash (max)	0.3

2.2.4. Tetramethylthiuram disulphide

Tetramethylthiuram disulphide (TMTD) was also used as an accelerator, and the supplier of TMTD was Nocil Ltd., Mumbai, with the specifications given in Table 2.5.

Table 2.5. Specifications of TMTD

Property	Value
Melting point (°C)	142-147
% ash (max)	0.3
Specific gravity at 25 °C	1.43

2.2.5. 2,2,4-Trimethyl-1,2-dihydroquinoline

The antioxidant 2,2,4-trimethyl-1,2-dihydroquioline (TMQ) is commonly utilised in dry rubber applications to maintain surface and physical properties such as superior heat resistance, strong anti-scorch, and high colour retention at low concentrations. The parameters of TMQ, which was bought from Sigma-Aldrich Chemicals Private Limited, Bangalore, are recorded in Table 2.6.

Table 2.6. Specification of TMQ

Property	Value
Appearance	Amber to brown
Melting point (°C)	90
Specific gravity	1.06
Form	Flakes

2.2.6. Sulphur

Sulphur was used as a vulcanising agent, supplied by Oriental Carbon and Chemicals Ltd., Gujarat and had the specifications listed in Table 2.7.

Table 2.7. Specifications of sulphur

Property	Value
Appearance	Yellow fine powder
Elemental sulphur (%)	80.0
Specific gravity	2.05
Acidity (%), (max)	0.05
Ash content (%), (max)	0.05

2.2.7. Solvents

The solvents, namely toluene, xylene, mesitylene, and hexane, were purchased from E. Merck (India) Ltd., Mumbai (AR grade, 99 % pure), and petrol was collected from Indian Oil Corporation Ltd. Table 2.8. lists the physical characteristics of the solvents that were used.

Table 2.8. Physical characteristics of solvents used

Solvent	Molecular weight	Density (kg/m^3)	Boiling point (^oC)	Solubility parameter ($MPa^{1/2}$)
Toluene	92.14	867	109	18.3
Xylene	106.17	860	137	18.2
Mesitylene	120.19	864	164.7	18.0
Hexane	86.18	661	68.7	14.4
Petrol	80-100	710-737	70-150	-

2.3. Experimental methods

The experimental methods for rubber compounding, formulation of NR mixes, sample designations and formulations of fabricated composites, moulding, various rheological and mechanical

parameters, and employed theoretical modelling techniques are explained below.

2.3.1. Rubber compounding

The compounding was performed using a laboratory 6"×12" two-roll mixing mill under ASTM D3184 (Figure 2.7). After three minutes of masticating the rubber through the mill, activators, fillers, processing aids, accelerators, and vulcanizing agents were added to the compounding materials. Two more minutes of mixing were required to ensure the homogeneous mixing of all components. After that, the compound was allowed to run five times through a narrow nip gap before being sheeted out at a 3 mm nip gap. The mill speed ratio, nip gap, and roll mixing duration remained constant for all the mixes. Before moulding, the compound was allowed to mature for a full day at room temperature.

Figure 2.7. Two-roll mixing mill

Table 2.9. provides the general formulation of the NR mixes.

Table 2.9. Formulation of the NR mixes

Ingredients	Amount (phr)
ISNR 5	100
Zinc oxide	5.0
Stearic acid	2.0
TMQ	1.0
CBS	0.6
TMTD	0.2
Sulphur	2.5

2.3.2. Compression moulding

The composites were vulcanised in conventional moulds using an electrically heated hydraulic press with a 12" × 12" platen size and 150 kg/cm^2 pressure at a predetermined temperature and ideal cure time. The specimens were quickly cooled by soaking them in water after moulding, and they were then cured for 24 hours at room temperature. The required samples were cut from the set sheets to create the test specimens.

2.3.3. Cure characteristics

A Rubber Process Analyser, RPA-2000, was used to analyse the compound's cure characteristics. The rubber process analyser uses two directly heated, opposite biconical dies. A circular disc-shaped specimen weighing about 5 g was held in the bottom die and oscillated

at a 0.5 deformation angle (100 cycles per minute frequency). The force is transferred through the rubber and sensed by the upper die's torque transducer. The computer receives the measurements produced by the torque transducer. The chosen attributes are measured, and the calculations and results are shown. The rheography can provide the following information.

The ideal cure time, or t_{90}, is the period required to generate 90 % of the maximal torque, determined using the following formula.

$$\text{Torque at optimum cure } = 0.9\ (M_H - M_L) + M_L \qquad (2.1)$$

Scorch time, t_{s2}: The time needed to increase 2 dNm of torque over the minimum torque.

Maximum torque, M_H: This is the highest torque recorded after the mixture is cured.

Minimum torque, M_L: The mix's lowest torque reading at the test temperature before cure begins.

The following equation determines the cure rate index (CRI) and measures how quickly the cure response occurs.

$$CRI = 100/(t_{90} - t_{s2}) \qquad (2.2)$$

Reversion time: After M_H has been attained, this is the time needed to reach 98 % of M_H.

2.3.4. Stress-strain measurements

The force applied per unit area of the original cross-sectional area when a specimen band is stated in megapascals (MPa) is known as tensile strength. The ability of rubber to stretch without breaking is known as elongation. It is equivalent to the extension created by applying a tensile force on a specimen that results in benchmarks. In relation to the initial distance between the markings, it is expressed as a percentage. An Instron Universal Testing Machine Model 3365 with a 5 kN load cell and a 500 mm/min displacement rate was used to conduct tensile tests under ASTM D412. A die was used to punch out specimens in the shape of dumbbells from the moulded sheets in the direction of the grain, as in Figure 2.8. Before testing, the sample's thickness was measured using a computerised gauge. These tests offer the composite's tensile strength, modulus values and elongation at break.

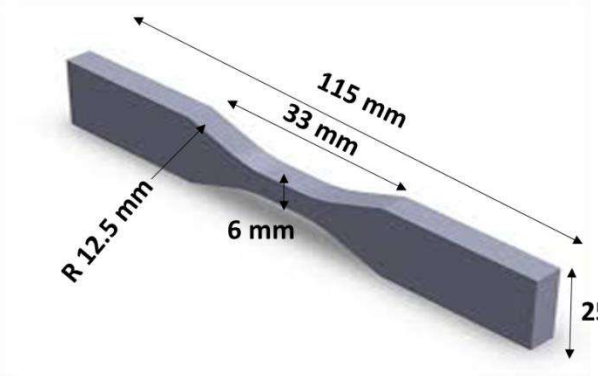

Figure 2.8. Test specimen for tensile testing of rubber

2.3.5. Tear strength

A test specimen's tear strength or resistance is determined by the highest force needed to tear it in a direction perpendicular to the direction of stress. The sample's tear resistance was tested under ASTM D624 using tab ends and an unnicked 90° angle on one side (Die C). The force operates on the test specimen in the direction of grasp separation in a direction parallel to the sample's tab ends. A 500 mm/min test speed was used, and the test specimen is shown in Figure 2.9.

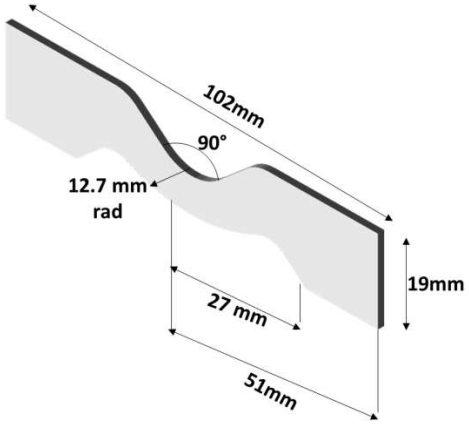

Figure 2.9. Test specimen for tear strength analysis

2.3.6. Hardness

The shore A hardness of compression moulded experimental samples was measured using a Bariess durometer under ASTM D2240. Unstressed samples with a thickness of 6 mm were used for the tests. Readings were collected after 10 seconds of indentation with an

applied load of 12.5 N when a solid contact had been made with the material.

2.3.7. Abrasion loss

Using a Bariess DIN abrader (Germany), the sample's abrasion resistance was assessed as per ASTM D5963. A 10 N load was applied, while a 16 ± 0.2 mm diameter sample piece was retained on a rotating sample holder. The sample was initially given a pre-run, and its weight was recorded. The weight of the sample piece after the final run was also noted. The formula used to determine the abrasion resistance index was

$$\text{Abrasion resistance Index (\%)} = \frac{\Delta m_1 . d_2}{\Delta m_1 . d_1} \times 100 \qquad (2.3)$$

where Δm_1 and Δm_2 are the mass losses in mg of the test piece and standard rubber, respectively, and d_1 and d_2 are the densities of the test piece and standard rubber, respectively.

2.3.8. Specific gravity

The mass of a material is compared to the mass of an equivalent volume of deionised water to determine its specific gravity. A solid piece of rubber is generally removed from a moulded test slab or button and weighed twice: once in air and once in water. The density or specific gravity is then calculated. The specific gravity was calculated using a Densimeter at room temperature under ASTM D297.

2.3.9. Compression set

The samples, which had a 12.5 mm thickness and 29 mm in diameter (ASTM D395), were subjected to compression to a constant deflection of 25 % and stored in duplicate at 70 °C in an air oven for 22 hours. The samples were then removed and allowed to attain room temperature for 30 minutes, and then the ultimate thickness was determined. The compression set was computed by using Equation (2.4).

$$\text{Compression set (\%)} = \frac{T_0 - T_i}{T_0 - T_n} \times 100 \qquad (2.4)$$

where T_n is the thickness of the utilised spacer bar, and T_0 and T_i are the specimen's initial and final thicknesses, respectively.

2.3.10. Heat build-up

According to ASTM D623, a heat build-up investigation was conducted using a Dynesco Goodrich Flexometer. Using a compression moulding machine, the test pieces were made in the shape of a cylinder with 17.8 ± 0.1 mm diameter and 25 ± 0.15 mm height. The test pieces were maintained for 30 minutes at 100 °C. Throughout the investigation, both the test load and the chamber temperature remained constant. A pyrometer was used to measure the sample's temperature after 25 minutes.

2.3.11. Rebound resilience

The elastic behaviour of elastomers under impact load is evaluated using rebound resilience. An elastomer sample is tested to

determine how much kinetic energy it can return following an impact. The type of material, the formulation of the material, and the test temperature all affect rebound resilience. An evaluation of a rubber material's aptitude for vibration-related tasks is based on its rebound resilience. DIN 53512 and ISO 4662 both explain the rebound resilience test in detail. The so-called push pendulum is hoisted, released at a predetermined speed, and strikes the test specimen that is fixed vertically. The hammer's deflection, or measured rebound height, calculates the rubber sample's rebound resilience.

2.4. Mechanical modelling to determine the strength of polymer particulate composites

The interfacial interaction between the filler and matrix was understood, and the tensile strength of NR-filler composites was confirmed using well-established theoretical modelling approaches. The mechanical properties of the composite depend on the filler's content, distribution within the matrix, morphology, and interaction with the matrix. In our investigation, three models were used to determine the composite's tensile strength: namely, the Nicolais-Narkis (N-N) model (123), the Lu model (124), and the Turcsányi-Pukànszky-Tüdõs (T-P-T) model (125) as analysed by Salam and Dong (126). These models are usually used to predict the tensile strength of rigid filler-polymer composites based on their interfacial properties.

2.4.1. Nicolais-Narkis model

Matrix-filler adhesion is not considered when using the Nicolais-Narkis (N-N) model for uniformly distributed spherical particles. There is no stress transfer from the matrix to the filler because there is no matrix-filler interfacial adhesion. As a result, the matrix carried the entire load by itself, which is used to evaluate the composite's lower-bound strength. However, the strength of the upper bound is established by supposing complete matrix-filler adhesion. As a result, the composite's strength is equal to that of the matrix or unfilled polymer ($\sigma_c \approx \sigma_m$). Thus, Equation (2.5) provides the composite's tensile strength.

$$\sigma_c = \sigma_m (1 - 1.21\emptyset^{2/3}) \tag{2.5}$$

where σ_c and σ_m represent the composite's and the matrix's respective tensile strengths and $\emptyset$ is the volume fraction of the filler.

2.4.2. Lu model

The Lu model is a variation of the N-N model that considers matrix-filler adhesion, as seen in Equation (2.6) below.

$$\sigma_c = \sigma_m(1 - 1.07\emptyset^{2/3}) \tag{2.6}$$

The strength of the matrix-filler interfacial bonding is determined by this equation, which considers all the properties discovered by micromechanical measurement, micromechanical analysis, and microdamage monitoring.

2.4.3. Turcsányi-Pukànszky-Tüdõs model

Strong particle-matrix interfacial bonding is assumed in the Turcsányi-Pukànszky-Tüdõs (T-P-T) Model, and an empirical relationship is suggested as given in Equation (2.7) below.

$$\sigma_c = \sigma_m (1 - \emptyset)/(1 + 2.5\emptyset)e^{(B\emptyset)} \quad (2.7)$$

The value of B, a hypothetical constant, is primarily determined by the following factors: interfacial bonding energy, particle surface area, density, and bonding between particles. The computation mentioned above does not account for the effects of porosity, voids, or particle size. According to this criterion, a rise in the volume proportion of filler strengthens the composite. Additionally, the T-P-T model can be applied to composites by including spherical and anisotropic particles.

2.5. Mechanical modelling to validate Young's modulus

Young's modulus is a unit used to measure and express a material's degree of stiffness (elastic modulus). The elastic modulus is constant in all directions for an isotropic material, although many composites have anisotropy. The following models, namely Einstein and Guth models, were employed.

2.5.1. Einstein Model

Einstein suggested an equation based on the presumption that a hard particle exists to predict the modulus of elasticity of metal-matrix composites, as shown below by Equation (2.8) (127).

$$E_c = E_m(1 + 2.5\emptyset) \quad (2.8)$$

Where E_c and E_m represent Young's moduli of the composite and matrix, and the filler's volume fraction is given by $\emptyset$. Einstein's equation remains true only at low filler volume fractions and presupposes excellent matrix-filler adhesion and homogenous filler particle dispersal.

2.5.2. Guth model

Equation (2.9) below illustrates Guth's extension of Einstein's theory to account for rubber reinforcement and the modulus rise by a rigid spherical filler (128).

$$E_c = E_m\,(1 + 2.5\emptyset + 14.1\emptyset^2) \quad (2.9)$$

2.6. Characterisation techniques

2.6.1. Fourier Transform infrared spectroscopy

A molecule's structure and functional groups can be assessed using Fourier Transform infrared (FTIR) spectroscopy by detecting the distinctive vibrational frequencies of molecules. Shimadzu IR Affinity-1S FTIR spectrometer with a range of 4000 cm^{-1} to 400 cm^{-1} was used in transmittance and attenuated total reflection (ATR) modes with a resolution of 4 cm^{-1}, and the number of scans was 32.

2.6.2. X-ray diffraction analysis

Using X-ray diffraction (XRD) research, crystalline materials are characterised, and their structures are determined. Constructive interference between monochromatic X-rays and a crystalline material

is the basis of X-ray diffraction. Every crystalline solid has a distinct X-ray powder pattern that can be used to identify it, much like a fingerprint. The industrial waste sample's XRD patterns were acquired using a Bruker AXS D8 Advance X-ray Powder Diffractometer operated at 40 kV and 35 mA, respectively, and Cu K_α radiation. The entire area of crystalline and amorphous peaks beneath the diffraction curve of crystalline and amorphous peaks in the XRD pattern was divided to determine the percentage crystallinity of a sample.

2.6.3. Dynamic light scattering analysis

The scientific dynamic light scattering (DLS) analyser Horiba Particamini-LA-350 was used to measure filler dispersion in water. The method, also known as photon correlation spectroscopy (PCS), works by measuring the irregular variations in the brightness of light scattered from a solution or a suspension. A rapid photon detector measures the fluctuations in the scattered light at a specified scattering angle after illuminating the sample with a laser beam.

2.6.4. Morphological studies - Scanning electron microscopy

High-resolution surface imaging can be achieved using scanning electron microscopy (SEM). Field emission scanning electron microscopy (FESEM) analysis (MIRA3 XMU, Czech Republic, and Hitachi SU8010, Japan) was used to examine the morphology of the surface fractured samples. In this process, electrons are accelerated towards an anode from a cathode made of tungsten or lanthanum hexaboride using thermionic emission; field emission is also an option. These concentrated high-intensity electron beams scan the object and

produce a range of surface signals. Various signals can be detected, including diffracted backscattered electrons, high-energy backscattered electrons, secondary electrons of low energy, and X-rays. Detectors (photomultiplier tubes) monitor and amplify these signals. Thus, a cathode ray tube is used to observe the specimen's tiny region under study, and a black-and-white camera is used to capture the image. The fracture surface of the tensile specimens on SEM observations is reported in the current investigation.

2.6.5. Energy dispersive X-ray spectroscopy

Energy dispersive X-ray spectroscopy (EDX) is used for qualitative elemental analysis, standardless quantitative analysis, and X-ray line scans. Since every element has a different atomic structure, it can emit X-rays with distinct peaks. The sample under examination is exposed to a high-energy stream of charged particles, such as electrons or X-rays, to stimulate the production of characteristic X-rays. EDX analysis was done using the JEOL JEM 2100 Plus high-resolution transmission electron microscope.

2.6.6. High-resolution transmission electron microscopy

High-resolution transmission electron microscopy (HRTEM) uses a rapidly charged electron beam (up to 300 kV), which scatters as it passes through an extremely thin material (almost 160 nm). The electron scattering during transmission decides the type of information about the sample. An accurate map of atomic arrangements can be obtained in the high-resolution imaging mode, providing a greatly enlarged perspective of micro and nanostructures. The samples are

spread out in the water and placed on the Cu-based TEM grid for imaging. Its thickness and mesh size range from a few to 100 μm, and its diameter is 3 mm. Before imaging, the material is dried at room temperature. The JEOL JEM 2100 Plus high-resolution transmission electron microscope was used for TEM imaging.

2.6.7. Brunauer-Emmett-Teller adsorption

Brunauer-Emmett-Teller (BET) surface area, pore diameter, and pore volume of the materials were assessed using a BET analyser (MicrotracBEL, Japan) with a nitrogen environment. Using the BET approach, the specific surface area was determined from the isotherms. At a relative pressure (P/P_0) of roughly 0.95, the volume of adsorbed nitrogen was used to compute the single-point total pore volume. Using the Barrett-Joiner-Halenda (BJH) approach, the pore size distribution was determined from the desorption branch of the isotherm (129).

2.6.8. Thermogravimetric analysis

Samples are subjected to thermogravimetric analysis (TGA) to find variations in weight with temperature. The analysis typically comprises a pan filled with the sample and a high accuracy balance. A thermocouple is used to precisely detect the temperature of the sample by placing it in a small electrically heated oven. Analysis was done by progressively increasing the temperature and plotting the weight in percentage against temperature. Utilizing a Hitachi STA7200 thermogravimetric analyser, the samples were heated at 10 ºC/min between 40 ºC and 600 ºC while being purged at a rate of 100 cc/min

of nitrogen. The temperatures recorded were of the onset (T_i), residue detected at 600 ºC, and the maximum value seen in the derivative thermogram (T_{max}). The associated weight changes were recorded using a sensitive microbalance.

2.7. Theoretical modelling of thermal degradation kinetics

The rate of thermal degradation reactions of solid polymers has been studied using a variety of methodologies, and in the TGA method, the rate is characterised by the following Equation (2.10).

$$\frac{d\alpha}{dt} = k(T)f(\alpha) \tag{2.10}$$

T and t denote the temperature and time, and α is the conversion factor provided by Equation (2.11).

$$\alpha = \frac{(m_0 - m_t)}{(m_0 - m_f)} \tag{2.11}$$

where f(α) is the conversion function, m_0, m_t, and m_f are the starting, actual, and final masses of the analyte, respectively, and k(T) is the rate constant (130). The Arrhenius Equation's rate constant is represented by Equation (2.12).

$$k(T) = A\exp\left(\frac{-E_a}{RT}\right) \tag{2.12}$$

Terms in Equation (2.12) include the pre-exponential factor (A) in s^{-1}, the universal gas constant (R), the activation energy (E_a) of the degradation in $kJmol^{-1}$, and the reaction temperature (T). Equation (2.12) is applied in Equation (2.10) to obtain,

$$\frac{d\alpha}{dt} = A \exp\left(\frac{-E_a}{RT}\right) f(\alpha) \quad (2.13)$$

Under dynamic circumstances, the temperature varies linearly with time. Therefore, T can be expressed as Equation (2.14).

$$T = T_0 + \beta t \quad (2.14)$$

where β is the heating rate ($\beta = \frac{dT}{dt}$) and on applying Equation (2.14) in Equation (2.13), we get,

$$\frac{d\alpha}{dT} = \frac{A}{\beta} \exp\left(\frac{-E_a}{RT}\right) f(\alpha) \quad \text{or} \quad \frac{d\alpha}{f(\alpha)} = \frac{A}{\beta} \exp\left(\frac{-E_a}{RT}\right) dT \quad (2.15)$$

The integral conversion function, g (α), can be obtained by integrating dynamic conditions of Equation (2.16).

$$g(\alpha) = \frac{A}{\beta} \int_{T_0}^{T} \exp\left(\frac{-E_a}{RT}\right) dT = \frac{A}{\beta} p(x) \quad (2.16)$$

where p (x) is the temperature integral in which $x = \frac{E_a}{RT}$ without any analytical solution.

Several approaches were put forth to investigate the kinetics of non-isothermal reaction degradation utilising TG analysis (131,132). The reported studies involve the application of Flynn-Wall-Ozawa (FWO) (133,134), Kissinger-Akahira-Sunose (KAS) (135,136), Tang (137,138), and Starink (139,140) methods by TG analysis with different heating rates to assess important kinetic parameters like E_a and A.

2.7.1. Flynn-Wall-Ozawa method

The Flynn-Wall-Ozawa (FWO) method, which makes use of Doyle's approximation, is an isoconversional kind strategy that was introduced by Flynn, Wall, and Ozawa (141) which uses experiments with various heating rates (β) to determine the temperature that corresponds to a fixed conversion degree (α). FWO method employs the formula given below in Equation (2.17) to assess the kinetic parameters which are deduced from modifying Equation (2.16) by the assumption, $\ln[p(x)] \approx -2.315 - 0.456x$.

$$\log \beta = \frac{-0.457E_a}{RT} + \left\{\log\left[\frac{AE_a}{g(\alpha)R}\right] - 2.315\right\} \quad (2.17)$$

The log β against the 1/T plot should yield a straight line, and the E_a is calculated from the slope ($0.457E_a/R$).

2.7.2. Kissinger-Akahira-Sunose method

The isoconversional model-free kinetic analysis method, known as Kissinger-Akahira-Sunose (KAS) analysis, determines how much E_a depends on the degree of conversion (α) for dynamic trials with various constant heating rates. Due to the accuracy of this isoconversional technique, Vyazovkin et al. recommend utilising it to measure kinetic parameters (142). Equation (2.18) provides the relationship between β and T at a given α as

$$\ln\left(\frac{\beta}{T^2}\right) = \ln\left(\frac{AR}{E_a g(\alpha)}\right) - \left(\frac{E_a}{RT}\right) \quad (2.18)$$

The slope ($-E_a/R$) of the linear fit of $\ln(\beta/T^2)$ and 1/T, obtainable from TGA data of various heating rates, can be used to determine E_a for each conversion.

2.7.3. Tang Method

Another integral isoconversional technique, adjusted as Equation (2.19) below, has been developed by Tang with a better approximation of the temperature integral.

$$\ln\left(\frac{\beta}{T^{1.8947}}\right) = \text{constant} - 1.00145\left(\frac{E_a}{RT}\right) \quad (2.19)$$

E_a can be evaluated from the plot of $\ln\left(\frac{\beta}{T^{1.8947}}\right)$ versus I/T in a linear least square fashion.

2.7.4. Starink Method

The temperature integral can be calculated using an alternative integral isoconversional method developed by Starink using a series of approximations, as shown in Equation (2.20).

$$\ln\frac{\beta}{T^{1.92}} = \text{constant} - 1.0008\frac{E_a}{RT} \quad (2.20)$$

Using the linear least squares approach, E_a has been calculated from the slope of $\ln\frac{\beta}{T^{1.92}}$ against $1/T$ plot.

2.8. Sorption studies

The diffusion, sorption, and penetration of solvents into elastomers have received much attention recently because they are fundamental processes crucial to many significant engineering and industrial fields (143,144). Qualities like chemical stability, dimensional invariance, and structural integrity in the presence of aggressive compounds are crucial in applications, including electronic

encapsulation, food packaging, filtration, and controlled medication release. Therefore, it is essential to conduct transport studies when designing and producing barrier rubber materials for their application in various industrial sectors (145).

Circular samples were cut from vulcanised sheets by using a standard die. The sample's weight, width, and thickness were initially measured, and the samples were preserved in diffusion bottles filled with 30 mL of the solvent. Periodically, the samples were taken out of the diffusion bottles, the adhering solvent was wiped off using tissue paper, and the samples were immediately weighed to the nearest ± 0.0001 g. The diffusion container was filled with the weighed samples again, and the experimental method continued until equilibrium swelling was attained. After drying, the sample's de-swollen weight was obtained. Since the weighing was completed in less than 40 seconds, the inaccuracy caused by solvent evaporation is minimal (146). A similar approach was reported by various researchers (99,147). Studies were performed in duplicates; the standard variation ranged between 0.06 and 0.1 mol %. Diffusion curves, which plot mol % or wt. % uptake against the square root of time in minutes was used to express the findings of diffusion tests. The diffusion studies provide the mol % uptake, denoted as moles of solvent sorbed by 0.1 kg of the sample, and the mol % uptake from the diffusion investigations is given by Qt (mol %), expressed by Equation (2.22).

$$Q_t = \frac{M_t/M_s}{M_p} \times 100 \qquad (2.22)$$

where M_t, M_s, and M_p stand for the mass of solvent absorbed at time t, the solvent's molecular mass, and the composite's mass, respectively. The resulting Q_t % values are plotted against the square root of time to obtain the sorption curves. Solvents such as petrol, xylene, mesitylene, hexane, and toluene were employed to examine the sorption behaviour of composites made of NR and industrial wastes.

The swelling index was examined to determine the degree of the composite's swelling behaviour. It is the proportion of original weight to swollen weight. The swelling index directly indicates crosslinking strength; the lower the ratio, the more crosslinking there is.

$$\text{Swelling index } (\%) = \frac{(W_1 - W_0)}{W_0} \times 100 \qquad (2.23)$$

W_o and W_1 are the specimen's weights before and after swelling. The crosslink density ($1/2M_c$) was calculated using an equilibrium swelling approach with toluene as the solvent, where M_c is the rubber chain's number-average molecular weight between crosslinks. The sample's weight was measured while it was bloated and after it had shrunk to its original weight after being dried in a vacuum. Using the technique described by Ellis and Welding, the volume fraction of rubber (Vr_f) in the swollen network was estimated from the following Equation (2.24) (148).

$$V_{rf} = \frac{(m_d - fm_i)\rho_r^{-1}}{(m_d - fm_i)\rho_r^{-1} + m_s\rho_s^{-1}} \qquad (2.24)$$

where ρ_r is the polymer density, ρ_s is the solvent density, f is the weight fraction of insoluble components, and m_s is the quantity of

solvent absorbed by the sample. The starting and de-swollen weights of the sample are m_i and m_d. The Flory-Rehner Equation was used to compute the crosslink density in Equation (2.25)(149).

$$\text{Crosslink density} = \frac{1}{2M_c} \tag{2.25}$$

where M_c is the molecular weight of polymer between crosslinks and is given in Equation (2.26)

$$M_c = \frac{-\rho_r V_s V_{rf}^{1/3} rf}{\ln(1-V_{rf})+V_{rf}+\chi V_{rf}^2} \tag{2.26}$$

where V_s is the solvent's molar volume (toluene has a molar volume of 106.2 cm3/mol), χ is the parameter describing the interaction between the rubber and solvent, and $\chi = 0.3795$ for the NR-toluene system.

2.9. Kinetic parameters of solvent transport

The following kinetic parameters, namely sorption, diffusion, and permeation coefficients, were evaluated from the diffusion studies of NR-industrial waste composites.

2.9.1. Diffusion coefficient

The following formula, Equation (2.27), is used to calculate the diffusion coefficient (D).

$$D = \pi\left(\frac{h\theta}{4Q_\infty}\right) \tag{2.27}$$

The mol % sorption at equilibrium is denoted by Q_∞, whereas the thickness of the sample and slope of the linear component of sorption

curves prior to attaining 50% of equilibrium are represented by h and θ.

2.9.2. Sorption coefficient

The sorption coefficient (S) is correlated to the solvent's equilibrium sorption and is estimated by Equation (2.28).

$$S = \frac{W_\infty}{W_p} \tag{2.28}$$

W_∞ is the mass of the penetrant solvent at equilibrium swelling, and W_p denotes the composite's mass.

2.9.3. Permeation Coefficient

The principal elements influencing the penetrant's penetration through a matrix are sorption and diffusion. As a result, according to Equation (2.29), the permeation coefficient (P) is calculated by multiplying the diffusion coefficient by the sorption coefficient.

$$P = D \times S \tag{2.29}$$

2.9.4. Mode of transport

Different mechanisms are followed to transport liquids through composite materials depending on various variables, including the chemical makeup of the filler and the polymer matrix, their compatibility, and interfacial adhesion. Three types of diffusion behaviour can occur depending on the relative speeds of polymer segmental relaxation and penetrant mobility (150,151). They include (1) anomalous behaviour, where the mobility of the penetrant and the

relaxation rates of polymer segments are similar; (2) Fickian behaviour, where the mobility of the penetrant is significantly lower than the relaxation rates of the polymer segments; and (3) non-Fickian behaviour, where mobility of penetrant is significantly higher than the relaxation rates of polymer segments. In the current study, the transport mechanism was investigated utilising the empirical relationship found in Equation (2.30)

$$\log \frac{Q_t}{Q_\infty} = \log k + n \log t \tag{2.30}$$

Q_t and Q_∞ are the amount of liquid that 100 g of sample absorbed at time t and at equilibrium swelling, respectively. The value *k* denotes the interaction of the penetrant with the polymer, and the term *n* indicates the mode of transport. The interfacial adhesion and the composition of the materials affect the constants *n* and *k*. The slope and y-intercept values of log Q_t/Q_∞ versus log t plots were used to get *n* and *k* values. The transport mechanism belongs to various types depending on the value of *n*. If *n* = 1, the behaviour is non-Fickian, or relaxation-controlled transport occurs. The value of *n* for Fickian behaviour is 0.5. The transport behaviour is anomalous if *n* is between 0.5 and 1. A constant that changes depending on the composite's structure, the factor *k* indicates how the composite and solvent interact. Lower values of *k* indicate lesser interaction between the composite and the solvent and lesser solvent absorption. According to the "like dissolves like" principle, whether the composite and solvent are polar or non-polar, the solubility increases, and *k* is also high. However,

solubility declines and the value of *k* also drops if the composite and solvent are of different kinds.

2.9.5. Activation energy of diffusion and permeation

The Arrhenius relationship can be used to determine the energy of activation for diffusion and permeation based on the temperature dependence of the transport coefficients (P, D, and S).

$$X = X_0 e^{-E/RT} \tag{2.31}$$

where E is the activation energy, T is the absolute temperature, R is the universal gas constant, and X is P, D, or S. X_0 denotes P_0, D_0, or S_0 constants. The activation energy of diffusion (E_D) and permeation (E_P) can be determined from the slopes of Arrhenius plots of log D vs 1/T and log P vs 1/T. The following equation, which details the molecular movement in the polymer matrix, can be used to calculate the heat of sorption (ΔH).

$$\Delta H = E_p - E_D \tag{2.32}$$

The required materials for fabricating NR-industrial waste composites and the methods to characterise them were explained. The rheological, mechanical, thermal, and sorption properties of these fabricated composites will be investigated to explore the possibility of using them in NR for the production of various industrial rubber components.

Chapter 3
Characterisation of Fillers

The properties of various industrial wastes, namely, rigid polyurethane waste (PUW) from the footwear industry, light magnesium carbonate waste (MCW) from the condom industry, and recovered sodium sulphate waste (SSW) from the pigment industry that have been gathered and employed as fillers for reinforcement in NR are fully explained in this chapter. There is also a brief description of clay's qualities, which is used as an additional filler along with PUW. The other impurities present were removed from the collected industrial wastes, powdered and characterised by various analytical techniques like Fourier Transform infrared spectroscopy (FTIR), X-ray diffraction (XRD), Thermogravimetry (TG), Field emission scanning electron microscopy (FESEM), Energy dispersive X-ray (EDX), High resolution tunnelling electron microscopy (HRTEM), Dynamic light scattering (DLS), and Brunauer-Emmett-Teller (BET) surface area analysis.

3.1. Introduction

The collected industrial solid wastes included rigid polyurethane-rich shoe sole waste, light magnesium carbonate waste, and recovered sodium sulphate waste from the footwear, condom, and pigment industries, respectively. These wastes are produced in vast amounts, and their landfill seriously pollutes the environment. Before being characterised, all the collected industrial wastes were adequately isolated from other wastes and powdered. Several analytical techniques were employed to characterise these wastes, including FTIR, XRD, FESEM, HRTEM, DLS, BET, EDX, and TG. These wastes were employed as reinforcing fillers in NR to fabricate NR-industrial waste composites to study the enhancement of NR's mechanical, thermal, and sorption properties for industrial applications in a circular economy strategy.

3.2. Characterisation of polyurethane waste

Polyurethane waste **(**PUW) collected from the footwear industry (Veekesy Elastomers Pvt. Ltd., Kozhikode, Kerala) was characterised by FTIR, FESEM, XRD, FESEM-EDX, and TGA techniques.

3.2.1. Fourier Transform infrared spectroscopic analysis of PUW

Figure 3.1 shows the FTIR spectra of PUW, which displayed three distinct absorption peaks at 3311 cm^{-1} (N-H stretching), 2974 cm^{-1} (-CH_2 stretching), and 2867 cm^{-1} (-CH_3 stretching), respectively. There were also other notable peaks found,

including those at 1700 cm^{-1} (urethane C=O stretching), 1527 cm^{-1} (C-H-N vibration), 1226 cm^{-1} (coupled C-N and C-O stretching), and 1076 cm^{-1} (C-O stretching). The observed peaks demonstrated the existence of different functional groups in PUW (152,153).

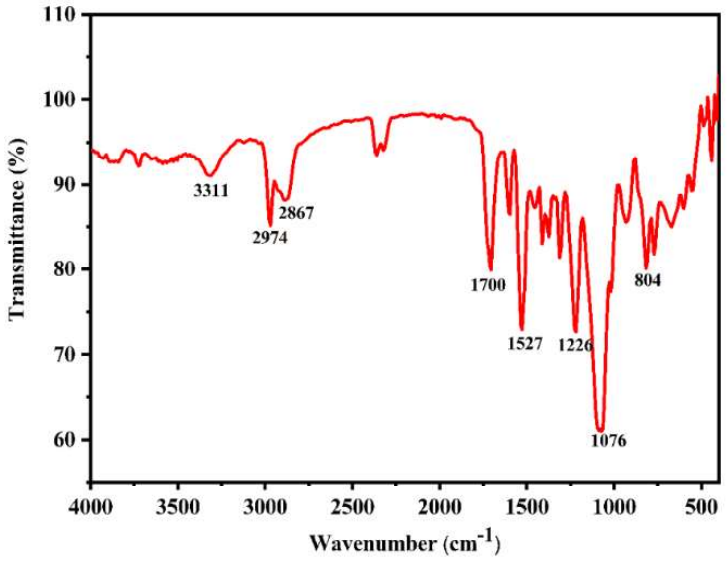

Figure 3.1. FTIR spectrum of PUW

3.2.2. X-ray diffraction analysis of PUW

The XRD pattern of PUW is displayed in Figure 3.2. The amorphous character of PUW is indicated by the prominent peaks at 2θ = 20° and 40°. Even though PUW has both hard and soft segments, their incorrect alignment reduces the crystallinity (154,155). The percentage crystallinity of PUW was found to be 31 %, as calculated using the XRD deconvolution method (153).

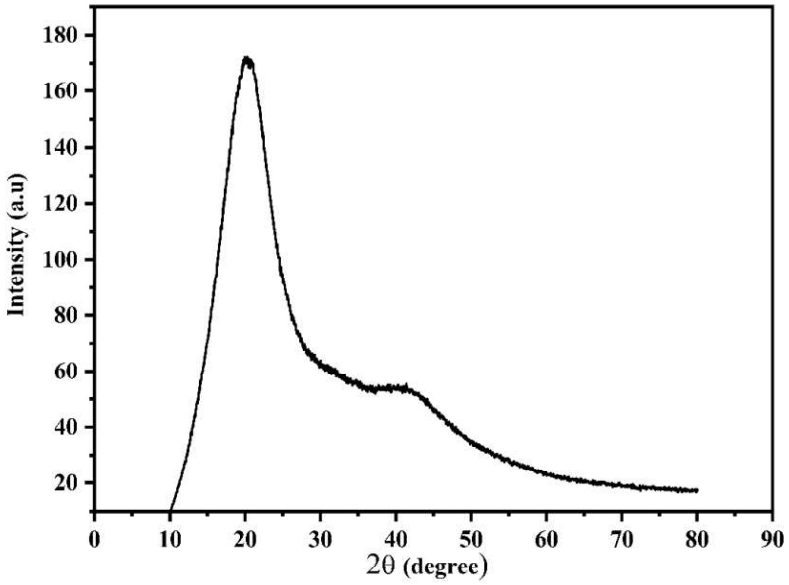

Figure 3.2. XRD pattern of PUW

3.2.3. Surface morphological analysis of PUW

Figure 3.3 shows the FESEM image of PUW, which is used to analyse the surface morphology of the material. The dispersion of particles with a non-spherical irregular shape and mild aggregation can be seen in Figure 3.3. The PUW powder is typically in a soft physical state, and the average particle size determined from the FESEM analysis is between 50 and 100 μm.

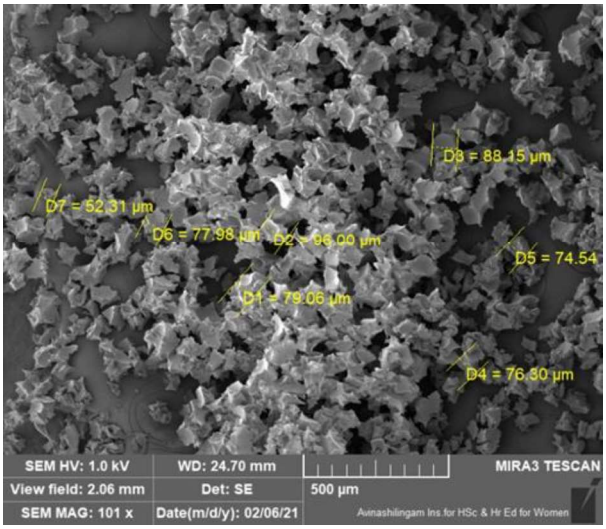

Figure 3.3. FESEM of PUW

3.2.4. Elemental analysis of PUW

Figure 3.4 displays the chemical composition of PUW, established by the FESEM-EDX analysis. Carbon, oxygen, and nitrogen were identified as the primary ingredients based on the EDX pattern. Traces of silicon were also found since it is used in the footwear industry as a mould-releasing agent while producing PU.

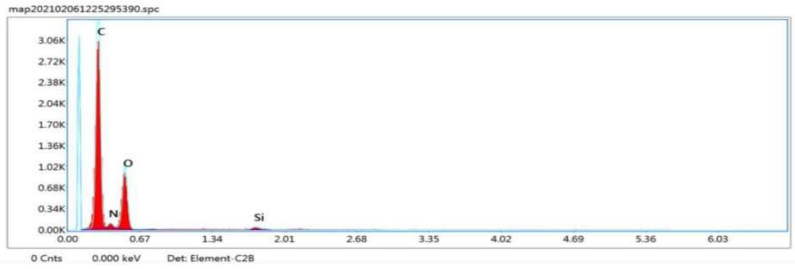

	Element	Weight %	Atomic %	Error %
▶	C K	59.64	66.15	4.62
	N K	5.81	5.53	22.11
	O K	33.30	27.73	9.67
	Si K	1.24	0.59	15.39

Figure 3.4. Elemental composition of PUW

3.2.5. Thermogravimetric analysis of PUW

Figure 3.5 illustrates the TG-DTG curves of PUW powder. The thermogram showed a two-stage decomposition that started at 260 °C and involved breaking urethane links and releasing volatile chemicals. The second stage involved the oxidation of the residues (156,157).

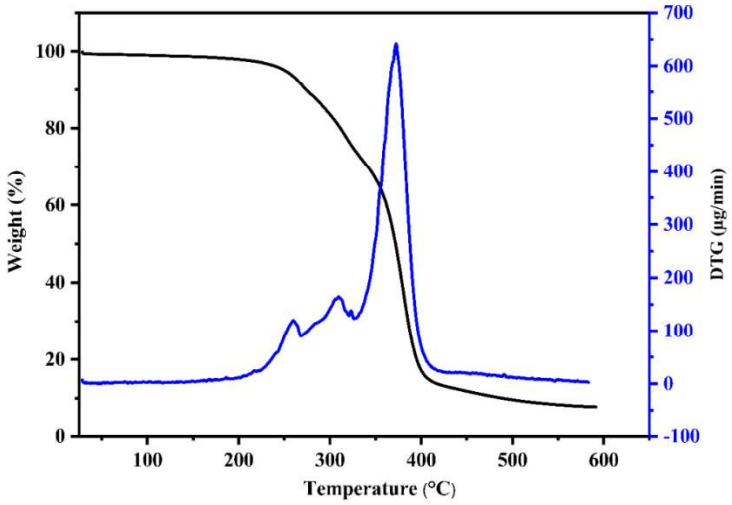

Figure 3.5. TG-DTG curves of PUW

3.3. Characterisation of light magnesium carbonate waste

The light magnesium carbonate waste (MCW) collected from the condom industry (HLL Lifecare Ltd., Thiruvananthapuram, Kerala) was characterised by FTIR, XRD, FESEM, HRTEM-EDX, BET, DLS, and TGA techniques.

3.3.1. Fourier Transform infrared spectroscopic analysis of MCW

Figure 3.6 displays the FTIR spectrum of MCW powder, denoting the essential details about the material's structure. Strong bands at 870 cm^{-1} signify the asymmetric deformation of CO_3^{2-} and are observed as doublets at 1481 and 1427 cm^{-1}, respectively, corresponding to the asymmetric stretching vibrations of C-O bonds. The carbonate group's C-O deformation (symmetric) vibration is responsible for the weak band seen at 1026 cm^{-1}. The calcite form of $CaCO_3$ has distinctive bands with notable peaks at 802 and 702 cm^{-1} (158,159).

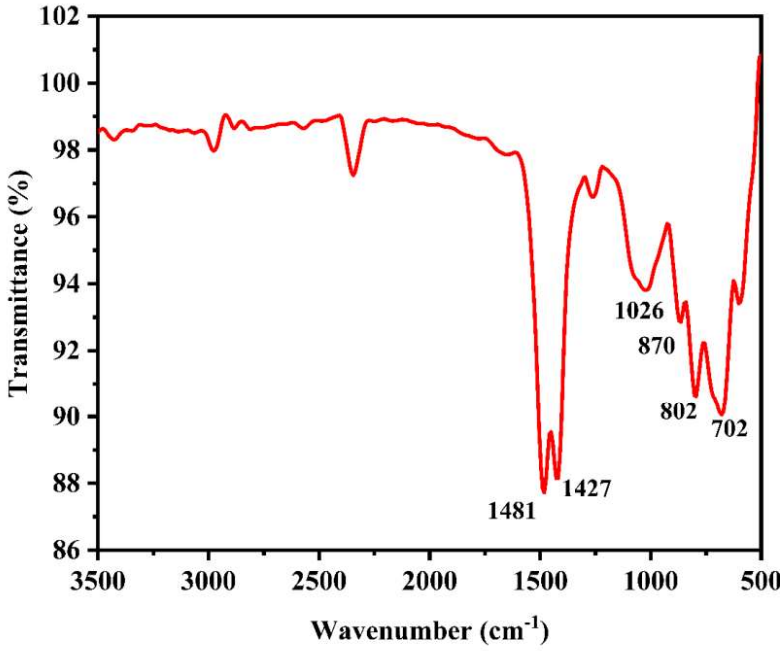

Figure 3.6. FTIR spectrum of MCW

3.3.2. X-ray diffraction analysis of MCW

Figure 3.7 shows the results of the XRD analysis used to determine the structural properties and phase of MCW powder. The characteristic peaks point to the crystalline form of the MCW powder with residues of $CaCO_3$. Peaks associated with $MgCO_3$ were found at 2θ = 32.68°, 35.82°, 43.21°, and 53.82°, respectively, which correspond to the hkl planes (104), (006), (113), and (116) and peaks associated to $CaCO_3$ at 2θ = 46.95° and 70.45° correspond to (202) and (300) planes (160,161).

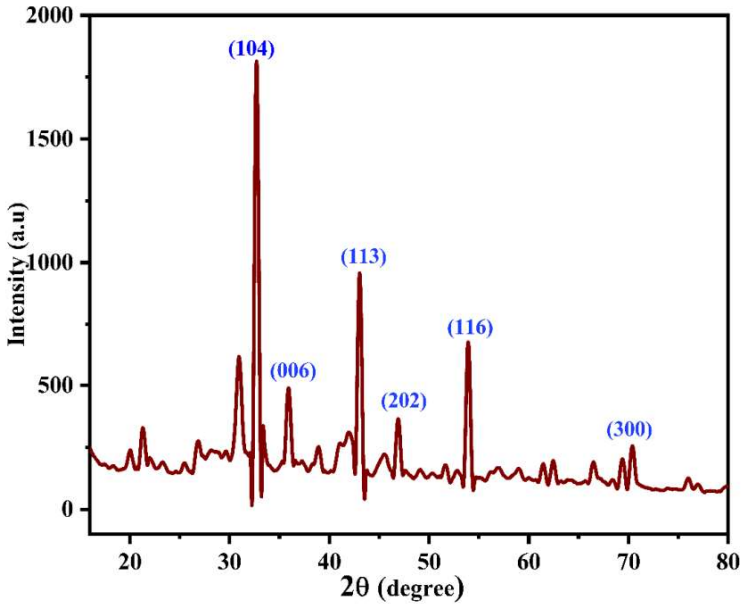

Figure 3.7. XRD pattern of MCW

3.3.3. Thermogravimetric analysis of MCW

The TGA of MCW in Figure 3.8 shows three distinct phases of MCW's deterioration. The first phase of breakdown is the removal of water from the crystallisation stage, which is completed at 236 °C. The second stage breakdown of magnesium carbonate into magnesium oxide and carbon dioxide, which occurred between 410 and 500 °C, was responsible for around 60-65 % of the total weight loss (162). In the third stage, at 600 to 800 °C, 30-35 % of $CaCO_3$ decomposes into CaO and CO_2 (163).

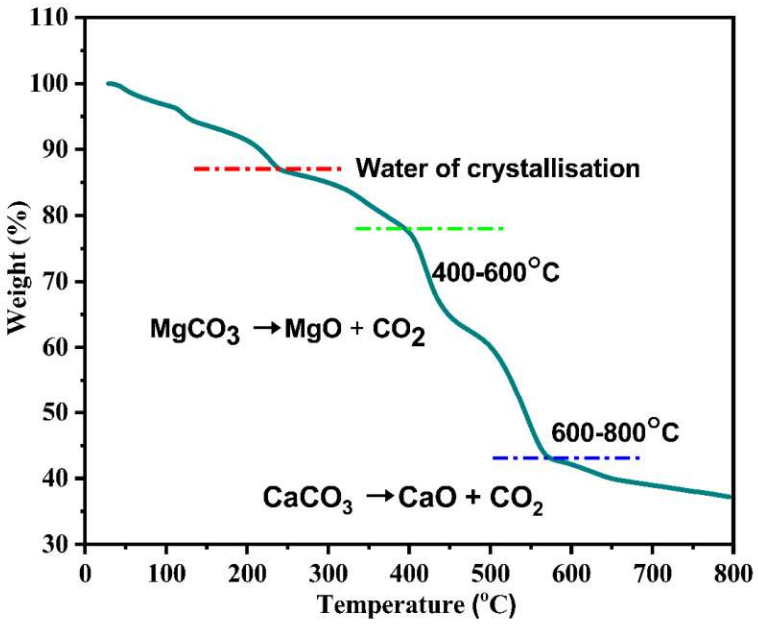

Figure 3.8. TGA curve of MCW

3.3.4. BET isotherm analysis of MCW

The nitrogen adsorption-desorption isotherms from the 16-hour BET analysis of MCW at 80 °C are shown in Figure 3.9. According to IUPAC categorisation, the obtained isotherms fall under category IV (129). Adsorbents of a mesoporous nature with pores between 6 and 10 nm in size are the most common places to find Type IV isotherms. When pore condensation occurs, the gas gets condensed as a phase that resembles liquid at a pressure (P) lower than the bulk liquid's saturation pressure (P_0). Consequently, capillary condensation is followed by hysteresis, and final saturation plateaus of different lengths can distinguish type IV isotherms. The nanosphere produces these pores, which comprise empty spaces between nanoparticles (164). The Barret-Joyner-Halenda (BJH) plot (inset of Figure 3.7) was used to analyse the MCW pore size distributions. The mean pore diameter is 9.61 nm, and the total pore volume is 1.6976 $\times 10^{-2}$ cm^3g^{-1}. As equilibrium pressure rises, the compound containing $MgCO_3$ and $CaCO_3$ has a greater adsorption capacity because of the condensation of N_2 molecules in mesoporous adsorbents at high pressures. The measured surface area, which is 7.0660 m^2g^{-1}, shows that the material has a decreased porosity as a result of the pre-treatment that was applied. The BET-specific surface area is a crucial statistic for adsorption investigations and is shown to be low due to the subpar porosity outcomes from the MCW distribution. As a result, this substance can be utilised to alter the properties of other materials to achieve desired results.

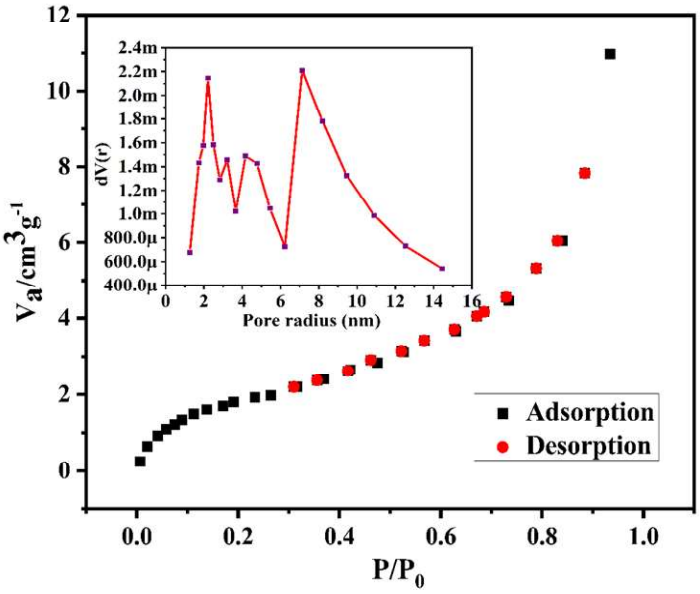

Figure 3.9. BET-adsorption-desorption isotherms of MCW (inset BJH plot)

3.3.5. Morphological analysis of MCW

Figure 3.10 (a-b) shows the results of the FESEM and HRTEM examination of the MCW and illustrates how the FESEM findings foretell the agglomerated structure of the combination of magnesium carbonate and calcium carbonate (165). The application of ultrasonication before HRTEM examination aided the separation of agglomerated nanoclusters. Figure 3.10 (b) evaluates the existence of rhombohedral nanoparticles connected to magnesium carbonate and calcium carbonate.

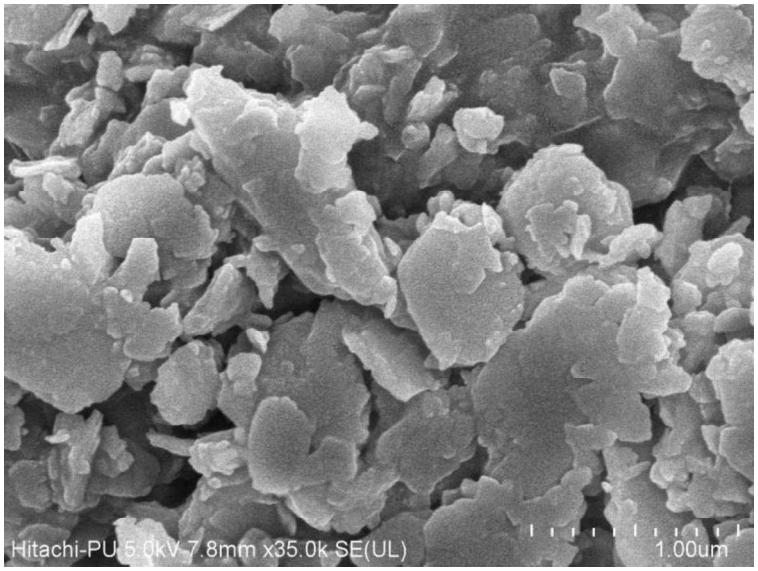

Figure 3.10 (a). FESEM image of MCW

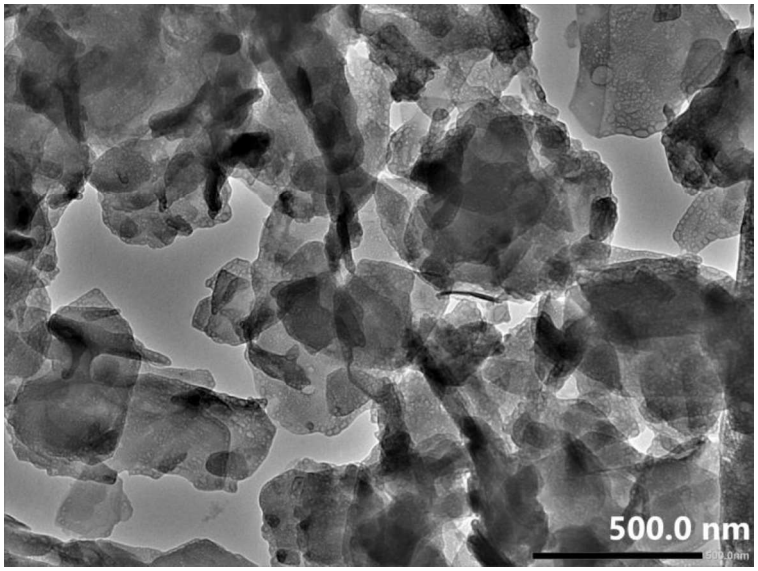

Figure 3.10 (b). HRTEM image of MCW

3.3.6. Elemental and particle size analysis of MCW

Figure 3.11 shows the result of the particle size analysis of the MCW. According to the DLS analysis, rhombohedral nanoparticles are typically between 100 and 200 nm in size. The scalenohedral $MgCO_3$ and $CaCO_3$ can produce particles between 400 and 500 nm in diameter. Figure 3.12 displays the HRTEM-EDX analysis used to perform the elemental analysis of MCW. According to Figure 3.12, magnesium (13.71 %), calcium (0.42 %), carbon (32.57 %), and oxygen (53.18 %) make up the majority of the elemental composition.

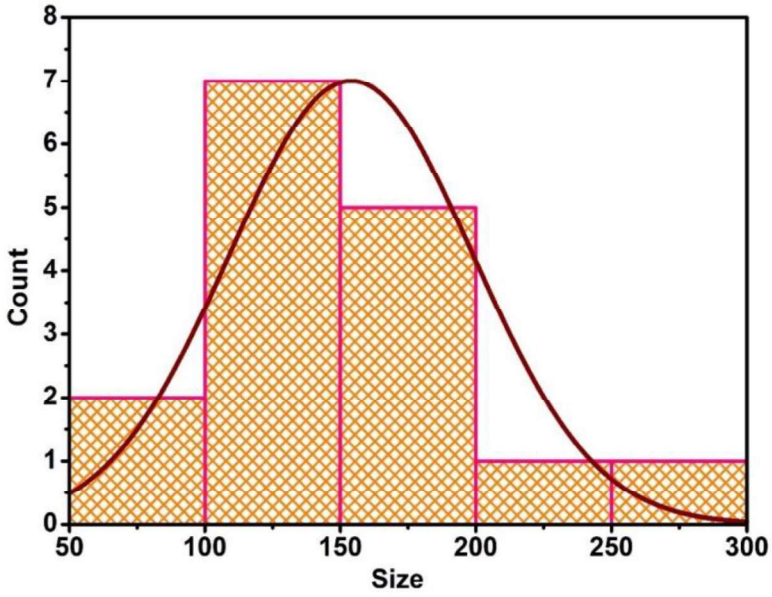

Figure 3.11. Average particle size of MCW

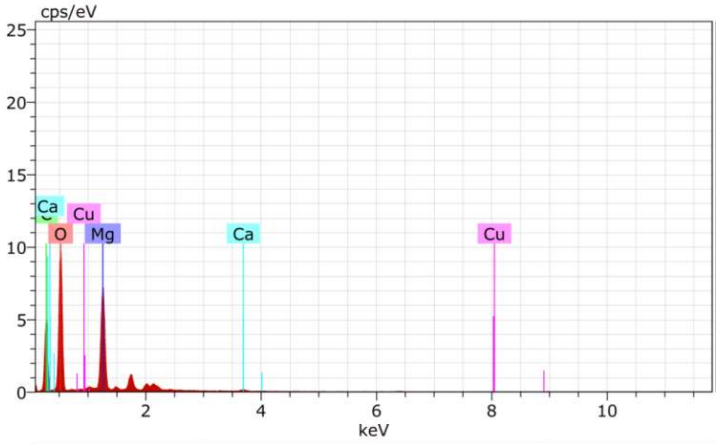

Element	Line type	Wt.%	Atomic %
Oxygen	K-series	53.18	50.27
Carbon	K-series	32.57	41.01
Magnesium	K-series	13.71	8.53
Calcium	K-series	0.42	0.16
Copper	K-series	0.11	0.3

Figure 3.12. Elemental analysis of MCW

3.4. Characterisation of sodium sulphate waste

The recovered sodium sulphate waste (SSW) collected from Ultramarine and Pigments Limited, Chennai, Tamil Nadu, was characterised by FTIR, FESEM, XRD, FESEM-EDX, and TGA techniques.

3.4.1. Fourier Transform infrared spectroscopic analysis of SSW

The chemical reliability of SSW was assessed by FTIR analysis and is given in Figure 3.13. Spectra of SSW revealed several significant peaks related to its nature. The absorption band in the range 3404-3495 cm^{-1} is due to the -OH stretching vibrations of water of crystallisation. The -OH bending modes are also present between 1600 and 1700 cm^{-1} (at 1635 cm^{-1}). This implies that during the separation

process, water has been retained by SSW. The peaks present at 1115 cm^{-1} and 615 cm^{-1} were indicative of asymmetric stretching and asymmetric bending of the SO_4^{2-} group, respectively. The bands observed below 700 cm^{-1} are attributed to both symmetric and asymmetric bending of the SO_4^{2-} group (166).

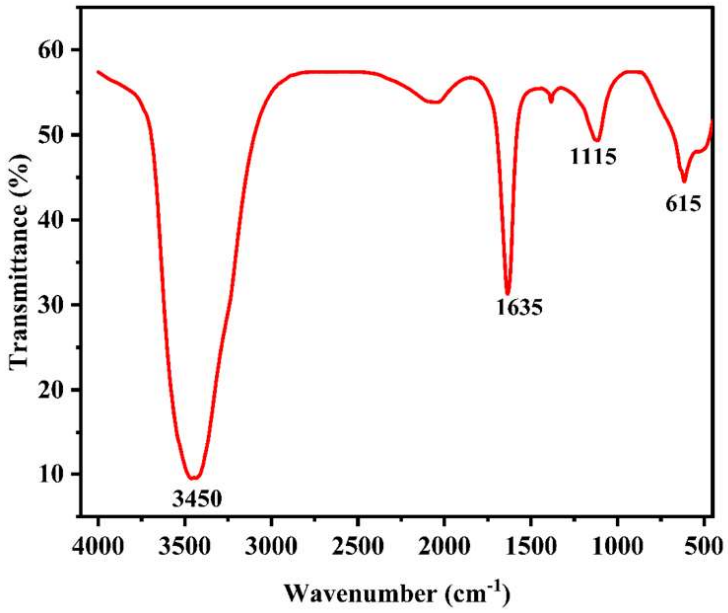

Figure 3.13. FTIR spectrum of SSW

3.4.2. X-ray diffraction analysis of SSW

The XRD pattern of SSW is given in Figure 3.14. Sharp peaks were obtained at 2θ = 27.65, 29.56, 43.44, 57.91, and 60 (JCPDS card No. 00-037-1465), which corresponds to the hkl planes, i.e., (113), (004), (041), (262), and (333), respectively, confirming the crystal structure of sodium sulphate. The SSW has undergone heating at high

temperatures during the manufacture of ultramarine blue pigment, and therefore, it often adopted the orthogonal phase (167,168).

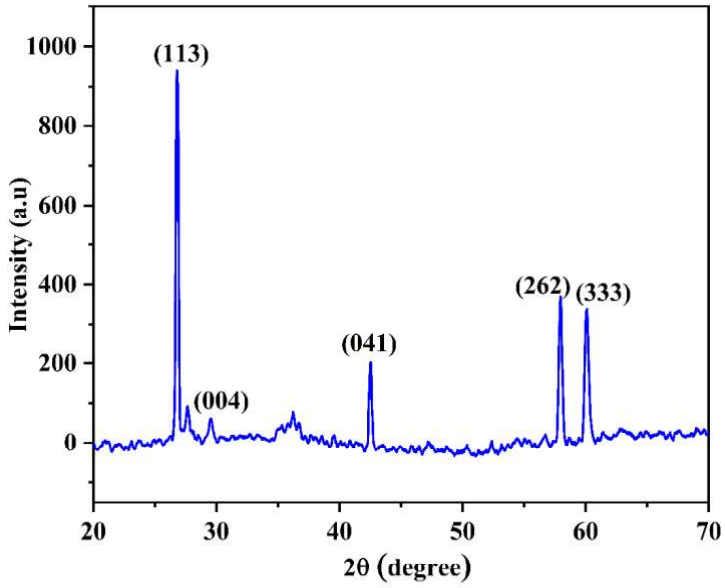

Figure 3.14. XRD pattern of SSW

3.4.3. Thermogravimetric analysis of SSW

The TGA thermogram for the SSW sample is displayed in Figure 3.15. The test run was conducted with a 100 cc/min nitrogen flow and a 10 °C/min heating rate. TG analysis confirmed that the recovered SSW crystals were completely dehydrated. In the 40 to 180 °C temperature range, the predicted weight loss, i.e., 4.8 %, is much less than that of hydrated Na_2SO_4. There was little impact on the thermally processed SSW sample between 200 and 800 °C (169,170).

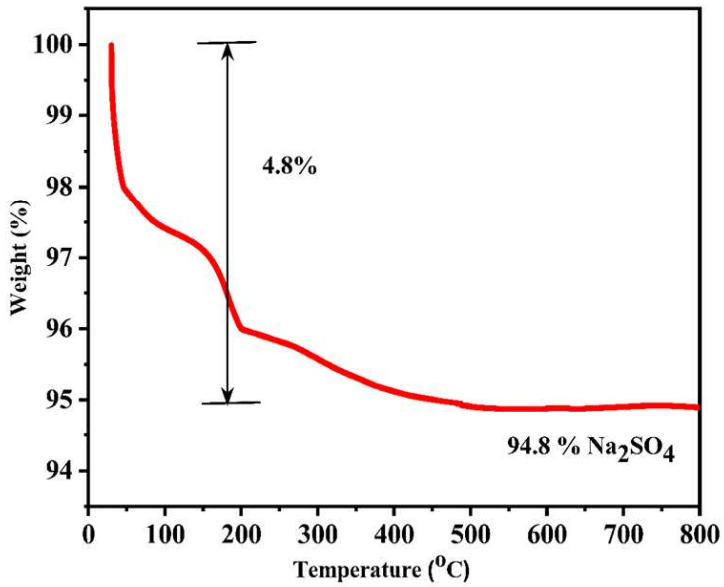

Figure 3.15. TGA thermogram of SSW

3.4.4. BET isotherm analysis of SSW

One crucial element that could influence how strong and resilient a material is its surface area (171). The SSW sample's surface area and pore size were ascertained using N_2 adsorption-desorption isotherms (172,173). A classical type-IV nitrogen isotherm with a hysteresis loop is visible in the adsorption/desorption isotherms (174). The calculated surface area of the SSW sample was found to be 1.944 m^2g^{-1}. The relative pore volume of SSW is measured to be relatively low (0.008 cm^3g^{-1}). The results demonstrate that the heating treatment may increase the surface area due to the activated form of the SSW sample. The Langmuir and BJH plots of SSW are given in Figures 3.16 and 3.17.

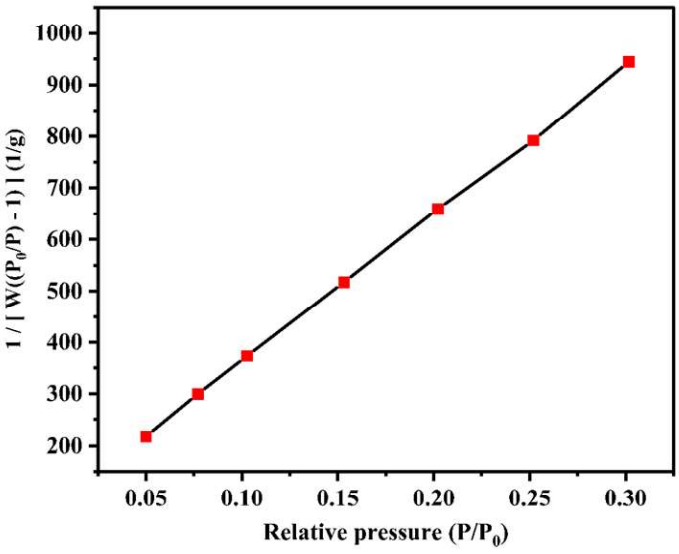

Figure 3.16. Multi-point BET plot of SSW

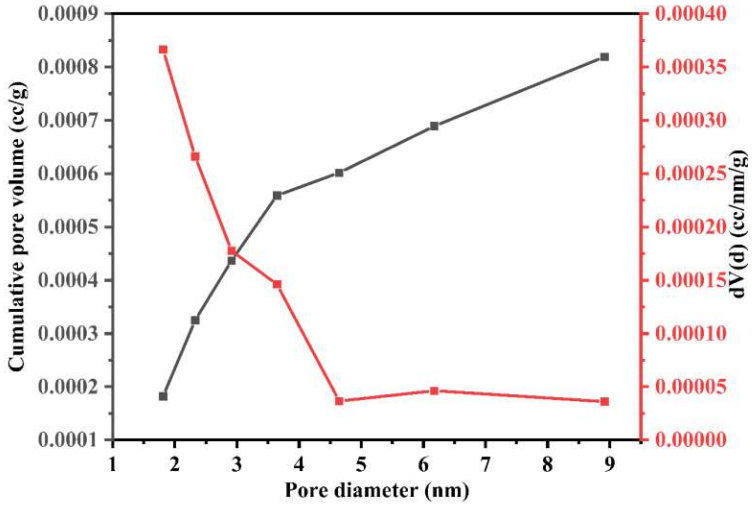

Figure 3.17. BJH plot of SSW

3.4.5. Morphological and elemental analyses of SSW

The size and surface morphological details of SSW were evaluated by FESEM analysis (Figure 3.18). The SSW sample showed octahedron geometry as a result of its processing at very high temperatures, as shown in Figure 3.18 (a-b) (175). The octahedron-type geometry consists of prismatic-like units of size varying between about 1-20 μm [Figure 3.18 (c)]. The elemental compositions obtained from the FESEM-EDX analysis ensure the presence of Na, S, and O_2 and indicate the existence of Na_2SO_4 [Figure 3.18 (d)].

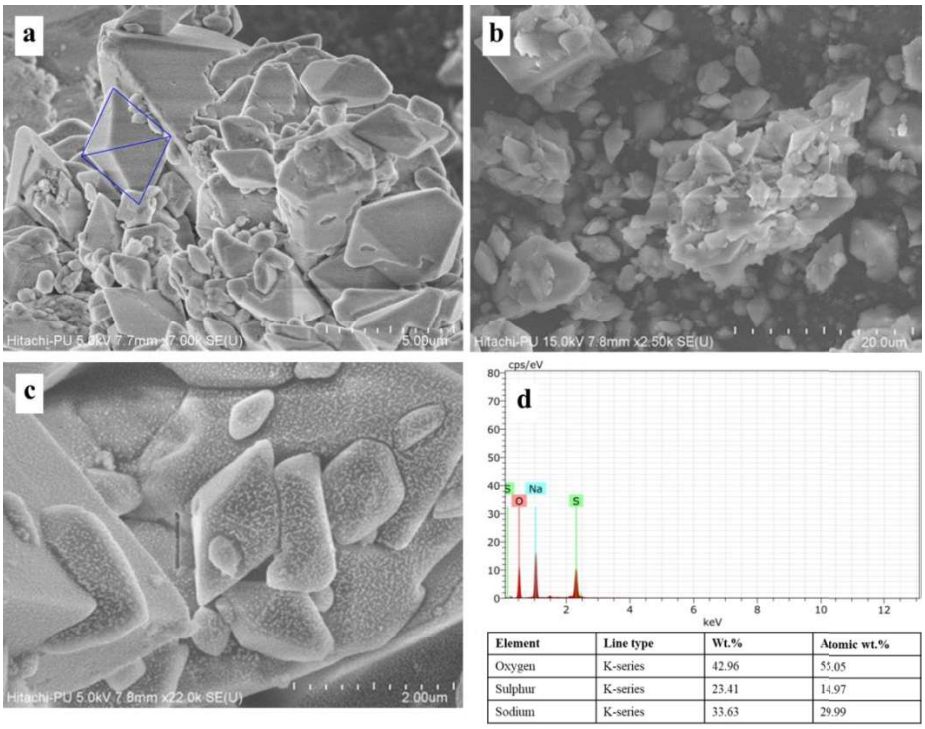

Element	Line type	Wt.%	Atomic wt.%
Oxygen	K-series	42.96	55.05
Sulphur	K-series	23.41	14.97
Sodium	K-series	33.63	29.99

Figure 3.18. FESEM and FESEM-EDX images of SSW

3.5. Characterisation of clay

Hydrated clay was collected from the English Indian Clays Ltd. (EICL), Thiruvananthapuram, Kerala and is characterised by FTIR, FESEM-EDX, and TGA techniques.

3.5.1. Fourier Transform infra-red spectroscopic analysis of clay

Figure 3.19 shows the FTIR spectrum of clay. The characteristic bands at 3690 and 3620 cm^{-1} correspond to stretching vibrations of -OH groups, and the Si-O bonds cause bands at 1115 and 1005 cm^{-1} (176,177). In addition, the bands at 780 and 675 cm^{-1} originate from the deformation vibrations of the Al-O-Si bonds, while the band at 912 cm^{-1} is attributable to the deformation vibration of the Al-OH (178,179).

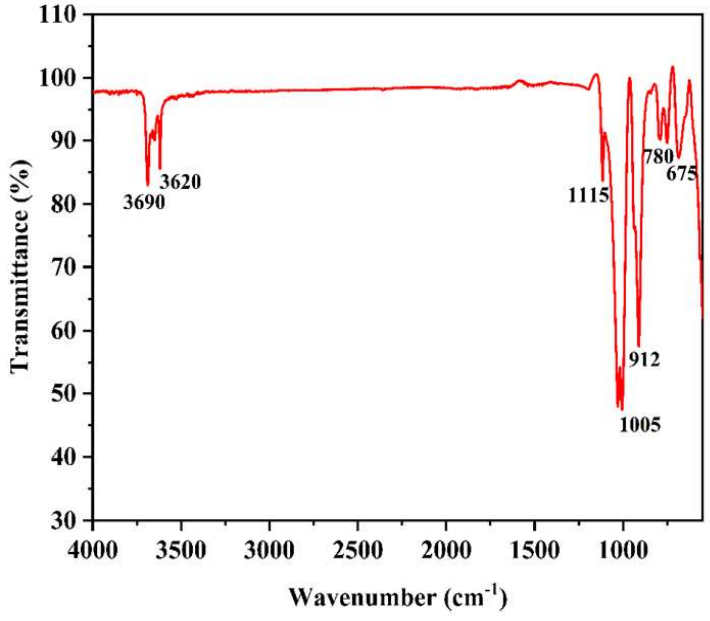

Figure 3.19. FTIR spectrum of clay

3.5.2. Elemental analysis of clay

The FESEM-EDX analysis was used to determine the clay's chemical composition, as shown in Figure 3.20 and revealed carbon, oxygen, aluminium, sulphur, silicon, and sodium as the main constituents.

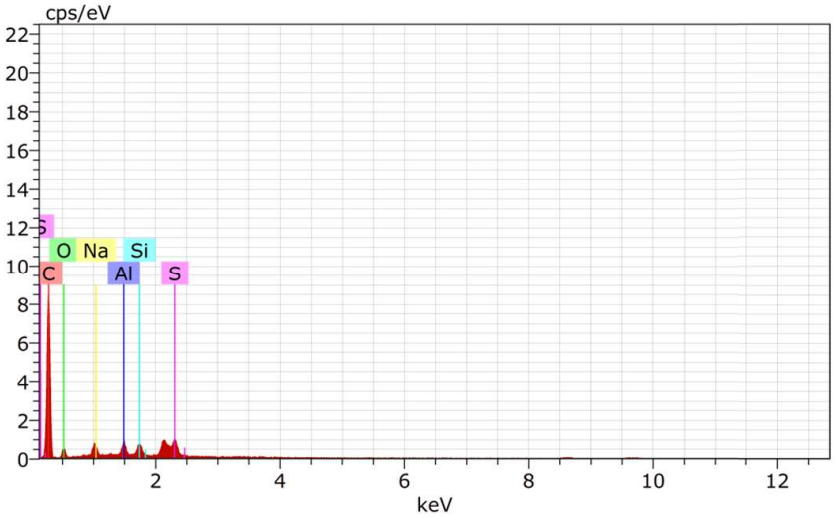

Element	Line type	Wt.%	Atomic wt.%
Carbon	K-series	81.06	87.84
Oxygen	K-series	9.61	7.82
Aluminium	K-series	1.81	0.87
Silicon	K-series	1.84	0.85
Sulphur	K-series	3.70	1.50
Sodium	K-series	1.98	1.12

Figure 3.20. Elemental analysis of clay

3.5.3. Thermogravimetric analysis of clay

TGA is used to analyse clay's thermal stability, and the TG-DTG curve is shown in Figure 3.21. Two primary stages of breakdown are visible in the thermogram. The removal of adsorbed and intercalated water from the clay causes the first loss to occur at 100 °C

and 240 °C, respectively (180). The temperature range for second weight loss is 440-670 °C, which is associated with the dehydroxylation of the various silicate phases found in clay (181).

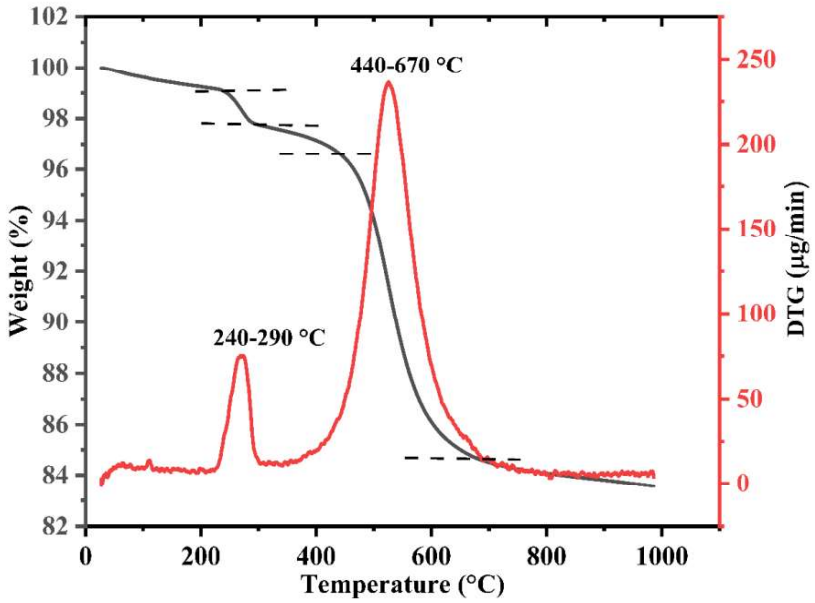

Figure 3.21. TG-DTG curves of clay

3.6. Conclusion

The collected industrial solid wastes (PUW, MCW, and SSW) were isolated from other impurities, powdered, and subjected to various analytical methods for characterisation. Additionally, the clay is also characterised. This work aims to investigate the potential use of these industrial wastes as reinforcing fillers in NR and examine the resulting composite's mechanical, thermal, and sorption properties. Clay is employed in studies of property enhancement coupled with PUW since it is already considered an excellent filler in NR.

Chapter 4
Mechanical, thermal and sorption studies of natural rubber-polyurethane waste composites

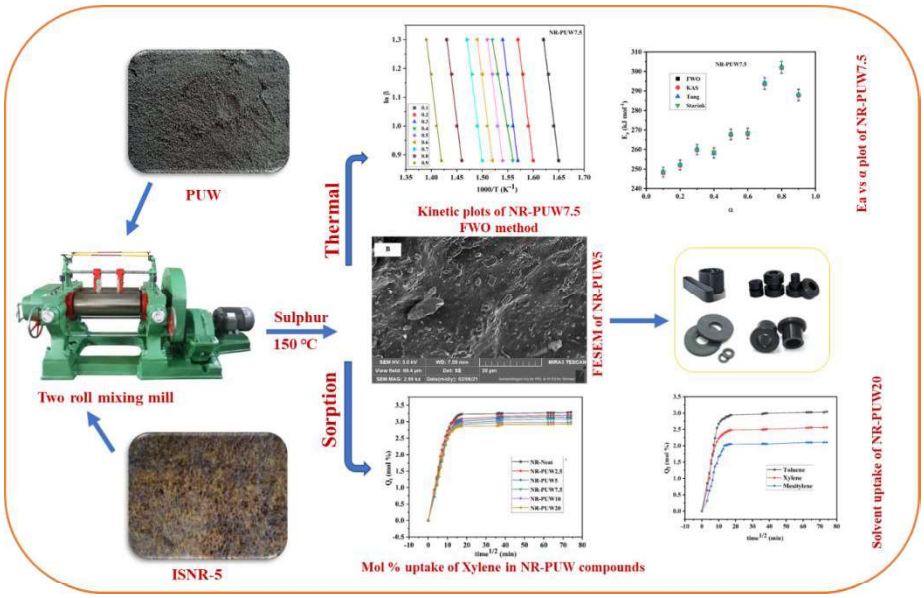

In this chapter, natural rubber-polyurethane waste (NR-PUW) composites were fabricated and thoroughly characterised. The procedures for evaluating the rheological, mechanical, thermal and sorption properties of the NR-PUW composites have been described. The Nicolais-Narkis (N-N), Lu, and Turcsányi-Pukànszky-Tüdõs (T-P-T) models were used to validate the tensile strength as well as the Einstein and Guth models to validate the Young's modulus of the fabricated composites. The reported study applies the Flynn-Wall-Ozawa (FWO), Kissinger-Akahira-Sunose (KAS), Tang, and Starink model-free methods to explore the kinetics of non-isothermal degradation using TG analysis. Various sorption parameters and the sorption characteristics of NR-PUW composites in different aromatic, aliphatic and industrial solvents have also been investigated.

Bashpa P. Mechanical, Thermal and Sorption Studies of Industrial Waste Reinforced Natural Rubber.
St. Joseph's College (AUTONOMOUS) Devagiri, University of Calicut. 2024

4.1. Introduction

Massive amounts of solid waste from numerous industries have been produced due to industrialisation, urbanisation, and economic growth (25,182). As a result, the difficulties in managing resources and disposing of garbage are also increasing quickly. In addition to posing serious environmental risks, poor disposal and handling also have detrimental effects on human health (183–185). It is crucial to treat waste effectively and sustainably, and it is unavoidable that waste management strategies be creative in order to design goods with additional value. Conventional techniques like incineration and landfilling are the least preferable because they harm the ecosystem and groundwater (186). Modern recycling practices use many different recycling procedures to replace traditional ones (187).

NR is a significant biopolymer primarily employed in the tyre industry because of its exceptional characteristics (188). Its most crucial properties are excellent strength and extraordinary fatigue resistance. NR has mediocre resistance to environmental degradation from light and heat. NR can adhere to other materials and to itself thanks to its great green strength and tack. NR-reinforced materials are, therefore, more practical for industrial purposes (189). The use of industrial waste-derived materials with strong reinforcing and processing capabilities as fillers in the rubber industry is gaining popularity due to the steep increase in the price of NR and other compounding components (190,191). NR combines with organic, inorganic, and bio-based waste additives for the desired qualities, and a

brief literature description is given in Tables 1.2 to 1.4 in the introduction part of this thesis.

The footwear industry commonly employs rigid PU as crosslinked microcellular foams to manufacture chappal and shoe soles. Due to the extensive use of PU in the footwear industry and the fact that it cannot be recycled, vast amounts are currently dumped in landfills worldwide, which poses a severe threat to the environment. The considerable impact of PUW on environmental contamination and ongoing changes in regulatory requirements have drawn attention to this issue on a global scale. Over several decades, various techniques, including mechanical degradation, incineration, and landfilling, have been tried (192,193). Alternative methods for disposing of PU goods are becoming more viable due to rising landfill costs and shrinking landfill space (194,195). PUW recycling has been explored using several techniques, including chemical processing, thermochemical processing, and mechanical recycling (196,197). The documented hygrothermal breakdown of polyester-urethane waste has led to the usage of the byproducts as fillers in NR, styrene-butadiene rubber (SBR), chloroprene, and nitrile rubber to enhance the cure and processing properties of these materials (198,199).

A developing, efficient, and cost-effective method of waste management is the mechanical recycling of the crosslinked PUW produced by the footwear industry. PUW is reused as a filler in elastomers by regrinding technology, a significant component of mechanical recycling (200,201). The use of PUW as a reinforcing filler in NR is investigated as an attempt to lower environmental pollution and production costs. The general formulation of NR compounding is

given in Table 2.9* of the Materials and Methods section. The sample designation and formulation details of NR-PUW composites are provided in Table 4.1.

Table 4.1. Sample designation and formulation of NR-PUW composites

Sample designation	NR	PUW
NR-Neat	100	0
NR-PUW2.5	100	2.5
NR-PUW5	100	5
NR-PUW7.5	100	7.5
NR-PUW10	100	10
NR-PUW20	100	20

*NR-100, ZnO-5.0, stearic acid-2.0, TMQ-1.0, CBS-0.6, TMTD-0.2 and sulphur-2.5 (in phr)

The fabricated composites underwent rheological, mechanical, thermal, and sorption investigations. Studies using established theoretical modelling methods on tensile strength and Young's modulus were also conducted to validate the experimental results. Degradation kinetics of NR-PUW composites were also studied using various model-free approaches.

4.2. Results & Discussion

4.2.1. Attenuated total reflectance-Fourier Transform infrared spectroscopic analysis

Figure 4.1 depicts the ATR-FTIR spectra of NR-Neat and NR-PUW composites, and the peaks obtained are explained in Table 4.2. An interaction between the functional groups in NR and PUW during

the curing reaction is ruled out by the lack of discernible changes in the position and intensity of peaks in the FTIR spectra.

Table 4.2. Prominent peaks in the ATR-FTIR Spectra

Band position (cm^{-1})	Assignment
2960	Symmetric and asymmetric stretching vibrations of the CH group
2911	Symmetric and asymmetric stretching vibrations of the CH_2 group
2840	Symmetric and asymmetric stretching vibrations of the CH_3 group (202)
831	Isoprene functional group (203)
1363	Symmetric vibration of CH_3 in NR
1448	Symmetric vibration of CH_2 in NR
1538	C-N-H vibration of PU confirming the presence of PUW (204)
1080	C-O-C stretching vibrations of PU (205)

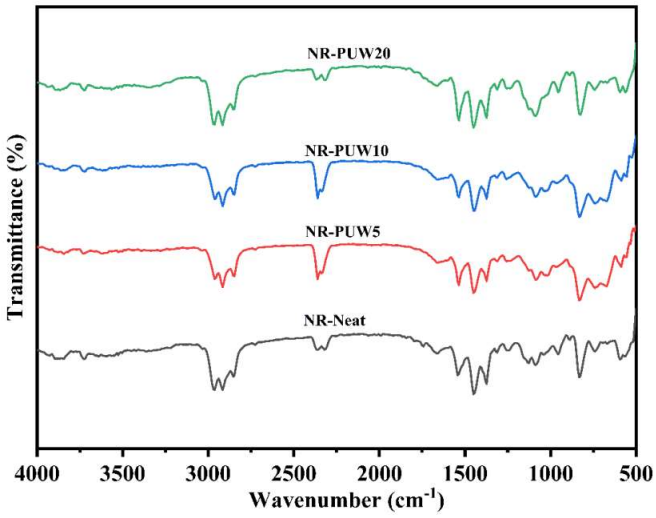

Figure 4.1. ATR-FTIR spectra NR-Neat and NR-PUW composites

4.2.2. Surface morphology of NR-Neat and NR-PUW composites

The FESEM surface morphology of NR-Neat and its composites with 5 phr, 10 phr, and 20 phr PUW, respectively, is shown in Figures 4.2 (a) to (d). These FESEM pictures demonstrate notable variations in the morphology of stress-fractured surfaces. Figure 4.2 (a) shows the presence of cavities harbouring tiny curative particles on NR, while Figure 4.2 (b) shows homogeneous PUW dispersion on NR with ridges and undulations that exhibit effective stress transfer. As the PUW loading increases, the filler particles start to aggregate. Figures 4.2 (c) and 4.2 (d) show PUW aggregates and cracks resulting from a breakdown in the shear yielding between neighbouring PUW particles.

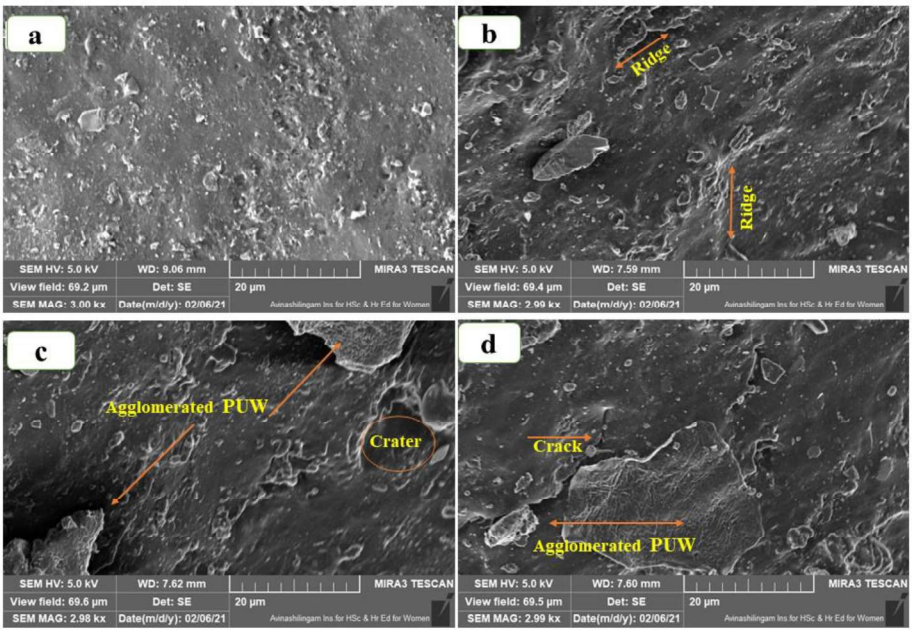

Figure 4.2. FESEM images of (a) NR-Neat, (b) NR-PUW5, (c) NR-PUW10 and (d) NR-PUW20

4.2.3. Cure characteristics of NR-PUW composites

Table 4.3 illustrates how PUW affected the cure properties of NR. All composites have identical additives (zinc oxide, stearic acid, TMQ, CBS, TMTD, and sulphur). NR-PUW composite's cure time (t_{90}) improved as filler loading was increased. The maximum torque value (M_H), which reveals the composite's stiffness, decreased upon adding filler because of the decrease in NR crosslinking brought about by the addition of PUW. It was found that the cure rate index (CRI), which measures the curing rate, dropped when the filler loading increased. The decrease in CRI could be attributed to the delayed cure brought on by PUW in NR because of the decreased matrix-filler interaction.

Table 4.3. Cure properties of NR-PUW composites

Cure characteristics	NR-Neat	NR-PUW2.5	NR-PUW5	NR-PUW7.5	NR-PUW10	NR-PUW20
Cure time, t_{90} (min)	3.67	4.1	4.18	4.35	4.38	4.4
Scorch time t_{S2} (min)	1.84	2.15	2.21	2.18	2.13	1.97
Minimum torque, M_L (dNm)	6	4.8	5.4	6.6	6.8	8.2
Maximum torque, M_H (dNm)	72.9	67.5	61.1	59.7	51.1	44.9
M_H-M_L (dNm)	66.9	62.7	55.7	53.1	44.3	36.7
Cure rate index (min^{-1})	54.65	51.28	50.76	46.08	44.44	41.15

4.2.4. Mechanical properties of NR-PUW composites

Figure 4.3. depicts the stress-strain graphs of NR-PUW composites. Composite with 5 phr PUW displayed the highest stress because the matrix and filler interacted better, increasing the potential for rupture (206).

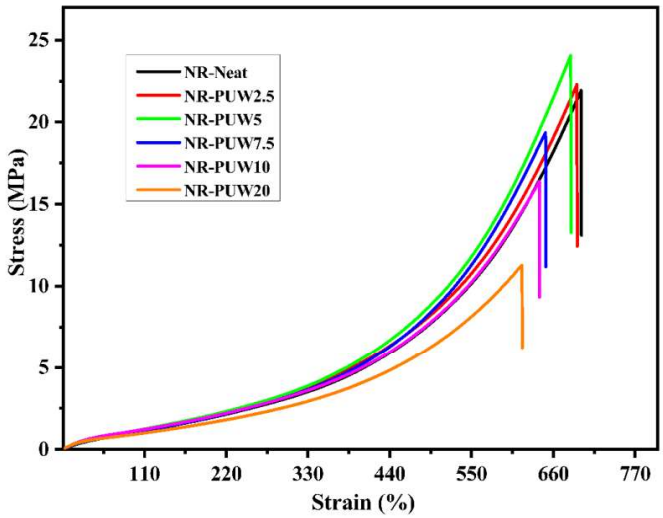

Figure 4.3. Stress-strain curves of NR-PUW composites

The tensile strength of NR-PUW composites increases up to 10 % on adding 5 phr PUW before rapidly declining with additional filler loading, as seen in the case of PU nanocomposites strengthened with nanosized zinc oxide (207). The formation of filler aggregates, which resulted in an uneven distribution of filler in NR, was the reason for the loss in tensile strength with increasing PUW loading. NR-PUW interactions are decreased, and PUW-PUW interactions are promoted when PUW volume exceeds its percolation threshold. PUW-PUW interactions did not enable stress transfer through the composites at higher filler loading (208).

Elongation at break slightly decreased up to 5 phr loading of PUW and significantly reduced at higher loading. The substantial decrease in elongation at break can be ascribed to the PUW filler in the composite, which limits the unrestricted mobility of molecular chains in the NR (209). The modulus at 300 % elongation increases by 9 % up to a filler loading of 5 phr before declining due to filler agglomeration at higher loading. A similar pattern could be seen in Young's modulus. Composite with 5 phr PUW showed maximum tear strength, and due to the filler particle's aggregation and poor dispersion on NR, it considerably decreased on further loading. Comparable actions were observed in additional systems, like ENR and NR, which were strengthened by carbon black and calcium carbonate (210). The NR-PUW composite's hardness rises steadily while abrasion loss diminishes up to 5 phr loading of PUW before rising steadily with additional loading. This may be because the matrix-filler interaction is better at lower PUW loading than at higher loading, and as a result, abrasion loss increases (69). Composites could withstand continuous strain because the compression set values increased with the filler loading. This could result from the NR-PUW link breaking down, the PUW building up under stress, or the restricted molecular chain mobility. The energy that a material absorbs in response to a specific applied deformation is called resilience. Friction is produced as the polymer chains and filler pass one another due to this deformation, releasing heat and raising the heat build-up values of NR-PUW composites. After adding PUW filler, the rebound resilience of NR exhibited a declining tendency (211). Table 4.4 gives the values of various mechanical parameters.

Table 4.4. NR-PUW composite's mechanical characteristics

Properties	**NR-Neat**	**NR-PUW2.5**	**NR-PUW5**	**NR-PUW7.5**	**NR-PUW10**	**NR-PUW20**
Hardness (Shore A)	41 ± 0.5	43 ± 0.5	44 ± 1	45 ± 1	46 ± 1.5	49 ± 1.5
Specific gravity	0.965 ± 0.005	0.969 ± 0.010	0.973 ± 0.010	0.977 ± 0.005	0.979 ± 0.017	0.983 ± 0.018
DIN abrasion loss (cc)	0.272 ± 0.15	0.260 ± 0.18	0.259 ± 0.15	0.282 ± 0.22	0.327 ± 0.18	0.339 ± 0.25
Tensile strength (MPa)	21.93 ± 0.3	22.3 ± 0.4	24.06 ± 0.2	19.36 ± 0.35	16.39 ± 0.25	11.28 ± 0.45
Elongation at break (%)	697 ± 18	692 ± 16	683 ± 20	649 ± 15	641 ± 17	618 ± 20
Modulus at 300 % elongation (MPa)	3.09 ± 0.17	3.31 ± 0.14	3.36 ± 0.16	3.18 ± 0.12	3.16 ± 0.18	2.58 ± 0.20
Young's modulus (MPa)	0.8991 ± 0.1	0.9491 ± 0.17	0.9706 ± 0.18	0.8951 ± 0.22	0.8814 ± 0.18	0.6958 ± 0.24
Tear strength (N/mm)	41.76 ± 1.2	40.41 ± 1.5	42.29 ± 1.65	39.55 ± 1.72	37.63 ± 2.2	34.96 ± 1.98
Rebound resilience (%)	78.48 ± 2.4	74.12 ± 2.8	70.25 ± 3.26	68.76 ± 3.4	63.36 ± 3.82	58.38 ± 3.46
Compression set (%)	18.68 ± 0.36	21.41 ± 0.28	24.09 ± 0.26	25 ± 0.22	26.09 ± 0.33	31.6 ± 0.32
Heat build-up (ºC)	1 ± 0.45	5 ± 0.32	7 ± 0.28	10.5 ± 0.66	15 ± 0.75	29 ± 0.82

4.2.5. Theoretical modelling of tensile strength of NR-PUW composites

The tensile strength of NR-PUW composites was confirmed, and the extent of interfacial interaction between NR and PUW was understood using various theoretical modelling tools. The composition, distribution, morphology, and interaction of the filler with the matrix all affect the mechanical properties of the composites. Three established theoretical models, namely, Nicolais-Narkis (N-N) (123), Lu (124), and Turcsanyi-Pukanszky-Tüdõs (T-P-T) (125), were used to validate the tensile strength of the composites as examined by Salam and Dong (126). Based on the interfacial characteristics of the rigid polymer-filler composites, these models typically show the tensile strength of the materials. Tensile strength values acquired empirically and those determined using these three theoretical models were compared, as shown in Figure 4.4.

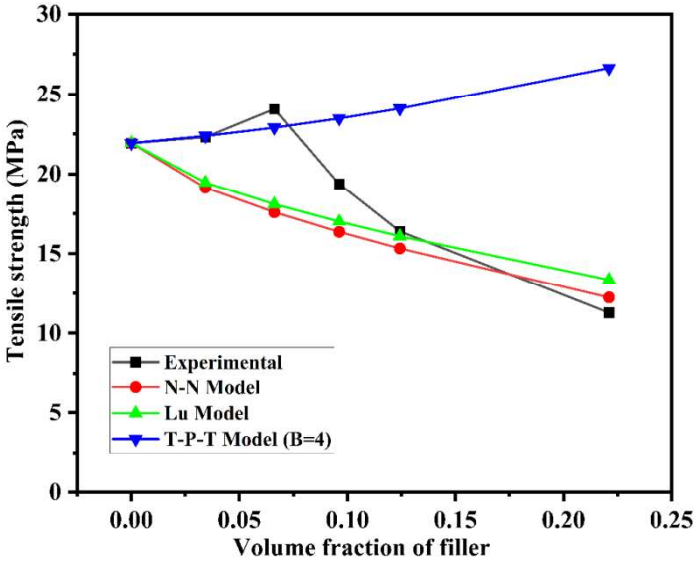

Figure 4.4. Tensile strength comparison between experimental results with theoretical models

According to Figure 4.4, up to 5 phr loading, the experimental results are consistent with the T-P-T model's (B = 4, where B is a hypothetical constant) superior matrix-filler adhesion assumption. The N-N and Lu models, which presume minimal adhesion between the matrix and the filler, are consistent with the experimental data at higher filler loadings.

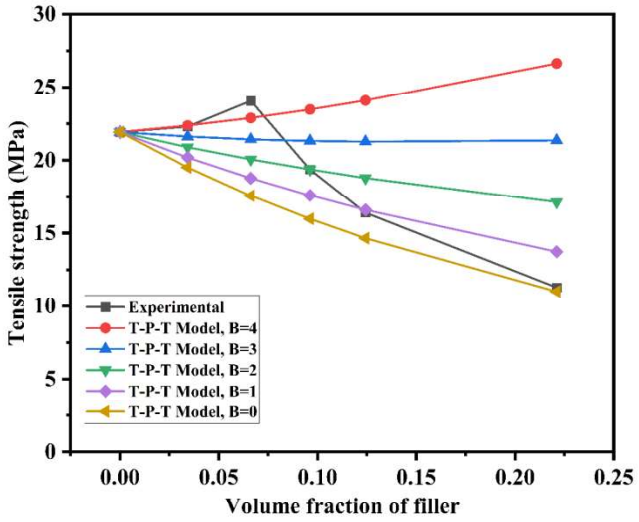

Figure 4.5. T-P-T model comparison of experimental tensile strength as a function of various B values

Figure 4.5 displays the T-P-T model used at various B values, including 0, 1, 2, 3, and 4. Matrix-filler interfacial bonding is better when B values are higher than 3 (212). By employing B value 4, the composite's experimental findings are consistent with the prediction of the T-P-T model up to 5 phr PUW loading. When the filler loading increases, the observed values deviate less from the projected values. The results align with the predictions for B values of 0 or 1, implying a weak matrix-filler interfacial interaction. The calculated value of B for

NR-PUW composites using the T-P-T model equation is displayed in Table 4.5.

Table 4.5. B values of NR-PUW composites

Composites	NR-PUW2.5	NR-PUW5	NR-PUW7.5	NR-PUW10	NR-PUW20
T-P-T model interaction parameter (B)	3.90	4.75	2.00	0.90	0.11

Higher interaction parameter (B) values and tensile strength were seen in the 5 phr PUW composite, indicating enhanced filler-matrix adherence and compatibility (213). It can be inferred from the theoretical prediction plots that up to a 5 phr loading of PUW, there is better miscibility and matrix-filler adhesion. The filler-filler cohesive contact may have overcome the matrix-filler adhesive interaction with increased filler loading, which caused the matrix-filler adhesion to collapse with higher loading.

4.2.6. Theoretical modelling of Young's modulus of NR-PUW composites

Young's modulus, or elastic modulus, is a unit used to measure and express a material's degree of stiffness. The elastic modulus is constant in all directions for an isotropic material, although many composites have anisotropy. Einstein first proposed an equation [Equation (2.8)] based on the supposition that a particle is rigid, and Guth later updated it as Equation (2.9) (127,128). Figure 4.6 compares the elastic modulus experimental results with Einstein and Guth's model.

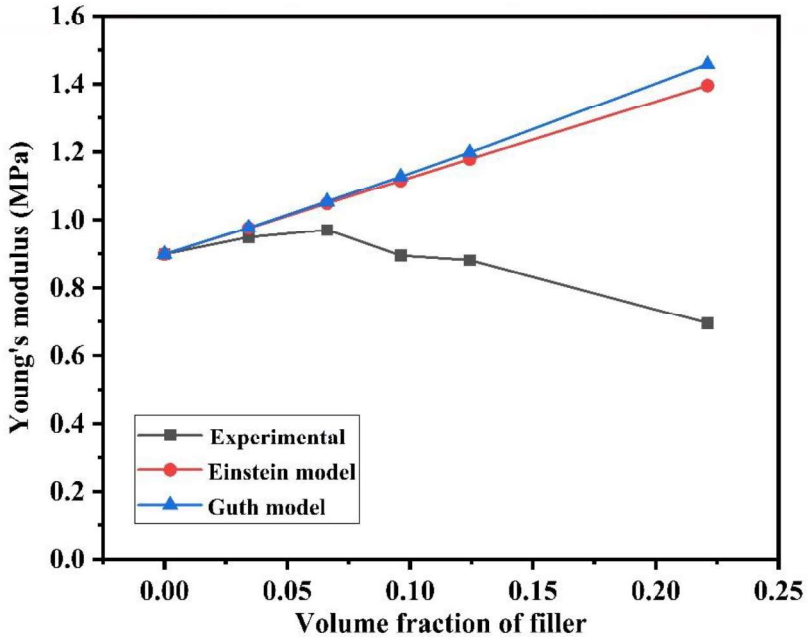

Figure 4.6. Experimental and theoretical Young's moduli comparison

At lower filler loading up to 5 phr PUW, the elastic modulus of the NR-PUW composites agrees well with the values predicted by the Guth model and the Einstein model, as seen in Figure 4.6. Improved matrix-filler adhesion and uniform filler distribution on the matrix could be the reason for this observation. However, the experimental values significantly differ from the theoretical predictions due to filler agglomeration and the absence of matrix-filler adhesion at higher PUW loading.

4.2.7. Thermogravimetric analysis of NR and NR-PUW composites

Table 4.6 presents the findings of the thermal study of NR and its PUW composites, and Figure 4.7 displays the TGA curves.

Table 4.6. Thermal degradation characteristics

Properties	NR-Neat	NR-PUW2.5	NR-PUW5	NR-PUW7.5	NR-PUW10	NR-PUW20
Onset degradation temperature, T_i (ºC)	336	339	339	341	342	342
Maximum degradation temperature, T_{max} (ºC)	386	387	387	388	389	389
Residue at 600 °C (%)	4.98	5.62	5.62	5.82	5.95	6.15

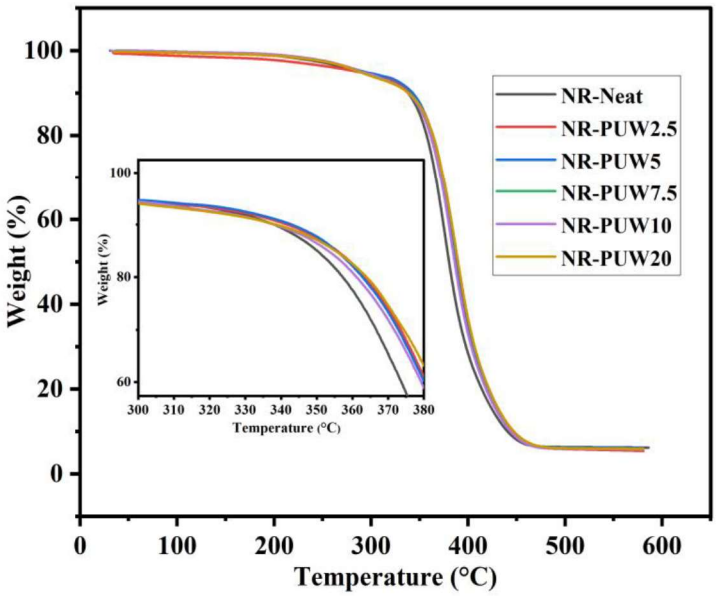

Figure 4.7. TGA curves of NR and NR-PUW composites

The initial and maximum degradation temperatures (T_i and $T_{max,}$ respectively) and residue at 600 °C were determined. NR and NR-PUW composites are degraded in one phase, and T_i of NR is about 336 °C. Integrating PUW improves the matrix's thermal stability, as evidenced by the composite's initial degradation temperature showing a noticeable rise. The integration of PUW on NR does not affect the maximum degradation temperature. Increasing PUW in all composites at the same temperature increases the amount of residue at 600 °C. The TGA data unequivocally demonstrate the composite's better thermal stability relative to NR.

4.2.8. Thermal degradation kinetics

TGA has been used to investigate the thermal stability and degradation dynamics of NR-PUW composites. Isoconversional model-free approaches like Flynn-Wall-Ozawa (FWO) (133,134), Kissinger-Akahira-Sunose (KAS) (135,136), Tang (137,138) and Starink (139,140) were proven to be effective for interpreting the kinetics of thermal degradation. Thermal degradation kinetics is vital because it clarifies the reaction mechanism and provides additional insight into the energy barriers for different processes (214). The FWO, KAS, Starink, and Tang methods were employed to compute E_a at various conversion levels ranging from 0.1 to 0.9, and for each, the least square method was used to fit a straight line. All composites displayed the same trend, and all model's neat and composite plots with 7.5 phr PUW are provided in Figures 4.8 - 4.11. The correlation coefficient values obtained for all linear fits demonstrate a robust linear link between the heating rate and temperature, which vary from 0.97 to

0.99. This is true for all the applied kinetic methods. The four applied model's various approximations cause a modest difference in E_a values due to the different approximations used in the employed models. Table 4.7 lists the calculated E_a for all conversions based on the graphs obtained.

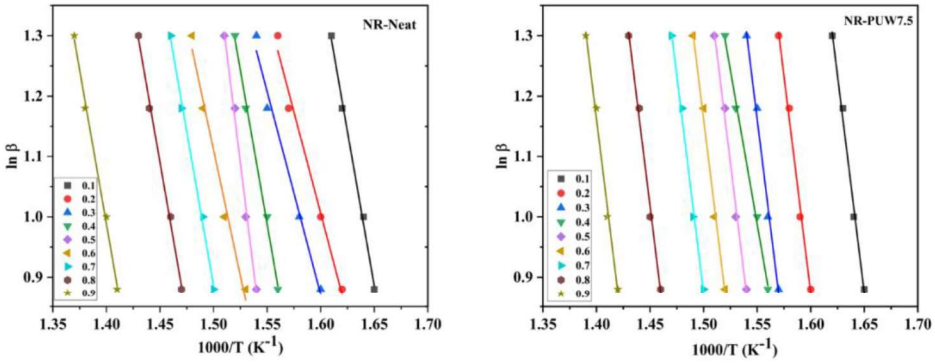

Figure 4.8. Kinetic plots of NR-Neat and NR-PUW7.5 by FWO method

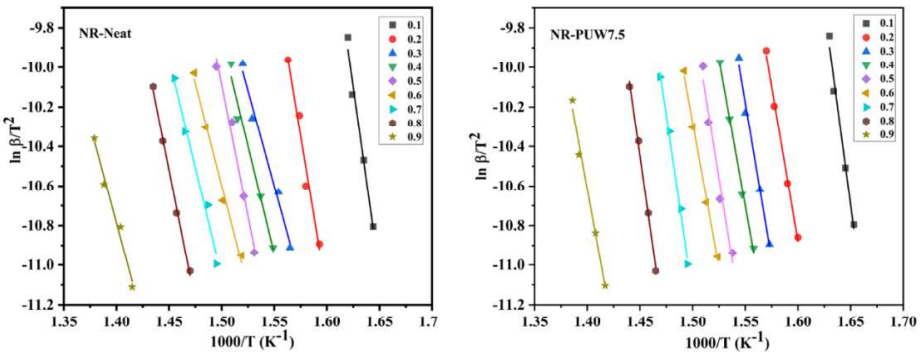

Figure 4.9. Kinetic plots of NR-Neat and NR-PUW7.5 by KAS method

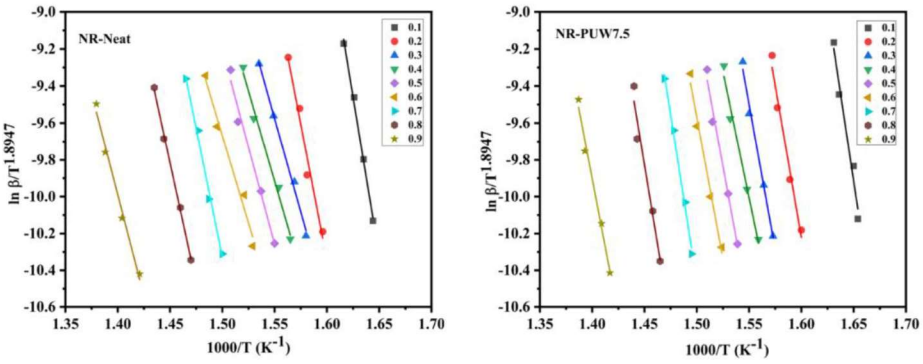

Figure 4.10. Kinetic plots of NR-Neat and NR-PUW7.5 by Tang method

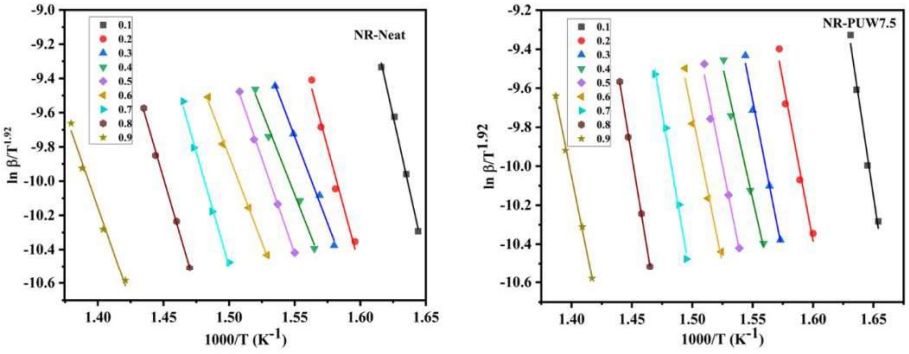

Figure 4.11. Kinetic plots of NR-Neat and NR-PUW7.5 by Starink method

Table 4.7. E_a values for FWO, KAS, Tang and Starink methods

Sample →		NR-Neat	NR-PUW2.5	NR-PUW5	NR-PUW7.5	NR-PUW10
Method ↓	**α**	**E_a ($kJmol^{-1}$)**	**E_a ($kJmol^{-1}$)**	**E_a ($kJmol^{-1}$)**	**E_a ($kJmol^{-1}$)**	**E_a ($kJmol^{-1}$)**
FWO	0.1	123.94	163.09	171.79	248.18	190.60
	0.2	129.81	181.67	184.05	252.01	177.29
	0.3	137.90	187.37	215.53	259.74	199.42
	0.4	148.52	210.52	191.27	255.17	218.93
	0.5	156.67	213.06	232.66	267.63	207.12
	0.6	157.38	215.71	241.33	248.17	224.12
	0.7	174.66	211.17	247.35	293.64	230.63
	0.8	194.16	268.68	233.98	301.9	187.08
	0.9	185.75	176.04	173.45	257.80	198.07
KAS	0.1	123.23	162.96	171.39	248.20	190.08
	0.2	129.11	180.09	183.99	251.82	176.88
	0.3	137.30	187.35	215.51	259.67	198.79
	0.4	148.27	210.54	190.88	255.35	218.63
	0.5	156.15	212.81	232.32	267.43	206.57
	0.6	157.48	215.47	241.25	247.83	223.80
	0.7	174.19	210.53	247.39	293.58	230.48
	0.8	193.76	268.76	233.72	301.93	187.15
	0.9	184.70	175.73	173.09	257.65	197.50

Tang	0.1	123.76	163.49	171.93	248.73	190.61
	0.2	129.66	180.40	184.55	252.37	177.44
	0.3	137.87	187.91	216.07	260.30	199.35
	0.4	148.84	210.80	191.45	255.92	219.20
	0.5	156.73	213.38	232.90	268.00	207.14
	0.6	158.06	216.05	241.83	248.41	224.38
	0.7	174.78	211.12	247.98	294.17	231.07
	0.8	194.36	269.36	234.32	302.54	187.75
	0.9	184.32	176.36	173.71	258.27	198.12
Starink	0.1	123.63	163.35	171.80	248.60	190.49
	0.2	129.53	180.27	184.41	252.24	177.30
	0.3	137.73	187.78	215.94	260.09	199.21
	0.4	148.70	210.67	191.32	255.79	219.07
	0.5	156.59	213.25	232.76	267.87	207.01
	0.6	157.48	215.91	241.69	248.27	224.24
	0.7	174.64	210.98	247.84	294.03	230.93
	0.8	194.22	269.22	234.18	302.09	187.61
	0.9	185.17	176.21	173.56	258.11	197.97

The initial lower E_a values imply that the kinetics of the early stages of degradation are restricted by weak link initiation. The higher E_a values observed during the later stages indicate that the degradation of composites becomes relatively constrained by the random scission initiated due to the initial degradation (215,216). All composites demonstrated higher E_a values for thermal degradation than NR-Neat, showing increased thermal stability on PUW addition. A rise in the composite's E_a values could be attributed to the mobility constraint of the polymer chains with higher PUW loading. Due to filler aggregation, E_a values of composites were found to drop after 7.5 phr PUW. The four kinetic model's E_a values all agree well with one another, demonstrating the applicability of these techniques to the investigation of thermal degradation.

4.2.9. Activation energy dependency on degree of conversion

The kinetics of the thermal degradation can be predicted using the dependence of activation energy (E_a) on the degree of conversion (α). According to Vyazovkin et al., the variation of E_a indicates that the thermal degradation process has numerous steps, each contributing equally to the overall rate (217). Figure 4.12 shows the variance of E_a for various conversion rates for NR-Neat and NR-PUW7.5.

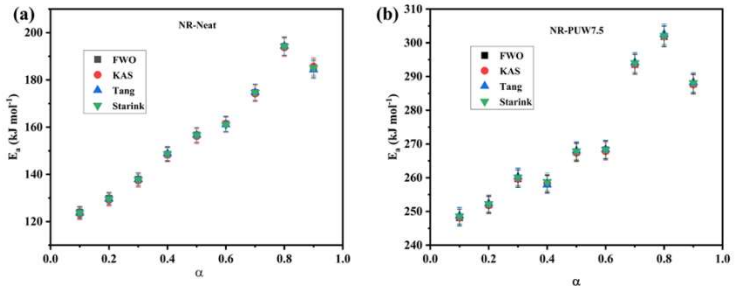

Figure 4.12. Variation of E_a with α for (a) NR-Neat and (b) NR-PUW7.5

Figure 4.12 (a) depicts a gradual increase in E_a values with an increase of α up to 0.8 in the case of NR-Neat. Then, it presents a declining trend during the latter stages, indicating the completion of degradation. Intriguingly, the NR-PUW composites exhibit an atypical relationship with α and a representative plot of NR-PUW7.5 is given in Figure 4.12 (b). The E_a values of composites are higher than those of NR-Neat, proving their better thermal stability. The complicated reaction steps in the degradation process are readily visible in the fluctuation in E_a obtained for the composites at higher conversion, demonstrating the multistep reaction path (218). The aforementioned findings indicate that all the employed model-free approaches furnished comparable E_a values across the whole conversion range under investigation. So, it is possible to suggest isoconversional models for precisely predicting the kinetics of thermal degradation of various NR composites.

4.2.10. Sorption properties of NR-PUW composites

The behaviour of different organic solvents as they move through various polymers and rubbers is of tremendous technological significance since it is crucial to several barrier applications (143,219). Various sorption characteristics and parameters were investigated, determined, and described below. Solvents like toluene, mesitylene, hexane, xylene, and petrol were employed to study the sorption behaviours of NR-PUW composites.

4.2.10.1. Mol % uptake of solvents

The plot of percentage uptake (Q_t %) of various solvents against the square root of time was drawn. The Q_t % is calculated using the Equation (2.21). All curves in each solvent are comparable, and Figure 4.13 shows a typical plot in toluene. As observed, swelling begins quickly and then slows to a plateau at equilibrium swelling. Due to a considerable concentration gradient and high levels of solvent stress, higher swelling is experienced in the initial stage. The concentration difference during equilibrium swelling is essentially non-existent (220).

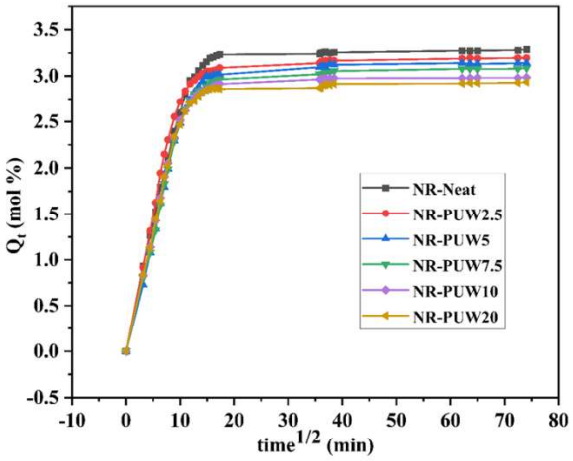

Figure 4.13. Mol % uptake of toluene through different NR-PUW composites at 30 ºC

4.2.10.2. Effect of filler loading

Flexible chains in NR-Neat showed the most significant solvent absorption. Lower sorption occurs due to the mobility of the polymer chains being constricted and becoming a barrier to the penetrant when

the amount of filler in NR increases. The fillers create physical and chemical crosslinks with the polymer chains, causing some immobilisation in the polymer segments, preventing the rearrangement of the polymer chain during solvent ingression, and reducing the free volume in the composites. This resistance to the penetrant's path results from these effects. Due to reduced free volume and the mobility of the polymer chains, solvent uptake reduces as filler concentration rises. The nature of the filler, degree of adhesion, and compatibility with the matrix all affect solvent diffusion in polymer composites. The filler occupies the polymer matrix's empty space and creates a difficult pathway for molecules trying to penetrate it. The filler's volume fraction and the particle's shape and orientation influence how tortuous the material is. The smaller transport area in the filled system and the tortuous path lower the solvent uptake (221,222). As can be seen from Figure 4.13, the composite with 20 phr PUW showed the lowest solvent absorption.

4.2.10.3. Effect of penetrant size

Table 4.8 lists the equilibrium mol % (Q_∞) values of the NR-Neat and NR-PUW composites in various solvents. The results are in the following order: toluene > xylene > mesitylene > petrol > hexane. The Hildebrand solubility parameter (δ) difference between the matrix and solvents can be used to explain this tendency. NR, toluene, xylene, mesitylene, and hexane each have δ values 16.6, 18.3, 18.2, 18 and 14.4, respectively. For toluene and xylene, the difference in value is smaller, resulting in the maximum solvent uptake. Due to the high solubility parameter difference and higher molar volume, hexane has

demonstrated minor diffusion compared to other solvents (223). Despite the closer δ values among xylene, mesitylene and toluene, both xylene and mesitylene have greater penetrant size and steric effect, which hinder their penetration through the composite. Petrol contains trace levels of olefins, ethanol, and a combination of other hydrocarbons such as paraffin, cycloalkanes, and benzene, according to Indian Oil Corporation Ltd.'s BS-VI criteria. Because of its composition, petrol has a larger average δ value than hexane, resulting in a higher petrol diffusion. The existence of hydrocarbons with a smaller molecular mass that may readily permeate the NR matrix could also be the cause of petrol's higher δ value (224). The solvent uptake of NR-PUW20 composite in various aromatic solvents is given in Figure 4.14.

Table 4.8. NR-PUW composite's Q_∞ values for different solvents

Sample	Q_∞ (mol %)				
	Toluene	**Xylene**	**Mesitylene**	**Hexane**	**Petrol**
NR-Neat	3.26	3.02	2.18	1.33	2.91
NR-PUW2.5	3.20	3.01	2.14	1.30	2.90
NR-PUW5	3.19	2.99	2.12	1.30	2.84
NR-PUW7.5	3.17	2.99	2.09	1.27	2.87
NR-PUW10	3.14	2.98	2.07	1.27	2.81
NR-PUW20	3.04	2.60	2.04	1.23	2.73

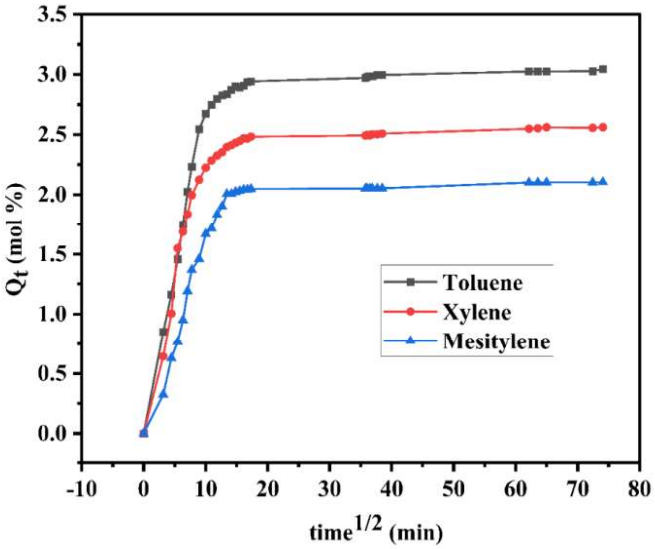

Figure 4.14. Solvent uptake of NR-PUW20 in various solvents

4.2.11. Diffusion coefficient, sorption coefficient, and permeation coefficient

Tables 4.9 and 4.10 show the values of the sample's permeation (P), sorption (S), and diffusion (D) coefficients in various solvents at room temperature. In all solvents, it is found that D, S, and P values steadily decline as the filler content rises. A decrease in free space, filler-matrix interaction at increased loading, filler-filler network development, and reduced chain mobility of polymers could all be contributing causes for the above observation. Another critical factor in the diffusion process is the penetrant's size; as it gets bigger, more energy is needed to facilitate the smooth transition of positions between the solvent molecule and the polymer chains (225).

Table 4.9. Values of D, S, and P of NR-Neat and NR-PUW composites in aromatic solvents

Sample ↓	Diffusion coefficient (D) × 10^{-4} (cm^2s^{-1})			Sorption coefficient (S)			Permeation coefficient (P) × 10^{-4} (cm^2s^{-1})		
	Toluene	Xylene	Mesitylene	Toluene	Xylene	Mesitylene	Toluene	Xylene	Mesitylene
NR-Neat	45.20	40.51	7.19	2.80	2.09	2.55	126.60	84.62	18.34
NR-PUW2.5	41.32	39.62	6.39	2.79	2.00	2.53	115.01	79.35	16.18
NR-PUW5	38.04	33.61	6.87	2.71	2.09	2.55	103.02	70.17	17.55
NR-PUW7.5	37.52	32.52	6.85	2.70	2.14	2.47	101.50	69.53	16.97
NR-PUW10	32.27	30.32	7.19	2.70	1.99	2.55	87.20	60.24	18.34
NR-PUW20	35.13	30.26	6.05	2.64	2.55	2.41	92.78	77.39	14.58

Table 4.10. D, S, and P values of NR-Neat and NR-PUW composites in petrol and hexane

Sample ↓	Diffusion coefficient (D) × 10^{-4} (cm^2s^{-1})		Sorption coefficient (S)		Permeation coefficient (P) × 10^{-4} (cm^2s^{-1})	
	Hexane	Petrol	Hexane	Petrol	Hexane	Petrol
NR-Neat	1.65	18.07	1.09	2.02	1.80	37.75
NR-PUW2.5	1.52	17.53	1.06	1.99	1.61	34.91
NR-PUW5	1.48	15.72	1.04	1.98	1.55	31.14
NR-PUW7.5	1.32	14.85	1.04	1.97	1.36	29.35
NR-PUW10	1.28	14.47	1.03	1.90	1.32	27.52
NR-PUW20	0.78	16.07	1.01	1.90	0.79	30.62

4.2.12. Mode of transport

Equation (2.29) can be used to evaluate the transport mechanism. When the chain relaxation exceeds the solvent diffusion rate ($n = 0.5$), the transport is referred to as Fickian. When *n* equals 1, the transport is referred to as non-Fickian, meaning solvent penetration exceeds chain relaxation. The conveyance is considered anomalous if the value falls between 0.5 and 1. Table 4.11 presents the results of the linear regression analysis of log (Q_t/Q_∞) against the log t plot, which was used to determine *n* and *k* values for the NR-Neat and NR-PUW composites.

According to the data, the values of *n* for xylene and toluene follow the Fickian transport mechanism. Simultaneously, hexane, petrol, and mesitylene displayed anomalous behaviour. The delayed and viscous polymer chain relaxation following filler replenishment is the cause of the anomalous mode. The value of *k* is used to evaluate the polymer's structural properties. Additionally, it offers insight into the way solvent and matrix molecules interact. The exact values of *k* discovered in the utilised solvents show how similarly the matrix and the solvents interacted (226). No correlation exists between *n* and the quantity of filler added to NR.

Table 4.11. Values of *n* and *k* for NR-PUW composites in different solvents

Sample ↓	*n*					*k*				
	Toluene	**Xylene**	**Mesitylene**	**Hexane**	**Petrol**	**Toluene**	**Xylene**	**Mesitylene**	**Hexane**	**Petrol**
NR-Neat	0.51	0.50	0.60	0.65	0.57	0.34	0.35	0.25	0.32	0.29
NR-PUW2.5	0.51	0.52	0.54	0.65	0.59	0.34	0.33	0.29	0.35	0.32
NR-PUW5	0.50	0.51	0.63	0.60	0.55	0.36	0.33	0.24	0.35	0.31
NR-PUW7.5	0.50	0.51	0.63	0.67	0.56	0.34	0.34	0.24	0.33	0.35
NR-PUW10	0.51	0.50	0.59	0.58	0.58	0.35	0.36	0.25	0.32	0.30
NR-PUW20	0.50	0.50	0.62	0.55	0.55	0.36	0.36	0.25	0.37	0.30

4.3. Conclusion

The NR-PUW composites were prepared by two roll mill mixing method and characterised using ATR-FTIR, FESEM, and TGA techniques. The fabricated composite's curing, mechanical, thermal, and sorption properties were examined, along with the viability of using rigid thermoset polyurethane waste - a byproduct of shoe sole manufacturing as an effectual reinforcing filler in NR. NR composites with 5 phr PUW exhibited significantly higher tensile strength, abrasion resistance, modulus at 300 % elongation, and tear strength than NR-Neat. Other mechanical parameters such as hardness, heat build-up, and compression set increased on the increase of filler loading. NR-PUW composite's surface morphology by FESEM demonstrated that PUW was uniformly dispersed on the NR surface up to 5 phr loading. The N-N, Lu, and T-P-T models were used to validate the findings of the tensile strength test. At B = 4, experimental data demonstrated significant conformity with the T-P-T model up to 5 phr PUW loading. The obtained Young's modulus values were tested with the Einstein and Guth models and showed good agreement up to 5 phr loading of PUW. This relationship with theoretical models demonstrates unequivocally that PUW adheres to NR surface up to 5 phr PUW loading.

Thermal investigation of NR-PUW composites showed improved thermal stability on adding PUW compared to NR-Neat. TGA examined the thermal degradation kinetics of the NR-PUW composites. Isoconversional, model-free FWO, KAS, Tang, and Starink approaches were used to ascertain the E_a values for the

breakdown of NR-Neat and the composites. During the thermal breakdown process, these isoconversional models were helpful in tracking the paths and predicting changes in E_a. The four employed isoconversional models predicted multistep deterioration kinetics for the produced composites.

Toluene has a higher swelling behaviour for the fabricated NR-PUW composites than the other solvents used. In all solvents, solvent intake reduces as filler loading increases. Kinetic parameters like diffusion, sorption, and permeation coefficients were assessed. With toluene and xylene, the method of transportation is consistent with Fickian theory, but with mesitylene, hexane, and petrol, it showed anomalous transport behaviour.

The enhanced mechanical, thermal, and sorption properties of the fabricated NR-PUW composites make them highly promising for producing common industrial rubber goods. Additionally, this work offers insight into tackling environmental pollution concerns by considering the possibility of reutilisation of PUW from the footwear industry in a circular economy perspective to develop a more economical, efficient, and high-performance composite.

Chapter 5
Mechanical, thermal and sorption studies of natural rubber-magnesium carbonate waste composites

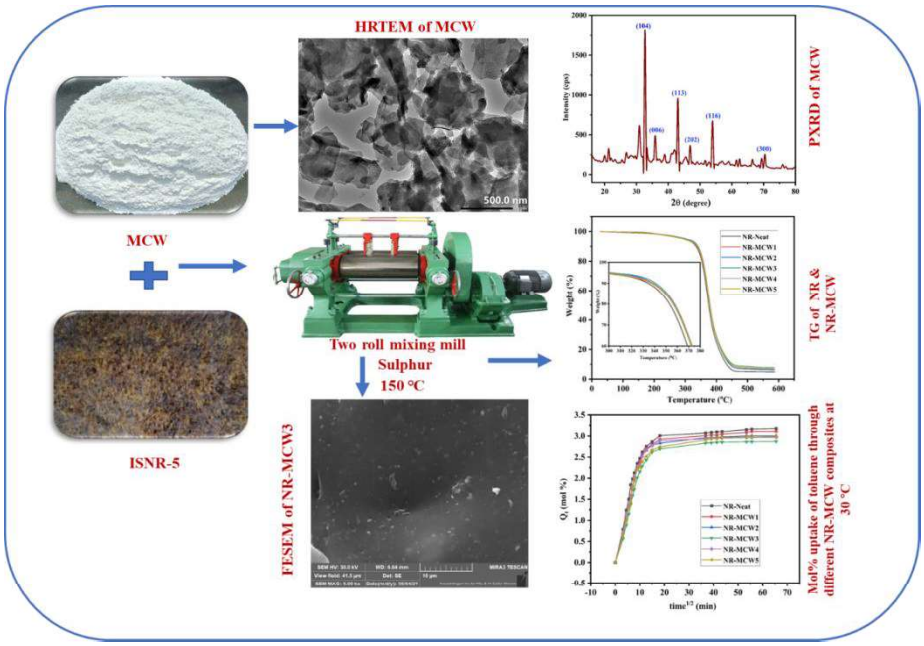

This chapter describes the fabrication and characterisation of natural rubber-magnesium carbonate waste (NR-MCW) composites. The curing, mechanical, thermal and sorption properties of the NR-MCW composites have been investigated and described. The experimental Young's modulus values were validated using Einstein and Guth models. Model-free methods like Flynn-Wall-Ozawa (FWO), Kissinger-Akahira-Sunose (KAS), Tang, and Starink were used to examine the kinetics of thermal degradation of NR-MCW composites. Various sorption parameters and the sorption characteristics of NR-MCW composites in different aromatic and aliphatic solvents have also been investigated.

Bashpa P. Mechanical, Thermal and Sorption Studies of Industrial Waste Reinforced Natural Rubber. St. Joseph's College (AUTONOMOUS) Devagiri, University of Calicut. 2024

5.1. Introduction

A condom is a sheath-shaped barrier device that is used during sexual activity to reduce the chance of getting pregnant or to guard against sexually transmitted diseases (STDs) (227). One of the most significant and well-liked birth control methods available today is the use of male condoms (112). Latex, which is vulcanised to boost the rubber's strength and durability, makes up the majority of condoms. During latex manufacturing, fatty acids are frequently used as binding agents and surfactants to stabilise the material. Zinc oxide, which guards against fungal and UV radiation attacks on rubber breakdown, is also added. Accelerators and antioxidants are also included to stop harmful nitrosamine formation and oxidative degradation. Powders of calcium carbonate and magnesium carbonate are frequently employed to lessen the stickiness of condoms (113). Many condom producers now utilise pharmaceutical-grade light magnesium carbonate (LMC) to alleviate the sticking property. The Indian condom market is projected to rise from an estimated USD 0.69 billion in 2021 to USD 1.02 billion by 2029 at a compound annual growth rate (CAGR) of 5.1 % between 2022 and 2029.

The largest producer of NR latex condoms in the Indian market is HLL Lifecare Limited, a Government-owned company with eight manufacturing facilities nationwide. The industrial facility in Thiruvananthapuram, Kerala, was built in 1969 with the assistance of M/s Okamoto Industries Inc., a technical partner from Japan. With a production capacity of 1947 million condoms annually, this unit has continuously upgraded. During the last phases of condom production,

LMC was used as a finishing powder. Around 75 to 85 tonnes of magnesium carbonate waste (MCW) are produced each year, and as of yet, no attempts have been made to reutilise it. The enormous amount of MCW generated during condom production, the difficulties in disposing of it, and the fact that its landfill is the main contributing factor to the hardness of water are the factors that lead to looking into the potential of its utilisation as a reinforcing filler in NR.

Table 2.9* in the Materials and Methods section describes the NR compounding, and Table 5.1 shows the sample designation and formulation of NR-MCW composites. Rheological, mechanical, thermal, and sorption experiments were done on the fabricated composites. Validation studies were also conducted using established theoretical modelling on the Young's modulus results. Several model-free methodologies were used to study the thermal degradation dynamics of NR-MCW composites.

Table 5.1. Sample designation and formulation of NR-MCW composites

Sample designation	NR	MCW
NR-Neat	100	0
NR-MCW1	100	1
NR-MCW2	100	2
NR-MCW3	100	3
NR-MCW4	100	4
NR-MCW5	100	5

*NR-100, ZnO-5.0, stearic acid-2.0, TMQ-1.0, CBS-0.6, TMTD-0.2 and sulphur-2.5 (in phr)

5.2. Results & Discussion

5.2.1. Attenuated total reflectance-Fourier Transform infrared spectroscopic analysis of NR-MCW composites

The ATR-FTIR spectra of the NR-Neat and NR-MCW composites are presented in Figure 5.1. Table 5.2 lists the prominent peaks that were obtained. In contrast to NR-Neat, NR-MCW composites had peaks associated with the symmetric deformation vibration of C-O and CO_3^{2-}.

Table 5.2. Prominent peaks in the ATR-FTIR spectra

Band position (cm^{-1})	Assignment
2995	CH stretching vibrations in NR (symmetric and asymmetric)
2910	CH_2 stretching vibrations in NR (symmetric and asymmetric)
2840	CH stretching vibrations in NR (symmetric and asymmetric)
2352	C-H vibrational mode of stearic acid in NR
1667	Stretching of C = C in NR (cis-1,4-isoprene units) (84)
831	C-H wagging in NR (84)
1447	C-O asymmetric stretching vibrations
1085	C-O symmetric deformation vibration (absent in NR) (228)
676	CO_3 symmetric deformation vibration (absent in NR) (228)

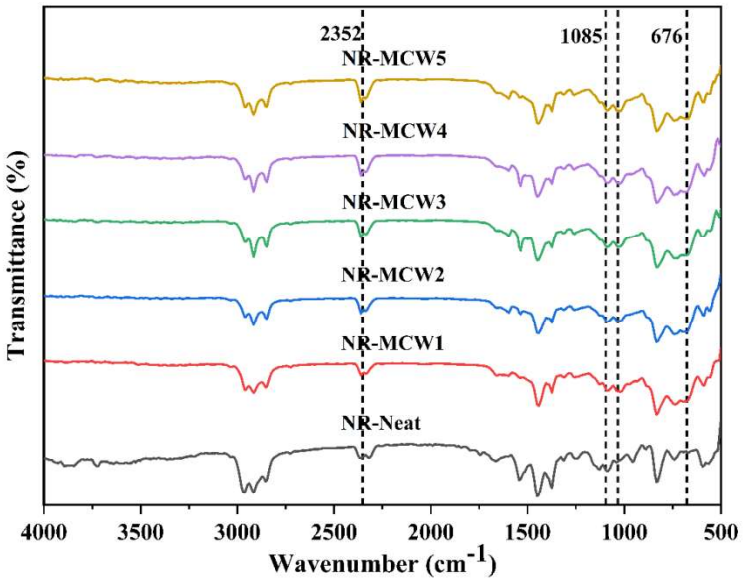

Figure 5.1. ATR-FTIR spectra of NR-Neat and NR-MCW composites

5.2.2. Surface morphology of NR-Neat and NR-MCW composites

The FESEM analysis of the tensile ruptured surface morphology of NR and its MCW composites is shown in Figure 5.2. Because of the surface's same chemical composition, the FESEM image of NR generalises its smooth morphology, as seen in Figure 5.2 (a) (229). Figure 5.2 (b) shows the uniform distribution of MCW particles on 3 phr loading on the surface of NR. Figure 5.2 (c) illustrates the cross-sectional analysis of NR-MCW3 in which some regions exhibit an epitaxial wavy structure due to chemical composition changes to the NR-MCW. But when MCW is loaded at 5 phr, the filler particles tend to clump together, resulting in an uneven surface morphology, as seen in Figure 5.2 (d) (230).

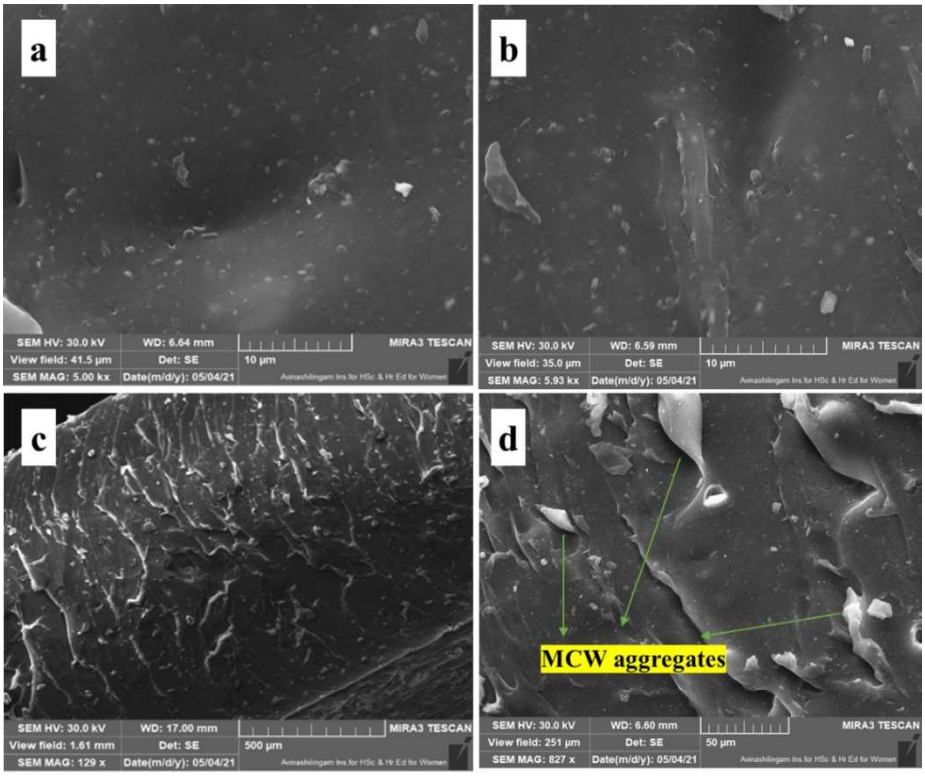

Figure 5.2. FESEM images of (a). NR-Neat (b). & (c). NR-MCW3, (d). NR-MCW5

5.2.3. Cure characteristics of NR-MCW composites

The effect of MCW loading on the cure characteristics of NR is described in Table 5.3.

Table 5.3. NR-MCW composite's curing properties

Cure characteristics	NR-Neat	NR-MCW1	NR-MCW2	NR-MCW3	NR-MCW4	NR-MCW5
Cure time, t_{90} (min)	4.18	4.12	4.07	3.68	3.87	3.93
Scorch time, t_{s2} (min)	2.15	2.37	2.24	1.95	1.99	2.27
Minimum torque, M_L (dNm)	6	6.5	7.8	6.3	7.6	6.6
Maximum torque M_H (dNm)	72.9	74.1	76	78.6	75.8	76.3
M_H-M_L (dNm)	66.9	67.6	68.2	72.3	68.2	69.7
Cure rate index ($min^{-1)}$	49.26	57.14	54.64	57.80	53.19	60.24

The MCW3 composite's cure time is reduced by 12 %, and all other composites also showed a significant reduction, demonstrating the filler's co-curing activity. The degree of curing is measured by the cure rate index (CRI), and NR-MCW composites have a higher CRI than NR, suggesting that the fabrication of composites is more feasible. All the composite's scorch times are nearly identical, while the NR-MCW3 composite showed the smallest value. With the addition of the filler, the M_L and M_H values increased, indicating a decrease in the mobility of the macromolecular chains in NR (85). The NR-MCW composite's maximum torque values increased, showing improved NR crosslinking after adding MCW. This is further supported by an

increase in the difference between the maximum and minimum torque values (M_H-M_L) (231).

5.2.4. Mechanical properties of NR-MCW composites

Table 5.4 provides a summary of the mechanical property values for NR-MCW composites.

The concept that NR becomes more elastic with the addition of MCW is supported by the stress-strain graphs of NR-MCW composites, which are displayed in Figure 5.3. This is explained by improved matrix-filler adhesion, which raises the stress required for the composite to rupture (206).

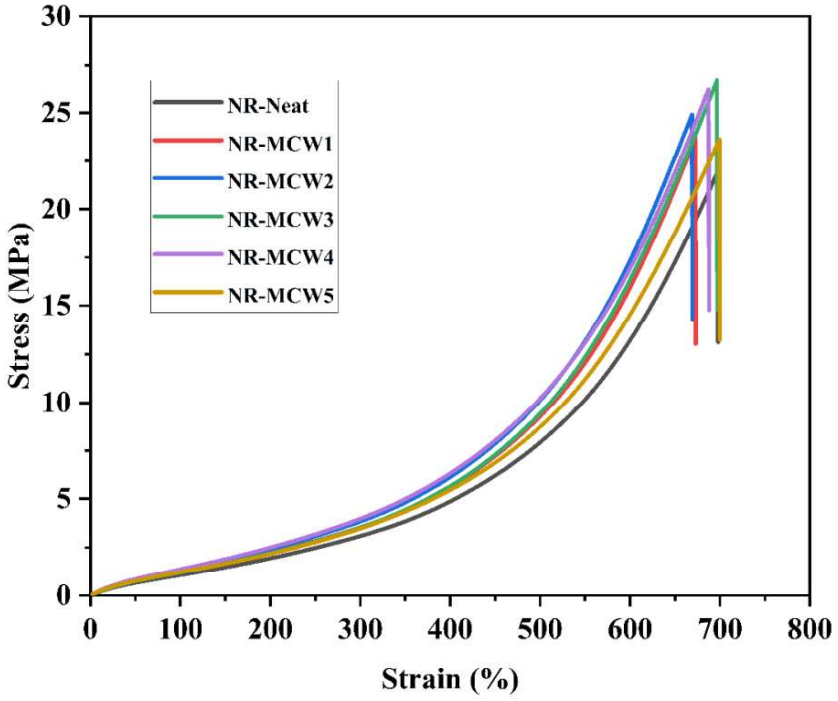

Figure 5.3. Stress-strain curves of NR-MCW composites

Table 5.4. Mechanical property values of NR-MCW composites

Properties	NR-Neat	NR-MCW1	NR-MCW2	NR-MCW3	NR-MCW4	NR-MCW5
Hardness (Shore A)	41 ± 0.5	40 ± 0.5	41 ± 1	43 ± 1	41 ± 1	41 ± 1.5
Specific gravity	0.965 ± 0.005	0.974 ± 0.005	0.978 ± 0.010	0.981± 0.012	0.981 ± 0.012	0.997± 0.015
DIN abrasion loss (cc)	0.272 ± 0.015	0.226 ± 0.022	0.228 ± 0.025	0.22± 0.018	0.23 ± 0.033	0.264 ± 0.035
Tensile strength (MPa)	21.93 ± 0.25	23.72 ± 0.34	24.91± 0.28	26.66 ± 0.46	26.21 ± 0.52	23.62 ± 0.55
Elongation at break (%)	697 ± 12	673 ± 18	669 ± 14	667 ± 15	687 ± 12	689 ± 16
Modulus at 300 % elongation (MPa)	3.09 ± 0.23	3.53 ± 0.25	3.83 ± 0.34	3.97 ± 0.22	3.52 ± 0.43	3.48 ± 0.32
Young's modulus (MPa)	0.899 ± 0.04	1.031 ± 0.03	1.138 ± 0.02	1.165 ± 0.02	1.049 ± 0.05	1.029 ± 0.02
Tear strength (N/mm)	41.76 ± 0.72	46.42 ± 0.65	47.42 ± 0.78	50.31 ± 0.84	48.01 ± 0.72	48.78 ± 0.68
Compression set (%)	18.68 ± 0.22	17.39 ± 0.24	15.49 ± 0.28	18.23 ± 0.25	18.86 ± 0.22	19.57 ± 0.26
Heat build-up (ºC)	1 ± 0.34	1 ± 0.22	2 ± 0.28	1± 0.36	2.5 ± 0.42	2.5 ± 0.34

The composite containing 3 phr MCW had the highest tensile strength with an increase of up to 22 % compared to NR-Neat, owing to the enhanced dispersion and robust interfacial bonding of MCW on the NR matrix. However, as more filler was added, it began to decline due to the MCW aggregation in the NR matrix. The NR-MCW interactions break down above 3 phr MCW loading, favouring the MCW-MCW interactions, which prevented the effective transfer of stress applied to the composite (208). In NR-MCW1 to NR-MCW3 composites, the elongation at break decreased, followed by a marginal rise on further addition, demonstrating the greater adhesion of MCW to NR up to 3 phr filler loading. The modulus values at 300 % elongation showed an upward trend (a 29 % rise for 3 phr MCW loading), but due to filler agglomeration, they began to drop on further MCW addition. The composite's Young's modulus was calculated using stress-strain graphs, indicating an increasing trend up to 3 phr MCW loading and then decreases on further addition of filler. The NR-MCW composite's tear strength increased up to 3 phr MCW (20 % increase) addition and steadily decreased with further addition. MCW aggregation is more pronounced at higher filler loading, which lowers the mechanical characteristics by causing uneven filler distribution on the NR matrix (232). NR-MCW3 showed higher hardness because of its ameliorated dispersion in the pores of NR. The superior dispersion of MCW up to 3 phr on NR is supported by the fact that all composites have less abrasion loss (volume loss) than NR. The NR-MCW composite's compression set values are nearly identical to the NR matrix's, demonstrating better matrix-filler interaction and homogeneous MCW dispersion on NR up to 3 phr loading.

5.2.5. Young's modulus of NR-MCW composites: A theoretical modelling approach

A material's stiffness degree is gauged by its Young's modulus (elastic modulus). Although many composites have anisotropy, the elastic modulus is constant in all directions for an isotropic material. Guth revised the equation that Einstein had proposed based on the assumption that spherical filler particles are rigid (127,128). Figure 5.4 shows the correlation between the experimental elastic modulus results with Einstein and Guth's model.

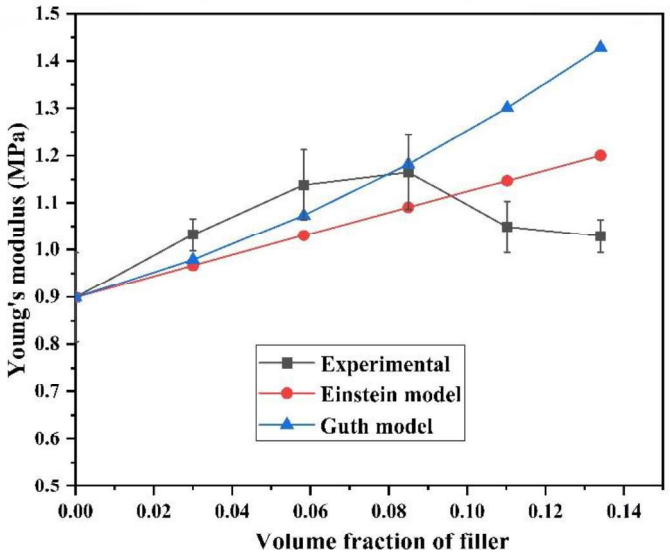

Figure 5.4. Experimental and theoretical Young's moduli comparison

Figure 5.4 shows the experimental and predicted values of Young's modulus with those of the Einstein and Guth models. At lower filler loadings, the predicted Young's modulus values from the Einstein and Guth models significantly correlated with the experimental values for NR-MCW composites, merging with the Guth model value at 3 phr

MCW loading. This behaviour suggests that MCW is distributed uniformly across NR and that NR-MCW adhesion is improved. The experimental Young's modulus values with higher filler loading deviated negatively from the theoretically expected values, most likely because the MCW agglomeration on NR weakens the NR-MCW interaction.

5.2.6. Thermogravimetric analysis of NR and NR-MCW composites

The thermal profiles of the NR-Neat and NR-MCW composites at various filler loadings are displayed in Figure 5.5. Table 5.5 gives the E_a for decomposition, amount of residue at 600 °C, highest thermal decomposition temperature (T_{max}) and onset decomposition temperature (T_i).

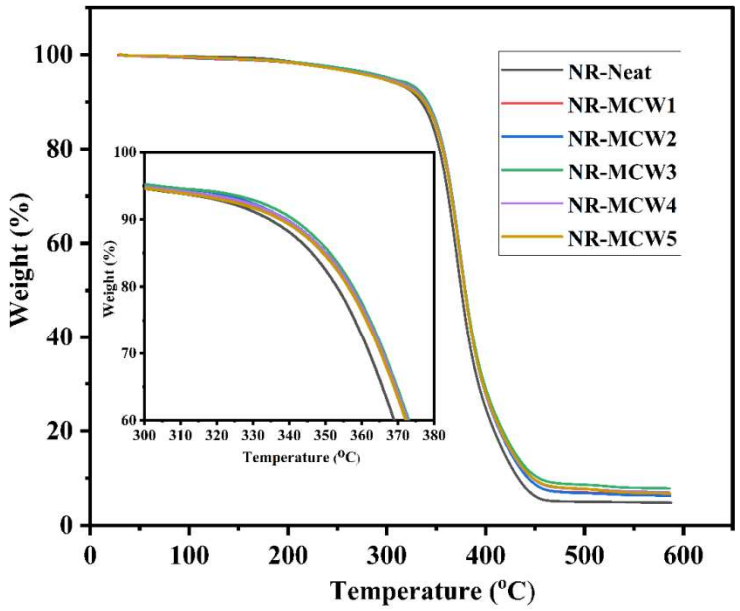

Figure 5.5. TGA curves of NR and NR-MCW composites

Table 5.5. Thermal degradation characteristics of NR-MCW composites

Properties	NR-Neat	NR-MCW1	NR-MCW2	NR-MCW3	NR-MCW4	NR-MCW5
Onset decomposition temperature, T_i (ºC)	326.7	327.9	328.8	332.2	330.5	327.1
Maximum decomposition temperature, T_{max} (ºC)	372	373.5	374.6	375.8	375.2	374.1
Residue at 600 °C (%)	4.86	5.52	6.04	7.06	6.23	6.90

Decomposition of NR-Neat has been shown to occur in one step and to begin at 326.7 °C. For NR-MCW composites, the results for the onset decomposition temperature increased up to 3 phr before decreasing as the breakdown process progressed (233). The composite's maximum degradation temperature rose slightly compared to NR, indicating improved thermal stability. The residue at 600 °C slightly increased as the filler quantity increased because the filler needed a high temperature to break down (234).

5.2.7. Thermal degradation kinetics

The thermal stability and degradation dynamics of NR-MCW composites have been studied using TGA. Isoconversional models, such as Flynn-Wall-Ozawa (FWO) (133,134), Kissinger-Akahira-Sunose (KAS) (135,136), Tang (137,138) and Starink (139,140), were

demonstrated to be helpful in understanding the kinetics of thermal decomposition. Thermal degradation kinetics is essential because it clarifies the energy boundaries for various processes and explains how reactions proceed (214). For every conversion level between 0.1 and 0.9, E_a was computed using the FWO, KAS, Starink, and Tang methods. A straight line was fitted using the least squares method for each process. Kinetic plots of NR-Neat and NR-MCW3 composites for all four models are displayed in Figures 5.6 - 5.9, and they all showed the same trend. The correlation coefficient values, ranging from 0.97 to 0.99, for all linear fits show a robust linear relationship between the heating rate and temperature. This is valid for all kinetic models that have been used. There is only a slight variance in E_a values obtained in all four models employed, possibly due to the difference in approximations of the models. Table 5.6 provides the calculated E_a for each conversion based on the generated graphs.

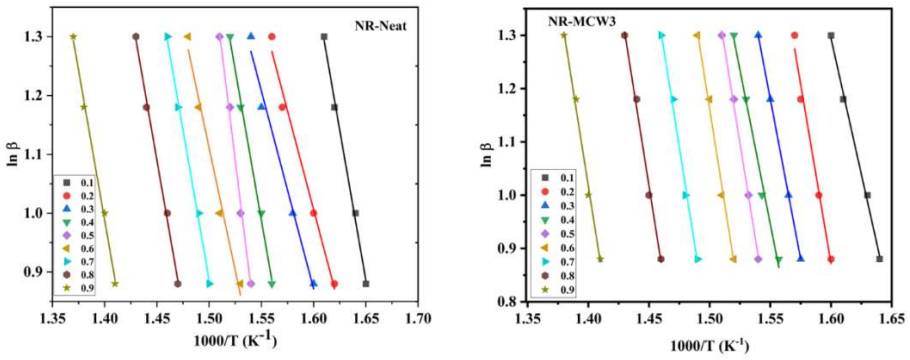

Figure 5.6. Kinetic plots of NR-Neat and NR-MCW3 by FWO method

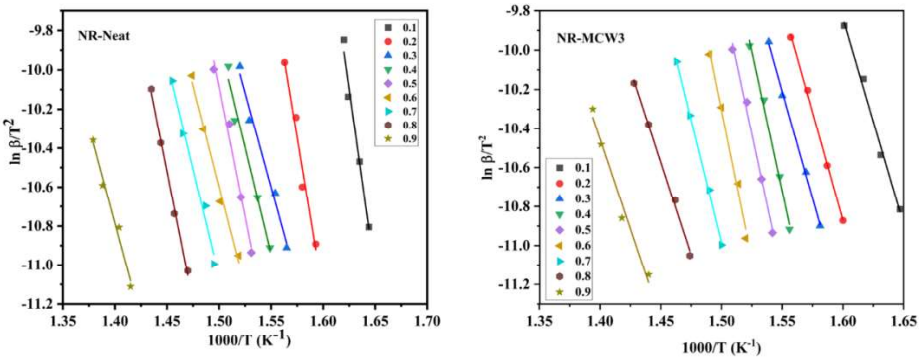

Figure 5.7. Kinetic plots of NR-Neat and NR-MCW3 by KAS method

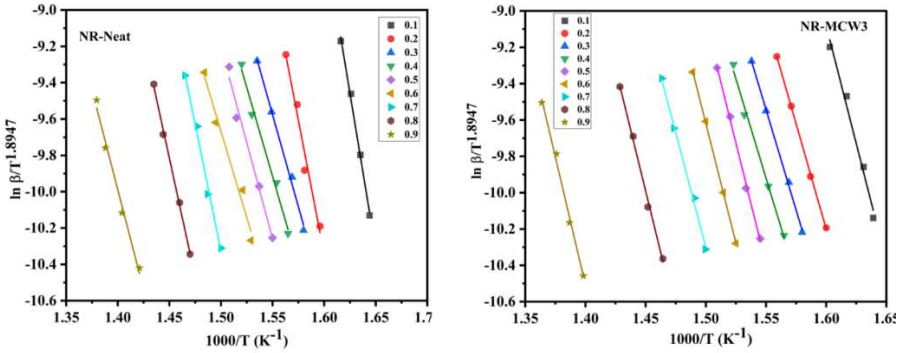

Figure 5.8. Kinetic plots of NR-Neat and NR-MCW3 by Tang method

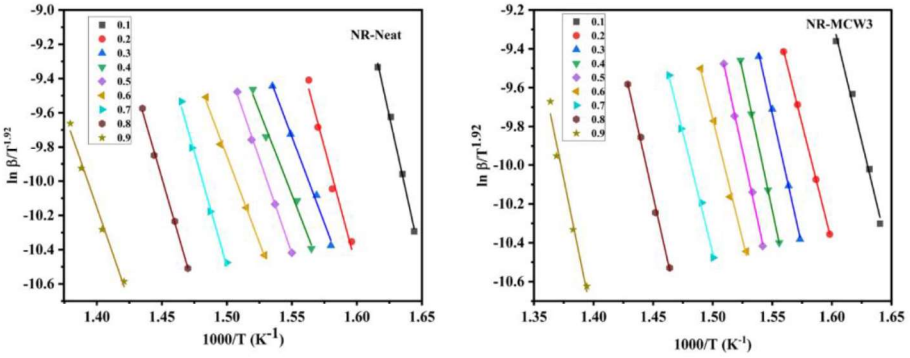

Figure 5.9. Kinetic plots of NR-Neat and NR-MCW3 by Starink method

Table 5.6. E_a values for FWO, KAS, Tang and Starink models

Samples →		NR-Neat	NR-MCW1	NR-MCW2	NR-MCW3	NR-MCW4	NR-MCW5
Method ↓	α	E_a (kJmol^{-1})	E_a (kJmol^{-1})	E_a (kJmol^{-1})	E_a (kJmol^{-1})	E_a (kJmol^{-1})	E_a (kJmol^{-1})
FWO	0.1	123.94	185.47	233.10	245.28	182.59	161.82
	0.2	129.81	214.76	224.37	251.24	222.83	197.56
	0.3	137.90	223.45	211.17	263.25	210.13	194.95
	0.4	148.52	220.09	190.14	264.4	207.49	206.64
	0.5	156.67	229.60	200.41	280.78	172.95	208.51
	0.6	157.38	229.47	233.15	300.75	220.85	212.35
	0.7	174.66	213.38	248.34	280.76	199.07	193.55
	0.8	194.16	239.5	234.20	265.2	221.53	190.19
	0.9	185.75	241.93	254.84	255.6	138.34	76.36
KAS	0.1	123.23	183.63	232.92	244.68	181.90	161.56
	0.2	129.11	214.48	224.01	252.04	222.38	196.01
	0.3	137.30	223.41	211.03	263.55	209.45	194.04
	0.4	148.27	219.77	188.83	263.4	206.58	205.69
	0.5	156.15	228.58	199.51	280.18	173.38	207.55
	0.6	157.48	228.32	236.78	300.55	220.74	211.94
	0.7	174.19	210.43	248.39	280.26	198.71	193.31
	0.8	193.76	237.85	233.85	265	219.55	191.12
	0.9	184.70	239.24	253.22	255.5	137.95	75.44

Tang	0.1	123.76	184.17	233.46	245.98	182.44	162.09
	0.2	129.66	215.03	224.56	251.84	222.94	196.55
	0.3	137.87	223.97	211.60	264.25	210.01	194.60
	0.4	148.84	220.34	189.40	265.4	207.15	206.26
	0.5	156.73	229.15	200.09	281.78	174.95	208.12
	0.6	158.06	228.91	237.36	301.75	221.32	212.52
	0.7	174.78	211.01	248.98	281.76	199.30	193.90
	0.8	194.36	238.45	234.46	266.23	220.16	191.72
	0.9	184.32	239.87	253.85	255.6	138.58	71.09
Starink	0.1	123.63	184.04	233.33	246.18	182.31	161.97
	0.2	129.53	214.90	224.42	252.64	222.80	196.42
	0.3	137.73	223.83	211.46	263.95	209.88	194.46
	0.4	148.70	220.20	189.27	266.4	207.01	206.13
	0.5	156.59	229.01	199.95	281.18	174.82	207.98
	0.6	157.48	228.77	237.23	301.95	221.18	212.38
	0.7	174.64	210.87	248.84	281.56	199.16	193.75
	0.8	194.22	238.31	234.31	266,25	220.01	191.57
	0.9	185.17	239.72	253.69	256.8	138.43	70.93

The lower initial E_a values suggest that weak link initiation limits the kinetics of the early stages of degradation. The increased E_a values obtained in the latter phases suggest that random scission-induced degradation further suppresses the composite's ability to degrade. Similar outcomes were previously reported (215,216). All composites exhibited higher E_a values for thermal degradation than NR-Neat up to 3 phr addition of MCW, indicating improved thermal stability. Due to the mobility restriction of the polymer chains with a higher MCW content, the composites may have higher E_a values. It was shown that filler aggregation caused the E_a values of the composites to drop above 3 phr MCW addition. The four kinetic model's E_a values agree with one another, proving the usefulness of these methods for studying thermal deterioration.

5.2.8. Activation energy dependency on degree of conversion

Isoconversional kinetic analysis is used to predict the kinetics and mechanism of a thermally driven process by analysing how activation energy (E_a) depends on the degree of conversion (α). The changes in E_a values suggest multistep processes, each contributing equally to the overall rate, according to Vyazovkin *et al*. (217). The E_a for different conversion rates for NR-Neat and NR-MCW3 against α is depicted in Figure 5.10.

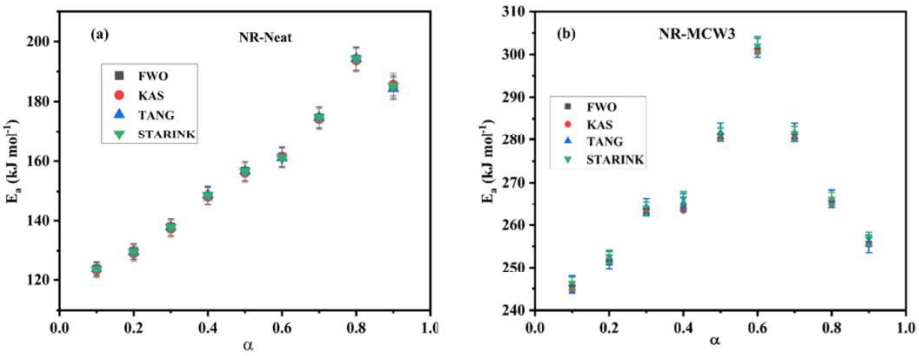

Figure 5.10. Variation of E_a with α for (a) NR-Neat and (b) NR-MCW3

Figure 5.10 (a) shows how E_a values gradually rise by up to 0.8 in the case of NR-neat. Then, in the latter phases, it displays a falling pattern, signifying that degradation has ended. Interestingly, the NR-MCW composites show an unusual association with α, and Figure 5.10 (b) shows a typical plot of NR-MCW3. Composites showed higher thermal stability since their E_a values are higher than NR-Neat's. The E_a values rise until they reach a value of 0.6 before declining. The complex reaction steps in the degradation reaction are illustrated by the variance in E_a seen for the composites at increased conversion, providing insight into the multistep reaction pathway (218). According to the above data, all four model-free approaches provided E_a values that were quite near to one another across the whole conversion range under consideration. It is, therefore, possible to suggest isoconversional models as a reliable tool for predicting the kinetics of heat degradation of various NR composites.

5.2.9. Sorption properties of NR-MCW composites

Molecular transport phenomena through polymeric systems are significant in many industrial sectors and influence many engineering fields (235). The various sorption properties and parameters determined are given below. The solvents employed for the study include toluene, xylene, mesitylene and hexane.

5.2.9.1. Mol % uptake of solvents

Equation (2.21) is used to calculate the Q_t % of solvent diffusion through various composites. A plot was made between the solvent's Q_t % and the square root of time. All of the curves in different solvents are comparable, and Figure 5.11 shows a plot typical for toluene.

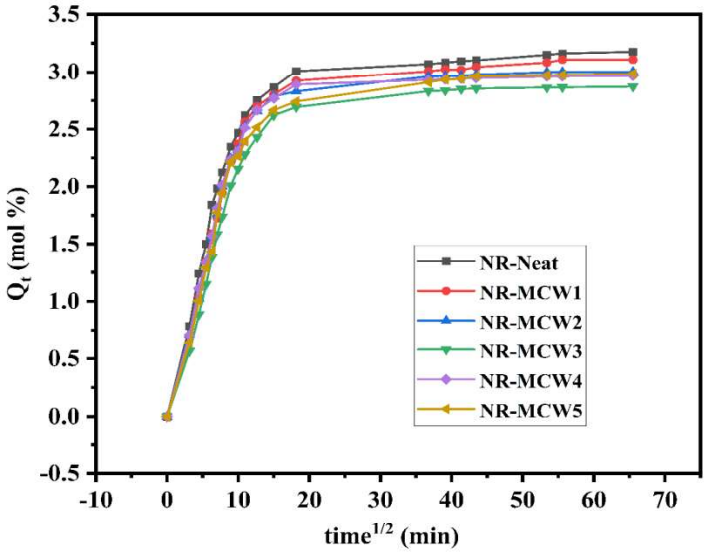

Figure 5.11. Mol % uptake of toluene through different NR-MCW composites at 30 °C

5.2.9.2. Effect of filler loading

Since the penetrant concentration gradient in the composite is quite large, it can be seen from Figure 5.11 that the solvent uptake initially continues at a relatively high pace. When the concentration gradient of the penetrant molecules is lowered, the rate of solvent uptake falls and reaches an equilibrium plateau. The observations mentioned above also make it evident that, as filler loading rises, solvent consumption first declines until 3 phr MCW, which begins to increase. This can be explained by the fact that reinforcing, resulting from a strong filler-polymer interaction, limits the mobility of the polymer following vulcanisation, making the polymer chains less flexible and reducing sorption behaviour up to 3 phr loading. Further filler addition causes agglomeration, which leaves gaps in the system that the solvent may easily penetrate.

The surface area of the reinforcing phase is increased by the nanofiller's effective dispersion within the matrix, greatly enhancing the nanocomposite's solvent resistance properties. The higher dispersion of MCW up to 3 phr loading is supported by FESEM images in Figure 5.2, as is the aggregation of filler beyond 3 phr. The free volume within the polymer matrix affects how easily solvent molecules diffuse across the polymer membrane. Nanofillers reduce the matrix's free volume, resulting in less equilibrium solvent uptake. The decline in solvent uptake in the filled systems can be explicated by the tortuous nature of the channel and the smaller transport area in the polymeric membrane when fillers are present (222).

5.2.9.3. Effect of penetrant size

Investigations are made into the composite's transport characteristics in aromatic and aliphatic solvents. Figure 5.12 shows the results for aromatic solvents: toluene > xylene > mesitylene.

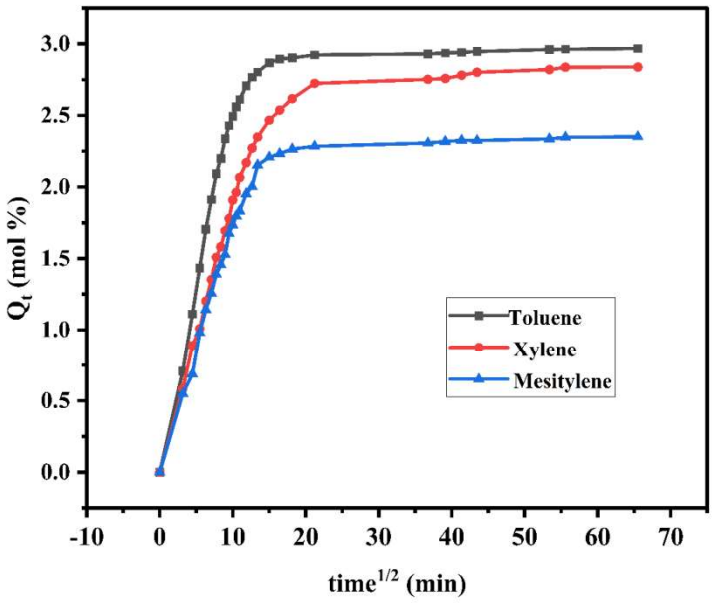

Figure 5.12. Solvent uptake of NR-MCW3 composite in various solvents

The equilibrium mol % (Q_∞) values of the NR-Neat and NR-MCW composites in different aromatic solvents and hexane are listed in Table 5.7. Even if the difference in the Hildebrand solubility parameter (δ) for aromatic solvents is lower, the bigger size of xylene and mesitylene and the steric factor restrict their penetration. Free volume theory can account for the reported drop in diffusivity as the penetrant's size increases (221,236). According to the free volume hypothesis, how easily polymer chains swap places with solvent

molecules significantly influences a molecule's diffusion rate. Solvent uptake is reduced when penetrant size increases because the ease of exchange reduces, particularly for most matrices. Low solvent absorption is also due to the big penetrant molecule's high activation energy requirement (237). When dealing with aliphatic liquids, the Q_∞ decreases as the alkyl chain's molar volume and chain length. The diffusion results for hexane show that aliphatic solvents have lower solvent diffusion values than aromatic solvents due to their higher molar volumes (238).

Table 5.7. NR-MCW composite's Q_∞ values for different solvents

Sample ↓	Q_∞ (mol %)			
	Toluene	**Xylene**	**Mesitylene**	**Hexane**
NR-Neat	3.5062	3.1193	2.9387	1.5260
NR-MCW1	3.4432	3.1092	2.8986	1.4520
NR-MCW2	3.3971	3.0224	2.8437	1.4238
NR-MCW3	3.3322	2.9948	2.6477	1.4082
NR-MCW4	3.3737	3.0035	2.7726	1.4462
NR-MCW5	3.3794	3.0905	2.7812	1.4492

5.2.9.4. Effect of temperature

Sorption tests in toluene were done at 4 °C, 30 °C, and 50 °C, respectively, to investigate the impact of temperature on the diffusion of solvents in the NR-MCW composites. Figure 5.13 demonstrates how the diffusion and solvent uptake rate increases as temperature rises because solvent molecules may diffuse more quickly at higher

temperatures due to the increased thermal energy. The solvent molecules become less viscous as the temperature increases, promoting the polymer segment's mobility. The increase in free volume within the matrix and the high rate of solvent diffusion are caused by the weakening of filler matrix adhesion and the creation of voids induced by the activation of diffusion with a temperature rise. The degree to which temperature increase activates the diffusion process and the temperature dependency of the transport parameters are demonstrated by the slope of the linear section of the curves at different temperatures. Similar patterns of an increase in the rate of solvent sorption with temperature have already been described (239,240).

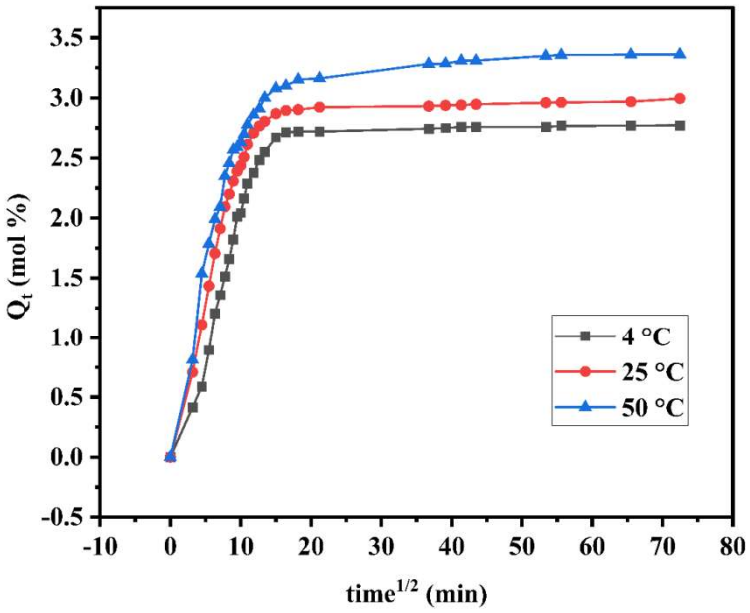

Figure 5.13. Mol % uptake of NR-MCW3 composite at various temperatures

5.2.10. Swelling index and crosslink density

In vulcanised composites, chemical crosslinks and rubber-filler interactions influence crosslink density (241). Table 5.8 shows the swelling index and crosslink density of the NR-MCW composites. According to the results, the solvent uptake regularly decreased up to 3 phr loading of MCW, and on further addition, the swelling index values slightly increased. The decrease in solvent uptake may be due to the improved matrix-filler interaction and fine dispersion of MCW up to 3 phr loading, and this uniform distribution of filler prevents solvent molecules from moving on NR. The further addition of MCW induces agglomeration, creating open spaces in the matrix that aid in solvent uptake.

Table 5.8. Crosslink density and swelling index values of NR-MCW composites

Sample's name	Crosslink density $\times 10^{-4}$ ($molg^{-1}$)	Swelling index (%)
NR-Neat	1.21 ± 0.01	289 ± 3
NR-MCW1	1.22 ± 0.03	286 ± 2
NR-MCW2	1.27 ± 0.02	278 ± 2
NR-MCW3	1.29 ± 0.03	275 ± 1
NR-MCW4	1.25 ± 0.02	277 ± 1
NR-MCW5	1.23 ± 0.01	279 ± 2

5.2.11. Diffusion, sorption and permeation coefficients

The sample's diffusion coefficient (D), sorption coefficient (S), and permeation coefficient in different solvents at room temperature are given in Table 5.9. In all solvents, up to 3 phr filler loading, a

constant decrease in D, S, and P values is shown. However, a minor increase in values is seen at higher filler loading. This may be caused by limited chain mobility of the polymers, the creation of filler-filler networks, contact between the filler and matrix with increased loading, and reduced free space. The diffusion process greatly depends on the size of the penetrant molecules because larger solvent molecules require higher activation energies to penetrate. Toluene, xylene, and mesitylene are the solvents in the order of molecular mass. As a result, the diffusion coefficient of the specific composite at the particular temperature is in the reverse order of the solvent's molecular masses, with toluene coming before xylene and mesitylene. The sorption and penetration coefficients also displayed a similar trend.

The values of coefficients of D, S, and P in toluene at various temperatures for NR-MCW composites are displayed in Table 5.10. The table shows that the diffusion rate rises as the temperature rises. The higher thermal energy produced by the temperature increase activates the diffusing molecules.

Table 5.9. Values of D, S, and P of NR-MCW composites in aromatic solvents at 30 °C

Sample ↓	Diffusion coefficient (D) × 10^{-4} (cm^2s^{-1})			Sorption coefficient (S)			Permeation coefficient (P) × 10^{-4} (cm^2s^{-1})		
	Toluene	Xylene	Mesitylene	Toluene	Xylene	Mesitylene	Toluene	Xylene	Mesitylene
NR-Neat	43.37	41.80	21.86	2.40	2.21	2.13	104.27	92.64	46.75
NR-MCW1	42.08	40.53	20.08	2.35	2.20	2.08	98.99	89.27	40.74
NR-MCW2	40.30	38.33	19.67	2.36	2.19	2.03	95.14	83.90	40.91
NR-MCW3	38.23	36.42	18.33	2.29	2.19	2.02	87.72	79.76	37.22
NR-MCW4	39.94	37.86	19.06	2.32	2.21	2.06	92.79	83.76	37.36
NR-MCW5	39.58	36.12	19.67	2.33	2.21	2.07	92.16	80.11	40.82

Table 5.10. D, S, and P values of NR-MCW composite in toluene at various temperatures

Sample ↓	Diffusion coefficient (D) × 10^{-4} (cm^2s^{-1})			Sorption coefficient (S)			Permeation coefficient (P) × 10^{-4} (cm^2s^{-1})		
Temperature (°C) ⟶	4	30	50	4	30	50	4	30	50
NR-Neat	26.15	43.37	48.77	2.14	2.40	2.57	51.25	104.27	125.46
NR-MCW1	25.13	42.08	45.36	1.94	2.35	2.53	48.93	98.99	114.64
NR-MCW2	23.35	40.30	43.98	1.89	2.36	2.51	41.84	95.14	110.79
NR-MCW3	20.54	38.23	42.80	1.87	2.29	2.50	38.62	87.72	107.05
NR-MCW4	23.06	39.94	43.73	1.88	2.32	2.50	45.43	92.79	108.87
NR-MCW5	24.24	39.58	42.27	1.87	2.33	2.49	47.78	92.16	107.59

5.2.12. Activation energy of diffusion and permeation

The activation energy for the diffusion (E_D) and permeation (E_P) processes can be determined using Equation (2.30) and the temperature dependence of the transport coefficients (P, D, and S). With correlation values of 0.97 to 0.99, linear regression analysis can be used for Arrhenius plots of log D vs 1/T and log P vs 1/T to find E_D and E_P. Table 5.11 lists the NR-MCW composite's estimated E_D and E_P values in toluene. Table 5.10 also includes the heat of sorption (ΔH), calculated using Equation (2.31).

Table 5.11. Values of E_D and E_P for toluene

Sample	E_D (kJmol^{-1})	E_P (kJmol^{-1})	ΔH (kJmol^{-1})
NR-Neat	9.19	12.17	2.98
NR-MCW1	9.53	13.79	4.26
NR-MCW2	10.21	15.74	5.53
NR-MCW3	11.85	16.45	4.6
NR-MCW4	10.32	14.12	3.8
NR-MCW5	9.97	13.01	3.04

It is evident from Table 5.11 that MCW-filled composites have a higher E_D than NR-Neat. A penetrant molecule can be imagined making a series of hops across a pile of tangled polymer chains and voids as it diffuses into a rubbery matrix. Thermal turbulence causes the cavities to reform and vanish continuously [238]. The migration of the penetrant molecule between cavities is influenced by a concentration gradient, which causes the overall diffusion process. For each jump, rubber-rubber and rubber-penetrant contacts must be

broken for the surrounding chains to rearrange and let the diffusing molecules pass. The energy required and the degree of this rearrangement are determined by the rubber's segmental mobility. The inclusion of filler reduces the rubber molecule's freedom of movement, which explains why the activation energy has increased (242). Table 5.11 shows the increase in E_a for diffusion up to 3 phr filler loading and a decreasing trend after 3 phr due to filler agglomeration that creates open spaces for the simple passage of penetrant molecules. Positive values of ΔH indicate that the process is endothermic, which supports the increase in diffusion rate and maximal solvent uptake with temperature [32].

5.2.13. Mode of transport

Equation (2.29) can be used to evaluate the transport mechanism. When $n = 0.5$, where chain relaxation outpaces solvent diffusion rate, the transport is referred to as Fickian. When $n = 1$, the transport is referred to as non-Fickian, and solvent penetration outpaces chain relaxation. The conveyance is considered anomalous if the value is between 0.5 and 1. The values of *n* and *k* for NR-Neat and NR-MCW composites were found using the results of the linear regression analysis of log (Q_t/Q_∞) against log t plot, as indicated in Table 5.12.

Table 5.12. NR-MCW composites: *n* and *k* values in different solvents

Sample ↓	*n*				*k*			
	Toluene	**Xylene**	**Mesitylene**	**Hexane**	**Toluene**	**Xylene**	**Mesitylene**	**Hexane**
NR-Neat	0.48	0.52	0.51	0.61	0.38	0.27	0.30	0.28
NR-MCW1	0.55	0.49	0.55	0.60	0.30	0.27	0.30	0.29
NR-MCW2	0.54	0.47	0.59	0.62	0.31	0.33	0.25	0.29
NR-MCW3	0.55	0.49	0.54	0.62	0.32	0.33	0.28	0.30
NR-MCW4	0.57	0.52	0.53	0.59	0.30	0.29	0.27	0.32
NR-MCW5	0.58	0.47	0.57	0.58	0.29	0.33	0.28	0.27

It is evident from the preceding table that xylene has *n* values that exhibit Fickian behaviour, but toluene, mesitylene, and hexane exhibit anomalous transport. There is no connection between the filler's composition and the *n* values. The values of *k* provide insight into the nature of the solvent-polymer interaction. The similarity of the *k* values found for different composites in the various solvents may indicate that the rubber composites and solvents interact similarly.

5.3. Conclusion

The NR-MCW composites were fabricated by mixing on a two roll mixing mill, and FTIR, FESEM, and TGA studies were performed to characterise the composites. Based on an analysis of the resulting composite's mechanical, thermal, and curing properties, MCW has been shown to be an effective reinforcing filler in NR. The NR

composite's tensile strength, modulus at 300 % elongation, tear strength, and abrasion resistance were significantly increased by 3 phr MCW loading compared to NR-Neat. As filler loading increases, so do other mechanical properties like hardness, compression set, and heat build-up. MCW was uniformly distributed on the NR surface up to 3 phr loading, according to FESEM analysis. Einstein and Guth's models validated Young's modulus values, demonstrating satisfactory agreement up to 3 phr filler loading. This connection to theoretical models proves the fine dispersion of MCW on NR surface up to 3 phr filler loading.

Thermal analysis of NR-MCW composites revealed a significant improvement in thermal stability compared to NR neat. The dynamics of the thermal degradation of the NR-MCW composites have been studied using TGA. The isoconversional, model-free FWO, KAS, Tang, and Starink techniques were used to determine the E_a values for the thermal degradation of NR-Neat and the composites. During the thermal decomposition, these isoconversional models successfully forecasted E_a changes and tracked the pathways. For the fabricated composites, the four isoconversional models indicated multistep degradation kinetics.

Compared to the other solvents used, toluene is found to have a more swelling behaviour for the NR-MCW composites. In all solvents, solvent consumption decreases up to 3 phr filler loading and gradually increases on further loading. It has been discovered that solvent intake rises as temperature rises and that the composite with a 3 phr MCW has the maximum E_a for diffusion. The diffusion, sorption, and

permeation coefficients were evaluated as kinetic parameters. The transport mechanism for xylene is consistent with Fickian theory. However, it exhibited anomalous transport behaviour for toluene, hexane, and mesitylene. The fabrication of NR-MCW composites holds excellent promise for substituting costly fillers in NR to manufacture typical rubber goods while lowering production costs. This approach also emphasises the circular economy concept of reutilising industrial wastes to reduce environmental pollution.

.

.

REFERENCES

1. Fuller R, Landrigan PJ, Balakrishnan K, Bathan G, Bose-O'Reilly S, Brauer M, et al. Pollution and health: a progress update. The Lancet Planetary Health. 2022;6(6):e535–47.

2. Ahmed F, Ali I, Kousar S, Ahmed S. The environmental impact of industrialization and foreign direct investment: empirical evidence from Asia-Pacific region. Environmental Science and Pollution Research [Internet]. 2022;29(20):29778–92. Available from: https://doi.org/10.1007/s11356-021-17560-w

3. Patnaik R. Impact of Industrialization on Environment and Sustainable Solutions – Reflections from a South Indian Region. IOP Conference Series: Earth and Environmental Science [Internet]. 2018 Mar;120(1):12016. Available from: https://dx.doi.org/10.1088/1755-1315/120/1/012016

4. Briggs D. Environmental pollution and the global burden of disease. British Medical Bulletin [Internet]. 2003;68(1):1–24. Available from: https://doi.org/10.1093/bmb/ldg019

5. Tandia PK, Pal BK. Strategies for industrial waste management in India - An overview. 2006;54:463–75.

6. MOEF. Hazardous and Other Wastes - Ministry of Environment and Forests. The gazzate of India. 2016;1981(i):1–68.

7. CPCB Annual Report 2019-2020. CPCB Annual Report. Cpcb [Internet]. 2022;145–287. Available from: https://cpcb.nic.in/uploads/plasticwaste/Annual_Report_2019-20_PWM.pdf

8. Gour AA, Singh SK. Solid Waste Management in India: A State-of-the-Art Review. Environmental Engineering Research [Internet]. 2023 Aug 27;28(4):220240–9. Available from: https://doi.org/10.4491/eer.2022.249

9. Kaza S, Yao L, Bhada-Tata P, Van Woerden F. What a Waste 2.0 Introduction -"Snapshot of Solid Waste Management to 2050." Overview booklet. Urban Development Series [Internet]. 2018;1–38. Available from: https://openknowledge.worldbank.org/handle/10986/30317

10. Karthikeyan L, Suresh VM, Krishnan V, Tudor T, Varshini V. The Management of Hazardous Solid Waste in India: An Overview. Environments [Internet]. 2018;5(9). Available from: https://www.mdpi.com/2076-3298/5/9/103

11. Abdel-Shafy H, Mansour M. Solid waste issue: Sources, composition, disposal, recycling, and valorization. Egyptian Journal of Petroleum. 2018 Dec 1;27:1275–90.

12. Kilpeläinen M, Happonen A. Awareness Adds to Knowledge. Stage of the Art Waste Processing Facilities and Industrial Waste Treatment Development. Current Approaches in Science and Technology Research Vol 4. 2021;(May):125–48.

13. MoHUA. Circular Economy in Municipal solid and liquid waste. Ministry of Housing and Urban Affairs, GOI. 2021;112.

14. Chand Malav L, Yadav KK, Gupta N, Kumar S, Sharma GK, Krishnan S, et al. A review on municipal solid waste as a renewable source for waste-to-energy project in India: Current practices, challenges, and future opportunities. Journal of Cleaner Production [Internet]. 2020;277:123227. Available from: https://www.sciencedirect.com/science/article/pii/S0959652620332728

15. Datta P, Mohi GK, Chander J. Biomedical waste management in India: Critical appraisal. Journal of laboratory physicians. 2018; 10(1):6–14.

16. Yadav VK, Gacem A, Choudhary N, Rai A, Kumar P, Yadav KK, et al. Status of Coal-Based Thermal Power Plants, Coal Fly Ash Production, Utilization in India and Their Emerging Applications. Vol. 12, Minerals. 2022.

17. Central Electricity Authority. Report on fly ash generation at coal/lignite based thermal power stations and its utilization in the country for the year 2019-2020. Ministry of Power, Government of India. 2020;(November):1–78.

18. Indian Minerals Yearbook 2017. Minerals Yearbook 2017, Part 2: Metals & Alloys, Indian Bureau of Mines. Government of India. 2017;56(2017):1–11.

19. Samal S, Ray AK, Bandopadhyay A. Proposal for resources, utilization and processes of red mud in India — A review. International Journal of Mineral Processing [Internet]. 2013;118:43–55. Available from: https://www.sciencedirect.com/science/article/pii/S0301751612001214

20. Patangia J, Saravanan TJ, Kabeer KISA, Bisht K. Study on the utilization of red mud (bauxite waste) as a supplementary

cementitious material: Pathway to attaining sustainable development goals. Construction and Building Materials [Internet]. 2023;375:131005. Available from: https://www.sciencedirect.com/science/article/pii/S0950061823007171

21. Jena SK, Dash N, Rath SS. Effective utilization of lime mud for the recovery of potash from mica scraps. Journal of Cleaner Production [Internet]. 2019;231:64–76. Available from: https://www.sciencedirect.com/science/article/pii/S0959652619317652

22. Saadaoui E, Ghazel N, Romdhane C Ben, Massoudi N. Phosphogypsum: potential uses and problems – a review. International Journal of Environmental Studies [Internet]. 2017;74(4):558–67. Available from: https://doi.org/10.1080/00207233.2017.1330582

23. Central Pollution Control Board. Annual Report 2019-20 on Implementation of Plastic Waste Management Rules. 2016;145–287.

24. Vidaurre-Arbizu M, Pérez-Bou S, Zuazua-Ros A, Martín-Gómez C. From the leather industry to building sector: Exploration of potential applications of discarded solid wastes. Journal of Cleaner Production [Internet]. 2021;291:125960. Available from: https://www.sciencedirect.com/science/article/pii/S0959652621001803

25. Kumar S, Smith SR, Fowler G, Velis C, Kumar SJ, Arya S, et al. Challenges and opportunities associated with waste management in India. Royal Society Open Science. 2017;4(3).

26. Biswas A, Chaudhary K, Singh R, Tewari S. WASTE-WISE CITIES Best Practices in municipal solid waste management [Internet]. NITI Aayog; 2021. 1–246 p. Available from: https://www.niti.gov.in/sites/default/files/2021-12/Waste-Wise-Cities.pdf

27. Yu Z, Khan SAR, Ponce P, Zia-ul-haq HM, Ponce K. Exploring essential factors to improve waste-to-resource recovery: A roadmap towards sustainability. Journal of Cleaner Production [Internet]. 2022;350:131305. Available from: https://www.sciencedirect.com/science/article/pii/S0959652622009349

28. Ayilara MS, Olanrewaju OS, Babalola OO, Odeyemi O. Waste Management through Composting: Challenges and Potentials. Vol. 12, Sustainability. 2020.

29. Lima PRL, Leite MB, Santiago EQR. Recycled lightweight concrete made from footwear industry waste and CDW. Waste Management

[Internet]. 2010;30(6):1107–13. Available from: https://www.sciencedirect.com/science/article/pii/S0956053X10000929

30. Chyliński F, Kuczyński K, Łukowski P. Application of Ilmenite Mud Waste as an Addition to Concrete. Materials (Basel, Switzerland). 2020 Feb;13(4).

31. Dimulescu C, Burlacu A. Industrial waste materials as alternative fillers in asphalt mixtures. Sustainability (Switzerland). 2021;13(14).

32. Hassanien R, Hassanien E, Ibrahim M. Recycling Waste Plastic Bags as a Replacement for Cement in Production of Building Bricks and Concrete Blocks Advanced Applications of Solar Energy in Greenhouses for Energy and Food Production. ID:33456 View project. Journal of Waste Resources and Recycling [Internet]. 2020;1(05300205020516009):1–13. Available from: www.annexpublishers.com

33. Kumar N, Amritphale SS, Matthews JC, Lynam JG, Alam S, Abdulkareem OA. Synergistic utilization of diverse industrial wastes for reutilization in steel production and their geopolymerization potential. Waste management (New York, NY). 2021 May;126:728–36.

34. Choudhary J, Kumar B, Gupta A. Utilization of Waste Glass Powder and Glass Composite Fillers in Asphalt Pavements. Lu G, editor. Advances in Civil Engineering [Internet]. 2021;2021:3235223. Available from: https://doi.org/10.1155/2021/3235223

35. Prathap MG, Balaji N, Sudarsan JS. Experimental study on usage of industrial waste in road construction. AIP Conference Proceedings [Internet]. 2020;2277(1):150001. Available from: https://doi.org/10.1063/5.0025309

36. Debbarma S, Ransinchung R.N. GD, Singh S, Sahdeo SK. Utilization of industrial and agricultural wastes for productions of sustainable roller compacted concrete pavement mixes containing reclaimed asphalt pavement aggregates. Resources, Conservation and Recycling [Internet]. 2020;152:104504. Available from: https://www.sciencedirect.com/science/article/pii/S0921344919304100

37. Irshidat MR, Al-Nuaimi N. Industrial Waste Utilization of Carbon Dust in Sustainable Cementitious Composites Production. Materials [Internet]. 2020;13(15). Available from: https://www.mdpi.com/1996-1944/13/15/3295

38. Julphunthong P, Joyklad P. Utilization of Several Industrial Wastes as Raw Material for Calcium Sulfoaluminate Cement. Materials. 2019 Oct 12;12:3319.

39. Altenbach H, Altenbach J, Kissing W. Classification of Composite Materials. In 2018. p. 3–18.

40. Kurian T, Mathew NM. Natural Rubber: Production, Properties and Applications. Biopolymers: Biomedical and Environmental Applications. 2011;403–36.

41. Porter M. Vulcanization of Rubber BT - Organic Chemistry of Sulfur. In: Oae S, editor. Boston, MA: Springer US; 1977. p. 71–118. Available from: https://doi.org/10.1007/978-1-4684-2049-4_3

42. Fröhlich J, Niedermeier W, Luginsland H-D. The effect of filler–filler and filler–elastomer interaction on rubber reinforcement. Composites Part A: Applied Science and Manufacturing [Internet]. 2005;36(4):449–60. Available from: https://www.sciencedirect.com/science/article/pii/S1359835X04002428

43. Ramesh M, Rajeshkumar LN, Srinivasan N, Kumar DV, Balaji D. Influence of filler material on properties of fiber-reinforced polymer composites: A review. e-Polymers [Internet]. 2022;22(1):898–916. Available from: https://doi.org/10.1515/epoly-2022-0080

44. Phumnok E, Khongprom P, Ratanawilai S. Preparation of Natural Rubber Composites with High Silica Contents Using a Wet Mixing Process. ACS Omega [Internet]. 2022 Mar 15;7(10):8364–76. Available from: https://doi.org/10.1021/acsomega.1c05848

45. Ulfah IM, Fidyaningsih R, Rahayu S, Fitriani DA, Saputra DA, Winarto DA, et al. Influence of Carbon Black and Silica Filler on the Rheological and Mechanical Properties of Natural Rubber Compound. Procedia Chemistry. 2015;16:258–64.

46. Kashfipour MA, Mehra N, Zhu J. A review on the role of interface in mechanical, thermal, and electrical properties of polymer composites. Advanced Composites and Hybrid Materials [Internet]. 2018;1(3):415–39. Available from: https://doi.org/10.1007/s42114-018-0022-9

47. Sethulekshmi AS, Saritha A, Joseph K. A comprehensive review on the recent advancements in natural rubber nanocomposites. International journal of biological macromolecules. 2022 Jan; 194:819–42.

48. Abdul Salim ZAS, Hassan A, Ismail H. A Review on Hybrid Fillers in Rubber Composites. Polymer-Plastics Technology and Engineering [Internet]. 2018 Apr 13;57(6):523–39. Available from: https://doi.org/10.1080/03602559.2017.1329432

49. Kuity A, Jayaprakasan S, Das A. Laboratory investigation on volume proportioning scheme of mineral fillers in asphalt mixture. Construction and Building Materials. 2014;68(C):637–43.

50. Sienkiewicz M, Janik H, Borzędowska-Labuda K, Kucińska-Lipka J. Environmentally friendly polymer-rubber composites obtained from waste tyres: A review. Journal of Cleaner Production. 2017 Jan 27;147.

51. Al Sheheri SZ, Al-Amshany ZM, Al Sulami QA, Tashkandi NY, Hussein MA, El-Shishtawy RM. The preparation of carbon nanofillers and their role on the performance of variable polymer nanocomposites. Designed monomers and polymers. 2019;22(1):8–53.

52. Sekharan RV, Abraham BT, Thachil ET. Utilization of waste expanded polystyrene: Blends with silica-filled natural rubber. Materials and Design. 2012;40:221–8.

53. Dwivedi C, Manjare S, Rajan SK. Recycling of waste tire by pyrolysis to recover carbon black: Alternative & environment-friendly reinforcing filler for natural rubber compounds. Composites Part B: Engineering [Internet]. 2020;200:108346. Available from: https://www.sciencedirect.com/science/article/pii/S1359836820333953

54. Simon-Stőger L, Varga C. PE-contaminated industrial waste ground tire rubber: How to transform a handicapped resource to a valuable one. Waste Management [Internet]. 2021;119:111–21. Available from:https://www.sciencedirect.com/science/article/pii/S0956053X20305481

55. Díaz S, Ortega Z, Mccourt MP, Kearns MP, Benítez AN. Recycling of polymeric fraction of cable waste by rotational moulding. Waste management. 2018;76:199–206.

56. Ferreira CT, Perez CAB, Hirayama D, Saron C. Recycling of polyamide (PA) from scrap tires as composites and blends. Journal of Environmental Chemical Engineering [Internet]. 2013;1(4):762–7. Available from: https://www.sciencedirect.com/science/article/pii/S2213343713001085

57. Sarioğlu E, Kaynak HK. PET Bottle Recycling for Sustainable Textiles. In: Camlibel NO, editor. Polyester [Internet]. Rijeka: IntechOpen; 2017. Available from: https://doi.org/10.5772/intechopen.72589

58. Abdou TR, Botelho Junior AB, Espinosa DCR, Tenório JAS. Recycling of polymeric composites from industrial waste by pyrolysis: Deep evaluation for carbon fibers reuse. Waste Management [Internet]. 2021;120:1–9. Available from: https://www.sciencedirect.com/science/article/pii/S0956053X20306267

59. Pajtášová M, Holcová K, Ondrušová D, Janík R, Skalková P, Ďurišová S, et al. The effect of alternative fillers based on polypropylene waste from fibers and foils production on properties of rubber compound. Vlakna a Textil. 2021;28(2):54–62.

60. Hiranobe CT, Tolosa GR, de Almeida Santos GT, de Oliveira JPJ, Budemberg ER, da Silva MJ, et al. Recycling waste polyurethane from the refrigeration industry as filler in SBR/NR composites for industrial applications. Journal of Applied Polymer Science [Internet]. 2023 Apr 10;140(14):e53709. Available from: https://doi.org/10.1002/app.53709

61. Włoch M, Ostaszewska U, Datta J. The Effect of Polyurethane Glycolysate on the Structure and Properties of Natural Rubber/Carbon Black Composites. Journal of Polymers and the Environment [Internet]. 2019;27(6):1367–78. Available from: https://doi.org/10.1007/s10924-019-01437-8

62. Zhang J-P, Zhang C-C, Zhang F-S. A novel process for waste polyvinyl chloride recycling: Plant growth substrate development. Journal of Environmental Chemical Engineering [Internet]. 2021;9(4):105475. Available from: https://www.sciencedirect.com/science/article/pii/S2213343721004528

63. Nabil H, Ismail H, Azura AR. Recycled Polyethylene Terephthalate Filled Natural Rubber Compounds: Effects of Filler Loading and Types of Matrix. Journal of Elastomers \& Plastics [Internet]. 2011;43(5):429–49. Available from: https://doi.org/10.1177/0095244311405503

64. Hayeemasae N, Salleh SZ, Ismail H. Using chloroprene rubber waste in rubber blends: optimizing performance by adding fillers. Green Materials [Internet]. 2019;7(4):156–67. Available from: https://doi.org/10.1680/jgrma.18.00086

65. Yehia A, Abdel Bary E, Mull M, Ismail M, Assem Y. New Trends for Utilization of Rubber Wastes. Macromolecular Symposia. 2012 Oct 1;320.

66. Colom X, Marín-Genescà M, Mujal R, Formela K, Cañavate J. Structural and physico-mechanical properties of natural rubber/GTR composites devulcanized by microwaves: Influence of GTR source and irradiation time. Journal of Composite Materials [Internet]. 2018 Mar 1;52(22):3099–108. Available from: https://doi.org/10.1177/0021998318761554

67. Demirhan E, Dinçler S, Saraç HI. Selection of Inorganic Fillers for Nontire Rubber Compounding. Polymer-Plastics Technology and Engineering [Internet]. 1994 Jan 1;33(1):83–8. Available from: https://doi.org/10.1080/03602559408010732

68. Kurlyand SK, Bykov EA, Karlina IA. A New Inorganic Filler for General- and Special-Purpose Rubbers. International Polymer Science and Technology [Internet]. 2008 Jan 1;35(1):35–8. Available from: https://doi.org/10.1177/0307174X0803500109

69. Rattanasom N, Saowapark T, Deeprasertkul C. Reinforcement of natural rubber with silica/carbon black hybrid filler. Polymer Testing. 2007;26(3):369–77.

70. Greenough S, Dumont M-J, Prasher S. The physicochemical properties of biochar and its applicability as a filler in rubber composites: A review. Materials Today Communications [Internet]. 2021;29:102912. Available from: https://www.sciencedirect.com/science/article/pii/S2352492821009004

71. Arroyo M, López-Manchado MA, Herrero B. Organo-montmorillonite as substitute of carbon black in natural rubber compounds. Polymer [Internet]. 2003;44(8):2447–53. Available from: https://www.sciencedirect.com/science/article/pii/S0032386103000909

72. Dananjaya SA V, Somarathna YR, Karunanayake L, Siriwardena S. Waste mica as filler for natural rubber latex foam composites. Journal of Polymer Research [Internet]. 2022;29(3):71. Available from: https://doi.org/10.1007/s10965-022-02930-w

73. Vinod A, Sanjay MR, Suchart S, Jyotishkumar P. Renewable and sustainable biobased materials: An assessment on biofibers, biofilms, biopolymers and biocomposites. Journal of Cleaner Production [Internet]. 2020;258:120978. Available from: https://www.sciencedirect.com/science/article/pii/S0959652620310258

74. Thomas SK, Parameswaranpillai J, Krishnasamy S, Begum PMS, Nandi D, Siengchin S, et al. A comprehensive review on cellulose, chitin, and starch as fillers in natural rubber biocomposites. Carbohydrate Polymer Technologies and Applications [Internet]. 2021;2:100095. Available from: https://www.sciencedirect.com/science/article/pii/S2666893921000633

75. Andrew JJ, Dhakal HN. Sustainable biobased composites for advanced applications: recent trends and future opportunities – A critical review. Composites Part C: Open Access [Internet]. 2022;7:100220. Available from: https://www.sciencedirect.com/science/article/pii/S2666682021001122

76. Kazemi H, Mighri F, Rodrigue D. A Review of Rubber Biocomposites Reinforced with Lignocellulosic Fillers. Vol. 6, Journal of Composites Science. 2022.

77. Dileep P, Varghese GA, Sivakumar S, Narayanankutty SK. An innovative approach to utilize waste silica fume from zirconia industry to prepare high performance natural rubber composites for multi-functional applications. Polymer Testing [Internet]. 2020;81:106172. Available from: https://doi.org/10.1016/j.polymertesting.2019.106172

78. Awad A, Aly A, Elgamsy R, Hazem Abdellatif M. A study of some thermal and mechanical properties of HDPE blend with marble and granite dust. Ain Shams Engineering Journal. 2019 Mar 23;10:353–358.

79. Dognani G, dos Santos R, Meirelles M, Rodrigues T, Klauck C, Rodrigues MA, et al. Natural rubber composites with Grits waste from cellulose industry. Journal of Material Cycles and Waste Management. 2020 Mar 21;22.

80. Xie T, Wang F, Xie C, Lei S, Yu S, Liu J, et al. Mechanical properties of natural rubber filled with foundry waste derived fillers. Materials. 2019;12(11).

81. Roy K, Debnath S, Bansod N, Pongwisuthiruchte A, Wasanapiarnpong T, Potiyaraj P. Possible use of gypsum waste from ceramics industry as semi-reinforcing filler in epoxidized natural rubber composites. Journal of Material Cycles and Waste Management. 2019 Nov 1;22.

82. Matei E, Predescu AM, Săulean AA, Râpă M, Sohaciu MG, Coman G, et al. Ferrous Industrial Wastes-Valuable Resources for Water and

Wastewater Decontamination. International journal of environmental research and public health. 2022 Oct;19(21).

83. Dasgupta M, Gupta S Das, Mukhopadhyay R, Bandyopadhyay A. Derivation of a New Compounding Ingredient for Rubber from Waste Marble Powder and Study on its Suitability in an Innerliner Compound of Tubeless Tyres. Progress in Rubber, Plastics and Recycling Technology. 2016;32(2):55–72.

84. Ahmed K, Nizami SS, Raza NZ, Mahmood K. Mechanical, swelling, and thermal aging properties of marble sludge-natural rubber composites. International Journal of Industrial Chemistry [Internet]. 2012;3(1):21. Available from: https://doi.org/10.1186/2228-5547-3-21

85. El-Sabbagh SH, Ahmed NM, Mahmoud DS, Mohamed WS. Silica and modified silica fume waste (mSF) as reinforcing fillers for rubber industry. Pigment & Resin Technology [Internet]. 2020 Jan 1;50(1):74–84. Available from: https://doi.org/10.1108/PRT-01-2020-0002

86. Orczykowski W, Bielinski D, Anyszka R, Gozdek T, Klajn K, Celichowski G, et al. Fly Ash from Lignite Combustion as a Filler for Rubber Mixes—Part II: Chemical Valorisation of Fly Ash. Materials. 2022 Aug 29;15:5979.

87. Shafik ES, Tharwat C, Abd-El-Messieh SL. Utilization study on red brick waste as novel reinforcing and economical filler for acrylonitrile butadiene rubber composite. Clean Technologies and Environmental Policy [Internet]. 2022; Available from: https://doi.org/10.1007/s10098-022-02457-0

88. Kondarage Y, Etampawala T, Pitawala J, Thangavel K, Edirisinghe D. Ceramic Waste-Based Natural Rubber Composites: An Exciting Way for Improving Mechanical Properties. Journal of Advanced Chemical Sciences. 2018 Sep 19;4.

89. Intiya W, Thepsuwan U, Sirisinha C, Sae-Oui P. Possible use of sludge ash as filler in natural rubber. Journal of Material Cycles and Waste Management [Internet]. 2017;19(2):774–81. Available from: https://doi.org/10.1007/s10163-016-0480-5

90. Krainoi A, Sripornsawat B, Toh-ae P, Kitisavetjit W, Pittayavinai P, Tangchirapat W, et al. Utilization of high and low calcium oxide fly ashes as the alternative fillers for natural rubber composites: A waste to wealth approach. Industrial Crops and Products [Internet].

2022;188:115589. Available from: https://www.sciencedirect.com/science/article/pii/S092666902201072X

91. Moustafa H, El Mogy S, Ibrahim S, Awad A, Darwish N. Bioenveloping Inorganic Filler-Based Eggshell Wastes for Enhancing the Properties of Natural Rubber Biocomposites. Tire Science and Technology. 2020 Dec 3;49.

92. Dominic C.D. M, Joseph R, Sabura Begum PM, Raghunandanan A, Vackkachan NT, Padmanabhan D, et al. Chitin nanowhiskers from shrimp shell waste as green filler in acrylonitrile-butadiene rubber: Processing and performance properties. Carbohydrate Polymers [Internet]. 2020;245:116505. Available from: https://www.sciencedirect.com/science/article/pii/S0144861720306792

93. Dominic M, Joseph R, Sabura Begum PM, Kanoth BP, Chandra J, Thomas S. Green tire technology: Effect of rice husk derived nanocellulose (RHNC) in replacing carbon black (CB) in natural rubber (NR) compounding. Carbohydrate Polymers [Internet]. 2020;230:115620. Available from: https://doi.org/ 10.1016/j.carbpol.2019.115620

94. Garcia NG, dos Reis EAP, Budemberg ER, Agostini DL da S, Salmazo LO, Cabrera FC, et al. Natural rubber/leather waste composite foam: A new eco-friendly material and recycling approach. Journal of Applied Polymer Science [Internet]. 2015 Mar 15;132(11). Available from: https://doi.org/10.1002/app.41636

95. Hang L, Do QV, Nguyen L, Doan V, Dang L, Dao V-D, et al. Utilization of Leather Waste Fibers in Polymer Matrix Composites Based on Acrylonitrile-Butadiene Rubber. Polymers. 2020 Dec 30;13:117.

96. Joshi G, Naithani S, Varshney VK, Bisht SS, Rana V. Potential use of waste paper for the synthesis of cyanoethyl cellulose: A cleaner production approach towards sustainable environment management. Journal of Cleaner Production [Internet]. 2017;142:3759–68. Available from: https://www.sciencedirect.com/science/article/pii/S0959652616317000

97. Santos RJ dos, Agostini DL da S, Cabrera FC, Reis EAP dos, Ruiz MR, Budemberg ER, et al. Sugarcane bagasse ash: new filler to natural rubber composite. Vol. 24, Polímeros. scielo ; 2014.

98. Lubura J, Kobera L, Abbrent S, Pavlova E, Strachota B, Bera O, et al. Natural Rubber Composites Using Hydrothermally Carbonized Hardwood Waste Biomass as a Partial Reinforcing Filler- Part I: Structure, Morphology, and Rheological Effects during Vulcanization. Polymers [Internet]. 2023;15(5). Available from: https://www.mdpi.com/2073-4360/15/5/1176

99. Sareena C, Ramesan MT, Purushothaman E. Transport Studies of Peanut Shell Powder Reinforced Natural Rubber Composites in Chlorinated Solvents. Fibers and Polymers. 2013 Oct 15;14:1674–87.

100. Masłowski M, Miedzianowska J, Strzelec K. Natural Rubber Composites Filled with Crop Residues as an Alternative to Vulcanizates with Common Fillers. Vol. 11, Polymers. 2019.

101. Güngör A, Akbay İ, Özdemir T. Waste walnut shell as an alternative bio-based filler for the EPDM: mechanical, thermal, and kinetic studies. Journal of Material Cycles and Waste Management. 2018 Aug 22;21.

102. Sahoo S, Basu D, Kumar A, Rasam P, Koundal A, Nawale M, et al. Systematic evaluation of a sustainable plasticizer derived from coconut shell bio-waste in a reinforced styrene butadiene copolymer system. Journal of Polymer Research [Internet]. 2023;30(6):248. Available from: https://doi.org/10.1007/s10965-023-03619-4

103. Głowacz-Czerwonka D, Zakrzewska P, Oleksy M, Pielichowska K, Kuźnia M, Telejko T. The influence of biowaste-based fillers on the mechanical and fire properties of rigid polyurethane foams. Sustainable Materials and Technologies [Internet]. 2023;36:e00610. Available from: https://www.sciencedirect.com/science/article/pii/S2214993723000453

104. Prochoń M, Przepiórkowska A, Tshela Ntumba Y-H. The Effect of Waste Fodder Potato Proteins on the Mechanical Properties of Carboxylated Acrylonitrile-Butadiene Rubber. Hazer B, Ratnam CT, editors. ISRN Polymer Science [Internet]. 2012;2012:810208. Available from: https://doi.org/10.5402/2012/810208

105. Sekar P, Noordermeer JWM, Anyszka R, Gojzewski H, Podschun J, Blume A. Hydrothermally Treated Lignin as a Sustainable Biobased Filler for Rubber Compounds. ACS Applied Polymer Materials [Internet]. 2023 Apr 14;5(4):2501–12. Available from: https://doi.org/10.1021/acsapm.2c02170

106. Harvey AJ, Leather NZ, Association SR. Footwear Materials and Process Technology [Internet]. Lasra; 1982. Available from: https://books.google.co.in/books?id=5GOCHAAACAAJ

107. Karkalic R, Radulovic J, Jovanovic D. Characteristics of polyurethane and elastomer parts for shoe industry produced by liquid injection molding technology. Vojnotehnicki glasnik. 2017;65(4):948–67.

108. Zavodna L, Trejtnarová L, Zavodny Pospisil J. A sustainable materials for footwear industry: Designing biodegradable shoes. Applied Researches in Technics, Technologies and Education. 2020 Feb 1;8:1–9.

109. Rajić I, Govorcin Bajsic E, Holjevac Grgurić T. Application of polyurethane in the production of shoe soles. Koža & obuća. 2021 Jan 1;69:7–9.

110. Galan RJ, Narayan T, Markovs RA. Novel Polyurethane Shoe Sole Systems Having Superior Low Temperature Flex Properties. Journal of Elastomers and Plastics. 1990;22:22–31.

111. Staikos JT, Rahimifard S. Post-consumer waste management issues in the footwear industry. Proceedings of the Institution of Mechanical Engineers, Part B: Journal of Engineering Manufacture. 2007;221(2):363–8.

112. Copen CE. Condom Use During Sexual Intercourse Among Women and Men Aged 15-44 in the United States: 2011-2015 National Survey of Family Growth. National health statistics reports [Internet]. 2017 Aug;(105):1—18. Available from: http://europepmc.org/abstract/MED/29155683

113. Kang N, Griffin D, Ellis H. The pathological effects of glove and condom dusting powders. Journal of Applied Toxicology [Internet]. 1992;12(6):443–9. Available from: https://analyticalsciencejournals.onlinelibrary.wiley.com/doi/abs/10.1002/jat.2550120614

114. Arieli D, Vaughan DEW, Goldfarb D. New Synthesis and Insight into the Structure of Blue Ultramarine Pigments. Journal of the American Chemical Society [Internet]. 2004 May 1;126(18):5776–88. Available from: https://doi.org/10.1021/ja0320121

115. Wang N, Dorman RA, Ingersoll CG, Hardesty DK, Brumbaugh WG, Hammer EJ, et al. Acute and chronic toxicity of sodium sulfate to four freshwater organisms in water-only exposures. Environmental toxicology and chemistry. 2016 Jan;35(1):115–27.

116. Gubari MQ, Zwain HM, Hassan WH, Vakili M, Majdi A. Desalination of pigment industry wastewater by reverse osmosis using OPM-K membrane. Case Studies in Chemical and Environmental Engineering [Internet]. 2023;8:100401. Available from: https://www.sciencedirect.com/science/article/pii/S2666016423001068

117. Benatti CT, Tavares CRG, Lenzi E. Sulfate removal from waste chemicals by precipitation. Journal of Environmental Management [Internet]. 2009;90(1):504–11. Available from: https://www.sciencedirect.com/science/article/pii/S0301479707004203

118. Košutić K, Novak I, Sipos L, Kunst B. Removal of sulfates and other inorganics from potable water by nanofiltration membranes of characterized porosity. Separation and Purification Technology [Internet]. 2004;37(3):177–85. Available from: https://www.sciencedirect.com/science/article/pii/S1383586603002065

119. Geurts JJM, Sarneel JM, Willers BJC, Roelofs JGM, Verhoeven JTA, Lamers LPM. Interacting effects of sulphate pollution, sulphide toxicity and eutrophication on vegetation development in fens: a mesocosm experiment. Environmental pollution (Barking, Essex : 1987). 2009 Jul;157(7):2072–81.

120. Vishnu G, Palanisamy S, Joseph K. Assessment of fieldscale zero liquid discharge treatment systems for recovery of water and salt from textile effluents. Journal of Cleaner Production [Internet]. 2008;16(10):1081–9. Available from: https://www.sciencedirect.com/science/article/pii/S0959652607001539

121. Iacob M, Tiron V, Stiubianu G-T, Dascalu M, Hernandez L, Varganici C-D, et al. Bentonite as an active natural filler for silicone leading to piezoelectric-like response material. Journal of Materials Research and Technology [Internet]. 2022;17:79–94. Available from: https://www.sciencedirect.com/science/article/pii/S2238785421015684

122. Masa A, Krem-Ae A, Ismail H, Hayeemasae N. Possible use of sepiolite as alternative filler for natural rubber. Materials Research. 2020;23(4).

123. Nicolais L, Narkis M. Stress-strain behavior of styrene-acrylonitrile/glass bead composites in the glassy region. Polymer Engineering \& Science [Internet]. 1971;11(3):194–9. Available from: https://onlinelibrary.wiley.com/doi/abs/10.1002/pen.760110305

124. Sinien L, Lin Y, Xiaoguang Z, Zongneng Q. Microdamage and interfacial adhesion in glass bead-filled high-density polyethylene. Journal of Materials Science [Internet]. 1992;27(17):4633–8. Available from: https://doi.org/10.1007/BF01165998

125. Turcsányi B, Pukánszky B, Tüdõs F. Composition dependence of tensile yield stress in filled polymers. Journal of Materials Science Letters [Internet]. 1988;7(2):160–2. Available from: https://doi.org/10.1007/BF01730605

126. Salam H, Dong Y. Theoretical Modelling Analysis on Tensile Properties of Bioepoxy/Clay Nanocomposites Using Epoxidised Soybean Oils. Karimi-Maleh H, editor. Journal of Nanomaterials [Internet]. 2019;2019:4074869. Available from: https://doi.org/10.1155/2019/4074869

127. Einstein A. Eine neue Bestimmung der Moleküldimensionen. Annalen der Physik [Internet]. 1906;324(2):289–306. Available from: https://onlinelibrary.wiley.com/doi/abs/10.1002/andp.19063240204

128. Guth E. Theory of Filler Reinforcement. Journal of Applied Physics [Internet]. 1945 Jan 1;16(1):20–5. Available from: https://doi.org/10.1063/1.1707495

129. Thommes M, Kaneko K, Neimark A V, Olivier JP, Rodriguez-Reinoso F, Rouquerol J, et al. Physisorption of gases, with special reference to the evaluation of surface area and pore size distribution (IUPAC Technical Report). Pure and Applied Chemistry [Internet]. 2015;87(9–10):1051–69. Available from: https://doi.org/10.1515/pac-2014-1117

130. Janković B, Mentus S, Jelić D. A kinetic study of non-isothermal decomposition process of anhydrous nickel nitrate under air atmosphere. Physica B: Condensed Matter [Internet]. 2009;404(16):2263–9. Available from: https://www.s ciencedirect. com/science/article/pii/S0921452609002361

131. Moussout H, Ahlafi H, Aazza M, Bourakhouadar M. Kinetics and mechanism of the thermal degradation of biopolymers chitin and chitosan using thermogravimetric analysis. Polymer Degradation and Stability [Internet]. 2016;130:1–9. Available from: https://www. sciencedirect.com/science/article/pii/S014139101630146X

132. Motaung TE, Luyt AS, Bondioli F, Messori M, Saladino ML, Spinella A, et al. PMMA-titania nanocomposites: Properties and thermal degradation behaviour. Polymer Degradation and Stability. 2012;97(8):1325–33.

133. Flynn JH, Wall LA. General Treatment of the Thermogravimetry of Polymers. Journal of research of the National Bureau of Standards Section A, Physics and chemistry. 1966;70A(6):487–523.

134. Ozawa T. A New Method of Analyzing Thermogravimetric Data. Bulletin of the Chemical Society of Japan [Internet]. 1965 Nov 27 [cited 2022 Jul 2];38(11):1881–6. Available from: http://www.journal.csj.jp/doi/10.1246/bcsj.38.1881

135. Kissinger HE. Reaction Kinetics in Differential Thermal Analysis. Analytical Chemistry [Internet]. 1957 Nov 1;29(11):1702–6. Available from: https://doi.org/10.1021/ac60131a045

136. Lim ACR, Chin BLF, Jawad ZA, Hii KL. Kinetic Analysis of Rice Husk Pyrolysis Using Kissinger-Akahira-Sunose (KAS) Method. Procedia Engineering [Internet]. 2016;148:1247–51. Available from: https://www.sciencedirect.com/science/article/pii/S1877705816309535

137. Tang W, Liu Y, Zhang H, Wang C. New approximate formula for Arrhenius temperature integral. Thermochimica Acta [Internet]. 2003;408(1):39–43. Available from: https://www.sciencedirect.com/science/article/pii/S0040603103003101

138. Li C-R, Tang TB. Dynamic thermal analysis of solid-state reactions. Journal of thermal analysis [Internet]. 1997;49(3):1243–8. Available from: https://doi.org/10.1007/BF01983680

139. Starink MJ, van Mourik P. Cooling and heating rate dependence of precipitation in an Al—Cu alloy. Materials Science and Engineering: A [Internet]. 1992;156(2):183–94. Available from: https://www.sciencedirect.com/science/article/pii/092150939290150Y

140. Starink MJ. The determination of activation energy from linear heating rate experiments: a comparison of the accuracy of isoconversion methods. Thermochimica Acta [Internet]. 2003;404(1):163–76. Available from: https://www.sciencedirect.com/science/article/pii/S0040603103001448

141. Doyle CD. Kinetic analysis of thermogravimetric data. Journal of Applied Polymer Science [Internet]. 1961;5(15):285–92. Available from: https://onlinelibrary.wiley.com/doi/abs/10.1002/app.1961.070051506

142. Vyazovkin S, Burnham AK, Criado JM, Pérez-Maqueda LA, Popescu C, Sbirrazzuoli N. ICTAC Kinetics Committee recommendations for performing kinetic computations on thermal analysis data. Thermochimica Acta [Internet]. 2011;520(1):1–19. Available from: https://www.sciencedirect.com/science/article/pii/S0040603111002152

143. Igwe IO, Ezeani OE. Studies on the Transport of Aromatic Solvents through Filled Natural Rubber. Isayev AI, editor. International Journal of Polymer Science [Internet]. 2012;2012:212507. Available from: https://doi.org/10.1155/2012/212507

144. Padhi S, Achary PG, Nayak N. Molecular transport behaviour of organic solvents through halloysite nanotubes filled ethylene–vinyl acetate copolymer. Bulletin of Materials Science. 2015 Aug 5;38.

145. Zemzem M, Vinches L, Hallé S. Molecular sorption and diffusion of organic solvents through maleated rubber/layered silicate nanocomposites. Journal of Elastomers and Plastics. 2021; 53(8):1015–32.

146. George S, Varughese KT, Thomas S. Molecular transport of aromatic solvents in isotactic polypropylene/acrylonitrile-co-butadiene rubber blends. Polymer [Internet]. 2000;41(2):579–94. Available from: https://www.sciencedirect.com/science/article/pii/S0032386199002086

147. John M, Thomas S, Varughese K. Comparison of Interaction of Aromatic Solvents in Hybrid and Textile Biocomposites. Journal of Elastomers and Plastics. 2009 Nov 4;41.

148. Ellis B, Welding GN. Estimation, from Swelling, of the Structural Contribution of Chemical Reactions to the Vulcanization of Natural Rubber. Part I. General Method. Rubber Chemistry and Technology [Internet]. 1964;37(2):563–70. Available from: https://doi.org/10.5254/1.3540348

149. Flory PJ, Rehner John J. Statistical Mechanics of Cross-Linked Polymer Networks I. Rubberlike Elasticity. The Journal of Chemical Physics [Internet]. 2004;11(11):512–20. Available from: https://doi.org/10.1063/1.1723791

150. Wu JC, Peppas NA. Modeling of penetrant diffusion in glassy polymers with an integral sorption deborah number. Journal of Polymer Science Part B: Polymer Physics [Internet]. 1993 Oct

1;31(11):1503–18. Available from: https://doi.org/10.1002/polb.1993.090311108

151. Rogers C. Sorption and diffusion in multicomponent polymers. Journal of Polymer Science: Polymer Symposia. 2007 Mar 8;72:301.

152. Strankowski M, Włodarczyk D, Piszczyk Ł, Strankowska J. Polyurethane Nanocomposites Containing Reduced Graphene Oxide, FTIR, Raman, and XRD Studies. Sitko R, editor. Journal of Spectroscopy [Internet]. 2016;2016:7520741. Available from: https://doi.org/10.1155/2016/7520741

153. Trovati G, Sanches EA, Neto SC, Mascarenhas YP, Chierice GO. Characterization of polyurethane resins by FTIR, TGA, and XRD. Journal of Applied Polymer Science [Internet]. 2010;115(1):263–8. Available from: https://onlinelibrary.wiley.com/doi/abs/ 10.1002/ app.31096

154. Yang JH, Chun BC, Chung YC, Cho JH. Comparison of thermal/mechanical properties and shape memory effect of polyurethane block-copolymers with planar or bent shape of hard segment. Polymer. 2003;44(11):3251–8.

155. Cullity BD. Elements of X-ray Diffraction. Second Edi. Addison-Wesley Publishing Company, Inc. Philippines; 1978.

156. Filip D, Macocinschi D, Vlad S. Thermogravimetric study for polyurethane materials for biomedical applications. Composites Part B: Engineering [Internet]. 2011;42(6):1474–9. Available from: https://www.sciencedirect.com/science/article/pii/S1359836811001910

157. Askari F, Barikani M, Barmar M, Shokrolahi F, Vafayan M. Study of thermal stability and degradation kinetics of polyurethane–ureas by thermogravimetry. Iranian Polymer Journal (English Edition). 2015 Sep 22;24:783–9.

158. Cai G-B, Chen S-F, Liu L, Jiang J, Yao H-B, Xu A-W, et al. 1{,}3-Diamino-2-hydroxypropane-N{,}N{,}N′{,}N′-tetraacetic acid stabilized amorphous calcium carbonate: nucleation{,} transformation and crystal growth. CrystEngComm [Internet]. 2010;12(1):234–41. Available from: http://dx.doi.org/10.1039/B911426M

159. Rey C, Renugopalakrishnan V, Collins B, Glimcher MJ. Fourier transform infrared spectroscopic study of the carbonate ions in bone

mineral during aging. Calcified tissue international. 1991 Oct; 49(4):251–8.

160. Xing Z, Hao Q, Ju Z, Xu L, Qian Y. Synthesis of MgCO3 microcrystals at 160°C starting from various magnesium sources. Materials Letters [Internet]. 2010;64(12):1401–3. Available from: https://www.sciencedirect.com/science/article/pii/S0167577X10002430

161. Zhao C, Lu Y, Zhao X, Khanal S, Xu S. Synthesis of MgCO3 particles with different morphologies and their effects on the mechanical properties of rigid polyvinyl chloride composites. Polymer-Plastics Technology and Materials [Internet]. 2021 Feb 11;60(3):316–26. Available from: https://doi.org/10.1080/25740881.2020.1811314

162. Choi S-B, Kim N-W, Lee D-K, Yu H. Growth mechanism of cubic MgO granule via common ion effect. Journal of nanoscience and nanotechnology. 2013 Nov;13(11):7577–80.

163. Yamaguchi N, Masuda Y, Yamada Y, Narusawa H, Han-Cheol C, Tamaki Y, et al. Synthesis of CaO-SiO₂ Compounds Using Materials Extracted from Industrial Wastes. Open Journal of Inorganic Non-metallic Materials. 2015;05(01):1–10.

164. Kadota K, Ibe T, Sugawara Y, Takano H, Yusof YA, Uchiyama H, et al. Water-assisted synthesis of mesoporous calcium carbonate with a controlled specific surface area and its potential to ferulic acid release. RSC Adv [Internet]. 2020;10(47):28019–25. Available from: http://dx.doi.org/10.1039/D0RA05542E

165. Åhlén M, Cheung O, Strømme M. Amorphous Mesoporous Magnesium Carbonate as a Functional Support for UV-Blocking Semiconductor Nanoparticles for Cosmetic Applications. ACS Omega. 2019;4(2):4429–36.

166. Kiefer J, Stärk A, Kiefer AL, Glade H. Infrared Spectroscopic Analysis of the Inorganic Deposits from Water in Domestic and Technical Heat Exchangers. Vol. 11, Energies. 2018.

167. Proydakova VY, Voronov V V, Pynenkov AA, Kuznetsov S V, Zykova MP, Nishchev KN, et al. Sodium Sulfate Polymorphism. Russian Journal of Inorganic Chemistry [Internet]. 2022;67(7):970–7. Available from: https://doi.org/10.1134/S0036023622070208

168. Linnow K, Zeunert A, Steiger M. Investigation of Sodium Sulfate Phase Transitions in a Porous Material Using Humidity- and Temperature-Controlled X-ray Diffraction. Analytical Chemistry [Internet]. 2006 Jul 1;78(13):4683–9. Available from: https://doi.org/10.1021/ac0603936

169. Lee SW, Hong KS, Condrate RA, Hapanowicz RP, Speyer RF. Characterization of gas components and deposits in bubbles in silicate glasses prepared with sodium sulphate. Journal of Materials Science [Internet]. 1992;27(18):4961–6. Available from: https://doi.org/10.1007/BF01105261

170. Yang S, Du W, Shi P, Shangguan J, Liu S, Zhou C, et al. Mechanistic and Kinetic Analysis of Na2SO4-Modified Laterite Decomposition by Thermogravimetry Coupled with Mass Spectrometry. PloS one. 2016;11(6):e0157369.

171. Dollimore D, Spooner P, Turner A. The bet method of analysis of gas adsorption data and its relevance to the calculation of surface areas. Surface Technology [Internet]. 1976;4(2):121–60. Available from: https://www.sciencedirect.com/science/article/pii/0376458376900248

172. Walton KS, Snurr RQ. Applicability of the BET Method for Determining Surface Areas of Microporous Metal−Organic Frameworks. Journal of the American Chemical Society [Internet]. 2007 Jul 1;129(27):8552–6. Available from: https://doi.org/10.1021/ja071174k

173. Brunauer S, Emmett PH, Teller E. Adsorption of Gases in Multimolecular Layers. Journal of the American Chemical Society [Internet]. 1938 Feb 1;60(2):309–19. Available from: https://doi.org/10.1021/ja01269a023

174. Guo Y, Zhang G, Gan H, Zhang Y. Micro/nano-structured CaWO4/Bi2WO6 composite: synthesis{,} characterization and photocatalytic properties for degradation of organic contaminants. Dalton Trans [Internet]. 2012;41(41):12697–703. Available from: http://dx.doi.org/10.1039/C2DT31376F

175. Xu K, Chen P, Zhou J, Zhan C, Qu Y, Yang Y, et al. Novel Metal−Organic Framework-Assisted Synthesis of ZnO Nanoparticle-Decorated {221} SnO 2 Octahedrons for Improved Triethylamine Gas Sensing. Industrial & Engineering Chemistry Research. 2023 Aug 10;62.

176. Madejová J, Gates WP, Petit S. Chapter 5 - IR Spectra of Clay Minerals. In: Gates WP, Kloprogge JT, Madejová J, Bergaya FBT-D in CS, editors. Infrared and Raman Spectroscopies of Clay Minerals [Internet]. Elsevier; 2017. p. 107–49. Available from: https://www.sciencedirect.com/science/article/pii/B9780081003558000059

177. Madejová J. FTIR techniques in clay mineral studies. Vibrational Spectroscopy [Internet]. 2003;31(1):1–10. Available from: https://www.sciencedirect.com/science/article/pii/S0924203102000656

178. Louati S, Baklouti S, Samet B. Geopolymers Based on Phosphoric Acid and Illito-Kaolinitic Clay. Nicolais L, editor. Advances in Materials Science and Engineering [Internet]. 2016;2016:2359759. Available from: https://doi.org/10.1155/2016/2359759

179. Jozanikohan G, Abarghooei MN. The Fourier transform infrared spectroscopy (FTIR) analysis for the clay mineralogy studies in a clastic reservoir. Journal of Petroleum Exploration and Production Technology [Internet]. 2022;12(8):2093–106. Available from: https://doi.org/10.1007/s13202-021-01449-y

180. Vieira CM, Monteiro S. Firing Behavior of the Clay Fraction of a Natural Kaolinitic Clay: Are They Different? Materials Research. 2019 Oct 1;22.

181. Ahrouch M, Gatica JM, Draoui K, Vidal H. Adding value to natural clays as low-cost adsorbents of methylene blue in polluted water through honeycomb monoliths manufacture. SN Applied Sciences [Internet]. 2019;1(12):1595. Available from: https://doi.org/10.1007/s42452-019-1636-4

182. Ferronato N, Torretta V. Waste Mismanagement in Developing Countries: A Review of Global Issues. International journal of environmental research and public health. 2019 Mar;16(6).

183. Evode N, Qamar SA, Bilal M, Barceló D, Iqbal HMN. Plastic waste and its management strategies for environmental sustainability. Case Studies in Chemical and Environmental Engineering [Internet]. 2021;4:100142. Available from: https://www.sciencedirect.com/science/article/pii/S2666016421000645

184. Perelygin VM, Rusakov N V. [Public health aspects of the assessment of industrial wastes at the present time]. Vestnik Akademii meditsinskikh nauk SSSR. 1991;(1):43–7.

185. Buczyńska A, Rolecki R, Tarkowski S. [Industrial wastes and health hazards]. Medycyna pracy. 1999;50(2):179–90.

186. Siddiqua A, Hahladakis JN, Al-Attiya WAKA. An overview of the environmental pollution and health effects associated with waste landfilling and open dumping. Environmental Science and Pollution Research [Internet]. 2022;29(39):58514–36. Available from: https://doi.org/10.1007/s11356-022-21578-z

187. Oladele IO, Okoro CJ, Taiwo AS, Onuh LN, Agbeboh NI, Balogun OP, et al. Modern Trends in Recycling Waste Thermoplastics and Their Prospective Applications: A Review. Vol. 7, Journal of Composites Science. 2023.

188. Brüning K. Natural Rubber BT - Encyclopedia of Polymeric Nanomaterials. In: Kobayashi S, Müllen K, editors. Berlin, Heidelberg: Springer Berlin Heidelberg; 2015. p. 1377–82. Available from: https://doi.org/10.1007/978-3-642-29648-2_302

189. John JM, Thomas GM, Vidhu H, Thomas S. Sustainable Composites Based on Natural Rubber and Biomass Resources [Internet]. Vol. 5, Current Applied Polymer Science. 2022. p. 140–50. Available from: http://www.eurekaselect.com/article/125788

190. Gargol M, Podkościelna B. The use of waste materials as fillers in polymer composites - synthesis and thermal properties. Physicochemical Problems of Mineral Processing. 2019;55(6):1549–56.

191. Setyarini PH, Purnomo P, Sulistyarini DH, Asfia A. The Effect of Addition of Waste Materials on Nitrile Butadiene Rubber to the Mechanical Properties of Roller Rubber. Key Engineering Materials [Internet]. 2020;851:47–52. Available from: https://www.scientific.net/KEM.851.47

192. Kemona A, Piotrowska M. Polyurethane Recycling and Disposal: Methods and Prospects. Polymers [Internet]. 2020 Aug 5;12(8):1752. Available from: https://pubmed.ncbi.nlm.nih.gov/32764494

193. Yang W, Dong Q, Liu S, Xie H, Liu L, Li J. Recycling and Disposal Methods for Polyurethane Foam Wastes. Procedia Environmental Sciences [Internet]. 2012;16:167–75. Available from: https://www.sciencedirect.com/science/article/pii/S1878029612005610

194. Nikje MMA, Garmarudi AB, Idris AB. Polyurethane waste reduction and recycling: From bench to pilot scales. Designed Monomers and Polymers. 2011;14(5):395–421.

195. Bhuvaneswari. G H. 3 - Degradability of Polymers. In: Thomas S, Rane AV, Kanny K, V.K. A, Thomas MG, editors. Recycling of Polyurethane Foams [Internet]. William Andrew Publishing; 2018. p. 29–44. (Plastics Design Library). Available from: https://www.sciencedirect.com/science/article/pii/B9780323511339000036

196. Gadhave R V., Srivastava S, Mahanwar PA, Gadekar PT. Recycling and Disposal Methods for Polyurethane Wastes: A Review. Open Journal of Polymer Chemistry. 2019;09(02):39–51.

197. Kemona A, Piotrowska M. Polyurethane recycling and disposal: Methods and prospects. Polymers. 2020;12(8).

198. Aprem AS, Jose S, Thomas S, Barkoula NM, Kocsis JK. Influence of hygrothermally degraded polyester-urethane on physical and mechanical properties of chloroprene rubber. European Polymer Journal. 2003;39(1):69–76.

199. Kumar CR, Karger–Kocsis J. Curing and mechanical behavior of carboxylated NBR containing hygrothermally decomposed polyurethane. European Polymer Journal. 2002;38(11):2231–7.

200. Gausas L, Kristensen SK, Sun H, Ahrens A, Donslund BS, Lindhardt AT, et al. Catalytic Hydrogenation of Polyurethanes to Base Chemicals: From Model Systems to Commercial and End-of-Life Polyurethane Materials. JACS Au [Internet]. 2021 Apr 26;1(4):517–24. Available from: https://doi.org/10.1021/jacsau.1c00050

201. Datta J, Kopczyńska P, Simón D, Rodríguez JF. Thermo-Chemical Decomposition Study of Polyurethane Elastomer Through Glycerolysis Route with Using Crude and Refined Glycerine as a Transesterification Agent. Journal of Polymers and the Environment. 2018;26(1):166–74.

202. Rolere S, Liengprayoon S, Vaysse L, Sainte-Beuve J, Bonfils F. Investigating natural rubber composition with Fourier Transform Infrared (FT-IR) spectroscopy: A rapid and non-destructive method to determine both protein and lipid contents simultaneously. Polymer Testing. 2015;43:83–93.

203. Stelescu MD, Manaila E, Craciun G, Chirila C. Development and characterization of polymer eco-composites based on natural rubber reinforced with natural fibers. Materials. 2017;10(7):1–20.

204. Fiayyaz M, Zia KM, Zuber M, Jamil T, Khosa MK, Jamal MA. Synthesis and characterization of polyurethane/bentonite nanoclay based nanocomposites using toluene diisocyanate. Korean Journal of Chemical Engineering. 2014;31(4):644–9.

205. Yang Z, Peng H, Wang W, Liu T. Crystallization behavior of poly(ε-caprolactone)/layered double hydroxide nanocomposites. Journal of Applied Polymer Science. 2010;116(5):2658–67.

206. Santos RJ, Agostini DLS, Cabrera FC, Budemberg ER, Job AE. Recycling leather waste: Preparing and studying on the microstructure, mechanical, and rheological properties of leather waste/rubber composite. Polymer Composites [Internet]. 2015;36(12):2275–81. Available from: https://onlinelibrary.wiley.com/doi/abs/10.1002/pc.23140

207. El Mogy SA, Youssef RS, Abd El Megeed AA. Processing of polyurethane nanocomposite reinforced with nanosized zinc oxide: Effect on mechanical and acoustic properties. Egyptian Journal of Chemistry. 2019;62(2):333–41.

208. Prasertsri S, Rattanasom N. Fumed and precipitated silica reinforced natural rubber composites prepared from latex system: Mechanical and dynamic properties. Polymer Testing. 2012;31(5):593–605.

209. Ahmed K. Hybrid composites prepared from Industrial waste: Mechanical and swelling behavior. Journal of Advanced Research. 2015;6(2):225–32.

210. Sadequl AM, Poh BT, Ishiaku US. Effect of Filler Loading on the Mechanical Properties of Epoxidized Natural Rubber (ENR 25) Compared with Natural Rubber (SMR L). International Journal of Polymeric Materials and Polymeric Biomaterials [Internet]. 1999;43(3–4):261–78. Available from: https://doi.org/10.1080/00914039908009689

211. Al-Hartomy OA, Al-Ghamdi AA, Farha Al Said SA, Dishovsky N, Mihaylov M, Ivanov M. Influence of carbon black/silica ratio on the physical and mechanical properties of composites based on epoxidized natural rubber. Journal of Composite Materials [Internet]. 2016 Feb 18 [cited 2021 Apr 24];50(3):377–86. Available from: http://journals.sagepub.com/doi/10.1177/0021998315575336

212. Zare Y. A model for tensile strength of polymer/clay nanocomposites assuming complete and incomplete interfacial adhesion between the polymer matrix and nanoparticles by the average normal stress in clay platelets. RSC Adv [Internet]. 2016;6(63):57969–76. Available from: http://dx.doi.org/10.1039/C6RA04132A

213. Švab I, Pustak A, Denac M, Škapin A, Leskovac M, Musil V, et al. Polypropylene Blends with m-EPR Copolymers: Mechanical and Rheological Properties. Acta Chimica Slovenica. 2018;65:344–53.

214. Li S-D, Kong L, Zhong J-P. Thermal Degradation Kinetics and Morphology of Natural Rubber/Silica Nanocomposites. Journal of nanoscience and nanotechnology. 2006;6:541–6.

215. Shih Y-F. Thermal degradation and kinetic analysis of biodegradable PBS/multiwalled carbon nanotube nanocomposites. Journal of Polymer Science Part B: Polymer Physics [Internet]. 2009;47(13):1231–9. Available from: https://onlinelibrary.wiley.com/doi/abs/10.1002/polb.21728

216. Shih Y-F, Chieh Y-C. Thermal Degradation Behavior and Kinetic Analysis of Biodegradable Polymers Using Various Comparative Models, 1. Macromolecular Theory and Simulations [Internet]. 2007 Jan 16;16(1):101–10. Available from: https://doi.org/10.1002/mats.200600059

217. Vyazovkin S, Sbirrazzuoli N. Isoconversional Kinetic Analysis of Thermally Stimulated Processes in Polymers. Macromolecular Rapid Communications [Internet]. 2006;27(18):1515–32. Available from: https://onlinelibrary.wiley.com/doi/abs/10.1002/marc.200600404

218. Rajeshwari PM, Dey TK. Thermogravimetric kinetics of degradation of HDPE based MWCNTs reinforced composites. International Journal of Plastics Technology. 2014;18:294–320.

219. Lee YM, Bourgeois D, Belfort G. Sorption, diffusion, and pervaporation of organics in polymer membranes. Journal of Membrane Science [Internet]. 1989;44(2):161–81. Available from: https://www.sciencedirect.com/science/article/pii/S0376738800833505

220. George SC, Thomas S, Ninan KN. Molecular transport of aromatic hydrocarbons through crosslinked styrene-butadiene rubber membranes. Polymer [Internet]. 1996;37(26):5839–48. Available from: https://www.sciencedirect.com/science/article/pii/ S0032386196004570

221. Dasan P. Solvent transport through carbon black filled poly(ethylene-co-vinyl acetate) composites. Express Polymer Letters - EXPRESS POLYM LETT. 2008;2:382–90.

222. Abraham J, Maria HJ, George SC, Kalarikkal N, Thomas S. Transport characteristics of organic solvents through carbon nanotube filled styrene butadiene rubber nanocomposites: the influence of rubber–filler interaction{,} the degree of reinforcement and morphology. Phys Chem Chem Phys [Internet]. 2015;17(17):11217–28. Available from: http://dx.doi.org/10.1039/C5CP00719D

223. Maria H, Lyczko N, Nzihou A, Mathew C, George S, Joseph K, et al. Transport of organic solvents through natural rubber/nitrile rubber/organically modified montmorillonite nanocomposites. Journal of Materials Science. 2013;48:5373–86.

224. Mathew L, Joseph KU, Joseph R. Swelling behaviour of isora/natural rubber composites in oils used in automobiles. Bulletin of Materials Science [Internet]. 2006;29(1):91–9. Available from: https://doi.org/10.1007/BF02709362

225. Al Minnath M, Unnikrishnan G, Purushothaman E. Transport studies of thermoplastic polyurethane/natural rubber (TPU/NR) blends. Journal of Membrane Science [Internet]. 2011;379(1):361–9. Available from: https://www.sciencedirect.com/science/article/pii/S0376738811004443

226. Jacob M, Varughese KT, Thomas S. A study on the moisture sorption characteristics in woven sisal fabric reinforced natural rubber biocomposites. Journal of Applied Polymer Science [Internet]. 2006 Oct 5;102(1):416–23. Available from: https://doi.org/10.1002/app.24061

227. Hatcher RA, Nelson AL, Trussell J, Cwiak CA, Cason P, Policar MS, et al. Contraceptive Technology [Internet]. Ayer Company Publishers, Incorporated; 2018. Available from: https://books.google.co.in/books?id=qsz8twEACAAJ

228. Datta J, Kosiorek P, Włoch M. Effect of high loading of titanium dioxide particles on the morphology, mechanical and thermo-mechanical properties of the natural rubber-based composites. Iranian Polymer Journal [Internet]. 2016;25(12):1021–35. Available from: https://doi.org/10.1007/s13726-016-0488-7

229. Zheng X, Jin Y, Chen J, Li B, Fu Q, He G. Mechanical properties and microstructure characterization of natural rubber reinforced by helical carbon nanofibers. Journal of Materials Science. 2019;54.

230. Datta J, Włoch M. Preparation, morphology and properties of natural rubber composites filled with untreated short jute fibres. Polymer Bulletin [Internet]. 2017;74(3):763–82. Available from: https://doi.org/10.1007/s00289-016-1744-x

231. Song SH. Influence of Eco-Friendly Processing Aids on Silica-Based Rubber Composites. Applied Sciences [Internet]. 2020;10(20). Available from: https://www.mdpi.com/2076-3417/10/20/7244

232. Dileep P, Varghese GA, Sivakumar S, Narayanankutty SK. An innovative approach to utilize waste silica fume from zirconia industry to prepare high performance natural rubber composites for multi-functional applications. Polymer Testing. 2020;81(September 2019): 106172.

233. Moonart U, Utara S. Effect of surface treatments and filler loading on the properties of hemp fiber/natural rubber composites. Cellulose [Internet]. 2019;26(12):7271–95. Available from: https://doi.org/10.1007/s10570-019-02611-w

234. Hayeemasae N, Ismail H, Matchawet S, Masa A. Kinetic of thermal degradation and thermal stability of natural rubber filled with titanium dioxide nanoparticles. Polymer Composites [Internet]. 2019;40(8):3149–55. Available from: https://onlinelibrary.wiley.com/doi/abs/10.1002/pc.25163

235. George SC, Thomas S. Transport phenomena through polymeric systems. Progress in Polymer Science [Internet]. 2001;26(6):985–1017. Available from: https://www.sciencedirect.com/science/article/pii/S0079670000000368

236. Sadrzadeh M, Saljoughi E, Shahidi K, Mohammadi T. Preparation and characterization of a composite PDMS membrane on CA support. Polymers for Advanced Technologies [Internet]. 2010 Aug 1;21(8):568–77. Available from: https://doi.org/10.1002/pat.1467

237. Stephen R, Joseph K, Oommen Z, Thomas S. Molecular transport of aromatic solvents through microcomposites of natural rubber (NR), carboxylated styrene butadiene rubber (XSBR) and their blends. Composites Science and Technology - COMPOSITES SCI TECHNOL. 2007 May 1;67:1187–94.

238. Seehra MS, Yalamanchi M, Singh V. Structural characteristics and swelling mechanism of two commercial nitrile-butadiene elastomers in various fluids. Polymer Testing [Internet]. 2012;31(4):564–71. Available from: https://www.sciencedirect.com/science/article/pii/S0142941812000311

239. Abdelmouleh M, Boufi S, Belgacem MN, Dufresne A. Short natural-fibre reinforced polyethylene and natural rubber composites: Effect of silane coupling agents and fibres loading. Composites Science and Technology [Internet]. 2007;67(7):1627–39. Available from: https://www.sciencedirect.com/science/article/pii/S026635380600248X

240. Aminabhavi TM, Khinnavar RS. Diffusion and sorption of organic liquids through polymer membranes: 10. Polyurethane, nitrile-butadiene rubber and epichlorohydrin versus aliphatic alcohols (C1-C5). Polymer. 1993;34(5):1006–18.

241. Lee J-Y, Park N, Lim S, Ahn B, Kim W, Moon H, et al. Influence of the silanes on the crosslink density and crosslink structure of silica-filled solution styrene butadiene rubber compounds. Composite Interfaces [Internet]. 2017;24(7):711–27. Available from: https://doi.org/10.1080/09276440.2017.1267524

242. Sareena C, Ramesan MT, Purushothaman E. Transport studies of peanut shell powder reinforced natural rubber composites in aromatic solvents. Polymer Composites [Internet]. 2012 Oct 1;33(10):1678–92. Available from: https://doi.org/10.1002/pc.22301

243. Arockiam JeyaSundar PGS, Ali A, Guo di, Zhang Z. 6 - Waste treatment approaches for environmental sustainability. In: Chowdhary P, Raj A, Verma D, Akhter YBT-M for SE and H, editors. Elsevier; 2020. p. 119–35. Available from: https://www.sciencedirect.com/science/article/pii/B9780128190012000061

244. Vignesh KS, Rajadesingu S, Arunachalam KD. Chapter Four - Challenges, issues, and problems with zero-waste tools. In: Hussain CMBT-C of AZWT, editor. Elsevier; 2021. p. 69–90. Available from: https://www.sciencedirect.com/science/article/pii/B9780128221839000040

245. Soliman NK, Moustafa AF. Industrial solid waste for heavy metals adsorption features and challenges; a review. Journal of Materials Research and Technology [Internet]. 2020;9(5):10235–53. Available from: https://www.sciencedirect.com/science/article/pii/ S2238785420315441

246. Vidya YS, Lakshminarasappa BN. Preparation, Characterization, and Luminescence Properties of Orthorhombic Sodium Sulphate. Pavesi L, editor. Physics Research International [Internet]. 2013;2013:641631. Available from: https://doi.org/10.1155/2013/641631

247. Chen D, Shao H, Yao W, Huang B. Fourier Transform Infrared Spectral Analysis of Polyisoprene of a Different Microstructure. Yang Z, editor. International Journal of Polymer Science [Internet]. 2013;2013:937284. Available from: https://doi.org/10.1155/2013/937284

248. Valera-Zaragoza M, Yescas-Yescas A, Juarez-Arellano E, Aguirre-Cruz A, Aparicio-Saguilán A, Ramírez E, et al. Immobilization of TiO2 nanoparticles on montmorillonite clay and its effect on the morphology of natural rubber nanocomposites. Polymer Bulletin. 2014 Jun 1;71:1295–313.

249. Sadok KH, Haouari M, Gallot-Lavallée O, Ben Ouada H. Effect of Na2SO4 substitution for Na2O on the structural and electrical properties of a sodium borophosphate glass. Journal of Alloys and Compounds [Internet]. 2019;778:878–88. Available from: https://www.sciencedirect.com/science/article/pii/S0925838818343329

250. Periasamy A, Muruganand S, Palaniswamy M. Vibrational studies of Na2so4, K2so 4, NaHSO4and KHSO4 crystals. Rasayan Journal of Chemistry. 2009;2(4):981–9.

251. Roy K, Debnath SC, Bansod ND, Pongwisuthiruchte A, Wasanapiarnpong T, Potiyaraj P. Possible use of gypsum waste from ceramics industry as semi-reinforcing filler in epoxidized natural rubber composites. Journal of Material Cycles and Waste Management [Internet]. 2020;22(1):285–94. Available from: https://doi.org/10.1007/s10163-019-00939-w

252. Ngamsurat S, Boonkerd K, Leela-adisorn U, Potiyaraj P. Curing Characteristics of Natural Rubber Filled with Gypsum. Energy Procedia [Internet]. 2011;9:452–8. Available from: https://www.sciencedirect.com/science/article/pii/S1876610211018042

253. Arayapranee W. Rubber Abrasion Resistance. Abrasion Resistance of Materials. 2012;

254. Hasnat A, Ghafoori N. Abrasion Resistance of Ultra-High-Performance Concrete for Railway Sleepers. Urban Rail Transit

[Internet]. 2021;7(2):101–16. Available from: https://doi.org/10.1007/s40864-021-00145-8

255. Utrera-Barrios S, Perera R, Leon N, Hernández M, Martínez N. Reinforcement of natural rubber using a novel combination of conventional and in situ generated fillers. Composites Part C: Open Access. 2021;5:100133.

256. Jung J, Sodano HA. Aramid Nanofiber Reinforced Rubber Compounds for the Application of Tire Tread with High Abrasion Resistance and Fuel Saving Efficiency. ACS Applied Polymer Materials [Internet]. 2020 Nov 13;2(11):4874–84. Available from: https://doi.org/10.1021/acsapm.0c00797

257. Mathew AP, Packirisamy S, Thomas S. Studies on the thermal stability of natural rubber/polystyrene interpenetrating polymer networks: thermogravimetric analysis. Polymer Degradation and Stability [Internet]. 2001;72(3):423–39. Available from: https://www.sciencedirect.com/science/article/pii/S0141391001000428

258. James J, Thomas G V, Pramoda KP, Thomas S. Transport behaviour of aromatic solvents through styrene butadiene rubber/poly [methyl methacrylate] (SBR/PMMMA) interpenetrating polymer network (IPN) membranes. Polymer [Internet]. 2017;116:76–88. Available from: https://www.sciencedirect.com/science/article/pii/S0032386117303282

259. Park GS. Transport Principles—Solution, Diffusion and Permeation in Polymer Membranes BT - Synthetic Membranes: Science, Engineering and Applications. In: Bungay PM, Lonsdale HK, de Pinho MN, editors. Dordrecht: Springer Netherlands; 1986. p. 57–107. Available from: https://doi.org/10.1007/978-94-009-4712-2_3

260. Obasi HC, Arukalam IO, Nwanonenyi SC, Eze IO, Chiemenem LI, Nwosu-Obieogu K, et al. Mechanical and Transport Properties of Natural Rubber Reinforced with Piassava (Raphia Hookeri) Fibre Composites. J Mater Environ Sci. 2019;10(2):119–31.

261. Joseph A, Mathai AE, Thomas S. Sorption and diffusion of methyl substituted benzenes through cross-linked nitrile rubber/poly(ethylene co-vinyl acetate) blend membranes. Journal of Membrane Science [Internet]. 2003;220(1):13–30. Available from: https://www.sciencedirect.com/science/article/pii/S0376738803001753

262. Welle F. Diffusion Coefficients and Activation Energies of Diffusion

of Organic Molecules in Polystyrene below and above Glass Transition Temperature. Vol. 13, Polymers. 2021.

263. Qian M, Zou B, Chen Z, Huang W, Wang X, Tang B, et al. The Influence of Filler Size and Crosslinking Degree of Polymers on Mullins Effect in Filled NR/BR Composites. Polymers. 2021 Jul;13(14).

264. Kumar V, Alam MN, Manikkavel A, Song M, Lee D-J, Park S-S. Silicone Rubber Composites Reinforced by Carbon Nanofillers and Their Hybrids for Various Applications: A Review. Polymers [Internet]. 2021;13(14). Available from: https://www.mdpi.com/2073-4360/13/14/2322

265. De Silva DJ, Abeysinghe H, Pamunuwa P, Nisansala D, Etampawala TNB. Carbon nanotube/rubber composites for pressure sensing applications. MRS Advances [Internet]. 2022;7(32):1004–9. Available from: https://doi.org/10.1557/s43580-022-00315-1

266. Ahmed K. Hybrid composites prepared from Industrial waste: Mechanical and swelling behavior. Journal of Advanced Research [Internet]. 2015;6(2):225–32. Available from: http://dx.doi.org/ 10.1016/j.jare.2013.12.002

267. Shafik ES, Tharwat C, Abd-El-Messieh SL. Utilization study on red brick waste as novel reinforcing and economical filler for acrylonitrile butadiene rubber composite. Clean Technologies and Environmental Policy [Internet]. 2023;25(5):1605–15. Available from: https://doi.org/10.1007/s10098-022-02457-0

268. Abdelsalam AA, El-Sabbagh SH, Mohamed WS, Khozami MA. Studies on swelling behavior, mechanical and thermal properties of ternary rubber blend composites in the presence of compatibilizers. Pigment & Resin Technology [Internet]. 2023 Jan 1;52(5):614–23. Available from: https://doi.org/10.1108/PRT-02-2022-0020

269. Neff F, Lion A, Johlitz M. Modelling diffusion induced swelling behaviour of natural rubber in an organic liquid. ZAMM - Journal of Applied Mathematics and Mechanics / Zeitschrift für Angewandte Mathematik und Mechanik [Internet]. 2019 Mar 1;99(3):e201700280. Available from: https://doi.org/10.1002/zamm.201700280

270. Rath JP, Chaki TK, Khastgir D. Development of Natural Rubber-Fibrous Nano Clay Attapulgite Composites: The Effect of Chemical Treatment of Filler on Mechanical and Dynamic Mechanical Properties of Composites. Procedia Chemistry [Internet]. 2012;4:131–7. Available from: https://www.sciencedirect.com/science/ article/ pii/S1876619612000204

271. Ogbebor O, Okieimen F, Ogbeifun D, Okwu U. Organomodified kaolin as filler for natural rubber. Chemical Industry and Chemical Engineering Quarterly. 2015 Oct 1;21:3.

272. Fiayyaz M, Zia KM, Zuber M, Jamil T, Khosa MK, Jamal MA. Synthesis and characterization of polyurethane/bentonite nanoclay based nanocomposites using toluene diisocyanate. Korean Journal of Chemical Engineering. 2014;31(4):644–9.

273. Yahaya L, Adebowale KO, Menon ARR, Olu-Owolabi B. Natural Rubber/ Organoclay Nanocomposite from Tea (Camellia S inensis) Seed Oil Derivative. American Journal of Materials Science. 2012;2:1–5.

274. Pinto-Salamanca C-E, Rigail-Cedeño AF, Mendoza Oliveros ME. Synthesis and characterization of natural rubber/clay nanocomposite to develop electrical safety gloves. Materials Today: Proceedings [Internet]. 2020;33:1949–53. Available from: https://www.sciencedirect.com/science/article/pii/S2214785320344084

275. Ibrahim N, Shokri AHM, Kamarun D, Mohd AF. Cure characteristic and mechanical properties of natural rubber vulcanizates with digested rice husk ash (RHA). AIP Conference Proceedings [Internet]. 2018;1985(1):40011. Available from: https://aip.scitation.org/doi/abs/10.1063/1.5047188

276. Jiang J, Zhai J, Kong L, Zhao D, Feng Y. Flame retardant chloroprene rubbers with high tensile strength and elongation at break via dual cross-linked networks. RSC Adv. 2022;12(42):27633–40.

277. Mohan TP, Kuriakose J, Kanny K. Effect of nanoclay reinforcement on structure, thermal and mechanical properties of natural rubber–styrene butadine rubber (NR–SBR). Journal of Industrial and Engineering Chemistry. 2011;17(2):264–70.

278. K Balan A, M P S, Vakyath S, Jinitha T, Subair N, Purushothaman E. Transport behavior of aromatic hydrocarbons through coconut shell powder filled thermoplastic polyurethane/natural rubber blend-composites. Vol. 1849, AIP Conference Proceedings. 2017. 20046 p.

279. Kim DY, Park JW, Lee DY, Seo KH. Correlation between the Crosslink Characteristics and Mechanical Properties of Natural Rubber Compound via Accelerators and Reinforcement. Polymers. 2020 Sep;12(9).

RESEARCH PUBLICATIONS

1. **P. Bashpa,** K. Bijudas, P. Dileep, Mehar Singh, Silviya Elanthikkal and Tania Francis, "Natural rubber composites reinforced with sodium sulfate waste from pigment industry: A circular economy approach for solid waste management", *Sustainable Chemistry and Pharmacy*, 2024; 40, 101628. https://doi.org/10.1016/j.scp.2024.101628

2. **P. Bashpa**, Annie Stephy, K. Bijudas and Tania Francis, "Thermal degradation kinetics and solvent transport behavior of natural rubber composites filled with polyurethane rich shoe sole waste from footwear industry", *Journal of Thermal Analysis and Calorimetry*, 2023; 148, 10871-10883. https://doi.org/10.1007/s10973-023-12425-5

3. **P. Bashpa,** K. Bijudas, P. Dileep, Mehar Singh, Silviya Elanthikkal and Tania Francis, "Mechanical and thermal characterization of condom industry waste reinforced natural rubber composites - Circular economy approach", *Environmental Engineering Research*, 2024; 29 (2): 230098. https://doi.org/10.4491/eer.2023.098

4. **P. Bashpa,** K. Bijudas, P. Dileep, Silviya Elanthikkal and Tania Francis, "Reutilization of polyurethane-based shoe sole scrap as a reinforcing filler in natural rubber for the development of high-performance composites", *Journal of Elastomers and Plastics*, 2022; 54 (6), 1040–1060. https:// doi.org/10.1177/ 00952443221108514

5. **Bashpa P,** Bijudas K, Tania Francis, "Enhanced dielectric and thermal properties of thermoplastic polyurethane/multi-walled carbon nanotube composites", *Materials Today: Proceedings*, 2022; 51 (8), 2254-2259. https://doi.org/10.1016/j.matpr. 2021.11.393

CONFERENCE PRESENTATIONS

1. **P. Bashpa,** Tania Francis, "High-Performance Natural Rubber Composites Reinforced with Sodium Sulphate Waste from the Pigment Industry", National Conference on Futuristic Materials in Science and Technology (NCFMST-2023), sponsored by Science and Engineering Research Board (SERB) and organized by Department of Chemistry, Bannari Amman Institute of Technology, Tamil Nadu on 05-10-2023 & 06-10-2023, ISBN: 978-93-5996-579-6

2. **P. Bashpa**, Tania Francis, "Light Magnesium Carbonate Rich Industrial Waste as a Reinforcing Filler in Natural Rubber: A Novel Attempt for Solid Waste Management", International Conference on Green Composites for a Sustainable Society (GCSS 2023), organized by Bhoomitrasena Club, Sacred Heart College, Thevara, Kochi, in collaboration with Directorate of Environment and Climate Change, Government of Kerala on 26-05-2023 & 27-02-2023.

3. **P. Bashpa**, Tania Francis, "Mechanical and Sorption Studies of Natural Rubber Composites Filled with Condom Industry Waste: A Novel Approach for Solid Waste Management", 2nd International Conference on Emerging Trends in Engineering, Sciences & Technology (ICETEST- 2023), organized by Faculty of Engineering & Technology, Poornima University, Jaipur on 24-02-2023 & 25-02-2023, ISBN: 978-93-5780-657-2

4. **P. Bashpa,** K. Bijudas, Tania Francis, "High performance natural rubber compounds filled with clay and polyurethane waste from footwear industry-A study on mechanical and thermal properties", International Research Conclave on Advances in Science and Technology (IRCAST 2023) organized by N. S. S. College, Ottapalam, Sanata Dharma University, Indonesia and Arunai Research Foundation on 18-02-2023 & 19-02-2023, ISBN: 978-81-952287-5-7

5. **Bashpa P,** Bijudas K, Tania Francis, "Enhanced dielectric and thermal properties of TPU/MWCNT composites, International

Conference on Advances in Materials Science (ICAMS, 2021), Arunai International Research Foundation & Department of Chemistry, University of Calicut on 11-09-2021 & 12-09-2021.

6. **Bashpa P,** Tania Francis, "Studies on the dielectric properties of TPU-MWCNT composites," Emerging Frontiers in Chemical Sciences (EFCS,2018), Department of Chemistry, Farook College, Calicut on 23-11-2018 & 24-11-2018, ISBN: 978-93-5321-807-2

7. Annie Stephy**, Bashpa P,** Namitha S Nath, Priyanka KJ and Tania Francis, "AStudy on the Dielectric Properties of EVA-CNT Composites, National Seminar on Current Trends in Chemistry, Department of Applied Chemistry, CUSAT, Kochi on 16th and 17th February, 2018.

Chapter 6
Mechanical, thermal and sorption studies of natural rubber-sodium sulphate waste composites

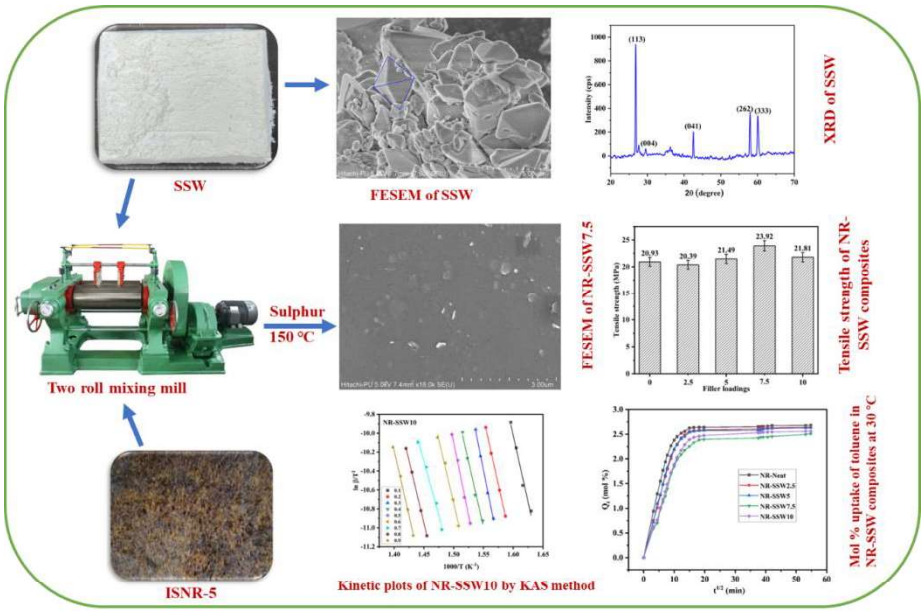

This chapter explains the fabrication and characterisation of the natural rubber-sodium sulphate waste (NR-SSW) composites. The rheological, mechanical, thermal and sorption properties of the fabricated NR-SSW composites have been discussed. Information on modelling studies of tensile strength by the established models like Nicolais-Narkis (N-N), Lu, and Turcsányi-Pukànszky-Tüdõs (T-P-T) has been provided. The kinetics of thermal degradation of NR-SSW composites have been studied by employing the model-free isoconversional methods, namely, Flynn-Wall-Ozawa (FWO), Kissinger-Akahira-Sunose (KAS), Tang, and Starink methods. Various sorption parameters and the sorption characteristics of NR-SSW composites in different solvents have been investigated.

6.1. Introduction

Environmental degradation is the primary issue brought on by fast urbanisation, industrialisation, and increased living standards. Any undesired solids, liquids, gases, or combinations released or expelled from an industrial operation are considered industrial waste. Due to their toxicity and environmental burden, industrial waste is one of the most significant issues all nations must deal with (243,244). Industrial waste can contaminate the groundwater, the air, and the land and can be defined as waste produced during various stages of industrial production. Industrial solid waste covers all forms of industrial waste, including recyclable, non-recyclable, reusable, and hazardous waste (245). Despite the measures adopted to manage and control industrial solid waste, there is a significant growth in its production. Consequently, the production of solid waste in industries has drawn a lot of attention, and the need to control it has led to the emergence of an active study field that brings together experts in chemical, environmental, and civil engineering.

Lapis lazuli is a semi-precious stone containing ultramarine blue pigment (sodium-alumino-silicate). It is a non-toxic, highly stable optical brightener and tinting agent and does not stain fabric. Extremely high concentrations of soluble inorganic salts, principally sodium salts and particularly sulphate, are present in the wastewater produced during the filtration of ultramarine blue slurry. Treatment of industrial effluents is significantly hampered and threatened by the presence of sulphate ions. It has been noted that sulphate consumption can have a laxative effect. Sulphate-rich irrigation water has the

potential to produce harmless white spots on tree leaves and fruits. Ultramarine and Pigments Ltd., Chennai, Tamil Nadu, the leading producer of inorganic pigments and surfactants, provided the recovered SSW.

As explained in section 2.1.4, SSW was collected, other impurities were removed, and it was used as a reinforcing filler in NR after being properly characterised using various analytical techniques. Table 2.9* of the Materials and Methods section discusses the general rubber compounding, and the sample designation and formulation of NR-SSW composites are given in Table 6.1. The fabricated composites were analysed for their rheological, mechanical, thermal and sorption properties. The experimental tensile strength results were also validated using well-established theoretical modelling methods. Various model-free methods were employed to examine the degradation dynamics of NR-SSW composites.

Table 6.1. Sample designation and formulation of SSW-filled NR composites

Sample designation	NR	SSW
NR-Neat	100	0
NR-SSW2.5	100	2.5
NR-SSW5	100	5
NR-SSW7.5	100	7.5
NR-SSW10	100	10

*NR-100, ZnO-5.0, stearic acid-2.0, TMQ-1.0, CBS-0.6, TMTD-0.2 and sulphur-2.5 (in phr)

6.2. Results & Discussion

6.2.1. Attenuated total reflectance-Fourier Transform infra-red spectroscopic analysis

The ATR-FTIR spectra of the NR-Neat and NR-SSW composites are shown in Figure 6.1, and Table 6.2 shows the obtained peaks. A unique peak of the SO_4^{2-} group in the composite's FTIR spectra and the lack of notable changes in peak positions rule out the possibility of chemical interactions between the functional groups in NR and SSW throughout the curing process (246).

Table 6.2. Prominent peaks in the ATR-FTIR spectra

Band position (cm^{-1})	**Assignment**
2960	Stretching vibrations (symmetric and asymmetric) of the CH group
2911	stretching vibrations (symmetric and asymmetric) of the CH_2 group
2840	stretching vibrations (symmetric and asymmetric) of the CH_3 group
831	Isoprene functional group (247)
1363	Symmetric vibration of CH_3 in NR (202)
1448	Symmetric vibration of CH_2 in NR (248)
1115-1035	Symmetric and asymmetric stretching vibrations of the SO_4^{2-} group (249)
616	Asymmetric bending vibrations of the SO_4^{2-} group (250)

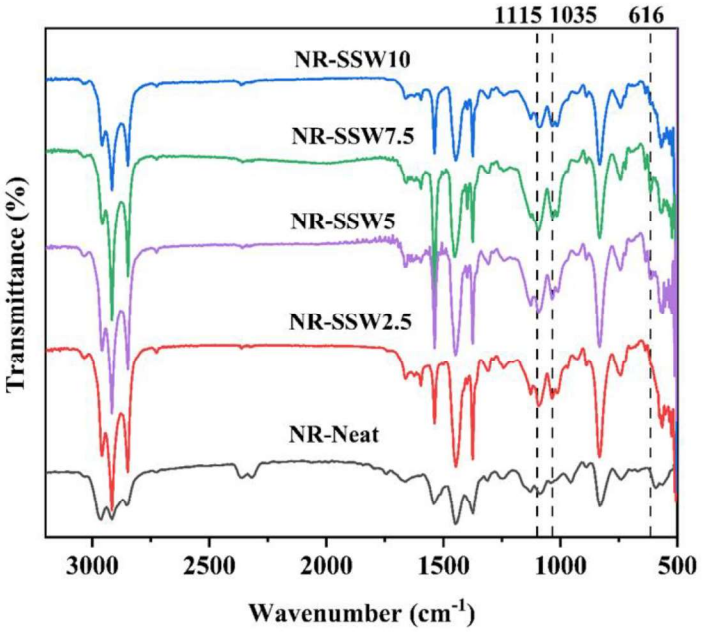

Figure 6.1. ATR-FTIR spectra of NR-Neat and NR-SSW composites

6.2.2. Surface morphology of NR and NR-SSW composites

Figures 6.2 (a) to (d) depict the surface morphology of NR-SSW composites with 2.5, 5, 7.5, and 10 phr SSW as determined by FESEM analysis. The stress-fractured surfaces of composites with different SSW loading were scanned to study the distribution of SSW on the NR matrix. The well-ordered distribution of SSW on lower filler loading is depicted in Figure 6.2 (a). Figures 6.2 (b) and (c) demonstrate the uniform distribution of SSW particles over the surface of the NR matrix without any chance of agglomeration up to 7.5 phr filler loading. However, Figure 6.2 (d) demonstrates that when the SSW loading surpasses 7.5 phr, the larger agglomerated SSW particles show less interaction between the matrix and filler.

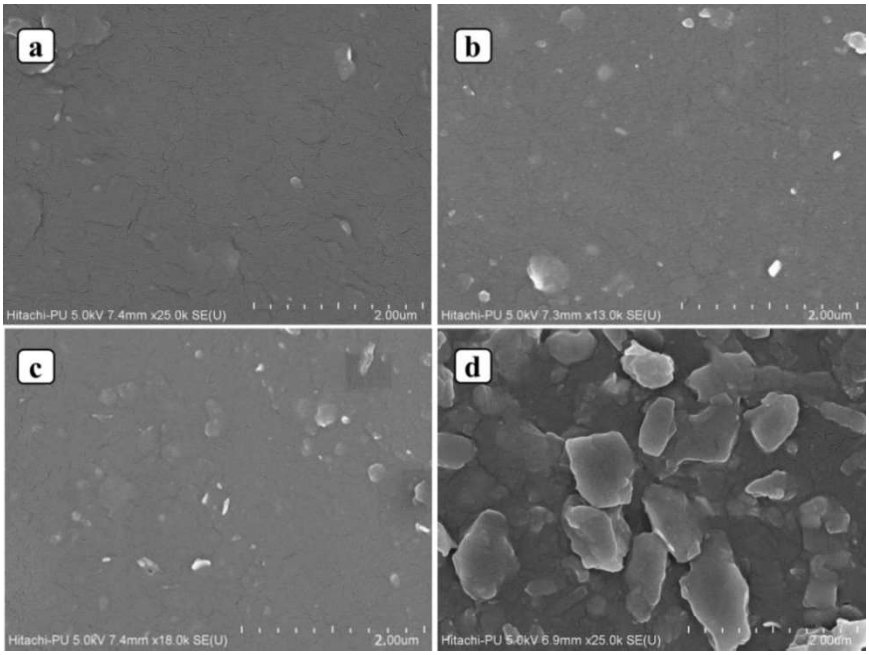

Figure 6.2. FESEM images of (a) NR-SSW2.5, (b) NR-SSW5, (c) NR-SSW7.5 and (d) NR-SSW10

6.2.3. Cure properties of NR-SSW composites

Table 6.3 illustrates the values of cure properties of NR-SSW composites.

Table 6.3. Cure properties of NR-SSW composites

Cure characteristics	NR-Neat	NR-SSW2.5	NR-SSW5	NR-SSW7.5	NR-SSW10
Cure time, t_{90} (min)	4.18	4.16	4.10	3.87	3.15
Scorch time t_{s2} (min)	2.15	2.25	2.21	2.06	1.88
Minimum torque, M_L (dNm)	6	5.4	6.4	6	5.5
Maximum torque, M_H (dNm)	72.9	68.8	70.4	75.2	78.6
M_H-M_L (dNm)	66.9	63.4	64	69.2	73.1
Cure rate index (min^{-1})	49.26	52.35	50.25	55.25	78.74

It is clear from the table that the optimum cure time (t_{90}) and scorch time decrease with an increase in SSW loading, proving that SSW is accelerating the curing of NR. The maximum torque value (M_H), representing the composite's stiffness, constantly increased with filler content. This can be explained by the fact that adding SSW reduces the mobility of polymer chains (251). Additionally, the torque difference (M_H-M_L) shows the quantity of cross-linkages that occur and is correlated with the compound's shear modulus, which rose with the amount of SSW. SSW's capacity to act as an accelerator in the curing of NR was further demonstrated by the rise in the cure rate index (CRI), which measures the curing rate upon adding filler (252).

6.2.4. Mechanical properties of NR-SSW composites

Figure 6.3 displays the graphs of stress and strain for NR-SSW composites. Composites with a filler loading of 7.5 phr, SSW showed the highest stress, proving its ability to withstand maximum strain because of the enhanced interaction of the matrix and filler (206).

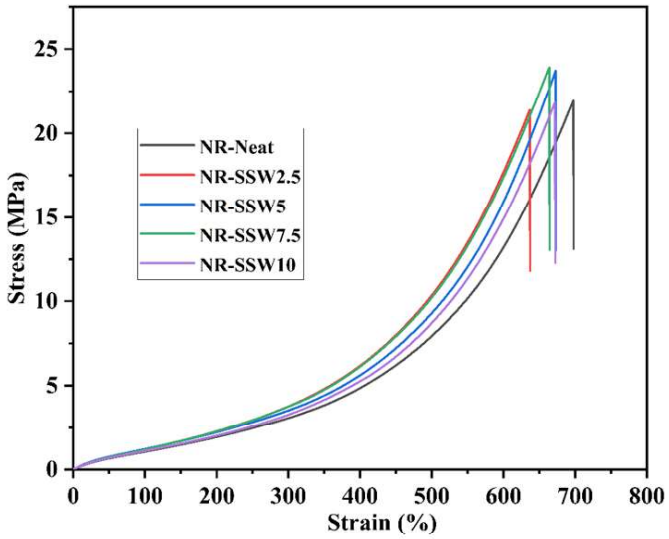

Figure 6.3. Stress-strain curves of NR-SSW composites

The tensile strength of NR-SSW composites increases by 9 % when 7.5 phr SSW is added; nevertheless, as filler loading increases, the strength rapidly decreases, as seen in the example of PU foam strengthened with nanosized zinc oxide (207). The reduction in tensile strength with increasing SSW loading was caused by the creation of filler aggregates, which led to an uneven distribution of filler in NR. NR-SSW interactions are inhibited, while filler interactions are promoted when SSW volume exceeds its percolation threshold. At higher filler loading, SSW-SSW interactions did not allow for stress transfer through the composites (208).

After adding SSW, the elongation at break showed a significant decrease compared to that of NR-Neat. This reduction in elongation at break could be brought on by SSW limiting the free movement of molecular chains in the NR (209). The modulus at 300 % elongation rises steadily to a filler loading of 7.5 phr (26 % increase for 7.5 phr SSW) and starts to decline on increasing SSW content due to filler

agglomeration. Young's modulus also exhibited the same pattern as the modulus at 300 % elongation. The tear strength showed a 14 % increase for 7.5 phr SSW loaded composite and gradually decreased on further addition due to poor dispersion of filler on NR and aggregation of SSW particles. Similar behaviour was shown in other systems, such as ENR and NR, reinforced with carbon black and calcium carbonate (210). Composite with 7.5 phr SSW showed minimum abrasion loss due to the better matrix-filler interaction (69). Heat build-up of NR-SSW composites increased progressively up to 7.5 phr filler loading before increasing sharply with further addition. An important factor affecting rubber material's performance, mainly when used in tyres and subjected to frequent abrasion, is the abrasion resistance index (ARI), which was evaluated to examine the durability towards abrasion. When a product is resistant to abrasion, it can withstand erosion brought on by rubbing, scraping, and other forms of mechanical wear. As a result, the substance is able to maintain its shape and integrity. This can be significant when a material's shape is essential to its ability to perform, as with precisely machined moving parts designed for maximum efficiency. When wearing becomes a problem, abrasion-resistant materials can be employed for moving and fixed elements (253,254). The NR-SSW7.5 composite had the highest ARI value, indicating its higher abrasion resistance property. The relevance of this improvement in abrasion resistance has already been described (255,256). The values of various mechanical parameters are provided in Table 6.4.

Table 6.4. NR-SSW composite's mechanical characteristics

Properties	**NR-Neat**	**NR-SSW2.5**	**NR-SSW5**	**NR-SSW7.5**	**NR-SSW10**
Hardness (Shore A)	41 ± 0.5	43 ± 0.5	44 ± 1	46 ± 1	46 ± 1.5
Specific gravity	0.965 ± 0.005	0.981 ± 0.010	0.993 ± 0.010	1.004 ± 0.005	0.979 ± 0.017
DIN abrasion loss (cc)	0.272 ± 0.15	0.277 ± 0.18	0.275± 0.15	0.260 ± 0.22	0.287 ± 0.18
Tensile strength (MPa)	21.93 ± 0.3	20.39 ± 0.4	21.49 ± 0.2	23.92 ± 0.35	21.81 ± 0.25
Elongation at break (%)	697 ± 18	647 ± 16	657 ± 20	669 ± 15	671 ± 17
Modulus at 300 % elongation (MPa)	3.09 ± 0.17	3.78 ± 0.14	3.82 ± 0.16	3.90 ± 0.12	3.36 ± 0.18
Young's Modulus (MPa)	0.8991 ± 0.02	1.0043 ± 0.04	1.0589 ± 0.01	1.1279 ± 0.05	0.9324 ± 0.01
Tear strength (N/mm)	41.76 ±1.2	44.30 ±1.5	46.10 ± 1.65	47.80 ± 1.72	44.80 ± 2.2
Heat Build-up (°C)	1 ± 0.45	1 ±0.32	2 ± 0.28	3.5 ± 0.66	6 ± 0.75
ARI	58 ± 2	57 ± 3	58 ± 3	62 ± 2	55 ± 4

6.2.5. Theoretical modelling of tensile strength of NR-SSW composites

The tensile strength of NR-SSW composites was confirmed using several theoretical modelling techniques, which also helped to establish the interaction between the matrix and filler at the interface. The mechanical properties of a composite are influenced by its filler content, filler distribution, filler morphology, and interaction with the matrix. In this work, three theoretical models, namely, Nicolais-Narkis (N-N) (123), Lu (124), and Turcsányi-Pukànszky-Tüdõs (T-P-T) (125), applied at various B values of 0, 1, 2, 3, 4, and 5, were used to predict the tensile strength of the composites. The experimental tensile strength values of the NR-SSW composites were more closely matched to those predicted by T-P-T models with B values above 3. Salam and Dong looked at these models and discovered that a B value above 3 indicates improved matrix-filler interfacial bonding (126). Based on the interfacial parameters of rigid filler-polymer composites, these models are frequently used to forecast the tensile strength of the materials. The values of tensile strength calculated with these three theoretical models and those obtained empirically are shown in Figure 6.4.

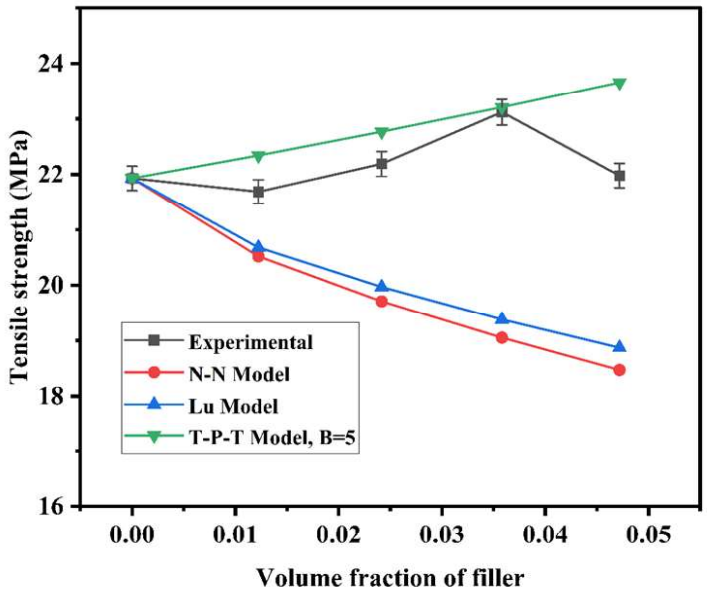

Figure 6.4. Tensile strength comparison between experimental results with theoretical models

The experimental results are consistent with the T-P-T model's (B = 5) better matrix-filler adhesion assumption up to 7.5 phr loading, as shown in Figure 6.4. The close agreement between experimental data and the T-P-T model suggests that the filler-matrix interfacial bonding of NR-SSW composites was better, resulting in efficient filler-matrix load transmission and a high reinforcing effect. Other models, such as the N-N, Lu, and T-P-T models with a B value below 3, underestimated the experimental tensile strength results. These models do not consider the filler-matrix adhesion and assume only weak interfacial bonding with no reinforcing effect.

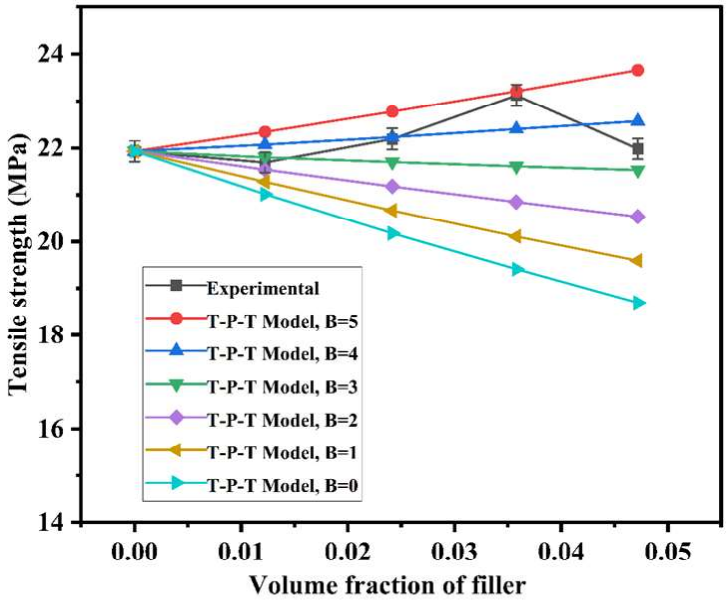

Figure 6.5. T-P-T model comparison of experimental tensile strength as a function of various B values

The T-P-T model is shown in Figure 6.5 at B values of 0, 1, 2, 3, 4, and 5. Matrix-filler interfacial bonding improves when B values exceed 3 (212). The experimental findings are compatible with the T-P-T model's prediction up to 7.5 phr SSW loading by using B value 5. The observed values differ from the expected values as the filler load rises. They align with predictions made using B values of 0 or 1, which assume a minimal interaction between the matrix filler and the interfacial medium. Table 6.5 shows the B values derived from the T-P-T model equation [Equation (2.7)] for NR-SSW composites.

Table 6.5. B values of NR-SSW composites

Composites	NR-SSW2.5	NR-SSW5	NR-SSW7.5	NR-SSW10
T-P-T model's interaction parameter (B)	1.43	3.93	5.84	3.44

It is evident from the above table that all composites had B values over 3, suggesting high filler-matrix adhesion and compatibility, except composite with filler content 2.5 phr SSW. NR-SSW7.5 composite displayed a higher B value and tensile strength, indicating improved filler-matrix adhesion (213). The theoretical prediction graphs for loading SSW up to 7.5 phr show higher matrix-filler adhesion and uniform SSW distribution on NR. The matrix filler adhesion collapses under increased loading. This may be because, with higher filler loading, cohesive contact between the filler and the filler outweighs adhesive interaction between the matrix and the filler.

6.2.6. Thermogravimetric analysis of NR and NR-SSW composites

TGA is used to examine the thermal behaviour of NR-Neat and NR-SSW composites at different filler loadings (Figure 6.6). As may be observed, there is just one stage of degradation for all composites. Table 6.6 gives the maximal thermal decomposition temperature (T_{max}), the amount of residue at 600 °C, and the initial decomposition temperature (T_i).

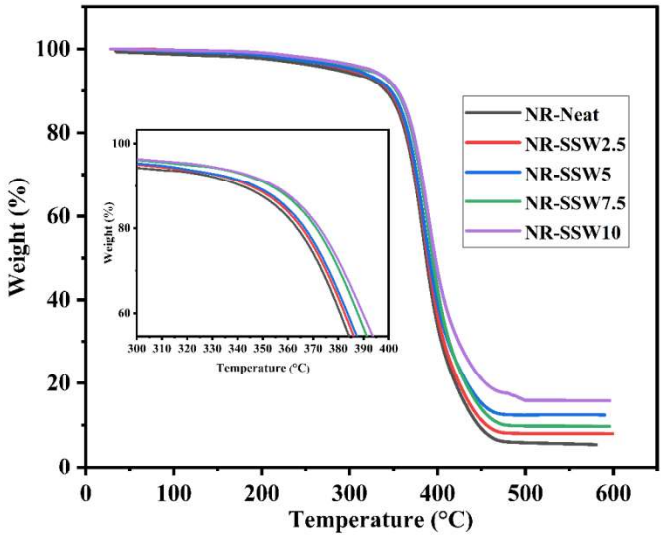

Figure 6.6. TGA curves of NR and NR-SSW composites

Table 6.6. Characteristics of NR-SSW composite's thermal deterioration

Properties	**NR-Neat**	**NR-SSW2.5**	**NR-SSW5**	**NR-SSW7.5**	**NR-SSW10**
Onset decomposition temperature, T_i (ºC)	326.7	326.8	328.2	331.5	333.6
Maximum decomposition temperature, T_{max} (ºC)	372	373.2	375.9	377.4	379.3
Residue at 600 °C (%)	5.39	7.90	9.80	12.26	15.82

NR-Neat and composites showed similar degradation behaviour. Volatilisation of breakdown products and weight loss occurs quickly during 330-450 °C, and roughly 6-7 % of weight loss occurs above 450 °C (257). Composites with 7.5 and 10 phr SSW

showed higher onset decomposition temperatures, suggesting better thermal stability than NR-Neat. Additionally, the maximum degradation temperature of the composites showed a gradual increase with that of NR-Neat. The filler's superior dispersion on the matrix causes higher thermal stability. As the filler percentage increases in the composites, there is an increase in the ultimate residue at 600 °C, which is only 5.39 % for NR-Neat. Composites showed increased thermal stability when adding the filler, as evidenced by the residue left behind following thermal breakdown.

6.2.7. Thermal degradation kinetics

The thermal stability and degradation dynamics of the NR-SSW composite have been studied using TGA. Thermal degradation kinetics have been successfully interpreted using isoconversional model-free methods such as Flynn-Wall-Ozawa (FWO) (133,134), Kissinger-Akahira-Sunose (KAS) (135,136), Tang (137,138), and Starink (139,140). Thermal degradation kinetics is vital because it clarifies the reaction mechanism and provides additional insight into the energy barriers for different processes (214). E_a values were calculated using the FWO, KAS, Starink, and Tang procedures at different conversion levels between 0.1 and 0.9. A straight line was fitted using the least square method for each method. Figures 6.7 - 6.10 show the NR-Neat and NR-SSW composite plots of all models with 10 phr SSW. All composites showed the same pattern. The correlation coefficient values, which range from 0.97 to 0.99, establish a strong

linear relationship between the heating rate and temperature for all linear fits. The four applied model's varying approximations account for a slight variance in E_a values. Table 6.7 lists the computed E_a for each conversion based on the presented graphs.

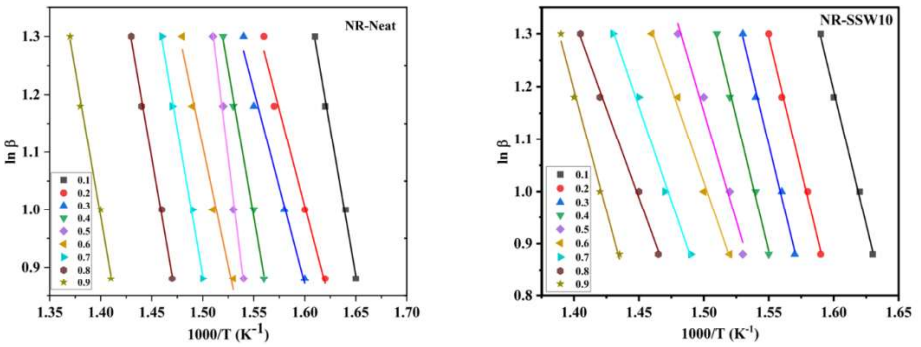

Figure 6.7. Kinetic plots of NR-Neat and NR-SSW10 by FWO method

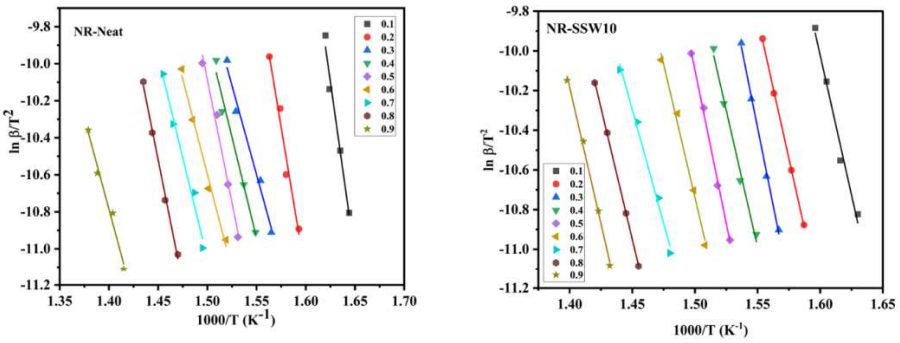

Figure 6.8. Kinetic plots of NR-Neat and NR-SSW10 by KAS method

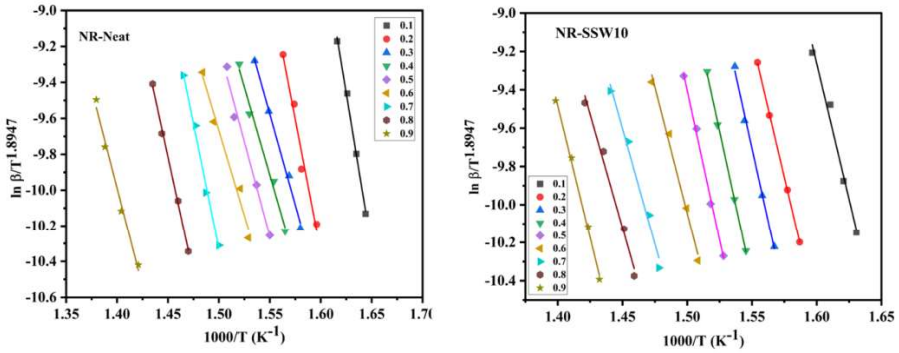

Figure 6.9. Kinetic plots of NR-Neat and NR-SSW10 by Tang method

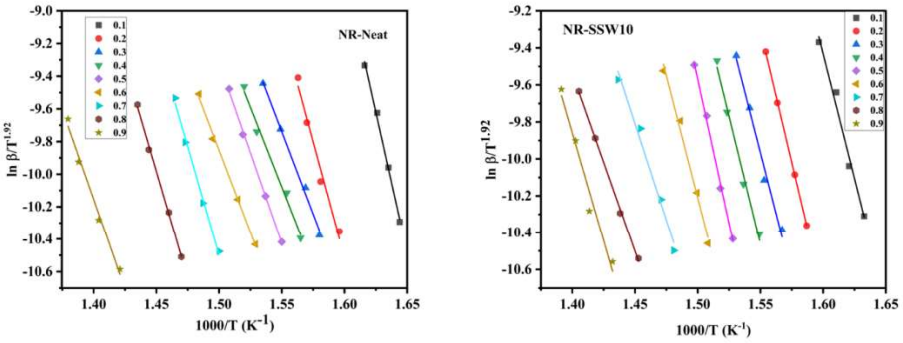

Figure 6.10. Kinetic plots of NR-Neat and NR-SSW10 by Starink method

Table 6.7. E_a values for FWO, KAS, Tang and Starink models

Samples →		NR-Neat	NR-SSW2.5	NR-SSW5	NR-SSW7.5	NR-SSW10
Method ↓	α	E_a ($kJmol^{-1}$)	E_a ($kJmol^{-1}$)	E_a ($kJmol^{-1}$)	E_a ($kJmol^{-1}$)	E_a ($kJmol^{-1}$)
FWO	0.1	123.94	194.40	174.71	170.09	219.19
	0.2	129.81	195.58	210.16	208.27	225.94
	0.3	137.90	214.08	203.97	178.98	245.72
	0.4	148.52	198.24	214.77	217.9	241.32
	0.5	156.67	210.02	240.98	240.61	239.77
	0.6	157.38	213.61	217.42	249.92	219.43
	0.7	174.66	217.68	207.05	183.38	213.13
	0.8	194.16	229.02	238.46	190.21	211.19
	0.9	185.75	172.06	118.15	120.73	207.65
KAS	0.1	123.23	193.85	174.39	170.24	218.89
	0.2	129.11	195.73	209.98	208.08	226.64
	0.3	137.30	213.97	204.33	179.24	248.42
	0.4	148.27	198.20	217.59	219.46	241.46
	0.5	156.15	209.55	240.93	240.59	241.86
	0.6	157.48	213.19	217.17	249.57	219.14
	0.7	174.19	217.28	206.68	183.30	213.57
	0.8	193.76	228.92	238.78	190.18	210.94
	0.9	184.70	172.12	118.00	120.70	207.24

Tang	0.1	123.76	194.39	174.93	170.78	219.37
	0.2	129.66	196.28	210.54	208.64	227.20
	0.3	137.87	214.53	204.90	179.80	248.99
	0.4	148.84	198.77	218.16	220.03	242.03
	0.5	156.73	210.13	241.51	241.17	242.44
	0.6	158.06	213.78	217.75	250.15	219.73
	0.7	174.78	217.87	207.30	183.89	214.16
	0.8	194.36	229.52	238.79	190.80	211.56
	0.9	184.32	172.75	118.65	121.32	207.85
Starink	0.1	123.63	194.26	174.80	170.65	219.24
	0.2	129.53	196.15	210.40	208.51	227.06
	0.3	137.73	214.39	204.76	179.67	248.55
	0.4	148.70	198.64	218.03	219.89	241.83
	0.5	156.59	209.99	241.37	241.03	242.30
	0.6	157.48	213.64	217.61	250.01	219.58
	0.7	174.64	217.73	207.15	183.75	214.02
	0.8	194.22	229.38	238.64	190.65	211.41
	0.9	185.17	172.60	118.49	121.17	207.71

The initial lower E_a values indicate that the breaking of weak linkages in the composites restricts the kinetics of the primary stages of degradation. The higher activation energy values observed during the later stages suggest that degradation of composites becomes relatively constrained and was further propagated by random scission of bonds and have already been reported (215,216). The variation of E_a values with different degrees of conversion illustrates the occurrence of parallel, consecutive, and irreversible reactions in the thermal degradation process. After adding SSW, all composites showed improved thermal stability with higher E_a values for thermal degradation than NR-Neat. Due to the mobility constraint of the polymer chains with increasing SSW content, E_a values for the NR-SSW composites may increase. The excellent agreement among the E_a values of the four kinetic models shows how these methods can be applied to study the thermal degradation of various composites.

6.2.8. Activation energy dependency on degree of conversion

The dependency of activation energy (E_a) on the degree of conversion (α) allows an adequate prediction of the reaction kinetics. The complicated multi-step reactions during pyrolysis, including competitive, parallel, and continuous reactions, may cause variations in E_a with conversion. Vyazovkin *et al*. stated that the change of E_a indicates that the process is divided into several phases, each contributing equally to the total rate (217). Figure 6.11 illustrates how E_a changes with conversion for NR neat and NR-SSW10 composites.

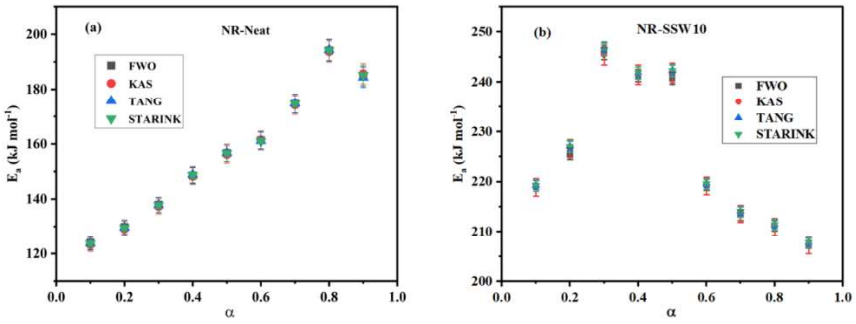

Figure 6.11. Variation of E_a with α for (a) NR-Neat and (b) NR-SSW10

As can be observed in Figure 6.10 (a), E_a steadily rises for NR-Neat up to α = 0.8 before declining at the end of the reaction. Each composite showed higher E_a than neat, and Figure 6.10 (b) shows an example of an NR-SSW10 plot. The variation of E_a for composite is not uniform; it first increases up to α = 0.5 and then declines sharply at later conversion stages. The E_a variation with conversion suggests a complicated, multistep breakdown of the reaction process. All the methods employed showed slight variation in the E_a due to the different approximations employed for the temperature integral.

6.2.9. Sorption properties of NR-SSW composites

The movement of different organic solvents and gases through polymers is crucial for many barrier applications and holds significant technological value. The matrix, type of penetrant, temperature, crosslink density, type of filler, interfacial adhesion between filler and matrix, and other variables all affect the transport mechanism through polymers (258,259). Solvents such as toluene, xylene, and mesitylene

were employed to investigate the sorption behaviour of NR-SSW composites.

6.2.9.1. Mol % uptake of solvents

The sorption characteristics of distinct solvents through the composites at varying filler loading were ascertained and shown as the solvent's molar percentage absorption (Q_t %) per gram. Equation (2.21) is used to calculate it. Q_t % is used to plot the sorption curves against the square root of time. Figure 6.12 displays a typical plot of sorption curves in toluene. All sorption curves in different solvents exhibit the same trend.

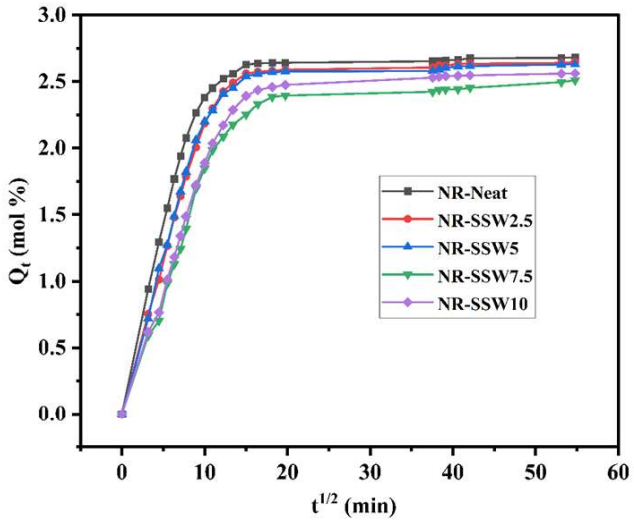

Figure 6.12. Mol % uptake of toluene through different NR-SSW composites at 30 °C

6.2.9.2. Effect of filler loading

The impact of filler loading on toluene diffusion in NR-SSW composites is depicted in Figure 6.12. The picture shows the greater concentration gradient of penetrant with the composites, which instigates the mol % of solvent uptake (Q_t) to increase initially at a high pace. As time passed, it reached an equilibrium similar to many other polymer systems, where the solvent extraction from the polymer counterbalanced the solvent intake. Rapid cavitations, which expose a larger surface area and improve solvent percolation, have been proposed as the cause of the higher early solvent absorption rates in polymers (144). It is clear that until 7.5 phr filler loading, the equilibrium solvent uptake falls; after that, it increases. Every filler particle acts as a barrier to the molecule that is diffusing. The amount of penetrating solvent decreases as the filler concentration in the rubber matrix rises because more and more barriers are formed to the diffusing molecule (52). The filler's reinforcement limits the polymer's freedom of movement and the composite's improved solvent resistance results from the polymer and filler network's improved interfacial adhesion. The tortuous path generated by the fillers is also indicated by the decrease in solvent diffusion in the filled polymer systems (260). Subsequently, a further increase in filler quantity causes agglomeration, which leaves gaps in the system that facilitate solvent penetration.

6.2.9.3. Effect of penetrant size

The order of the results, depicted in Figure 6.13, is toluene > xylene > mesitylene regarding the transport properties of NR-SSW composites in aromatic solvents.

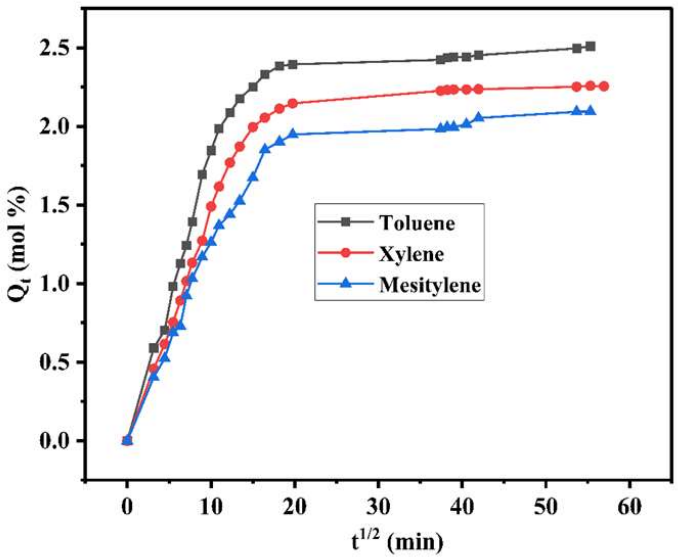

Figure 6.13. Solvent uptake of NR-SSW7.5 composite in various solvents

As penetrant size increases, the composite's Q_t % values start to decline. Numerous researches have observed that diffusivity decreases when penetrant size increases (143,261). Free volume theory explains this pattern, stating that the ease with which solvent molecules and polymer chains interchange locations determines the diffusion rate. Solubility decreases as exchange becomes more difficult due to increased molar volume or penetrant size. Moreover, larger activation energies are needed for the diffusion of bigger molecules (262). The equilibrium mol % (Q_∞) values of the NR-Neat and NR-SSW

composites in different aromatic solvents are listed in Table 6.8. Mesitylene has the lowest uptake values, whereas toluene has the greatest.

Table 6.8. NR-SSW composite's Q_∞ values for different solvents

	Q_∞ (mol %)		
Sample	**Toluene**	**Xylene**	**Mesitylene**
NR-Neat	2.6696	2.3122	2.2725
NR-SSW2.5	2.6238	2.3007	2.2637
NR-SSW5	2.6190	2.2898	2.2203
NR-SSW7.5	2.5805	2.2552	2.1943
NR-SSW10	2.5978	2.2638	2.2055

6.2.10. Swelling index and crosslink density

In vulcanised composites, chemical crosslinks and rubber-filler interactions influence a special characteristic called crosslink density (219,263). The main parameters affecting solvent transport through the NR matrix are the polymer chain's mobility, the composite's free volume, and the solvent's molecular size. Table 6.9 shows the swelling index and crosslink density of the NR-SSW composites. Based on the obtained results, the swelling index values indicated a minor rise upon additional filler addition, and the solvent absorption exhibited a consistent reduction upon increasing the SSW concentration up to 7.5 phr SSW. This could be because of the improved matrix-filler relationship. The uniformly distributed SSW in NR restricts the solvent molecule's mobility on NR up to 7.5 phr SSW addition. After that, SSW particles begin to agglomerate, creating open spaces in the matrix

that aid in solvent uptake. The composite's crosslink density peaked at 7.5 phr SSW and declined with additional filler addition because of the decreased NR-SSW interaction and SSW aggregation at higher loading (84). The NR-SSW composite's tensile strength and hardness strongly correlated with the crosslink density variation.

Table 6.9. Crosslink density and swelling index values of NR-SSW composites

Sample's name	Crosslink density $\times 10^{-4}$ (molg^{-1})	Swelling index (%)
NR-Neat	1.58 ± 0.02	245 ± 3
NR-SSW2.5	1.61 ± 0.01	242 ± 2
NR-SSW5	1.63 ± 0.02	241 ± 2
NR-SSW7.5	1.66 ± 0.03	236 ± 1
NR-SSW10	1.65 ± 0.02	238 ± 1

6.2.11. Diffusion coefficient, sorption coefficient and permeation coefficient

The values of the sample's permeation (P), sorption (S), and diffusion (D) coefficients in various solvents at room temperature are displayed in Table 6.10. D, S, and P values are found to be at their highest in unfilled systems because NR with flexible chains may readily adapt to solvent penetration. All solvents show a constant drop in values as the filler content is increased up to 7.5 phr filler loading. However, there is a modest increase in values at higher filler loading. This may result from decreased free space, filler-matrix interaction at increased loading, filler-filler network development, and reduced chain mobility of polymers. Due to the large activation energy requirement

for penetration as the solvent size grows, the size of the penetrant is also significant in the diffusion process. Solvents have molecular masses in the following order: toluene < xylene < mesitylene. As a result, the diffusion coefficient of the specific composite at a given temperature is reversed in the liquid's molecular mass order, with toluene being more than xylene and mesitylene. The trends in the sorption and penetration coefficients are likewise comparable.

Table 6.10. Values of D, S, and P of NR-SSW composites in aromatic solvents at 30 °C

Sample	Diffusion coefficient (D) × 10^{-4} (cm^2s^{-1})			Sorption coefficient (S)			Permeation coefficient (P) × 10^{-4} (cm^2s^{-1})		
	Toluene	Xylene	Mesitylene	Toluene	Xylene	Mesitylene	Toluene	Xylene	Mesitylene
NR-Neat	29.70	19.62	14.57	2.38	2.31	1.83	70.59	44.10	26.73
NR-SSW2.5	24.43	19.20	13.06	2.37	2.32	1.89	57.99	44.65	24.77
NR-SSW5	22.94	15.49	10.39	2.37	2.31	1.84	54.36	35.85	18.73
NR-SSW7.5	21.54	10.45	10.05	2.24	2.18	1.80	48.25	22.77	18.54
NR-SSW10	22.60	10.56	11.90	2.32	2.28	1.86	52.61	24.05	21.01

6.2.12. Mode of transport

It is possible to assess the transport mechanism using Equation (2.29). The solvent diffusion rate is less than the chain relaxation of the polymer chain when $n = 0.5$, indicating that the transport mode is normal Fickian. When $n = 1$, the transport is referred to as non-Fickian, meaning solvent penetration exceeds chain relaxation. If the value is in the range of 0.5 to 1, the transport is deemed anomalous. Table 6.11 presents the results of the linear regression analysis of log (Q_t/Q_∞) against log t plot, which was used to determine the values of *n* and *k* for the NR-Neat and NR-SSW composites.

Table 6.11. Values of *n* and *k* in different solvents for NR-SSW composites

Sample ↓	*n*			*k*		
	Toluene	Xylene	Mesitylene	Toluene	Xylene	Mesitylene
NR-Neat	0.48	0.53	0.61	0.38	0.37	0.30
NR-SSW2.5	0.45	0.52	0.59	0.33	0.35	0.31
NR-SSW5	0.50	0.53	0.54	0.35	0.31	0.30
NR-SSW7.5	0.51	0.50	0.57	0.32	0.29	0.29
NR-SSW10	0.47	0.50	0.57	0.37	0.35	0.30

According to the data, the values of *n* for xylene and toluene follow the Fickian transport mechanism. Additionally, mesitylene displayed anomalous behaviour. The delayed and viscous polymer chain relaxation following filler replenishment is the cause of the

anomalous mode. The value of *k* is used to evaluate the polymer's structural properties. Additionally, it offers insight into the way solvent and matrix molecules interact. The similar values of *k* discovered in the utilised solvents show how similarly the matrix and the solvents interacted (226). No correlation exists between n and the quantity of filler added to NR.

6.3. Conclusion

FTIR, FESEM, and TGA were used to characterise the NR-SSW composites, which were made using two roll mill mixing procedure. This study assessed the reuse of recovered SSW generated during the production of ultramarine pigment and examined the fabricated NR-SSW composite's curing, mechanical, thermal, and sorption properties. NR composites with 7.5 phr SSW showed noticeably higher tear strength, modulus at 300 % elongation, tensile strength, and enhanced abrasion resistance than NR-Neat. With increased filler loading, other mechanical properties, such as hardness, heat build-up, and compression set, are observed to rise. Up to 7.5 phr loading, the SSW was evenly distributed over the NR surface, as shown by the FESEM surface morphology of the NR-SSW composites. The tensile strength values were verified using the N-N, Lu, and T-P-T models. The T-P-T model and experimental tensile strength values agreed significantly up to 7.5 phr of SSW loading at B = 5. This relationship with theoretical models clearly shows the homogeneous distribution of SSW over the NR surface up to SSW loading of 7.5 phr.

Comparing NR-SSW composites to NR neat, thermal studies revealed the composite's better thermal stability. TGA has been used to investigate the kinetics of the heat deterioration of the NR-SSW composites. Isoconversional, model-free FWO, KAS, Tang, and Starink methods were used to calculate the E_a values for the breakdown of NR-neat and composites. These isoconversional models helped predict changes in E_a and trace the paths followed during thermal degradation. Multi-step degradation kinetics were anticipated by the four isoconversional models for the resulting composites.

It is found that compared to the other solvents used, toluene exhibits a higher swelling behaviour. The increase in filler loading in any solvent results in a decrease in solvent intake. The kinetic parameters like sorption, penetration, and diffusion coefficients were studied. The transportation method with mesitylene exhibited anomalous transport behaviour, whereas toluene and xylene align with Fickian theory. The NR composite with 7.5 phr SSW may be a better alternative to NR in common rubber products due to its exceptional mechanical, thermal, and sorption properties. This work also addresses environmental pollution issues by exploring the reutilisation of SSW from the pigment industry from a circular economy perspective.

Chapter 8

CONCLUSIONS

The substantial increase in industrialisation has a negative impact on the biosphere because of the excessive release of various industrial wastes. Landfills and other traditional methods are no longer sufficient to address the overproduction of industrial waste. Recycling these wastes is therefore growing in popularity. It is essential to effectively utilise different industrial wastes to reduce production costs and prevent pollution. High-performance rubber composites are critically needed for various applications in addition to recycling industrial waste. Numerous articles discuss the use of biomaterials as rubber fillers in particular contexts. However, the literature lacks information about the reutilisation of industrial solid wastes from the footwear, condom, and pigment industries. Large amounts of the aforementioned wastes are produced and typically dumped in landfills, seriously contaminating the ecology. As a result, a lot of attention was paid to using these industrial wastes as fillers in conjunction with reinforcement in NR to produce NR-waste composites, which would improve NR's sorption, mechanical, and thermal properties.

In addition to traditional filler clay, three different kinds of industrial wastes are employed as fillers in NR. Before the composite was prepared, the gathered wastes were made free from other materials and characterised by various analytical techniques like FTIR, FESEM, HRTEM, XRD, BET, DLS, HRTEM/FESEM-EDX, and TGA. NR composites containing PUW, MCW, SSW, and NR-PUW-clay compounds were fabricated using a two-roll mill mixing process. The composites were characterised and underwent rheological, mechanical, thermal, and sorption investigations. Theoretical modelling studies

were used to validate the mechanical and thermal results. The following lists the main findings drawn from the results obtained.

The NR-PUW composite's various mechanical characteristics were investigated. NR-PUW5 composite showed superior mechanical properties because the filler was more evenly distributed throughout the matrix, and there was greater matrix-filler interaction up to 5 phr loading of PUW. This composite showed high stress with the most efficient load distribution across the matrix. When compared to NR-Neat, the tensile, tear, and modulus of NR-PUW5 rose by 10 %, 2 %, and 9 %, respectively. The FESEM images of the tensile fractured surface provide additional proof of the fine dispersion of PUW on NR. While Young's modulus data were compared with Einstein and Guth models, the experimental tensile strength of NR-PUW composites was compared with the recognised theoretical modelling techniques (N-N, Lu, and T-P-T models). All modelling methodologies validate the improved matrix-filler interaction up to 5 phr PUW loading.

When the mechanical characteristics of NR-MCW composites were examined, it was discovered that the composite with 3 phr MCW had a significant improvement over NR-Neat in terms of tear strength (20 %), modulus at 300 % elongation (29 %), and tensile strength (22 %). The FESEM images of surface fractured composites demonstrated the superior distribution of MCW on NR up to 3 phr loading. The NR-MCW3 composite's experimental Young's modulus values strongly agreed with the Guth and Einstein models.

The analysed mechanical properties of the NR-SSW7.5 composite revealed a significant improvement over NR-Neat, with tensile strength and modulus increasing by 9 % and 26 %, respectively. According to the FESEM investigation, the system exhibits filler agglomeration at increased filler loading, which causes a reduction in properties. As filler loading increases, the mobility of polymer chains is restricted, resulting in a decrease in elongation at break. Similar trends were seen in other characteristics, such as rebound resilience, abrasion loss, and hardness. The well-known theoretical modelling techniques (N-N, Lu, and T-P-T models) were compared with the experimental tensile strength of NR-MCW composites. Better matrix-filler interaction is confirmed by all modelling methodologies used up to 7.5 phr SSW loading.

The NR-PUW5-C10 compound showed good tensile and tear strength after adding clay to the optimised NR-PUW5 composite. The characteristics remained unchanged even after increasing the amount of clay. The mechanical features of the optimised composites are displayed in Table 8.1.

Table 8.1. Mechanical properties of the optimised composites

Properties	**NR-Neat**	**NR-PUW5**	**NR-MCW3**	**NR-SSW7.5**	**NR-PUW5-C10**
Tensile strength (MPa)	21.93 ± 0.3	24.06 ± 0.2	26.66 ± 0.46	23.92 ± 0.35	26.3 ± 0.4
Modulus at 300 % elongation (MPa)	3.07 ± 0.17	3.36 ± 0.16	3.97± 0.22	3.90 ± 0.12	4.5 ± 0.15
Tear strength (N/mm)	41.76 ± 0.12	42.29 ± 1.65	50.31 ± 0.84	47.80 ± 1.72	44.85 ± 1.85
DIN abrasion loss (cc)	0.272 ± 0.15	0.259 ± 0.15	0.22 ± 0.018	0.260 ± 0.22	0.267 ± 0.25
Elongation at break (%)	697 ± 18	683 ± 20	667 ± 15	669 ± 15	645 ± 18

The thermal stability of all NR composites with PUW, MCW, and SSW, as well as NR-PUW-clay compounds, was investigated using TGA. It was discovered that all the composites and compounds significantly increased the onset degradation temperature, demonstrating their greater thermal stability than NR. The thermal stability of the produced composite is bolstered by an increase in the final residue at the end of the reaction. Activation energy and thermal degradation kinetics calculations at different degradation phases were assessed utilising isoconversional model-free techniques such as FWO, KAS, Tang, and Starink. When compared to NR-Neat, NR-PUW7.5, NR-MCW3, and NR-SSW10 showed the highest activation energy. The optimised composite's activation energies at 50 % conversion are reported in Table 8.2.

Table 8.2. Activation energy of NR composites at 50 % conversion

Method ↓	**Activation energy ($kJmol^{-1}$)**			
	NR-Neat	**NR-PUW7.5**	**NR-MCW3**	**NR-SSW10**
FWO	156.67	267.63	280.78	240.77
KAS	156.15	267.43	280.18	241.86
Tang	156.73	268.00	281.78	242.44
Starink	156.59	267.87	281.18	242.30

All of the applicable model's E_a values demonstrated strong correlations with one another. As the thermal decomposition proceeds through successive phases, the variation of E_a indicates a multistep degradation kinetics for the generated composites. NR-MCW3 composite showed the highest E_a values because MCW is a nanosized filler, allowing better matrix dispersion on NR than other fillers.

Various aliphatic and aromatic solvents examine the fabricated composite's sorption behaviour. It was established how temperature, penetrant size, and filler loading affected the values of mol % uptake. The solvent's absorption decreased with an increase in penetrant size and filler addition till optimised composite composition. Among all the aromatic solvents in the composites, toluene exhibited the highest diffusion, whereas mesitylene displayed the lowest. Aliphatic solvents dispersed more slowly than aromatic solvents. This is due to the considerable solubility parameter variation between aromatic and aliphatic solvents. The solvent uptake increased with an increase in temperature as solvent molecules are activated at high temperatures and also due to the weakening of matrix-filler interaction creating free volume for the easy diffusion of solvents. The estimated diffusion, sorption, and penetration coefficients also showed a similar trend as that of mol % uptake. The activation energy of diffusion was also computed using the Arrhenius Equation. The method of transportation was assessed based on *n* values. The optimised composite's sorption characteristics in toluene were compiled in Table 8.3.

Table 8.3. Q_∞ values of optimised composites in toluene

Sample	Q_∞ values (mol %)
NR-Neat	3.51
NR-PUW20	3.04
NR-MCW3	3.33
NR-SSW7.5	2.58
NR-PUW5-C20	2.17

The investigations revealed the improved qualities of NR composites reinforced with industrial wastes. NR-PUW, NR-MCW, NR-SSW, and NR-PUW-clay compounds demonstrated improved mechanical, thermal, and sorption properties. Using these compounds instead of NR would be advantageous when fabricating common industrial rubber goods requiring high tensile strength, temperature resistance, and solvent absorption resistance. Another significant finding of the study is how crucial it is to reuse industrial wastes from a circular economy perspective to reduce production costs and prevent pollution.

Chapter 9

RECOMMENDATIONS

Industrial solid waste generation has increased dramatically in India due to rapid industrialization following economic liberalisation. Traditionally, industries have disposed of their waste materials into the environment without pretreatment. This industrial pollution has catastrophic effects on the environment, biodiversity, and public health. To lessen the negative impacts of industrial pollution and safeguard the delicate balance of our planet's ecosystem, we must prioritise sustainable practices and technology. Reusing industrial wastes assumes fundamental relevance in the era of the circular economy. A circular economy is characterised by markets that promote product reuse rather than discarding them and extracting new resources. All waste materials, including old electronics, scrap metal, and abandoned clothing, are recycled or put to better use. In addition to protecting the environment, this can help create new industries, jobs, and skills and better use of natural resources.

One of Kerala's most significant districts, Kozhikode, is home to more than 150 PU-based footwear production units, each backed by 300 auxiliary facilities. Approximately 20 - 25 kg of PUW is produced daily in a unit, posing a primary environmental concern. In a similar vein, massive amounts of LMC, which is used as a finishing powder during the final stages of producing condoms, are discarded by landfills, causing water pollution. The pigment industries have a large quantity of recovered sodium sulphate as waste while manufacturing pigments, causing soil and water pollution. The aforementioned industrial wastes were gathered, unwanted materials removed, powdered and reused in NR as reinforcing fillers to investigate how

they can improve NR's mechanical, thermal, and sorption behaviours. The impact of clay on enhancing the above properties of NR-PUW composites is also studied.

The fabricated composites outperformed NR in mechanical characteristics, making them suitable for usage in various sectors needing high tensile and tear strength and dimensional stability, such as machinery components, footwear, and automobiles. Several theoretical models can be used to demonstrate the extraordinary mechanical qualities resulting from the improved adhesion between the matrix and the filler. As a result, these composites can produce common rubber goods like mud flaps, drive couplings, washers, anti-vibration mounts, pad assemblies, and conveyor belts flawlessly in place of NR due to their superior features.

The NR-industrial waste composites exhibited comparatively high thermal stability, rendering them appropriate for manufacturing high-temperature resistant rubber products in industries functioning at a higher temperature. The thermal degradation studies, utilising various model-free techniques for determining activation energy, can be extended to establish the thermal degradation mechanism.

The fabricated composites and compounds demonstrated high solvent resistance and have potential applications in any industry where machine parts come in contact with liquids. The better sorption resistance properties encourage their exploration in the design and fabrication of rubber materials for liquid transportation and packaging applications.

Furthermore, this work offers insight into addressing environmental pollution concerns and cost reduction from a circular economy perspective by examining the possibility of reusing solid wastes from various industries to produce inexpensive, high-performing composites. Additionally, this method may be used to build rubber composites with excellent performance for various industrial applications employing different rubber systems, such as SBR, NBR, ENR, etc.